RoboCity16

Robots for citizens

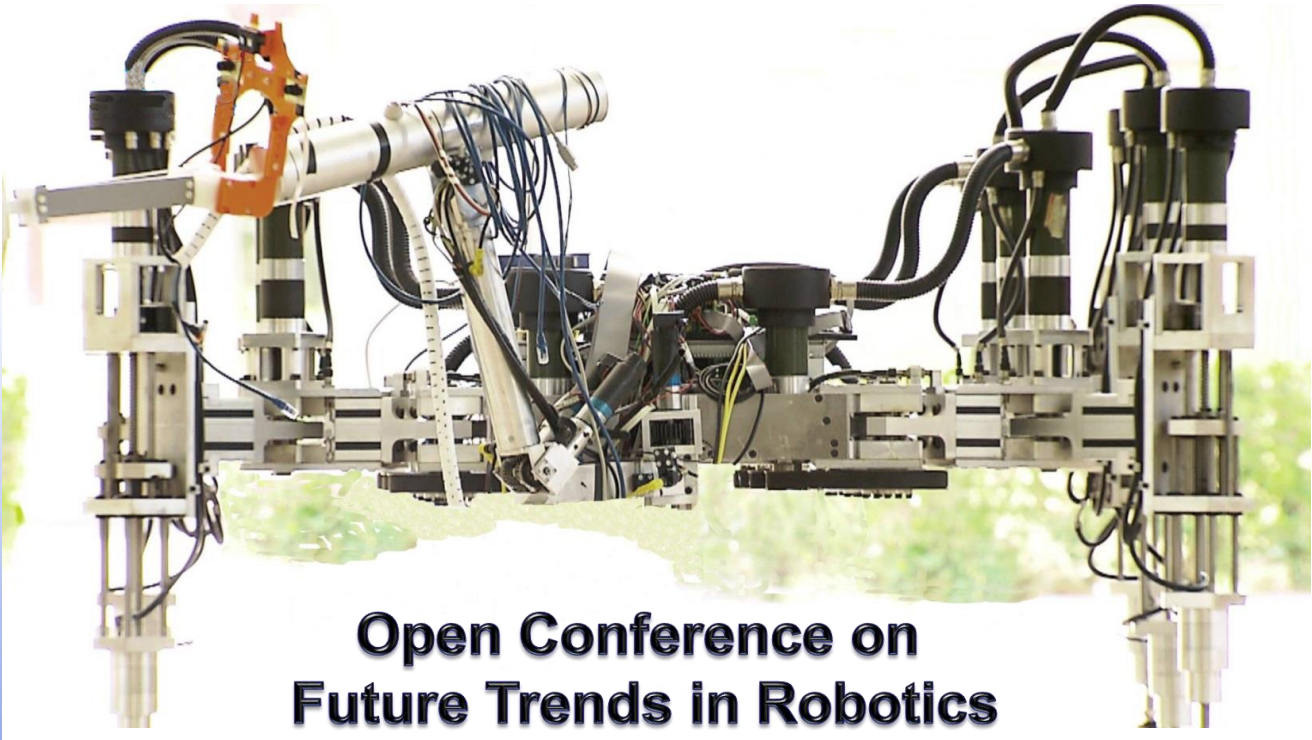

Open Conference on Future Trends in Robotics

Edited by:
Roemi E. Fernández
Héctor Montes

RoboCity2030.org

Comunidad de Madrid

UNIÓN EUROPEA
Fondos Estructurales
Invertimos en su futuro

Universidad Carlos III de Madrid

CSIC
Consejo Superior de Investigaciones Científicas

POLITÉCNICA

Universidad de Alcalá

Universidad Rey Juan Carlos

UNED

May 2016

RoboCity16 Open Conference on Future Trends in Robotics

Editors
Roemi E. Fernández Saavedra
Héctor Montes Franceschi

Madrid, 26 May 2016

Edited by: Consejo Superior de Investigaciones Científicas
Printed by: AFERTA SG S.L.
Legal Deposit: M-17804-2016
ISBN: 978-84-608-8452-1

PROLOGUE

It is my pleasure to present the RoboCity16 Open Conference on Future Trends in Robotics, a conference focused on presenting the efforts of Madrid´s robotic hub RoboCity2030. The science and innovation developed during the last 10 years by our Madrid hub were always oriented to joint regional efforts with an European dimension. This why, this year conference is Open and includes also the contributions of our collaborators and colleagues from other Spanish regions and European countries. We are welcoming them and hope to continue our fruitful collaboration.

This year conference has three main pillars: 1) *science in robotics*, where 42 contributions in nine Technical sessions and two Plenary speakers (from Space and Brain robotics fields) will be presented; 2) *entrepreneurship in robotics*, with two outstanding new activities such as "RobotizeYourIdea" competitions, for disruptive approaches, and a Brokerage Event oriented to support robotics spin-offs and start-ups; and 3) *societal & governmental issues of robotics*, with several workshops focused in different aspects as voice of end-users, new robotic society in a wide range of aspects such as education, culture, economy, sociology and law.

The implications of robotics in the new technological society will be very important for RoboCity2030, one of the biggest regional robotic long term hub in Europe (since 2006). It is formed by the six leading R&D robotics centers in Madrid with more than 100 researchers in the field, half of them PhDs. The main objective of the hub is the development of robotic projects and related technologies in order to increase the quality of life of citizens living in metropolitan areas.

The hub also includes more than 30 companies, some of them SMEs, from different sectors interested in testing robotic technologies and their applications. Another important aspect is a business incubator with about 10 robotic established spin-offs/star-ups and regular workshops with hundreds of students discussing and learning about future robotics applications. The network of Madrid´s regional and municipalities authorities is also involved in our activities and helps us to establish realistic targets to solve societal problems.

RoboCity16 Conference will be an excellent forum for exchange of knowledge and experiences among researchers, industry, end-users, administrations and society. The conference will pay special attention to recent advances in robotics and includes contributions presenting not only concepts and methodologies but also their practical validation and experimental testing in the lab and/or in the field. We hope that this two day conference will contribute to the future trends in robotic research and their applications.

Carlos Balaguer
RoboCity2030-CM Coordinator

INTRODUCTION

Despite the great progress made, the potential of Robotics is still far from achieving its maximum dimensions. It is expected that in the near future, innovative robotic systems will be able to confront the most challenging fields of application, providing solutions that contribute to improve the quality of life of the human beings. However, a great research effort is still required not only to develop faster, more intelligent, and more autonomous robots, but also to endow these systems with new cognitive skills, and with ability to learn and adapt to complex and changing environments.

The book consists of 45 chapters that collect widespread experimental and theoretical results on Assistive and Rehabilitation Robotics, Telerobotics and Remote Handling, Computer Vision and Image Processing, Humanoid Robotics, Human Robot Interaction, Locomotion and Actuation Systems, Localization, Mapping and Navigation, Multirobot Systems, Swarm Robotics, Tactile and Haptic Devices and New Mechatronics Designs. Most of these research works have been carried out by the different research groups from *Universidad Carlos III de Madrid*, *Universidad Politécnica de Madrid*, *Universidad de Alcalá de Henares*, *Universidad Rey Juan Carlos*, *Universidad Nacional de Educación a Distancia* and *Consejo Superior de Investigaciones Científicas*, within the framework of the ROBOCITY2030-III-CM project, funded by *Programas de Actividades* I+D from the Regional Government of Madrid and cofounded by Structural Funds of the EU.

The book is intended to be a valuable source of references for the robotics community. The scientific quality of the publication is supported by the innovative character of the works presented and the vast experience of the researchers who have authored them.

Finally, Editors would like to thank the great effort carried out by more than 110 researchers, authors of the different chapters, for conducting the difficult task of translating into a few sheets, the excellent results of their research activities.

Roemi E. Fernández Saavedra
Héctor Montes Franceschi

INDEX

The research leading to these results has received funding from the RoboCity2030-III-CM project (*Robótica aplicada a la mejora de la calidad de vida de los ciudadanos. fase III*; S2013/MIT-2748), funded by *Programas de Actividades I+D en la Comunidad de Madrid* and cofunded by Structural Funds of the EU.

CHAPTER 1

DEVELOPMENT OF A BRAIN-COMPUTER INTERFACE, BASED ON EMOTIONS FOR THE CONTROL OF ROBOTICS APPLICATIONS

D. PEÑA, A. VERONESI, G. LIBERT, R. SALTAREN, R. ARACIL and A. RODRÍGUEZ

Universidad Politécnica de Madrid, Centro de Automática y Robótica (CAR) CSIC-UPM, babeth69@gmail.com; veronesi-arthur@hotmail.com; grego525@hotmail.com; rsaltaren@etsii.upm.es; rafael.aracil@upm.es; alejandro.rbarroso@upm.es

This work refers to the development of a brain computer interface, based on electroencephalographic signals obtained through technologies such as Emotiv EPOC, responsible for measuring bioelectric potentials through electrodes placed on the scalp, thus, allowing it to be used to generate output signals, the use of which may allow movement or task execution based on the user's intentions, without the need to generate a direct physical action. This is possible with the use of tools such as Matlab, OpenViBE, Testbench, they have allowed the processing, noise reduction, feature extraction and classification of signals generated by the visual and auditory stimulation of a platform based on a game virtual reality (VR).

Keywords: Brain-Computer Interfaces (BCI), electroencephalogram (EEG), features extraction and classification, sensorimotor rhythms.

1 Introduction

Human computer interaction has been a topical research since the birth of the computer. Over the years, methods of computer interaction have progressed rapidly. At the beginning, the mouse and the keyboard were created, and now there exist a multitude of innovative technologies to allow human to interface with a computer for the purpose of data entry, control or communication. Most of the efforts over the years have been dedicated

to the design of user friendly and ergonomic systems to produce a more efficient and comfortable means of communication. Interfaces such as voice recognition, gesture recognition and other technologies based on physical movement have received enormous research attention over the years and successful examples of these technologies are being rolled out commercially as a consequence. The past two decades have seen an explosion of scientist research in a completely and novel approach of interacting with a computer (Wolpaw, 2010). Inspired by social recognition of people who suffer from severe neuromuscular disabilities or paralyzed, an interdisciplinary field of research has been created to offer direct human computer interaction via signals generated by the brain itself: Brain Computer Interface, and thus improve the quality of life of people.

The BCI systems are very varied, from how brain activity is recorded, and methodology for general potentials or stimuli based on the requirements and needs of the user, classified as follows: **1.** *Invasive techniques*, which require surgery to incorporate receivers or transmitters near or adjacent to areas to be analyzed. **2.** *Non-invasive techniques,* that do not require surgery, eliminating the disadvantages resulting from surgery, so its use is simpler and has good precision. **3.** *Exogenous Systems,* depend on the electrophysiological activity evoked by external stimuli to produce a series of physiological responses that will be modulated voluntarily by the subject by cognitive tasks. Voluntary modulation of these physiological responses cause different patterns of brain activity to be used in BCI systems **4.** *Endogenous Systems,* do not require any external stimulation to generate brain activity needed for operation and rely on the ability of user to control certain characteristics of their electrophysiological activity, and amplitude in a frequency band specific electroencephalographic signal recorded on a particular area of the cerebral cortex. Such systems are especially useful for users with ALS advanced stages or whose sensory organs have been affected cerebral.

One of the most used configurations for the implementation of a BCI system is the following (Wolpaw, 2010): **1. Subject:** Person who controls the device in the BCI system, for it intentionally modifying their brain activity in order to generate control signals, acting on the device. **2. Electrodes:** convert that brain activity into electrical signals. **3. Amplifier:** amplifies electrical signals. **4. Digitization:** Conversion of the analog-digital, necessary for the post processed signal. **5. Feature extraction:** the amplified electrical signals and parameters characterizing brain activity modified by the subject are transformed. **6. Classification:** are assigned to the parameters that characterize the electrical signals, a control logic signals. Ultimately it comes to classifying the different input parameters among a number of possible states. **7. Control Interface:** translates logic

control signals into an appropriate control signals for a given device**. 8. Device Driver**: Transforms the control signals from the control interface necessary to act on the physical device signals. **9. Device:** As in any control system, the number of devices on which a BCI system can act, can be unlimited. **10. Environment action:** Refers to the physical conditions of the environment on which you are using the BCI system, as well as objects and people present in that environment. These factors usually can be controlled in the laboratory.

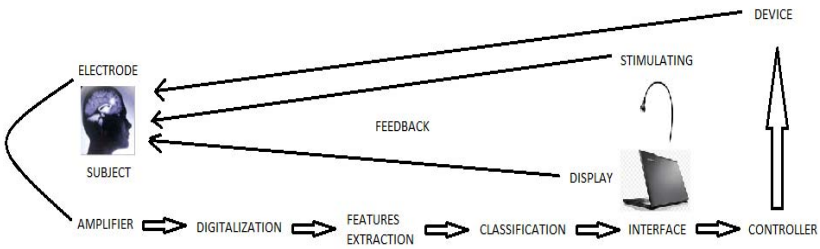

Fig. 1. General structure of a BCI system.

Among the techniques used by BCI systems, we have electroencephalography (EEG) is a non-invasive system, which measure the electrical activity of the cerebral cortex or the scalp, through an electrode with a distribution according to the 10/20 (Klem , 1999) rule, see Fig. 2. These signals contain physical, physiological and pathological information, being very important for rehabilitation or assistance applications to people with reduced movility. With This information you can make two types of measures: 1. Continuous Oscillations of potential, which together form what is EEG. These oscillations are known as the rhythms of brain activity or brain rhythms. 2. potential changes are in response to the occurrence of a certain event, which can be internal or external to the subject. These potentials are known as event-related potentials (ERP) and are derived from the EEG itself. These brain rhythms have certain characteristics, such as being in a range of values from 0 to 100 microvolts at frequencies of 0-40 Hz [1]; These frequencies are classified: as follows: (. 12 to 30 Hz, dominant in waking state and during the performance of any mental activity) Beta, Alpha (8 to 12 Hz, dominant in a state of relaxation.), Theta (4 to 8 Hz, occur before sleep), Delta (0.5 to 4 Hz, dominant during deep sleep) and Gamma (from 30 Hz, and are dominant in states of stress and anxiety). Another type of EEG signals are the Mu waves (8 to 12Hz, occur specifically in the area of the motor cortex and are related to the movement of upper and lower extremities), see Fig. 3.

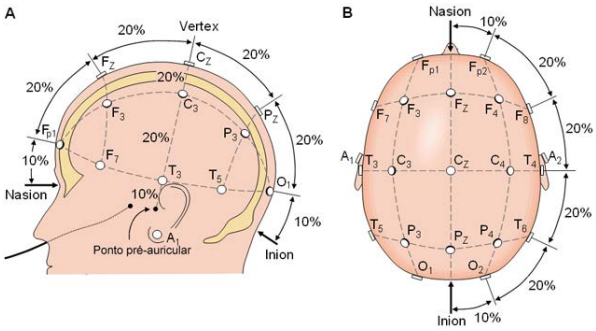

Fig. 2. System 10/20.

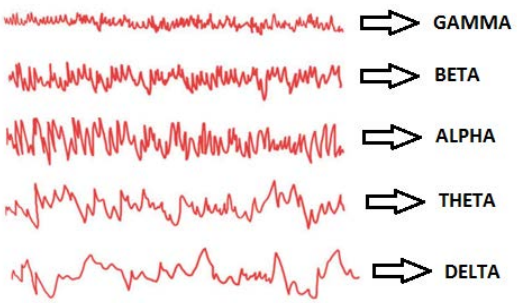

Fig. 3. Brain Wave Patterns.

The purpose of this article is to develop a non-invasive BCI system, based on encephalographic signals, able to recognize the brain activity of users through stimulations performed by video games of virtual reality, whose purpose is to achieve the movement of robotic applications. To make this possible, a mathematical algorithm and an interface for processing the EEG signals, based on the tools of Matlab, where a program that is responsible for removing noise, performing feature extraction and classification signals. In addition, other programs such as Testbench and OpenViBE as a graphical tool for analyzing the behavior of brain activity were used in the dimension of time and frequency. Then it will be emphasized in the description of the BCI system developed, followed by a section concerning the analysis and conclusions reached, obtained so far, since the system is still in development.

2 BCI description system

The implemented BCI system is detailed below, see Fig. 4:

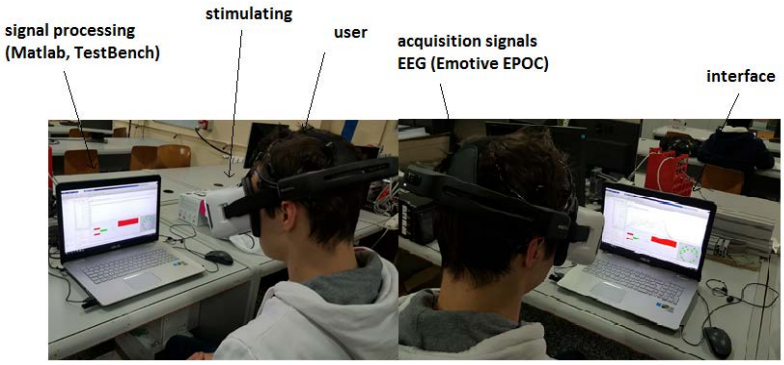

Fig. 4. Configuration of the BCI system.

2.1 Acquisition of EEG signals

EPOC® the Emotiv technology for capturing EEG signals was used. These signals are amplified and sent to the computer wirelessly. The sampling time of the system is 128 Hz, also it has 14 channels of reception and its use is simple. This system has a software called TestBench and Control Panel, which check that the connection has been made properly, as well as view, export and store EEG signals acquired in real time during the stage of stimulation, see Fig. 5.

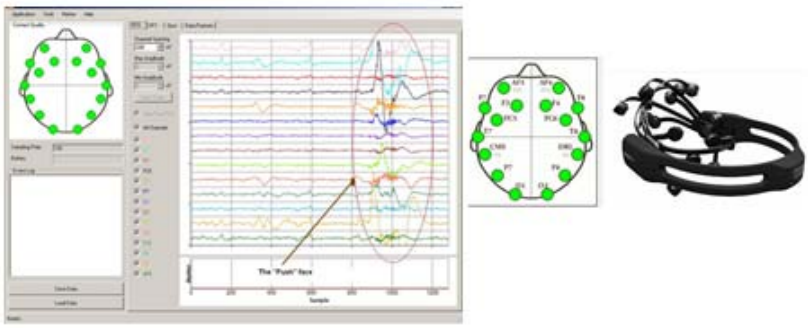

Fig. 5. Emotiv EPOC system.

Additionally, software OpenViBE was used to obtain the graphical representation of the electrical activity, acquired during implementation of BCI system, see Fig. 6.

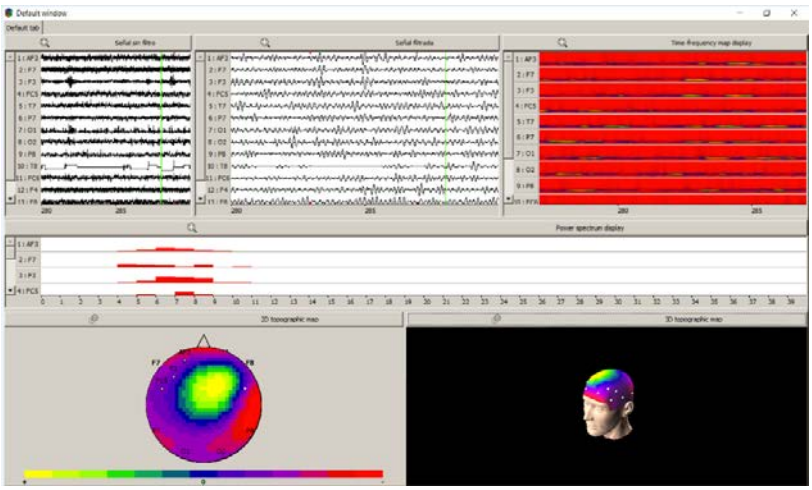

Fig. 6. Stage for the analysis of brain activity of implemented BCI system.

2.2 Remove Noise, Extraction and Classification of Signals EEG.

For the classification, there are two steps needed to obtain good results: The first thing to do is use filters to remove noise and artefact of signals to obtain a better quality of signals.

The second step consist of create a pattern with an algorithm like super vector machine (SVM) to establish a classification. When the classification is done, we can compare the signal in near real time (each second) with the model previously created to see if the signal corresponds to the model. We will record data during some period of time from a lot of different person to have a huge quantity of data. If we have more data, the model will be more precise. With the aim of having more precision, we will establish two models: one will be based on temporal signal; the other will be based on power of each band of frequency signal (alpha, beta, theta, and delta).

The following explain the processing of the EEG signals during the acquisition stage of the BCI system: **1. Record Data:** to record data, we use the tools provide by Emotiv: TestBench, this tool is very complete and allows us to have good data in EDF format with all information needed later. So we take stimuli like video games, sounds, pictures and many others stimuli to simulate emotion like fear, sad or joy. After this step; we have enough data to create our model. **2. Removal artefact:** to remove artifact,

we use a bandpass filter and a zero-phase filter. The low pass is fixed with the value 40 Hz and the high pass has the value 5 Hz. After this, we obtain a signal with less artifact and more clear. The signals obtained are normalized, using the statistical method of standard deviation, to identify mental states obtained during the stimulation phase; it allows us to remove some difference between each subject. In fact, each signal from the brain can be different depending on person. In this case, the normalization allows us to remove some of these differences. **3. Creation of Models: -** *frequency model,* to establish this model, we use a power spectral density to obtain the magnitude of the signal for each part of signal each second. After this, we use the result to establish a support vector machine models. - *band model*, like the precious model, we calculated the power spectral density estimate of the signal but this time, we use overlap to create more precision. After that, we use a power band extraction to obtain the average value of the power of a frequency band. Both model use fast Fourier transform to convert the temporal signal into a frequencies signals. **4. Super Vector Machine (SVM): t**he super vector machine is an algorithm which allows us to make a classification of data. Super Vector Machine can classify two tasks by two tasks. In our case, we need to classify more than two tasks; we have created a loop of classification which created some model depending on the task two by two. We use a 4-order polynomial function to create classification. So, to create model, we use the tools of matlab. **5. Comparison in Real Time:** When model are establish, we need to use our Emotiv EPOC in real time to compare data each second to our both model. Before the comparison, we will make a filter on the signal. After that, we use next lines of code to determine which task can be associated with the segment of data. We made it for both model and we compared the score. If the score are the same, we can conclude than the segment of data correspond to the task and so we can send the corresponding command, see Fig. 7.

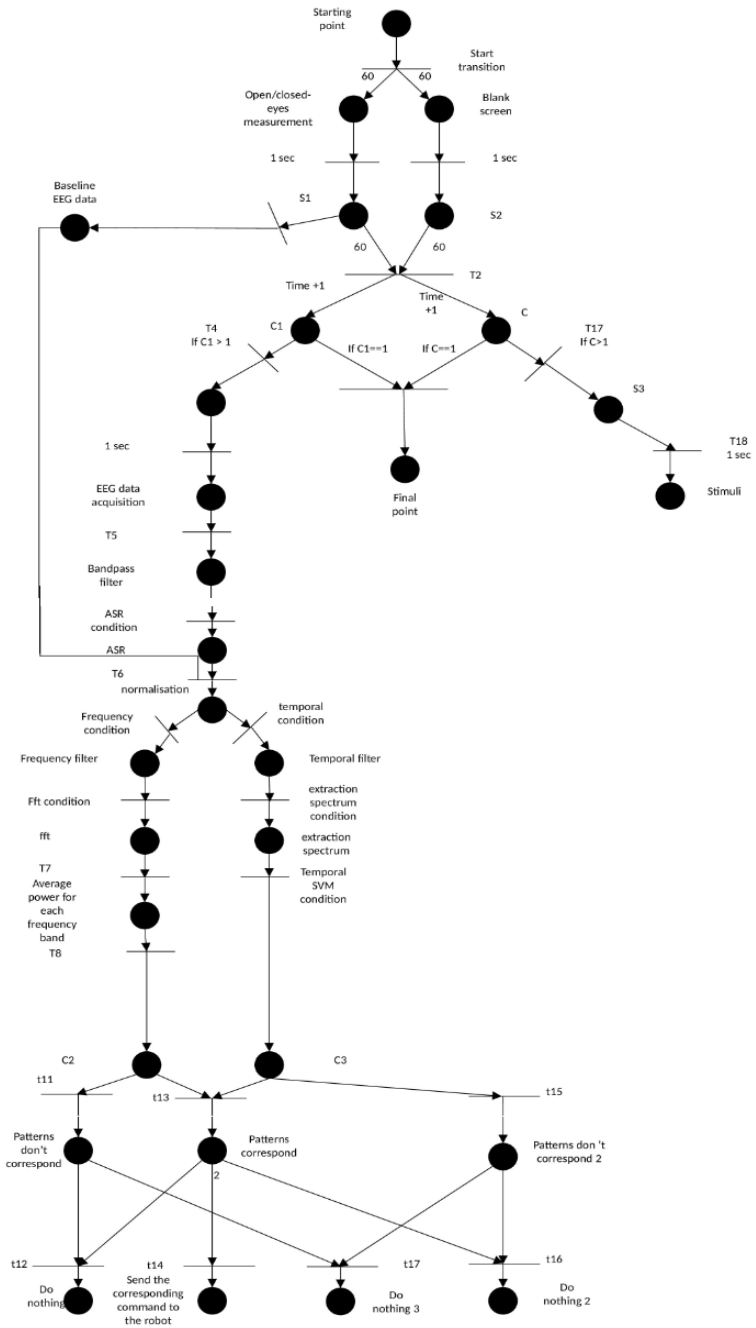

Fig. 7. BCI configuration system of Preti networks.

3 Conclusion and future research

The BCI system developed so far shows good behavior, regarding the acquisition of EEG signals of the brain activity of the user, based on brain rhythms stimulation, allowing its extraction and classification, for both, space time and frequency, making it a future alternative, such as controlling robotic systems or as an alternative rehabilitation.

Implementing other methods for the reduction of artifacts like the wavelet transform, besides hybrids, use mathematical algorithms to improve the feature extraction and classification of EEG signals obtained during the training phase and the online status of the BCI system, based on emotions, making this more natural for the user system.

Acknowledgements

Universidad Politécnica de Madrid project Ref. AL14-PID-15, and the RoboCity2030-III-CM Project (Robótica aplicada a la mejora de la calidad de vida de los ciudadanos. Fase III; S2013/MIT-2748), founded by "Programas de Actividades I+D en la Comunidad de Madrid", and cofounded by Structural Funds of the EU.

References

Alwasiti, H. H., Aris, I., and Jantan, A. Brain computer interface design and applications: Challenges and future. World Applied Sciences Journal 11, 7 (2010), 819–825.

Bayliss, J. D. A flexible brain-computer interface. PhD thesis, University of Rochester, 2001.

Cheng, M., Gao, X., Gao, S., and Xu, D. Design and implementation of a brain-computer interface with high transfer rates. Biomedical Engineering, IEEE Transactions on 49, 10 (2002), 1181–1186.

Cossio, E. G., and Gentiletti, G. G. Brain computer interface (icc) based on event-related potential p300: analysis of the effect of the dimension of the matrix stimulation on performance. Biomedical Engineering Magazine 2, 4 (2008), 26–33.

Devore, J. Probability And Statistics For Engineering And Sciences. Cengage Learning Editores, 2008.

Ding, M., Bressler, S. L., Yang, W., and Liang, H. Shortwindow spectral analysis of cortical event-related potentials by adaptive multivariate autoregressive modeling: data preprocessing, model validation, and variability assessment. Biological cybernetics 83, 1 (2000), 35–45.

Hornero, R., Corralejo, R., Alvarez, D., and Martín, L. Diseño, desarrollo y evaluación de un sistema brain computer interface (bci) aplicado al control de dispositivos domóticos para mejorar la calidad de vida de las personas con grave discapacidad. Trauma 24, 2 (2013), 117–125.

J. J. Vidal, "Real-time detection of brain events in EEG," Proc. IEEE, vol. 65, pp. 633–664, Mayo 1977.

Klem, G. H., Luders, H., Jasper, H., and Elger, C. "The tentwenty electrode system of the international federation". the international federation of clinical neurophysiology. Electroencephalography and clinical neurophysiology. Supplement 52 (1999), 3.

Schalk, G., and Mellinger, J. A Practical Guide to Brain Computer Interfacing with BCI2000: General-Purpose Software for BrainComputer Interface Research, Data Acquisition, Stimulus Presentation, and Brain Monitoring. Springer, 2010.

Smith, R. C. (2004). *Electroencephalograph based Brain.* Dublin, Ireland.

Wolpaw, J. R., Birbaumer, N., McFarland, D. J., Pfurtscheller, G., and

Vaughan, T. M. Brain–computer interfaces for communication and control. Clinical neurophysiology 113, 6 (2002), 767–791.

CHAPTER 2

KINEMATIC AND KINETIC SIMULATION OF UPPER BRACHIAL PLEXUS INJURY IN THE ARM ROTATION

M. A. DESTARAC, C. E. GARCÍA CENA, R. SALTARÉN PAZMIÑO and R. ARACIL SANTONJA

Centro de Automática y Robótica-CSIC-UPM, C/José Gutiérrez Abascal 2, 28006, Madrid, Spain, ma.destarac@alumnos.upm.es

This work presents a 3D upper limb musculoskeletal model and the simulation of arm rotation for the case of a healthy human subject and one with upper brachial plexus injury (UBPI). Then, the length change in muscles, range of movement and muscle force was obtained and compare for both cases. The results show a notable difference between the two cases and can be used to define an effective rehabilitation therapies for this injury and to develop a rehabilitation exoskeleton.

1 Introduction

People with movement disabilities, such as UBPI, require assistive technology to feed themselves and perform other daily activities. In recent years, several examples of the use of robotic exoskeleton can be found in the rehabilitation of upper limb injuries (Colombo, 2005; Loureiro, 2011; Perry, 2007). The advantage offered by these systems is the capacity to replicate with a patient the movements performed by a therapist during the treatment and to provide accurate data to monitor the recovery of the patient (Ruiz, 2006).

For clinical applications, as diagnoses or study of a particular shoulder injury, a musculoskeletal model is needed. The software that currently exists for musculoskeletal modeling is varied and most of them have advanced features for proper analysis and study of motion simulations (Damsgaard, 2006; Delp, 1995).

The aim of this work was the development of a 3D musculoskeletal model of the human upper limb to simulate and analyze the length change in muscles and force generation for the arm rotation of the case of a patient with UBPI in comparison with a healthy subject. The musculoskeletal model provides critical information that will be used for the design of an upper limb rehabilitation exoskeleton.

2 Material and methods

The model of the upper limb was developed using the 2.2 version of *MusculoSkeletal Modeling Software* (MSMS), a free software created by the University of Southern California (Davoodi 2003; Davoodi 2004). This software can automatically create a simulation model that can be executed in Simulink®.

2.1 Musculoskeletal model

The model kinematic was described in a previous works (Destarac, 2015; García, 2013). Muscles shown in Table I were added to the model presented in (Destarac, 2015) as line-segment and the muscle architecture parameters for an adult male are taken from (Garner, 2001; Holzbaur, 2005; Doyle, 2003). Fig. 1 shows the model created which have 15 muscles represented by 24 segments.

Table 1. Muscle architecture.

Muscle	Mass (g)	Optimal fascicle length (cm)	Optimal tendon length (cm)	Maximal muscle-tendon length (cm)
Latissimus dorsi thoracic	183,2	25,4	12	42,1
Latissimus dorsi lumbar	183,2	34,8	19,9	56
Latissimus dorsi illiac	183,2	27,9	14	57,2
Pectoralis major clav	235	22,6	2,9	28,9
Pectoralis major stern	243,3	16,6	9	32,2
Pectoralis major ribs	198	17,8	9,6	34,3
Subscapularis	318,5	8,7	3,3	13,1

2.2 Simulations

After convert the musculoskeletal model to a Simulink® blocks diagram, the simulation of external/internal arm rotation was done for the range of

motion provided by (Kapandji, 2007), as can be seen in Fig.1. Simulations are made for the case of a healthy subject and for a patient with UBPI.

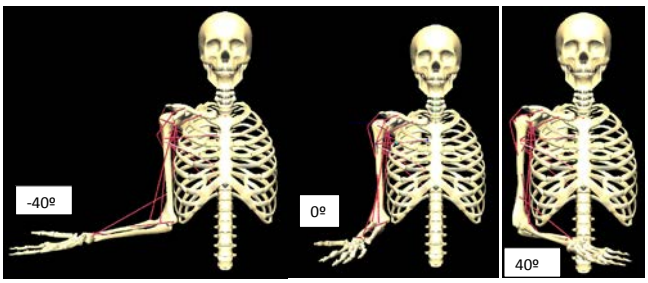

Fig. 1. Range of motion of the arm rotation. (Right) Maximum internal rotation. (Center) Anatomic position for arm rotation. (Left) Maximum external rotation.

MSMS has a simulation tool to convert the musculoskeletal model in a Simulink® blocks diagram. One of the blocks has as input parameters the activation signals of each muscle of the model and will generate (as output) a determined force to move the segment to which they are attached and a length change signal. Both programs are able to communicate with each other and the kinematic behavior that is obtained with the activation signals can be seen directly on the model.

The muscles that are activated for external rotation are the deltoid (scapular section), infraspinatus, and teres minor. For the internal rotation were activated the deltoid (clavicular section), the pectoralis major (clavicular and sternal sections) and subscapularis. The other muscles provide stability to the model and not were activated to simulate this movement.

A pulse train was used to activate them, simulating the Functional Electrical Stimulation (FES) as is indicated in (Davoodi, 2003). For all the muscles a pulse train with amplitude of 1 and a period of 2 seconds and pulse width of 50%. An active delay of 1 second was selected for antagonist muscles, while agonist have no delay. MSMS restricts the range of the excitation signal from 0 to 1, and this range represents the percentage of muscle activation. For the case of a healthy subject the muscles are active at 100% and to simulate the UBPI they were active at 20% (Midha, 2004).

3 Results

In Fig.2 are shown the graphs of the length change in the muscles for the case of a healthy subject. Starting in the limit of external rotation (-40º), the muscles responsible of the internal rotation decreases the length until the arm is in front of the thorax (internal rotation). When the arm reaches the limit internal rotation (40º), the length of this muscle group increases. The opposite results was obtain for the muscles responsible of external rotation.

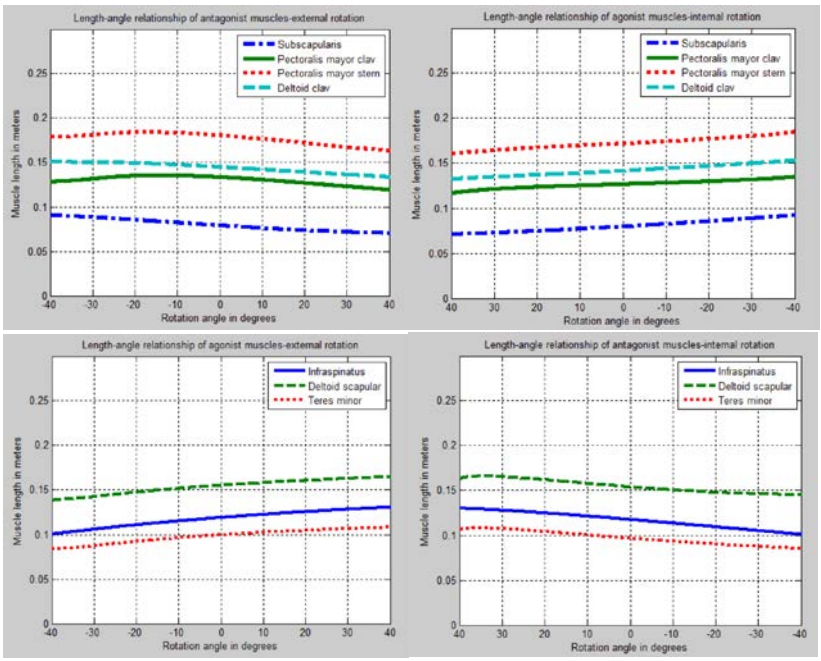

Fig. 2. Length change (in meters) in muscles that perform internal / external rotation of the arm of a healthy subject. (Above) Length change in muscles that perform internal rotation. (Bottom) Length change in muscle group responsible for external rotation.

The graphs of the force response along the movement were also obtained and are shown in Fig.3. It can be seen that the deltoid clavicular and infraspinatus are exerting the greater force.

Simulating the case of a patient with upper brachial plexus injury, the arm remains in internal rotation and moves within the range from 20 to 40°. During external rotation the muscle length remains virtually the same, as is shown in Fig.4, because is not possible to make this movement. For

internal rotation, similar behavior of a healthy subject is observed, although the variation is not linear.

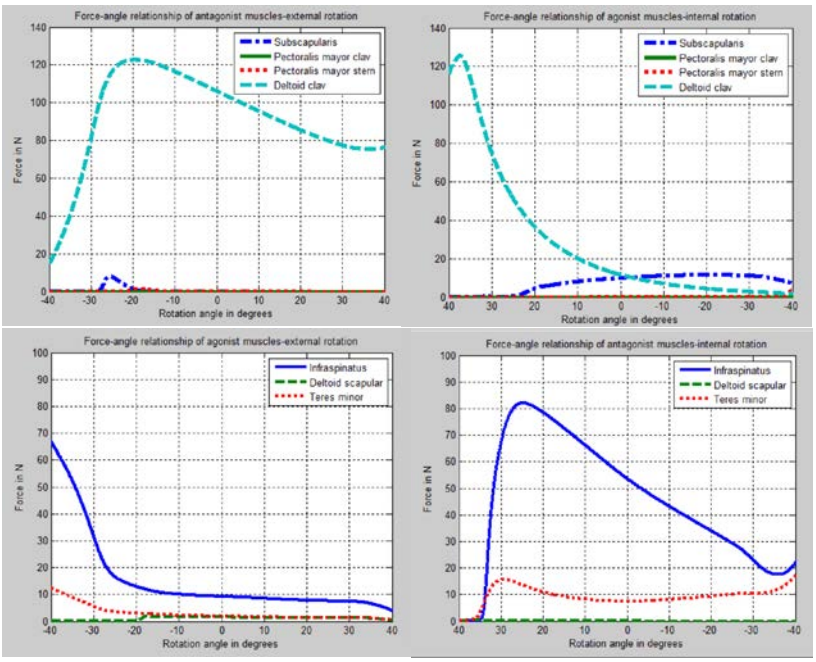

Fig. 3. Force response in muscles that perform internal / external rotation of the arm of a healthy subject. (Above) Muscles that perform internal rotation. (Bottom) Muscle group responsible for external rotation.

The force response for a patient with UBPI is shown in Fig. 5. In this case, the activated muscles generally develop a lower force, except the deltoid clavicular.

4 Discussion

Through simulations it was possible to compare the difference of range of motion and length change in healthy muscle and one affected by the UBPI. Observing Fig. 2 and 4, the length change difference produced in both cases is obvious.

For healthy muscles, the model shows that they can change enough the length to rotate the arm in complete range of motion. In the simulation of the case of a patient with UBPI, the length change is lower and the kinematic and dynamic of the movement is seriously affected.

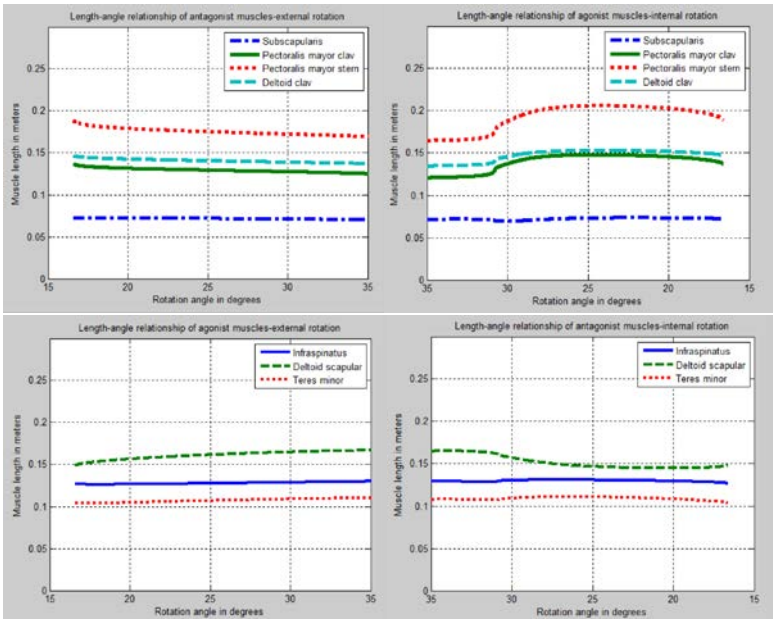

Fig. 4. Length change (in meters) in muscles that perform internal / external rotation of the arm of a patient with UBPI. (Above) Length change in muscles that perform internal rotation. (Bottom) Length change in muscle group responsible for external rotation.

Through simulations, it was possible to compare the difference of force production in healthy muscle in contrast to a patient with UBPI. For healthy muscles, the model shows that they produce enough force to rotate the arm in complete range of motion. The muscles produced the maximum force in the limits of the movement, as can be seen in Fig. 3, because they opposes the movement.

In the simulation of the case of a patient with UBPI, the force produced by the muscles to make the arm rotation is not sufficient, which justifies the use of a rehabilitation device. By observing Fig. 5, a dramatically decrease of the force generated by the muscles, except the deltoid clavicular, can be noted. The decrease in amplitude of the activation signal also reduces the force produced. This affects the response of the deltoid clavicular, which is forced to increase its force due to the dynamic imposed by the model.

5 Conclusions

The study and analysis in this work on aspects related to UBPI and musculoskeletal modeling have been the foundation necessary to develop rehabilitation exoskeletons. In addition, the musculoskeletal model is a useful medical tool for both clinical practice and research.

Future work includes the improvement of the musculoskeletal model, adding the missing muscles related to the movement of the shoulder. Other data can be obtained and study, as the joint moment.

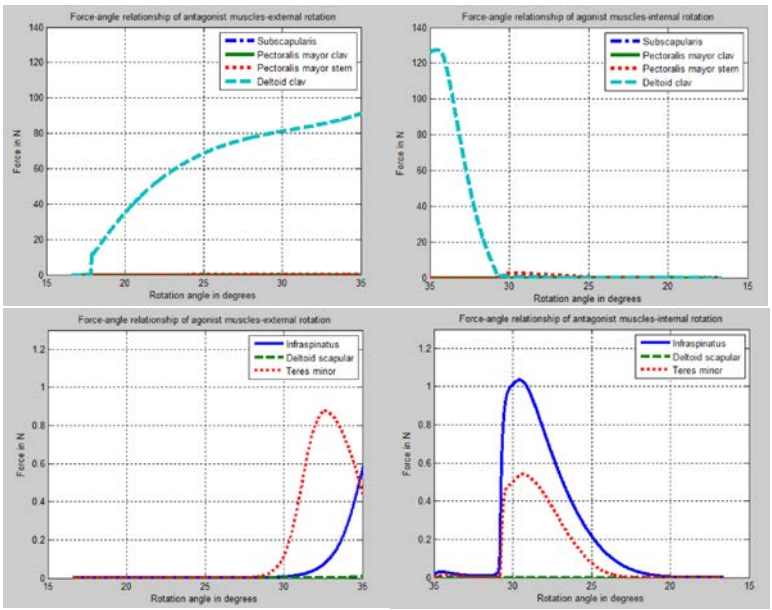

Fig. 5. Force response in muscles that perform internal / external rotation of the arm of a patient with UBPI. (Above) Muscles that perform internal rotation. (Bottom) Muscle group responsible for external rotation.

Acknowledgements

The research leading to these results has received funding from the Spanish Government CICYT Project Ref. DPI2014-57220-C2-1-P, the Spanish Ministry of Economy and Competitiveness Ref. DI-14-06967 and the RoboCity2030-III-CM project (Robótica aplicada a la mejora de la calidad de vida de los ciudadanos. Fase III; S2013/MIT-2748), funded by

Programas de Actividades I+D en la Comunidad de Madrid and cofunded by Structural Funds of the EU.

References

Colombo, R., et al. 2005. Robotic techniques for upper limb evaluation and rehabilitation of stroke patients. IEEE Trans. Neural. Syst. Rehab. Eng., 13(3):311-324.

Davoodi, R. et al. 2003. Advanced modeling environment for developing and testing FES control systems. Med. Eng. Phys., 25(1):3-9.

Davoodi, R., et al. 2004. Development of Clinician-Friendly software for Musculoskeletal Modeling and Control. In IEEE EMBS Proc. 26th Ann. Intern. Conf., San Francisco, California, pp.4622-4625.

Damsgaard, M., et al. 2006. Analysis of musculoskeletal systems in the AnyBody Modeling System. Simul. Model. Pract. Theory, 14(8):1100-1111.

Delp, S.L., et al. 1995. A graphics-based software system to develop and analyze models of musculoskeletal structures, Comput. Biol. Med., 25(1): 21-34.

Destarac, M.A., et al. 2015. Modeling and Simulation of Upper Brachial Plexus Injury. IEEE Syst. J. DOI: 10.1109/JSYST.2014.2387426.

Doyle, J. and Botte, M. 2003. Surgical anatomy of the Hand & Upper Extremity, Philadelphia, PA, USA: Lippincott Williams & Wilkins, pp.98-107

García, C., et al. "Skeletal Modeling, Analysis and Simulation of Upper Limb of Human Shoulder under Brachial Plexus Injury," in Advances in Intelligent Systems and Computing ROBOT 2013 edited by M.A. Armada et al., Ed. New York, NY, USA: Springer-Verlag, pp.195-207, 2013.

Garner, B., et al. 2001. Musculoskeletal Model of the Upper Limb based on the visible human male dataset. Comput. Methods Biomech. Biomed. Engin., 4(2):93-126.

Holzbaur, K., et al. 2005. A model of the upper extremity for simulating musculoskeletal surgery and analyzing neuromuscular control. Ann. Biomed. Eng., 33(6):829-840.

Kapandji, A. I. 2007. Fisiología Articular del miembro superior: Madrid, Spain: Editorial Médica Panamericana, pp.76-102.

Loureiro, R., et al. 2011. Advances in upper limb stroke rehabilitation: a technology push. Med. Bio. Eng. Comput., 49(10):1103-1118.

Midha, R. 2004. Nerve transfers for severe brachial plexus injury: a review. Neurosurg. Focus, 16(5), pp. 1-2.

Perry, J., et al. 2007. Upper-limb powered exoskeleton design. IEEE/ASME Trans. Mechatron., 12(4):805-810.

Ruiz, A., et al. 2006. Exoskeletons for rehabilitation and motor control. In First IEEE/RAS-EMBS Intern. Conf. Biomed. Robot. Biomecha., Pisa, Italy, pp.601-606.

CHAPTER 3

A PILOT STUDY ON THE DESIGN CONSIDERATIONS AND USER IMPRESSIONS OF AN ASSISTIVE AFFORDABLE DEVICE

E. OÑA[1], A. JARDÓN[1], C. BALAGUER[1], A. MARTÍNEZ[2], P. SÁNCHEZ-HERRERA[2], J.C. MIANGOLARRA[2, 3]

[1] Robotics Lab, Universidad Carlos III de Madrid; eona@ing.uc3m.es
[2] LAMBECOM, Universidad Rey Juan Carlos; [3] Servicio de Medicina Física y Rehabilitación, Hospital Universitario Fuenlabrada;

PRESSMATIC is a portable electromechanical device which was designed to assist people whose manual dexterity has been impaired for any reason (ageing, illness, paralysis, etc.). Its goal is restoring the loss of functionality of the thumb and forefinger in certain tasks that require pinching movements (e.g. grabbing scissors, tweezers, etc.). In this paper, a study on design considerations and user experience of PRESSMATIC is presented. For that purpose, pilot trials were conducted at healthcare facilities. Target users evaluated several prototypes of PRESSMATIC and their opinions were registered. Based on this, the original design specifications were reviewed. First, the methodology used in the study is presented. Participants, devices and tasks are described too. Then, trial results are shown and the system requirements will be discussed taking into account user experience. Finally, the study conclusions are shown.

1 Introduction

Currently, in Spain and the rest of the world there are millions of people who have some kind of functional diversity (WHO, 2011). According to their level of mobility many of them are in a situation in which, while retaining much of the functionality of their upper limbs, they have difficulty to perform tasks that require some manual dexterity. Thereby, employing little tools used in daily living activities (DLA) such as scissors, tweezers,

nail clippers, etc. is difficult or even impossible for people with this kind of injury. Among the causes of this situation are spinal cord injuries, osteoarthritis, paralysis by stroke, etc. This population requires help from third parties to perform basic activities of daily living. Therefore, to develop systems to increase their independence is a need.

Related to this, arose the PRESSMATIC assistive device to restore the ability to grip of their users through automatically generate opening and closing movements. It includes several exchangeable tools suitable for activities of daily living.

In this paper, a pilot study focused on reviewing the original design specifications based on user experience is presented. First, the methodology used in the study is explained also describing testers, devices and trials. Then, the test results are shown and the usefulness of the system elements will be discussed considering the user opinions. Finally, the study conclusions are presented.

2 Methodology

The portable assistive device PRESSMATIC has been designed to automatically generate opening and closing movements in their tip. It is aimed to assist people, who lack manual dexterity required for using everyday tools such as scissors, nail clippers or tweezers. Through its technology this device is able to restore the lost ability by the user. From the design and specifications defined in (Barroso, 2012) and (Jardón, 2013), three prototypes with some morphological differences, but keeping the same functionality, were developed.

A pilot study to investigate the impressions of individuals using PRESSMATIC in some common activities is conducted at two healthcare facilities. First trial was conducted at Asociación de Parapléjicos y Personas con Gran Discapacidad Física de la Comunidad de Madrid (ASPAYM-MADRID) where individuals with different levels of spinal cord injury participated. Second trial was conducted at Laboratorio de Análisis del Movimiento, Biomecánica, Ergonomía y Control Motor (LAMBECOM) where other individuals participated, whose physical conditions and the inclusion criteria will be detailed in the next section.

2.1 Participants

A total of twelve individuals participated in this study, of which nine were individuals with both restricted mobility and dexterity manual problems.

The remaining three individuals were medical professionals from the healthcare facilities. Trials were performed in two sessions and two different healthcare centers. The first trial was performed at ASPAYM-MADRID facility, which specializes in the care and support for people with spinal cord injuries. People with this kind of lesion may retain some motor functionality depending on the exact localization of injury at spinal cord. A previous study in (Barroso, 2012) suggests that potential users to employ PRESSMATIC present a level of injury between C5 and C7, including some cases of C4. On this basis, five individuals who have spinal cord injury between level C5 and C6 were selected by medical professionals to compose the Group 1.

However, after completing the test with the first group it was revealed that generally the main requirement for a person to use PRESSMATIC is to be able to hold it and to maintain the same cognitive ability which is necessary to control a smartphone. On this basis, the individuals that were part of Group 2 were selected according to the following inclusion criteria, which Group 1 also satisfies:

a) Affectation of the upper extremity,
b) Gripping ability,
c) Spasticity according Modified Ashworth Scale $\leq$ 2,
d) Ability to understand Mini-mental test instructions $\geq$ 24.

Four individuals participated in the second trial carried out in LAMBECOM. Three of the subjects had hemiparesis, in two cases caused by a hemorrhagic stroke and the other in the aftermath of brain tumor. The fourth subject had akinetic-rigid syndrome caused by neurodegenerative Parkinson's disease. Demographic data and the experience on controlling a smartphone, of the participating groups in the study, are shown in Table 1. Besides, the group of medical professionals, who were present during the performance of the tests, is added.

Table 1. Demographics of the groups which participated in the study.

Group	**Avg. Age (Std. Dev.)**	**Gender**		**Smartphone experience**		
		Female	**Male**	**Beg***	**Inter.***	**Adv.***
Group 1	34 (4.18)	0	5	0	1	4
Group 2	47.5 (16.4)	2	2	0	1	3
Healthcare professionals	34.7 (2.89)	2	1	0	0	3

*Beg – Beginner (call); *Inter – Intermediate (multimedia, use simple apps);
*Adv – Advanced (email, phone settings).

2.2 The portable assistive device PRESSMATIC

The PRESSMATIC original idea, consists of three basic elements: main body, exchangeable tool heads and control interfaces. These elements are described as follows:

i) *Main Body*: is the device itself, it hosts the actuator, transmission, control interface, battery and charger circuits (in the corresponding model). Also, it allows to connect the tool heads by means of special anchor docks and it moves them in linear guide. The external shape of the body was designed also to be ergonomic and functional.

ii) *Exchangeable tool heads:* thanks to diverse attachable tool heads the tip and therefore the functionality of PRESSMATIC changes from scissor tool, to small gripper, to tweezers or to whatever small tool, adapted to be mounted on the device. In this way, the same aid could develop a huge variety of tasks that require fine grasping abilities.

iii) *Control Interface:* PRESSMATIC by default is commanded by an embedded touch panel interface, which presents a menu of choices related with the attached tool head. For example, first the user chooses the type of tool connected depending on the task she/he wants to perform, and then the touch screen presents the right options to perform automatic pre-programmed movements in a suitable way for such tool.

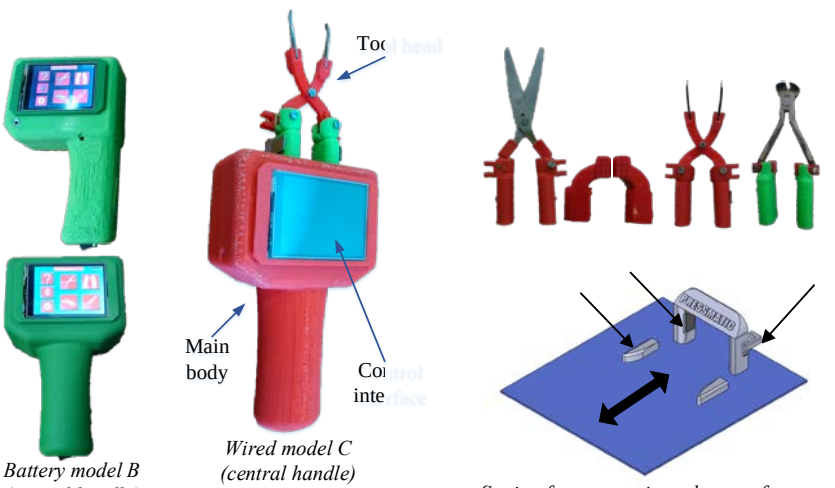

Fig. 1. PRESSMATIC system with complete tool heads set and station for automatic exchange of tool heads.

PRESSMATIC system and all its components is shown in Fig. 1. Currently, there are three prototypes with morphological differences among them while keeping the same functionality (See Fig. 1 left). Models A and B are battery powered and their handle is placed either laterally or in the center, respectively. Model C is mains-powered and it has central handle. Moreover, there are four tool heads as accessories: scissors, nippers, tweezers and nail clippers (See Fig. 1 upper right corner). An automated system for exchanging tools (See Fig, 1 lower right corner) has been implemented to facilitate the use of them.

A tool-oriented functionality has been implemented to control the device (See Fig. 2). That is, the user chooses the type of tool head connected depending on the task she/he wants to perform, and then the device generates automatic pre-programmed movements in a suitable way for such tool head.

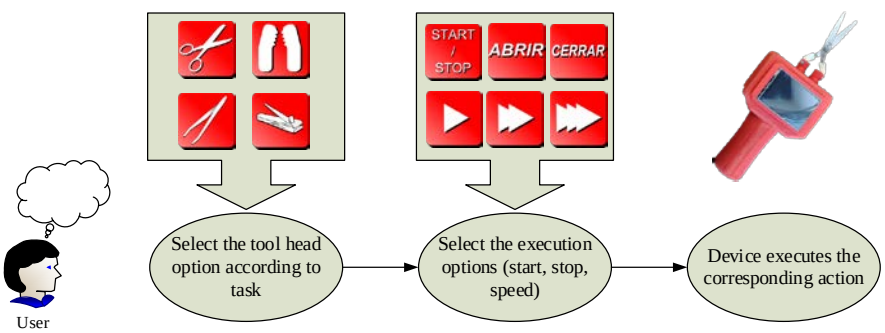

Fig. 2. Description of tool-oriented functionality of PRESSMATIC.

There are two ways to choose the tool heads to operate them: through embedded touch screen or through a app. The previous two options are mutually compatible and its graphical interface was developed under accessibility and usability criteria. The mechanical design, device functionality, the graphical interface and the app are described in detail in (Jardón, 2016).

2.3 Design of the trials

Three tasks were proposed to perform, two of them using two different tool heads, and the last one to evaluate the automated system for exchanging tool heads. The first proposed task was to cut several simple geometric figures printed on a sheet using PRESSMATIC with the scissors tool head.

At first, the individual tries to place the tool head by herself/himself. In case of not being able, an evaluator should place the tool head for her/him.

Related to controlling the device, the individuals could choose between the touch screen or the app. As second task and using either the tweezers or nippers tool heads, it was proposed to pick up a series of small objects placed inside a box, and then put them out. In this way, both the comfort to manipulate PRESSMATIC and if the device eases the tasks performance, were assessed. Finally, the third task consisted of tool heads exchange by using the station for automatic exchange. The functionality of the system was evaluated.

3 Pilot study results

The PRESSMATIC features and its control interfaces were individually evaluated by each user, who expressed their opinions via a range of satisfaction scores, from -2 to +2. Regarding the number of users for a proper usability assessment, (Virzi, 1992) and, more recently (Turner, 2006) have published influential articles on the topic of the sample size in usability testing. According to these authors, five is a proper number for usability testing. Taking into account this criteria, and since one subject was unable to attend the second trial, the results have been processed as an only group. Questions were classified on four categories and the results are summarized in the Fig. 3.

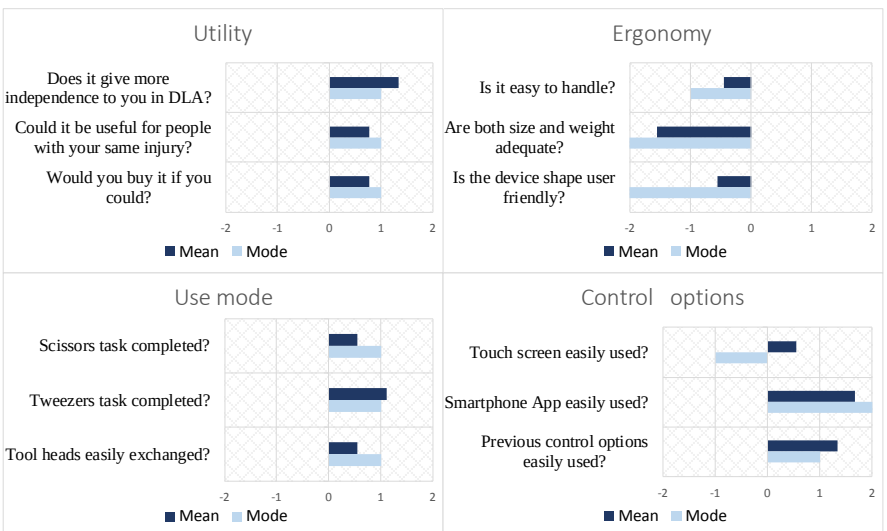

Fig. 3. Results for the usability questionnaires.

On one hand, the best results were obtained in both categories "Utility" and "Control options". Thus, PRESSMATIC was found easy to control by the individuals and that it could be useful in their daily living activities. Also, a favorable result is achieved for the "Use Mode" category, and it has an added value, when the fact that all participants were able to perform the proposed tasks is considered. On the other hand, the "Ergonomy" category has obtained the worst results. All the participants agreed on that current device weight decreases its usability.

a) b) c)

Fig. 4. Participants performing the tasks proposed.

Some pictures of participants performing the tasks proposed in tests are presented in Fig. 4. Some activities such as picking up a small object by controlling PRESSMATIC through a smartphone (See Fig. 4-a), cutting a sheet (See Fig. 4-b) or exchanging a tool heads using the automated station (See Fig. 4-c) are shown.

4 Discussion

The PRESSMATIC approach to improve user independence in their daily living activities was positively accepted. While the tests were performed, the participants raised suggestions and comments, which provided insight into a range of general design opportunities and user-experience requirements of PRESSMATIC.

4.1 Alternative design considerations

One part of the study was focused on gathering the opinion of the participants, that could be included in the next version. A general conclusion was

the integrated touch screen removal, since using the app the control was better. It was suggested, that a handle support such as a strap that wraps around either the hand or forearm could be included. Other suggestion was that PRESSMATIC could be fixed to a desk, allowing the users to free their hands.

4.2 Assessment design specifications

The original system requirements are mentioned as follows: a) Performs automatic grip movements; b) Multi-tool; c) Portable; d) Ergonomic; and e) Lightweight. All prototypes comply the previous items.

These considerations were reviewed through user experience. A system made up of a main body and exchangeable tool heads is strongly accepted and the multi-tool approach is highlighted by participants. The tool head set is positively valued but an extension with more tools is requested. The device portability of both models A and B is well appreciated, but the wired condition of model C does not decrease its usability.

Regarding device weight, all participants ask for its reduction. The current device weight is 630 grams, though not optimal, it allowed manipulate PRESSMATIC properly. For that purpose, to remove the touch screen is a good option. As shown in previous Table 1, all participants had some experience using a smartphone. The idea of controlling PRESSMATIC from their own smartphone was highlighted.

The reformulation of original design requirements based on impressions and user experience are summarized in Table 2. As shown in this table, the device portability and its operating principle do not change regarding to the originals. Also, ergonomy, weight and multi-tool function do not change, but the users marked them as important. Besides, two new specifications were added as result of this study. One of them, is to remove the embedded touch screen in order to control the device only with a smartphone. The other one, is to include the station for automatic tool heads exchange approved by users.

Table 2. New system requirements for design.

Remain	Important	New
a. Performs automatic grip movements	b. Multi-tool	f. Control by smartphone (without touch screen)
c. Portable	d. Ergonomic	g. Station for automatic exchange of tool heads
	e. Lightweight	

5 Conclusions

In this paper, a pilot study on the design considerations and user experience of an assistive device is presented. For that purpose, usability trials were conducted at two different healthcare facilities. A total of nine subjects performed a series of tasks such as picking up small objects, cutting a sheet of paper or exchanging tool heads. All tasks were performed using PRESSMATIC and an appropriated tool head.

From trials, some suggestions to improve the PRESSMATIC functionality were proposed by participants, such as tool head set extension, weight decrease and touch screen removal.

Based on the user experience, the original design specifications were reformulated. Thus, new requirements were obtained. It must be highlighted, participants think that embedded touch screen could be removed, and a better way for controlling the device is through the app. This consideration could reduce size and weight of the device.

A new version of the app is currently under development. This version includes user experience, since controlling PRESSMATIC through a smartphone was positively accepted. Besides, introducing new technology to reduce the device current weight is also considerate.

Acknowledgements

To Fundación Caser by I+D award, to Fundación Universia by funding this project, and to Robotics Lab Team. The research leading to these results has received funding from the RoboCity2030-III-CM project (Robótica aplicada a la mejora de la calidad de vida de los ciudadanos. Fase III; S2013/MIT-2748), funded by Programas de Actividades I+D en la Comunidad de Madrid and cofunded by Structural Funds of the EU.

References

Barroso, G. 2012. Dispositivo automático de apoyo para uso de herramientas requeridas de movimiento manual de pinzado. Master's thesis, Universidad Carlos III de Madrid.

Jardón, A. 2013. Dispositivo automático de apoyo para uso de herramientas requeridas de movimiento manual de pinzado, VII Congreso Iberoamericano de Tecnologías de Apoyo a la Discapacidad (IberDiscap).

Jardón, A. 2016. PRESSMATIC: Dispositivo automático para uso de herramientas que requieren de movimiento manual de pinzado. Descripción del Sistema y evaluación preliminar. Revista Iberoamericana de Automática e Informática Industrial RIAI (Pending publish).

Turner, C. W. 2006. Determining usability test sample size. International Encyclopedia of Ergonomics and Human Factors, 3084-3088.

Virzi, R. 1992. Refining the test phase of usability evaluation: How many subjects is enough? Hum. Factors 34 (4), 457-468.

World Health Organization, 2011. World report on disability.

CHAPTER 4

MODELLING AND SIMULATION OF SERVOMOTORS FOR A REHABILITATION EXOSKELETON

L. J. MONGE[1], M. A. DESTARAC[2], C. E. GARCIA[2] and S. HERNÁNDEZ[1,2]

[1] ETSIDI, Universidad Politécnica de Madrid, luis.mchamorro@alumnos.upm.es; [2] Centro de Automática y Robótica, Universidad Politécnica de Madrid

This work presents the modeling of the MX-64 and RX-64 servomotors from Robotis® and the analysis of their influence in some biomechanical movements for the rehabilitation of the upper brachial plexus injury. The model of each motor was introduced in a musculoskeletal model of the upper limb in order to compare their response and contribution in the movements made by a patient. The results have verified the feasibility of using these servomotors in an exoskeleton for the rehabilitation process of the injury.

1 Introduction

In recent years, several examples of the use of robotic exoskeletons can be found in the rehabilitation of upper limb injuries (Colombo, 2005; Perry, 2007; Loureiro, 2011). Nevertheless, there are only a few examples of them developed specifically for the rehabilitation of patients with brachial plexus injury (UBPI) (Slack, 1992; Rahman, 2004). The lesion may require nerve graft and after surgery, rehabilitation and nerve reeducation therapy would be necessary to improve strength sensitivity and movement of the affected extremity (Sutcliffe, 2007). An exoskeleton can be used after the surgery with the intent to make the rehabilitation process more intense and controlled.

The main contributions of this work are the analysis of the dynamic response of two servomotors and, the study of their influence in the biomechanical movements related with the injury. This study aims to select the optimum servomotor for an exoskeleton taking into account the injury parameters and the musculoskeletal model of the patient.

2 Material and methods

To modeling and simulate the response of the motors chosen for this work, Simulink® software is used. The rehabilitation therapies for upper brachial plexus injury were simulated with a musculoskeletal model that can be executed in Simulink®.

2.1 Servomotors modeling

The servomotors selected for this study are the Dynamixel MX-64 and RX-64 of Robotis®. The MX-64 is a position, speed, acceleration, and torque controllable servomotor, which integrates a gain configurable PID controller as an internal control.

To modeling the physical components of the MX-64, we distinguish DC motor, a gear and a PID controller. The DC motor is modeled following the classic patterns of a permanent magnet motor, due to the transformation of the input voltage in torque, and also is modeling the electromotive force. We use Simulink® to modeling and simulate the response of both motors.

The RX-64 integrates an unknown control method, but the manufacturer gives details about the torque response regarding to the error in angular position (Appendix 1).

The response offered by this servomotor is incompatible with a PID controller, because the torque response does not use the same mathematical function in all the operational phases. Therefore, we can model the dynamic response in Simulink using switches to change the dynamic response of the motor according to the operational phase.

2.2 Musculoskeletal model

Previous work of our research group are based on the development of a musculoskeletal model of the upper limb that allows some movements such as the elbow flexion/extension and shoulder abduction/adduction

(García, 2013; Destarac, 2015), two of the basic movements of arm rehabilitation. In (Destarac, 2015) can be found the results of the simulations of both movements for the case of a healthy subject and one with upper brachial plexus injury.

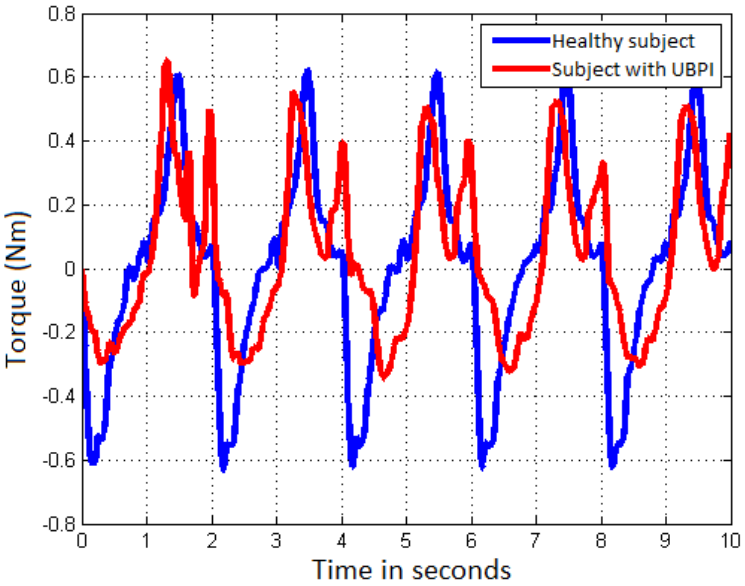

Fig. 1. Comparison of the muscle torque in the elbow joint between healthy subject and an upper brachial plexus injury patient.

The model of the upper limb was developed using the 2.2 version of MusculoSkeletal Modeling Software (MSMS), developed by the University of Southern California (Davoodi, 2004; Khachani, 2007). MSMS is a free software which offer different tools to perform animations and simulations of the biomechanical behavior of musculoskeletal models.

MSMS has a simulation tool to convert the musculoskeletal model in a Simulink® blocks diagram. Using this model, we can incorporate the motor diagram to actuate in some joints of the musculoskeletal model for the case of a patient with upper brachial plexus injury.

Fig. 1 shows the simulation comparison of the muscle torque in the elbow joint between healthy subject and an upper brachial plexus injury patient.

3 Results

We introduced a sinusoidal signal with the objective of observing the influence of their variation. MX-64 has a PID controller, that anticipating the motor action to the position error. For the case of the RX-64, integrate a control with compliance margins.

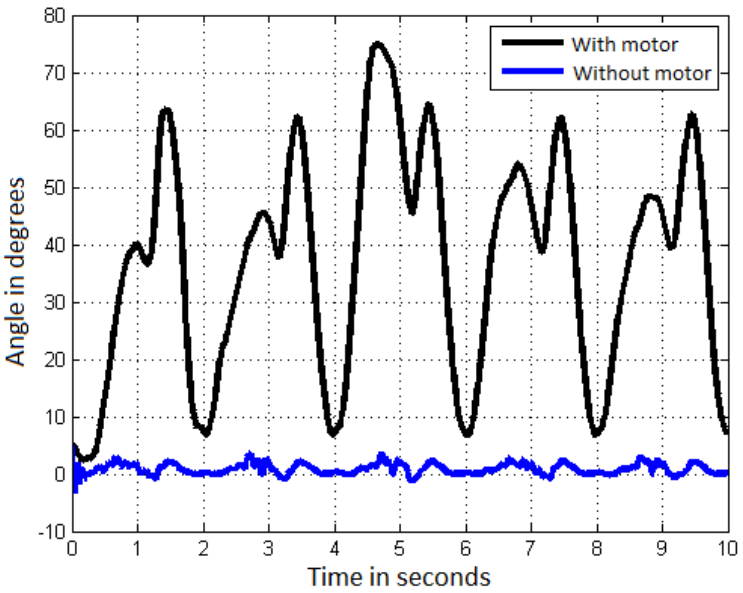

Fig. 2. Comparison of compliance error in an upper brachial plexus injury patient with and without MX-64 motor influence.

To analyzing the influence of the servomotor, we compared the results of their integration into the musculoskeletal model. Fig. 2 shows the compliance error made by the model when is configured as an affected patient with and without the assistance of the MX-64. It can be seen that the position error is practically zero when the motor is present.

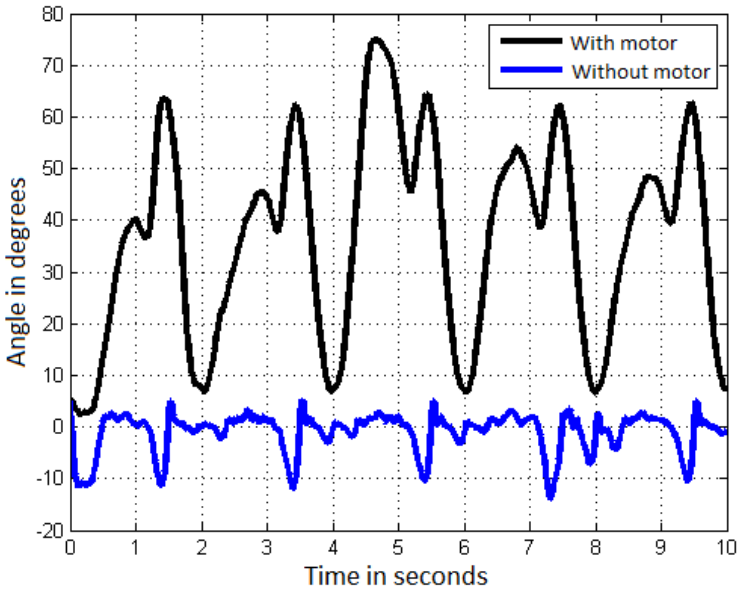

Fig. 3. Comparison of compliance error in an upper brachial plexus injury patient with and without RX-64 motor influence.

Fig. 3 shows the compliance error results for the RX-64. We can observe a less fine adjustment to the movement. This is due to the characteristics of the servomotor, which offer a margin of compliance to the patient before produce torque. Despite these small deviations, the results are acceptable.

4 Discussion

After perform simulations, we can see the differences in the response obtained with each of the servomotors. The MX-64 offers a quick and proactive response and a high value of compliance is achieved. With this motor is possible to obtain a satisfactory reproduction of the desired movement and an effective correction of path deviations.

The RX-64 model, however, provides an error margin to reach the desire trajectory without trying to correct the error. The width of this margin is configurable, as well the slope compliance. This gives to RX-64 characteristics that place it in a position of advantage over the MX- 64 for their implementation in a rehabilitation exoskeleton, because patients not always can accurately perform a movement due of the injury.

5 Conclusions

After the development of a model for MX-64 and RX-64 servomotors and the simulation of their contributions in biomechanical movements, the positive results has verified the feasibility of using the servomotors in an exoskeleton for the rehabilitation process of the upper brachial plexus injury.

The compliance characteristics of the RX-64 motor make it more suitable for a rehabilitation exoskeleton. However, and as future work, is necessary to make some tests with the physical devices to verify this point.

Acknowledgements

This work was supported by grants from Spanish Government CICYT Project Ref. DPI2014-57220-C2-1-P and Comunidad de Madrid who supports the project RoboCity2030-III-CM (Robótica aplicada a la mejora de la calidad de vida de los ciudadanos. Fase III; S2013/MIT-2748), funded by Programas de Actividades I+D en la Comunidad de Madrid and cofunded by Structural Funds of the EU.

References

Colombo, R., et al. 2005. Robotic techniques for upper limb evaluation and rehabilitation of stroke patients. IEEE Trans. Neural. Syst. Rehab. Eng., 13(3):311-324.

Davoodi, R., et al. 2004. Development of Clinician-Friendly software for Musculoskeletal Modeling and Control. In IEEE EMBS Proc. 26th Ann. Intern. Conf., San Francisco, California, pp.4622-4625.

Destarac, M.A., et al. 2015. Modeling and Simulation of Upper Brachial Plexus Injury. IEEE Syst. J. DOI: 10.1109/JSYST.2014.2387426.

García, C., et al. “Skeletal Modeling, Analysis and Simulation of Upper Limb of Human Shoulder under Brachial Plexus Injury,” in Advances in Intelligent Systems and Computing ROBOT 2013 edited by M.A. Armada et al., Ed. New York, NY, USA: Springer-Verlag, pp.195-207, 2013.

Khachani, M., et al. 2007. “Musculo-skeletal modeling software (msms) for biomechanics and virtual rehabilitation,” in: Proc. of American Soc. Biomech. Conf.

Loureiro, R., et al. 2011. Advances in upper limb stroke rehabilitation: a technology push. Med. Bio. Eng. Comput., 49(10):1103-1118.

Perry, J., et al. 2007. Upper-limb powered exoskeleton design. IEEE/ASME Trans. Mechatron.., 12(4):805-810.

Rahman, T., et al. 2004. Design and testing of WREX. Advances in Rehabilitation Robotics, LNCIS 306, pp.243-250. Springer-Verlag Berlin Heidelberg.

Slack, M., and Berbrayer, D. 1992. A Myoelectrically Controlled Wrist-Hand Orthosis for Brachial Plexus Injury: A Case Study. J. Prosth. Orth., 4(3).

Sutcliffe, T. 2007. Brachial plexus injury in the newborn. Neo Reviews: An official Journal of the American Academy of Pediatrics., 8(6):239-246.

Appendix 1

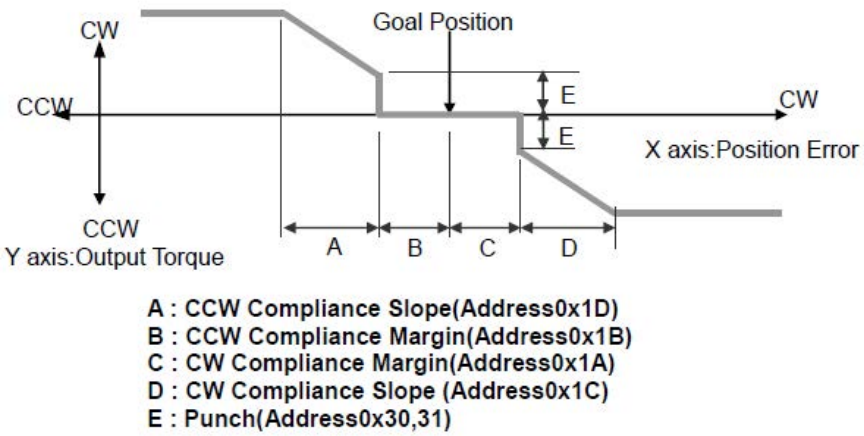

Fig. 4. Compliance diagram of RX-64 servomotor.

The diagram of the Fig. 4 shows the relationship between output torque and position error of the RX-64 servomotor. This diagram has been provided by Robotis®.

CHAPTER 5

SHOULDER EXOSKELETON FOR REHABILITATION ACTUATED WITH SHAPE MEMORY ALLOY

D. COPACI, A. FLORES, D. BLANCO and L. MORENO

RoboticsLab, Universidad Carlos III de Madrid; dcopaci@ing.uc3m.es

This paper presents the preliminary design of a rehabilitation exoskeleton for the shoulder joint with three degrees of freedom (DOF), actuated with Shape Memory Alloy (SMA) based actuators. Due to the actuation system, the proposed exoskeleton presents a light weight, low noise and everything in a simple design structure. The number of actuators and the preliminary designed was calculated after a biomechanical simulation of the human body with a specific category of patients.

1 Introduction

The upper limbs play an important role in daily life but neurological disorder and accidents such as stroke (cerebrovascular accident (CVA)) or spinal cord injury (SCI); significantly affect the normal rhythm of life, letting a partial or total trauma in the motor function with consequent medical and social care consuming a huge amount of healthcare resources. One part of these traumas can be recuperated through traditional rehabilitation therapy performed by therapists (each patient needing one or more therapists, resulting in elevated costs), and in the last decades through the rehabilitation robotic devices. It has been demonstrated that the use of the robot-aide in the rehabilitation therapy has a good result even better than the manual therapy in the patient motor function recuperation. Rehabilitation engineering has carried out a great effort in recent years in order to develop new technologies that should help to recover mobility of upper limbs. The technological advances in this area have been very remarkable. Among the most promising technologies, it is considered that therapies with robotic

exoskeletons are very beneficial for the rehabilitation of patients that require repetitive treatments in order to teach movements that were previously lost (Pons, 2008).

The shoulder joint is the most dynamic and mobile joint in the human body. It consists of the glenohumeral, acromioclavicular, sternoclavicular, and scapulothoracic articulations and the muscular structures that act on them. These articulations give the possibility to a complex range of motion, measured in terms of flexion and extension in the sagital plane, abduction in the coronal plane, and internal-external rotation about the long axes of the humerus. For this reason, very few robotic devices have been designed so far for its rehabilitation. The vast majority of conventional robotic devices for shoulder rehabilitation have been based on rigid, heavy and uncomfortable electromechanical components (Maciejasz et al., 2014) (ORTE, 2016). Among their primary design goals, the new devices should consider patient comfort, low weight and cost reduction to allow a widespread use. It is necessary to investigate compact, lightweight, portable and affordable solutions that allow these tools to be accessible to general public. The mechanical structure of the device must take into account issues such the pain, security, comfort, noise, weight, autonomy and the possibility of portability. These aspects have a strong connection with the system of actuation, forcing to search solution in the no conventional actuators. The aim of the robotic exoskeleton presented in this paper is to provide more efficiently rehabilitation therapies for shoulder joint with a very light and noiseless exoskeleton. Here the focus will be on over-actuated low-cost systems. The main objectives are to build a shoulder exoskeleton fully actuated by SMA wires (Moreno, 2009), demonstrating that this technology is a viable alternative when investigating possible improvements of the existing devices in terms of weight, volume and cost (DeLaurentis, 2002), (Duering, 1999), (Morgan, 2004), (Pittacio, 2012). The mechanical design of the exoskeleton should allow the typical movements of the most common therapies in rehabilitation.

2 Mechanical design

This paper presents a rehabilitation exoskeleton for the shoulder joint with 3DOF, actuated with SMA for the right upper limb where the characteristic of patient are: male with 75Kg of weight and 1.75 m of height.

2.1 Biomechanical simulation

Nowadays, in the development of any robotic device the simulation tools play an important role due to their capacity to analyze the expected performance of the system designed prior to manufacture. To estimate the necessary torques in the articulations for a specific patient, simulation software Biomechanics of Bodies (BoB) was used. The software is capable to simulate the inverse dynamic behavior of the human body, receiving as input: the height, weight and motion of the patient, and giving as output, among other data, the torque of articulations (Wagner et al. 2013). In this case the simulation was configured with the next parameters: weight 75Kg, height 1.75m, a trajectory in the right shoulder joint between -45 and 120 degrees in flexion-extension and 0 and 120 degrees in abduction with a frequency of movement 0.25Hz. As it can results in the simulation, to complete the rehabilitation task in the shoulder articulation successfully it is necessary a torque no more than 12Nm (Fig. 1). This case assumes that the patient has definitively lost the motor function and all the force is made by the exoskeleton.

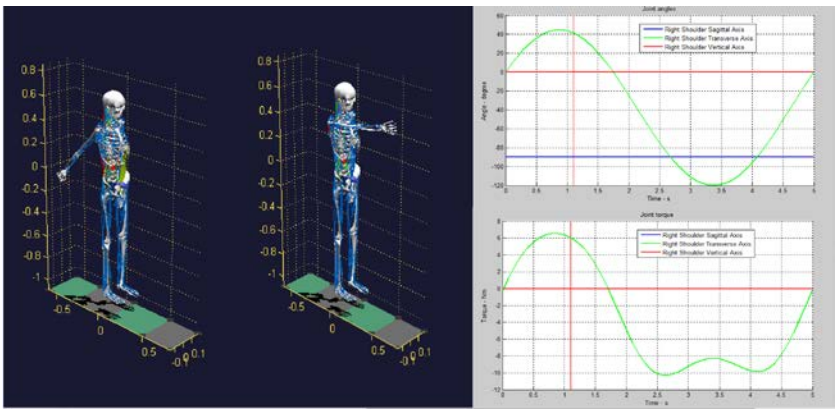

Fig. 1. In the left part the Biomechanics of Bodies simulator configured in the flexion-extension of the shoulder joint. In the right part the input trajectory and the results of simulation, the necessary torque in the shoulder joint.

2.2 SMA based actuators

The first result of the viability of the SMA actuator for soft wearable robots was presented in the past publication (Villoslada et al., 2014). Considering 12Nm the necessary torque in the shoulder exoskeleton joint and ranging the parameters such as: radio of pulley to pas from a translation motion to rotary motion, the diameter of the SMA wire, the SMA composition (NiTi and in composition with other alloys) a simulation program (see Fig. 3) capable to calculate the number of actuators and the length of this was done. In function of these results an optimal configuration for 165 degrees of angular motion (45 degrees in extension and 120 degrees in flexion) was chosen: 8 SMA wires with a length of 2.2 m and a radio of pulley of 30 mm. For the abduction-adduction motion was necessary 145 degrees (120 degrees abduction and 15 degrees adduction) resulting: 8 SMA wires with a length of 2m and a radio of pulley of 20 mm. The better alloy in this case is SmartFlex® with the diameter of 500mm. Moreover, the SMA wires were introduced in the Bowden cable that in addition of the fixed structure (one of the extremity of the SMA is crimp in the extremity of Bowden) have effect of heat dissipation. The election of the number of was done taking into account the additional weight of the exoskeleton and a possible additional weight in the hand, the total torque generated by the exoskeleton surpassing the 12 Nm.

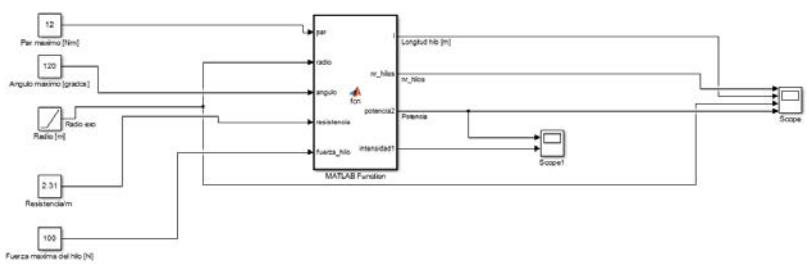

Fig. 2. Matlab/Simulink program for calculate the optimal actuator characteristics in function of the exoskeleton pulley

2.3 Exoskeleton design

In function of the biomechanics analysis and the chosen actuators an exoskeleton designed are proposed (Fig. 3). This is made of simple parts how give the possibility to easy assembly and adjustable them in function of the patient. In addition was designed such a low cost system give the possibility to build them with a 3D printer. The design of the exoskeleton shows

three DOF. The first DOF (2 of Fig. 3) give the possibility to abduction – adduction movement, 4 give the possibility of flexion-extension movement and 7 permit a passive scapulohumeral movement necessary in abduction movement.

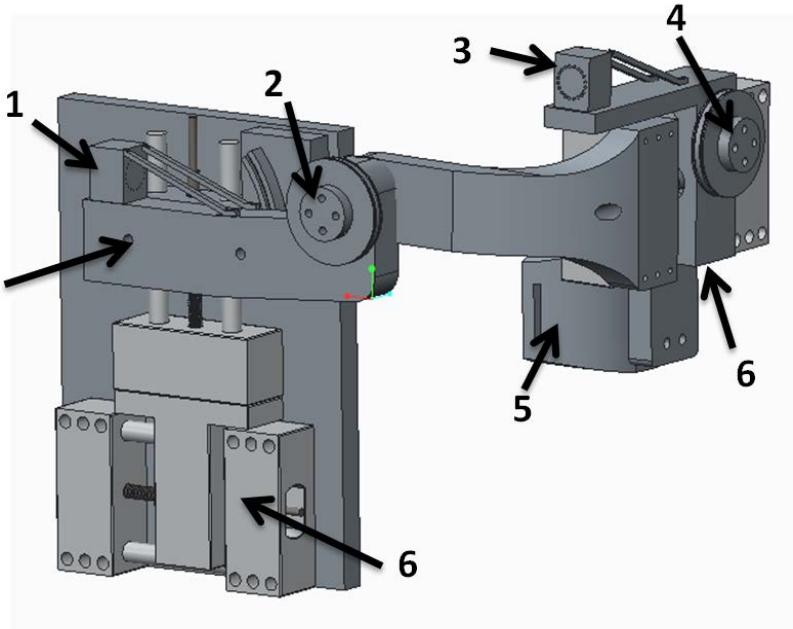

Fig. 3. SMA actuated exoskeleton: 1, 3 – fixed points for Bowden cable termination, 2, 4- pulley to switch from linear movement to rotary motion, 5 – attached point with the arm, 6 – configurable system in function of the patient, 7- passive DOF for scapula movement.

Based in the parameters such as: mobility, comfort, safety and easiness to put it on patient, the proposed design of the exoskeleton compared with the actually solution present a significantly evolution. The main advantages are given by the SMA based actuators that drastically reduce the weight of the structure, less than 2.5Kg, and in the same time with a very low noise - due to the lack of gears and motors in the mechanism. For the comfort all intern part in contact with the patient was covered with a very soft hypoallergenic material.

3 Controls

3.1 Control strategy

The main difficulty when controlling SMA based materials is the hysteresis, which appears in the phase of transition (Martín, 2014). It introduces in the system nonlinear behaviors which make difficult the controls algorithms for this type of actuator. Moreover in this structure the problem become more complicated when controlling for actuators mounted in parallel. In this work a four-term bilinear PID controller was used. The performance of this type of regulator used in control of SMA based single actuators was presented in (Villoslada et al., 2015).

3.2 Control hardware architecture

The control hardware architecture equipment was based IEC 61508, IEC 60601, SIL 4 according to the security criterion of the medical equipment (Fig. 4). This was based in a NRF51822 Bluetooth with a 32-bit ARM® Cortex™ M0 CPU ideally for soft devices (Flores, 2012). With the electronics, the control hardware architecture is capable to manage 8 controllers for 8 distinct actuators. In the case for the shoulder articulation only needing 2 controllers.

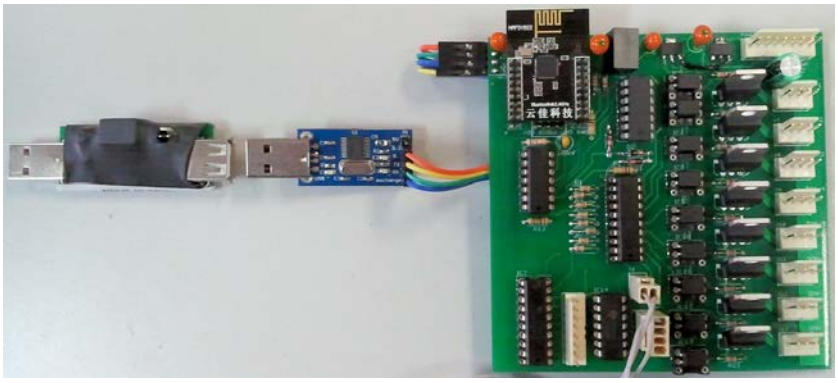

Fig. 4. Control hardware architecture.

4 Conclusions

In this paper it was presented the preliminary design for a wearable shoulder exoskeleton actuated with SMA based actuators (without motors) which permit to reduce drastically the weight of the exoskeleton (less than 2.5kg) and achieve a quiet operation characteristic that increase the comfort of the system.

The preliminary design of exoskeleton was built as a low cost and easy to use rehabilitation device, which can be made with a 3D printer, with a low cost electronics and actuators, which can be adjustable depending on the patients.

Acknowledgements

The research leading to these results has received funding from the RoboHealth (DPI2013-47944-C4-3-R) spanish research project and the from the RoboCity2030-III-CM project (Robótica aplicada a la mejora de la calidad de vida de los ciudadanos. Fase III; S2013/MIT-2748), funded by Programas de Actividades I+D en la Comunidad de Madrid and cofunded by Structural Funds of the EU.

References

DeLaurentis, K. J., C. Mavroidis. 2002. Mechanical design of a shape memory alloy actuated prosthetic hand. Technology and HealthCare, 10(2): 91-106.

Duerig, T.W. A. Pelton, D. Stöckel. 1999. An overview of nitinol medical applications. Materials Science and Engineering: A 273: 149-160.

Flores, A., DS.Copaci, A.Martín, D.Blanco, L.Moreno. 2012. Smooth and Accurate control of multiple Shape Memory Alloys based actuators via low cost embedded hardware. IEEE/RSJ Int. Conf. on Intelligent Robots and Systems. IROS.

Maciejasz, P., J. Eschweiler, K. Gerlach-Hahn, A. Jansen-Troy and S. Leonhardt. 2014. A survey on robotic devices for upper limb rehabilitation Journal of Neuro Engineering and Rehabilitation, 11:3.

Martín Clemente, A. 2014. Modelado y Control de Sistemas No Lineales de tipo SMA. Supervisors: L.Moreno; D.Blanco. Ph.Thesis, Universidad Carlos III de Madrid.

Moreno, L., M.L. Muñoz, S. Garrido, D. Blanco. 2009. Materiales inteligentes: aleaciones con memoria de forma (SMA). Revista de la Real Academia de Ciencias Exactas, Físicas y Naturales.

Morgan, N.B. 2004. Medical shape memory alloy applications—the market and its products. Materials Science and Engineering: A 378.1: 16-23.

ORTE. 2016. Robotics exoskeleton for shoulder rehabilitation. http://www.upm.es

Pittaccio, S., S. Viscuso. 2012. Shape Memory Actuators for Medical Rehabilitation and Neuroscience. INTECH Open Access Publisher.

Pons. J. 2008. Wearable Robots: Biomechatronic Exoskeletons. Wiley Online Library.

Villoslada, A., A. Flores, D. Copaci, D. Blanco, L. Moreno. 2014. High-displacement flexible Shape Memory Alloy actuator for soft wearable robots. Robotics and Autonomous Systems, Special Issue on Wearable Robotics for Motion Assistance and Rehabilitation.

Villoslada, A., N. Escudero, A. Flores, F. Martin, C. Rivera, L. Moreno, M. Collado. 2015. Position control of a shape memory alloy actuator using a four-term bilinear PID controller. Sensors and Actuators A Physical 236.

Wagner, D.W., Stepanyan, V., Shippen, J.M., DeMers, M.S., Gibbons, R.S., Andrews, B.J., Creasey, G.H., and Beaupre, G.S. 2013. Consistency Among Musculoskeletal Models: Caveat Utilitor. Annals of Biomedical Engineering 41 (8), 1787-1799.

CHAPTER 6

VISION DRIVEN CONTROL OF ROBOTS: REVIEW FOR FUTURE APPLICATIONS IN CERN ACCELERATORS HARSH ENVIRONMENTS

M. DI CASTRO[1, 2], M. FERRE[1] and A. MASI[2]

[1] Centre for Automation and Robotics UPM-CSIC, [2] CERN, European Organization for Nuclear Research, Mario.Di.Castro@cern.ch

Nowadays, computer vision has become part of our daily life. Computer vision is used, for example, in the medical field to support medical research by image data, which provides various information such as blood flow, the structure of an organ, or assessing the quality of medical treatments. It is also largely used in industry to support manufacturing processes. Computer vision is also widely used in robotics, where tasks such as measuring the position and orientation of an object to be picked up by a robotic arm and inspecting the final product in order to find defects are all done by computer vision. Vision driven control of multi-axis robotic systems is a fundamental need in telemanipulation tasks committed to unstructured and harsh environments. Several approaches have been exploited in the last decade showing that no single solution could be applied for unstructured and hazardous environment like the ones at CERN. In this article, the state of the art in robotic vision driven control is presented, as well as possible application scenarios in unstructured and hazardous environment where intelligent vision based systems are needed to adapt to unforeseen environmental conditions.

1 Introduction

During recent decades the technological development has made great strides, allowing to get more powerful components improving the quality of products. This has led to the market presence of excellent products for vision, ranging from the simple webcams or cameras with full HD quality,

stereo cameras, to 3D camera ranger where a mono camera is supported with an IR sensor for detecting depth information. Active vision and the next-best-view problem for 3D reconstruction are problems seen in the past in the computer vision and robotics literature (Aloimonos 1988, Bajcsy 1988). The current state of the art in reconstructing spatially bounded objects using active vision, as opposed to exploration, leverages estimation of information gain that could be obtained from candidate views in order to choose where next to observe the object (Vasquez-Gomez 2014, Kriegel 2015). Robot guidance using machine vision techniques in structured and industrial environments is a topic well studied in the last years allowing robots to be the main actors in industrial scenarios (Pérez 2016).

The vision for robotic purpose can be used in different ways, depending on its intended. It could be used to give back images of the environment in which the robot is localized, like for the inspection purpose, helping, at the same time, the remote operator moving inside it. The visual information could be insert within the control loop, generating commands which can drive the manipulator during the execution of its task and there could be the possibility to merge visual information with depth information, obtained using a stereo camera or 3D camera in order to recreate a virtual environment of the real one around the robot.

In order to construct a proper vision based control system, two main aspects have to be taken into account. The first one is the camera system that could be in-built with the end-effector (eye-in-hand configuration), or fixed in the space (eye-to-hand configuration). Different advantages and disadvantages correspond to each configuration. The eye-in-hand configuration allows a higher accuracy, avoiding occlusions problems and a more precise sight of the scene, but we will have a partial view of what happen into the robot's workspace. The eye-to-hand has a global view of the work environment, but could be not maneuverable enough to explore the scene leading a loss in accuracy. The second main aspect that a vision based control has to take into account is the image processing. In this case the vision sensors produce a lot of data and in order to reduce the computational time, specific hardware is require.

The presented work is focused on the aspects explained above and aims to provide a general knowledge on possible uses of vision and kind of controls, which incorporate visual feedback, available up to now in literature. Initially, basic concept about the Visual Servoing (VS) control are considered, and then a number of possible examples will be considered. Finally, some considerations in applying novel computer vision for CERN accelerators hazardous and unstructured environments are presented.

2 Review of visual servo control

In general, before starting to implement a VS control, several things has to be considered:

- Camera location: eye-in-hand or eye-to-hand
- Camera: mono or stereo
- Control: image-based or position-based
- Processing: remote(pc) or local(embedded)

Visual Servo Control means the use of visual data in order to control the movement of a manipulator. As well known in control theory, the control loop sends proper command to the robot in order to minimize as much as possible an error generated respect a reference. Generally, this reference is for a specific pose (Cartesian domain) in the workspace of the manipulator or a particular joint configuration (Joint domain). In VS control, instead, the error, which let the robot move, is defined into the Image domain:

$$e(t) = f(t) - f^* \tag{1}$$

where $f(t)$ is a vector of *n* features extract from the image at the instant *t,* and f^* is the desired value of that features. For the first time, in 1980, Sanderson proposed a classification of VS control in two main architectures:

- Image-Based Visual Servoing (IBVS) Control
- Position-Based Visual Servoing (PBVS) Control

In the IBVS control the error is directly computed on the values of the features extracted on the 2D image plane. The robot should move in order to reduce the error between the current image features and the desired features. As well described by Francois Chaumette (1998), the main issue for this control is the image Jacobian or interaction matrix J_s, defined from:

$$\dot{f} = J_s * \begin{pmatrix} V \\ \Omega \end{pmatrix} \tag{2}$$

In the J_s matrix is used to transform velocities in the features space to in camera velocities (V is the translational component and Ω is the rotational one). The interaction matrix deeply depends by the camera intrinsic parameters and by the Z coordinate of the point relative to the camera frame, which is not always known. For that reason the image Jacobian needs to be approximate or estimate (Hutchinson 1996).

In PBSV control, instead, the information extract from the image are compared with a geometric model of the target, in order to reconstruct the current 3D pose of an object.

Combining this information with the knowledge of a desired 3D pose, a generated Cartesian error drives the robot. This kind of control is very similar to the normal robot control, but it's require a 3D model, heavy processing end is very frail to noise and errors on camera calibration. Different ways to obtain 3D information are listed below:

- Using active ranger sensors (optical or ultrasonic).
- Photogrammetric techniques affected by complex computation and the necessity of a good camera calibration and a model of the target.
- Stereo Vision, being careful to the matching and correspondence problem.
- Depth from motion, with monocular or motion stereo, in which the target in the scene has not to move significantly between the views.

Table 1. Imaged-based vs position-based visual servoing.

	PBVS	IBVS
PROS	Cartesian space motion control similar to normal robot control	Robust to noise and errors 3D model not required
CONS	3D model required heavy processing (image + pose), estimation and camera calibration play a big role	image space motion motion of Cartesian space unknown

A new control approach has been presented in the past (Malis 1999) which can be described as a "halfway" approach between the two explained before, in order to avoid their respective disadvantages. In fact, this control does not need any geometric 3D model of the object and it ensures the convergence of the control law in the whole task space. Shared and traded telerobotic visual control combines the abilities and the experience of a human operator (manual control) with the efficacy of simple autonomous visual tracking and servoing modules (autonomous control). In the shared control mode, the autonomous mode can compensate the low visual reactiveness of the human operator but the human operator and the autonomous modules are not allowed to command the some degree of freedom. In the trade control mode, the problem of the contrast on the degree of freedom is solved.

Haptically Guided Teleoperation for Learning Manipulation Tasks is another well-established technique presenting a methodology that utilizes visual inputs directly in producing force guidance data and creating a potential field that modulates the haptic feedback in order to assertively guide the user toward the target location (Howard 2007).

Haptic Virtual Fixtures for Robot-Assisted Manipulation introduces the concept of haptic virtual fixtures. The haptic virtual fixtures are software-generated force and position signals applied to human operators in order to improve the safety, accuracy, and speed of robot-assisted manipulation tasks (Habboit 2007). Most of the telemanipulation task need the grasping option keeping the tool center point (TCP) and/or features of a target object tracked by the vision system (stereo camera) and the algorithms in the control loop try to bring the TCP to a desired position and orientation (Vahrenkamp 2008, Jiao 2014). Some other work using arm grasping have used Kinect or stereo vision and have obtained RGB frames and depth frames about the desired object also using fuzzy controls (Vasiljevic 2012, Ali 2015). Past work have been focused on Trajectory Generation for Obstacle Avoidance of Uncalibrated Stereo Visual Servoing without 3D Reconstruction (Hosoda 1995, Torres 2015).

Another known type of control of robotic telemanipulators by means of vision information is the uncalibrated stereo visual Servoing for manipulators using virtual impedance control (Cai 2014). This paper presents an implementation of uncalibrated, position-based stereo visual servoing with obstacle avoidance. Another work has been carried on integrating the uncalibrated visual servoing with obstacle avoidance using SQP method (Fu 2009). This method ensures that the robot avoids the obstacle safely and tracks the target as accurately as possible, requiring a priori knowledge of intrinsic and extrinsic parameters for the cameras. It is based on an SQP method which is commonly used in nonlinear constrained optimization and for solving static optimization problems. This method works when the cameras are fixed and the obstacle is static.

With the increasing of controllers and communication speed, real-time vision and super-low-latency based controller systems work have been carried over (Yang 2015, Katsuki 2015). Other works have been done obtaining collision-free visual servoing of an Eye-in-Hand manipulator using constraint-aware planning and control (Cahn 2011). In this case, the control law is designed for a robot manipulator with an uncalibrated camera mounted on its end-effector. The method uses an image-based command to describe the desired end-effector position with respect to an object with an unknown position. The visual servoing control law is implemented via a nonlinear model predictive control framework to generate feasible and realistic robot trajectories that respect the robot's joint and velocity limits. The control law explicitly keeps the target object within the camera's field of view and avoids potential collisions with workspace obstacles. In order to improve operator performance and understanding within remote envi-

ronment, a work has been carried on towards vision-based virtual force guidance for tele-robotic system (Ni 2013).

Mendiburu (2013) proposed system integrates a trajectory planning method into the controller of a five-degree-of-freedom manipulator aiming to simplify object handling and obstacle avoidance. The control scheme is composed by several blocks with a specific function. The vision from the fix camera (Kinect) is used for reconstruct the workspace and recognize the obstacles, instead the hand camera is used for extracting the features and computing the pose estimation. Other works have been done towards telerobotic tracker (Yuan 1990), where the manipulator, equipped with an end-effector-mounted camera, automatically tracks the motion of the target so that, in the absence of any operator command, the camera image of the latter remains stationary.

3 Conclusions and future work for CERN hazardous environment

In this work, a review on the state of the art in vision driven control for robots, which could be useful for harsh environments, has been presented. CERN accelerators hazardous and unstructured environment present several constraints and obstacles and the use of industrial standards telerobotic controls is often not satisfying. Therefore, a novel approach is needed and it could be foreseen in a close future. The fundamental challenges of 3D reconstruction for maintenance in hostile environments include reduced view spaces due to tightly installed equipment and the complexity of the objects needing to be reconstructed. The perception vision based system of a robot could rely on several key innovations in order to navigate through the environment, localize itself with respect to targets, identify and interact with particular equipment components, and make all of the information that it gathers available for the user via interactive visualizations and simulation. Estimating the feasible space of views that the sensor arm can take, based on an evolving map of the obstacles, and could be a key innovation. Additionally, a part-focused reconstruction algorithm that will focus the reconstruction on the components that are critical for the current manipulation task, and less time on the static elements that will not be interacted with could be developed. Future works could integrate the information coming from the vision part directly in the low level robotic control.

References

Ali, M. 2015. Arm grasping for mobile robot transportation using Kinect sensor and kinematic analysis. Instrumentation and Measurement Technology Conference (I2MTC), 2015 IEEE International.

Abbott, JJ. 2007. Haptic virtual fixtures for robot-assisted manipulation. Robotics research. Springer Berlin Heidelberg. 49-64.

Aloimonos, I. 1988. Active vision, Int. Journal of Computer Vision, vol. 1, no. 4, pp. 333-356.

Abbott, JJ. 2007. Haptic virtual fixtures for robot-assisted manipulation. Robotics research. Springer Berlin Heidelberg. 49-64.

Aloimonos, I. 1988. Active vision, Int. Journal of Computer Vision, vol. 1, no. 4, pp. 333-356.

Bajcsy, R. 1988. Active perception. Proceedings of the IEEE 76.8. 966-1005.

Cai, C. 2014. Uncalibrated stereo visual servoing for manipulators using virtual impedance control. Control Automation Robotics & Vision (ICARCV), 13th International Conference on. IEEE.

Chan, A. 2011. Collision-free visual servoing of an eye-in-hand manipulator via constraint-aware planning and control. American Control Conference (ACC), IEEE.

Chaumette, F. 1998. Potential problems of stability and convergence in image-based and position-based visual servoing. The confluence of vision and control. Springer London, 66-78.

Fu, Q. 2009. Uncalibrated visual servoing with obstacle avoidance using SQP method. Mechatronics and Automation. ICMA. International Conference on IEEE.

Hosoda, K. 1995. Trajectory generation for obstacle avoidance of uncalibrated stereo visual servoing without 3d reconstruction. Intelligent Robots and Systems 95. Human Robot Interaction and Cooperative Robots , Proceedings. IEEE/RSJ International Conference. Vol. 1. IEEE.

Howard, AM. 2007. Haptically guided teleoperation for learning manipulation tasks.

Hutchinson, S. 1996. A tutorial on visual servo control. Robotics and Automation, IEEE Transactions on 12.5, 651-670.

Jiao, J. 2014. Autonomous grasp of the embedded mobile manipulator with an eye-in-hand camera. Networking, Sensing and Control (ICNSC), IEEE 11th International Conference on. IEEE.

Katsuki, Y. 20105. Super-Low-Latency Telemanipulation Using High-Speed Vision and High-Speed Multifingered Robot Hand. Proceedings of the Tenth Annual ACM/IEEE International Conference on Human-Robot Interaction Extended Abstracts. ACM.

Kriegel, S. 2015. Efficient next-best-scan planning for autonomous 3D surface reconstruction of unknown objects. Journal of Real-Time Image Processing 10.4: 611-631.

Malis, E. 1999. 2½D visual servoing. Robotics and Automation, IEEE Transactions on 15.2: 238-250.

Mendiburu, F. 2013. Visual feedback trajectory planning for object handling and obstacle avoidance. Industrial Electronics Society, IECON 2013-39th Annual Conference of the IEEE.

Ni, T. 2013. Vision-based virtual force guidance for tele-robotic system. Computers & Electrical Engineering 39.7: 2135-2144.

Pérez, L. 2016. Robot Guidance Using Machine Vision Techniques in Industrial Environments: A Comparative Review. Sensors 16.3: 335.

Sanderson, A. C. 1980. Image-based visual servo control using relational graph error signals. Proc. IEEE 1074.

Torres, L. G., 20105. A motion planning approach to automatic obstacle avoidance during concentric tube robot teleoperation. Robotics and Automation (ICRA), IEEE International Conference.

Vahrenkamp, N. 2008. Visual servoing for humanoid grasping and manipulation tasks. Humanoid Robots. 8th IEEE-RAS International Conference on. IEEE.

Vasiljevic, G. 2012. Kinect-based Robot Teleoperation by Velocities Control in the Joint/Cartesian Frames. Robot Control. Vol. 10. No. 1.

Vasquez-Gomez, J. 2014. Volumetric next-best-view planning for 3d object reconstruction with positioning error. International Journal of Advanced Robotic Systems 11.

Yang, Y. R. 2015. Real-time human-robot interaction in complex environment using kinect v2 image recognition. Cybernetics and Intelligent Systems (CIS) and IEEE Conference on Robotics, Automation and Mechatronics (RAM), IEEE 7th International Conference on. IEEE.

Yuan, J. S. 1990. Telerobotic tracker. U.S. Patent No. 4,942,538. 17 Jul. 1990.

CHAPTER 7

COMPARISON BETWEEN A HYBRID RATE-POSITION CONTROL AND OTHER METHODS IN A LARGE WORKSPACE TELEMANIPULATION TASK

L. E. RUBIO[1], J. M. BREÑOSA[1], F. J. SUAREZ[2], M. FERRE[1] and R. ARACIL[1]

[1]Centre for Automation and Robotics UPM-CSIC, Madrid, [2]School of Mechanical and Aerospace Engineering, NTU, Singapore

This paper exposes the results of an experiment which compare a hybrid rate-position controller with other algorithms, like force-position and indexing position-position, used in remote handling and telemanipulation. Under the assumption that a hybrid controller optimizes the benefits of position and rate controllers for tasks that involve large workspaces with smaller haptic master devices, we propose an experiment which measures the difficulty of telemanipulation with fragile objects in structured environments. This experiment has been realized using a slave robot from Kraft Telerobotics and different haptic devices as a master device. Master devices involved in this paper are: commercial Kraft Telerobotics master and 3 Finger Haptic Device (3F-HD, a haptic device with three force feedback fingers developed by Centre for Automation and Robotics). Results show that a hybrid controller provide higher accuracy than a force-position controller spending a similar amount of time, and reduces considerably the time used in an indexing position-position keeping the accuracy and dexterity needed to perform the task successfully.

1 Introduction

Remote Handling is an important field associated to robotic research when using autonomous tasks is not always possible. Actually, the complexity and dexterity of some tasks need human skills. Artificial intelligence has

been reaching important steps but there is still a long time until humans may delegate all the task control to robots. Mainly, remote handling has been used to improve human capabilities in environments where operator could have some risks or difficulties.

Remote handling is based on bilateral control architecture (fig. 1), which has three different parts: master, slave and communications channel. Bilateral controllers on teleoperation are designed to provide stability and transparency to the system (Lawrence, 1992)

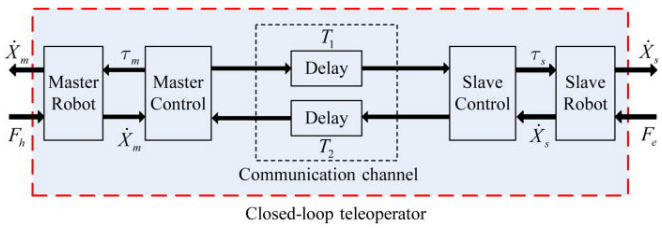

Fig. 1. Bilateral control architecture.

Master device is the tool which operator uses to control the robot, being advisable to use haptic devices able to provide force feedback to the operator for a correct performance. It depends of the controller used with the master device, it can manage slave robot through position or rate information. This slave robot will be in the remote environment and will follow commands sent by master device, providing back position and force information detected in its sensors. Finally, slave and master will be connected through a communication channel; master and slave information has to be updated at 1 kHz of frequency in order to maintain system stability.

As commented before, we need a robust system able to perform teleoperated tasks in unstructured environments. So it is important designing robust controllers to maintain the stability of the system, and having in consideration topics like impedance controllers (Miller, 2000), coupled stability (Colgate, 1988), transparent performance (Lee, 1997) and time-delays in communication channel (Hirche, 2007)

Most used control modes are based in rate control or position control, and depend on the task requirements (Kazi, 2001). The information sent through communication channel is provided by the controllers conditioning the control algorithm methodology.

Position control presents a more intuitive control between the master and slave. In (Kim, 1987) it is 1.5 times faster than rate control when master and slave workspaces are more or less similar. In the other way, rate control present more benefits when these workspaces are really different

(usually slave workspace bigger than master workspace). It means position control offer better performance when movements are short and precise, and rate control does when we need large and precise movements in rigid environments (Kontz, 2003).

Currently, there are different technics to work in large workspaces with a small master workspace in addition to rate control. Most common of them imply indexing techniques by using a button to synchronize or desynchronize master and slave, or even variable-scaling by commuting between high or low scaling using a button. Indexing method causes reference problems due to change the reference frame continuously, obtaining a less intuitive controller. In the case of variable-scaling, operator has to switch his mind every time that he changes the scaling to avoid do risky movement depending to the scaling mode. However, both has the inconvenience about using an extra button.

The proposed control in this situations is a hybrid rate-position controller (Barrio, 2012), that combines both rate and position control benefits without using a button. Although there is another hybrid rate-position controller but used on mobile robots (Farkhatdinov, 2007) or virtual haptic applications (Dominjon 2005), this combined control methodology has not been previously applied in Telerobotics field. In this paper we compare those three controllers and demonstrate benefits of hybrid controller in telemanipulation systems.

2 Experimental Setup

In order to performance the experiment, a test-bed has been designed. We divide the test-bed configurations in three different parts: master devices, slave robotic arm including the gripper and the communication channel.

2.1 Master Devices

Kraft Master: The Grips Manipulator system by Kraft Telerobotics, includes a slave and a haptic master device (fig. 2a) that are kinematically equivalent and hence a joint-to-joint control is sufficient to teleoperate the system covering the reachable workspace.

3-Finger Haptic Device: The 3-Finger haptic device shown in Figure 2b has ten actuators and 19 DoFs for movements. Each finger has its own mechanical structure with six DoF. The first three DoF are actuated and allow reflecting forces to the user in any direction. The last three allow

reaching and measuring any orientation within the device workspace. The mechanical structures of the three fingers are linked to the base through a redundant actuated joint that increases the workspace.

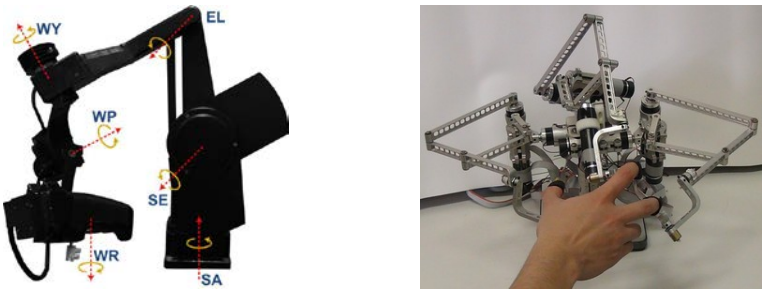

(a) Manufacturer Kraft Master (b) 3F HD

Fig. 2. Master devices

2.2 Slave Devices

Robotic arm: The slave robot, Fig. 3b, is a six DoF electrohydraulic manipulator equipped with a 3-finger gripper. Its potentiometers and double effect actuators feedbacks position and force in each joint. The slave workspace is 180 degrees wide, with a maximum reachable length of 1290 mm.

(a) Robotiq Hand (b) Robotic arm Grips from Kraft Telerobotics

Fig. 3. Slave devices

Robotiq Hand: For dexterity or high complex grasping tasks we need a gripper with high adaptability. A 3-Finger Adaptive Robot Gripper from Robotiq (fig. 3a) performs complex grasping in the experiment. This gripper has three fingers with joint redundancy which allow implement adaptive grasping by wrapping objects with its flexible finger configuration.

2.3 Communication channel

For the communication channel we must to have in consideration the possibility of time delay between our master and slave system. In order to

simplify the model we choose a wired communication through Ethernet and a LAN network which allow the connection of our different devices. We use IP communication through UDP protocol in order to maximize the frequency datagram exchange and giving priority to real time information: this protocol allows us to work at the maximum velocity of our system, in our case 1 KHz, to guarantee the stability of the system.

3 Experiment: Telemanipulation of fragile objects in unstructured environments

The most widely used methods for remote teleoperation in large environments are either use a master device which is kinematically identical or similar to the slave device. However, it is common to find haptic devices which have a significantly lower workspace than slave's; for these cases, methods such as indexing or scaling are usually implemented.

In this experiment, the rate-position method, the indexing method and the use of kinematically similar devices are compared. The simple scaling option is not compared here, since it would imply a significant loss in precision which would not be safe for a robot that is transporting a fragile robotic hand at the end--effector.

The indexing method has been implemented for the 3-Finger Haptic Device so that, while the user presses a button (space bar at the keyboard), the movement of the master device end-effector is decoupled from the movement of the slave device. When the user releases the button, the position of the haptic device end-point and the slave end-effector are synchronized and the system continues in position control mode. In our implementation, the orientation is not indexed since the orientations that the haptic device and the slave robot can achieve are the same.

3.1 Experimental Procedure

The experimental task consists on manipulating a fragile object: a light bulb. The steps for the task are the following:

1. The task begins with the robot in a designated position, located one meter away from the target;

2. The user has to approximate to the manipulation area where the light bulb is located on top of a glass and position the robot in the pre-grasp pose;
3. The user will command the robotic hand to grasp the light bulb;
4. The user will command the robot back to the starting position without breaking or releasing the light bulb;
5. The user will move back to the manipulation area (still holding the light bulb) where the fragile object was located and position the robot in a pre-release pose.
6. The user will command the robotic hand to place the light bulb at its starting position.

Fig. 4. A user performing the dexterous teleoperation task with the 3-Finger Haptic Device.

During the experiment, two subjects carried out the task 30 times for each of the three methods; the task involved performing manipulations with a robot that included a fragile robotic hand at the end-effector, a mistake by the operator would cause the hand to break; therefore, we were not allowed to perform this experimental procedure with people from outside our research group. Both users had previous experience with the 3-Finger Haptic Device and with the manufacturer controllers, but they were not familiar with the indexing or the rate-position controller. Preparatory trials were not performed given that the operators were used to the haptic device to evaluate the intuitiveness and learning effect for each control. Fig.4 shows a user during the grasping stage of the task.

3.2 Time to task Completion

As show in fig. 5, the time to perform the fragile dexterous manipulation task, for the rate--position controller is in average, 68.9 seconds; while for the indexing control, the average time spent to perform the task is 75.33

seconds. Using the kinematically-similar master with the robotic hand controllers, the time goes in average to 70.67 seconds.

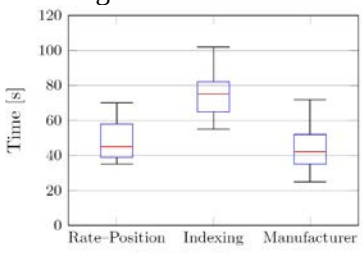

ANOVA Table

Source	SS	df	MS	F	*p*-value
Columns	17401	2	8700.51	52.64	1.04×10^{-15}
Error	14378.6	87	165.27		
Total	31779.6	89			

Fig. 5. ANOVA: Timing comparison when performing a dexterous manipulation task with different control methods

It can be seen that the indexing method has a higher average time to complete the task than any of the others. Moreover, subjects were more tired after finishing the trials with the indexing method than the others. The very small p-value indicates that differences between column means are highly significant. Reason is they had to move their arm forward and backward continuously and press a button when covering large distances. The rate-position method is similar in time to those obtained by using a kinematically similar master and some sliders by two people, which is intuitive since one person is only focused in the control of the hand, while the other subject is in charge of moving the robotic arm with a scale 1:1.

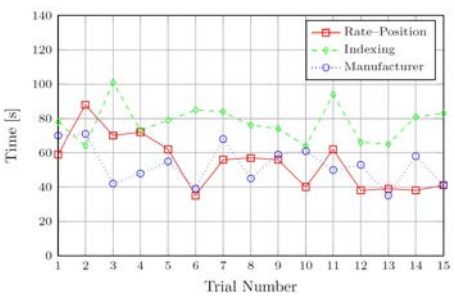

Fig. 6. Training time when performing a dexterous manipulation task with different control method.

Fig. 6 shows that the training time for the rate-position control drops from 70 to 45 seconds after five trials; the indexing mode it remains constant at about 80 seconds, and does not reduces during the 15 trials; for the manufacturer controller, the time lowers from 65 to 45 seconds after the

3rd trial. This shows that five trials are enough to get used to the rate-position control method to perform a dexterous task; which is admissible. Since subjects are usually trained to use computer interface with an indexing control mode, such as a computer mouse; it seemed very intuitive for them to move the robot around with this control. However, the longer time is due to the fact that they had to move more distance in the slave device than in the master device and they needed to keep a button pressed in order to decouple both systems.

3.3 Task success rate

Moreover, in fig.7 it can be seen that while the rate-position and indexing controllers have achieved a 100% success rate; for the manufacturer controllers, this percentage drops to 93.33%. After questioning the subjects, they mentioned that the main difficulty when using the manufacturer controller was the coordination between fingers when closing the hand with the sliders and keeping the robotic arm still while doing this. 93.33% may seem a high success rate, but for some situations that involve risk such as bomb dismantling, tele-surgery or maintenance of nuclear reactor, a drop of 6.67 points in the percentage may not be admissible, this failures could be explained because users have force-feedback and feel the grasping, despite the sliders don't provide this information and the operator has to ensure a proper grasping visually.

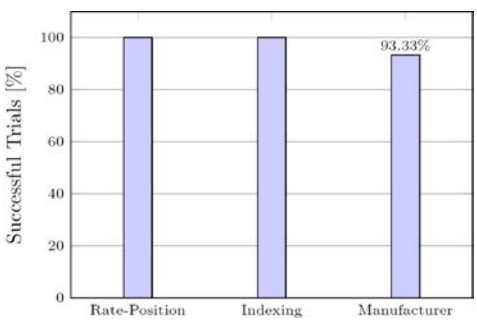

Fig. 7. Successful manipulations when performing a dexterous manipulation task with different control methods

4 Discussion and conclusion

This experiment proposes a manipulation that involves dexterity to work with fragile objects and different control methods used in large workspac-

es. In the sight of results obtained, we can compare the control methods in terms of effectiveness and efficiency. First at all, attend to effectiveness, both of three methods used have obtained a big rate of reliability based the results of the fig. 7. In this case, we emphasize that the minimum error produced by manufacturer master device could not be allowed in restrictive environments without an appropriate grasping method.

If we focus on efficiency, we have to consider the time spent during the task. Time differences between rate-position control and force-position control with manufacturer master device are really similar. Moreover, another control method is added to the comparison. Indexing mode, which it is one of the most common methods used in teleoperation with large workspaces, presents good results in the fragile manipulation task as a rate-position control does. The important difference now is the time during the task; rate-position control shows an improvement respect to indexing method, which loses time during desynchronized moments of the algorithm. Due to this, we obtain two methods with good results for teleoperation in large workspaces but rate-position is faster than indexing to perform a trajectory thanks to the velocity behavior of the first one, and even without tiring the operator.

This experiment emulates a case of dexterous manipulation of fragile objects, and it has been demonstrated that rate-position control reduces task time comparing with another control methods used in large-workspaces like indexing control or manufacturer controllers for the robotic hand and the slave robot. Moreover, rate-position control method keeps a high accuracy of the system that allows completing correctly the dexterous manipulation of fragile object task.

To conclude, the main strengths of this method are the possibility to control a slave with large workspace using a small haptic device and the great accuracy achieved due to the combination of the two operation modes.

References

Barrio, J., Suarez-Ruiz, F., Ferre, M., & Aracil, R. 2012. A rate-position haptic controller for large telemanipulation workspaces. In Intelligent Robots and Systems (IROS), 2012 IEEE/RSJ International Conference on (pp. 58-63). IEEE.

Colgate, J. E., & Hogan, N. 1988. Robust control of dynamically interacting systems. International journal of Control, 48(1), 65-88.

Dominjon, L., Lecuyer, A., Burkhardt, J. M., Andrade-Barroso, G., & Richir, S. 2005. The" Bubble" technique: interacting with large virtual environments using haptic devices with limited workspace. In Eurohaptics Conference, 2005 and Symposium on Haptic Interfaces for Virtual Environment and Teleoperator Systems, 2005. World Haptics 2005. First Joint (pp. 639-640). IEEE.

Farkhatdinov, I., & Ryu, J. H. 2007. Hybrid position-position and position-speed command strategy for the bilateral teleoperation of a mobile robot. In Control, Automation and Systems, 2007. ICCAS'07. International Conference on (pp. 2442-2447). IEEE.

Hirche, S., Hinterseer, P., Steinbach, E., & Buss, M. 2007. Transparent data reduction in networked telepresence and teleaction systems. part i: Communication without time delay. Presence: Teleoperators and Virtual Environments, 16(5), 523-531.

Kazi, A. 2001. Operator performance in surgical telemanipulation. Presence: Teleoperators and Virtual Environments, 10(5), 495-510.

Kim, W. S., Tendick, F., Ellis, S. R., & Stark, L. W. 1987. A comparison of position and rate control for telemanipulations with consideration of manipulator system dynamics. Robotics and Automation, IEEE Journal of, 3(5), 426-436.

Konz, M. E., & Book, W. J. 2003. Position/rate haptic control of a hydraulic forklift. In ASME 2003 International Mechanical Engineering Congress and Exposition (pp. 801-808). American Society of Mechanical Engineers.

Lawrence, D. A. 1993. Stability and transparency in bilateral teleoperation. Robotics and Automation, IEEE Transactions on, 9(5), 624-637.

Lee, H. K., Shin, M. H., & Chung, M. J. 1997. Adaptive controller of master-slave systems for transparent teleoperation. In Advanced Robotics, 1997. ICAR'97. Proceedings., 8th International Conference on (pp. 1021-1026). IEEE.

Miller, B. E., Colgate, J. E., & Freeman, R. A. 2000. Guaranteed stability of haptic systems with nonlinear virtual environments. Robotics and Automation, IEEE Transactions on, 16(6), 712-719.

CHAPTER 8

GRAPHICAL USER INTERFACES FOR ROBOTIC SYSTEMS IN HAZARDOUS FACILITIES

G. LUNGHI [1,2], M. DI CASTRO[1], R. MARIN PRADES[2], A. Mosca[1]

[1]CERN, Geneva, Switzerland, [2]Universitat Jaume I, Castellon de la Plana, Spain, Giacomo.Lunghi@cern.ch.

Currently robotic systems are becoming fundamental actors in industrial and hazardous facilities scenarios. Teleoperated robots need user friendly and intuitive control tools to be safely deployed in harsh environment where the intervention scenarios are unstructured and most of the time dangerous for human intervention. In this paper general guidelines for developing Graphical User Interfaces (GUI) which allow Human-Robot Interaction (HRI) with robotic systems used in harsh and unstructured facilities are presented.

1 Introduction

A Graphical User Interface is an interface which allows a user to interact with a system. According to the definition given by the Association for Computing Machinery (ACM), the Human-Machine interaction (HMI) is *"a discipline concerned with the design, evaluation and implementation of interactive computing systems for human use and with the study of major phenomena surrounding them"* (Hewett, 1992). The goal of the Human-Machine interaction is to improve the relations between users and machines by making machines more usable and receptive to the user's needs.

The development of an HMI must follow a series of steps starting from the identification of the needs of the users. The collected data are then analyzed and formalized in order to propose a design of the HMI. According to the proposed design, a prototype is developed and evaluated. During the evaluation, more data are collected and analyzed, a new design is proposed

and a new prototype is developed. When all the user requirements are fulfilled, the HMI is finally implemented and deployed.

In this paper, we address the problem of finding the main needs for a HMI that is able to control safely and easily a robotic system deployed in a harsh environment. The needs for such a HMI must be well defined and well related in order to provide, together with the usability and the learnability of the HMI, a very high level of safety to react to user control errors and to unexpected events in the robot workspace. Later on, a series of basic functionalities that a HMI must provide for the control of robotic systems are presented.

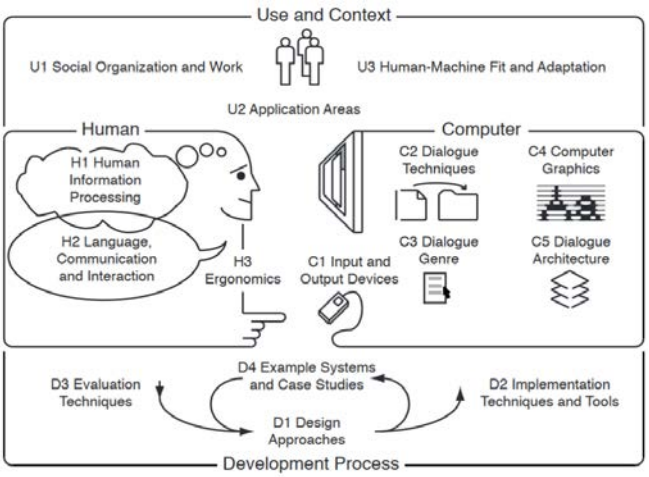

Fig. 1. Development process for a HMI system.

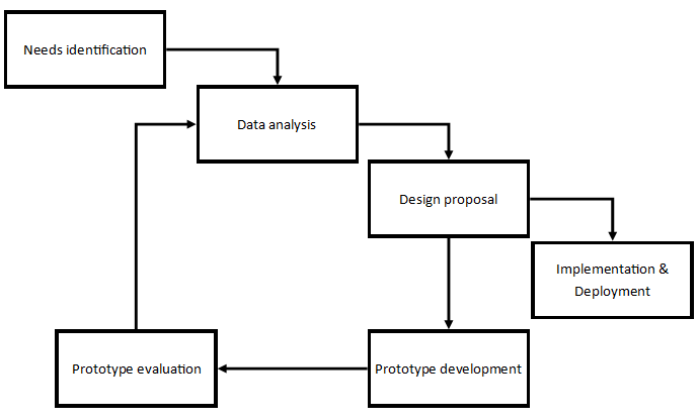

Fig. 2. Steps to be implemented for the realization of a HMI system.

2 Graphical User Interface development process

Designing Human-Machine Interfaces is becoming a significant challenge for designers. Embedded devices are shrinking in size, making it difficult to develop useful and intuitive HMIs with the right combinations of features in a short time-to-market window. Software tools can help manufacturers build user interfaces at a high level using programs like Photoshop for graphics and Visio for screen flow. Developers can then integrate those pieces of technology into actual code that can run on the device itself. Implementing prototypes for analyzing and evaluating a concept's usability is just as indispensable as formulating a complete and consistent specification for the HMI. Model-based software development using modern tool chains and existing sub-models provides clarity in ensuring a high level of quality from the very start. To achieve a reliable, safe and satisfying HMI, different steps have to be taken into account (Fig. 1 and Fig. 2). In the following, the main stages to develop a suitable HMI are listed and explained.

2.1 Identification of the operators

When developing a robotic platform, the first step is to identify who will be the operators that will use the final system. Three kind of operators can be usually identified:

- *Expert operators* who have a long experience in robot teleoperation, they followed specific teleoperation courses and they already performed several teleoperation tasks.
- *Project-involved operators* who do not have the complete knowledge of the system, but they have been involved during the development process. During this period they gained experience, which allows them to be more confident in the usage.
- *Entry-level operators* who never had the possibility to see the system and they are attempting to use it for the first time.

A robotic Graphical User Interface must be complete in the sense that must provide clear enough feedbacks to the operator which can be easily understood by an entry-level operator, but enough detailed information which can be useful for an expert operator.

Operator analysis is usually performed with the following techniques:

- Questionnaires
- Interviews
- Observation of users performing tasks

2.2 Needs identification and data analysis

After identifying the operators, the next part of the process is the identification of the needs. When developing a robotic system for unstructured and harsh scenarios, the safety of the robot, of the facility and of the operator are the most important requirements of the system. The Graphical User Interface must provide, then, a complete series of indicators of the status of the robotic system, and a series of well visible alarms which attract the attention of the operator in case of problem.

The feedback to the operator are usually visual and they can be integrated with audio feedback, for example to indicate that the battery of the system is low, and vibration feedbacks, for example warning the user of robot collisions with the environment.

With the aim to increase safety, an emergency safety stop have always to be implemented. The position of the emergency stop is critical and it depends on the input device that is used by the operator. If the operator is using a PC graphical using interface, an emergency stop button on the GUI must be positioned. This button can be triggered by the mouse, the keyboard, or any other input device connected to the GUI (e.g. a joypad, a haptic device etc.). The position of the button on the GUI is also critical and should be placed taking care of the Fitts Law (MacKenzie, 1992).

It is very common in the development of such a GUI the usage of the iconic knowledge of the operator (Fig. 3). The iconic knowledge of the operator associate an icon to a behavior. The behavior of the icon is connected to the affordance of the icon. The perceived affordance of the icon must be the same of the actual affordance. It is possible to integrate icons with text, in order to help the operator in the comprehension of the affordance.

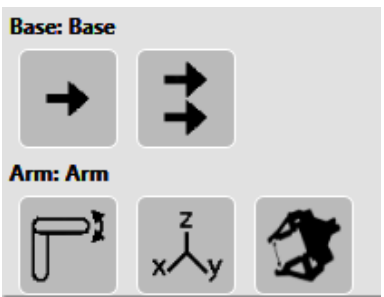

Fig. 3. Example of iconic knowledge on a robotic GUI

Operating a robot in critical situation is usually very stressful for the operator. According to the experience gained during teleoperated robotic interventions run at the accelerators of the European Organization for Nucle-

ar Research (CERN), the attention of the operator during the task operation tend to drop down very fast for multiple reasons: stress, limited time, gaining confidence etc. The Graphical User Interface have to be intuitive in order to reduce the stress of the operator and to focus all his/her attention on the task, and not in the comprehension of the functionalities.

An important factor that must be taken in to account is the working memory used during the operation: according to Baddeley (1992) an operator uses two types of memory, the short-term memory, faster and more resource demanding, and the long-term memory, slower. The use of the short-term memory is usually more stressful for the user. The GUI, then, must not overload the short term memory of the operator, who has to remember not more than 7-9 items. Furthermore, anxiety reduces dramatically the short-term memory performances and the number of items that can be remembered by the user drops off. In these items, some items are particularly important, like the emergency stop. The battery level, instead, can be excluded from these items, for example, if associated with an alarm sound when critical.

Fig. 4. Example of connecting procedure. Only two steps are necessary (selection of the robot and pressing the connect button). The short-term memory is not stressed.

In order to maximize the performances of the long-term memory, instead, the Graphical User Interface must be consistent during time. The process of forgetting depends on two factors: decay (information is lost gradually but very slowly – logarithmic law of decay) and for interferences. In particular, interference in the memory can happen if new information replaces old information (retroactive interference) or old information interfere with new information (proactive inhibition). Indicators

then must not change and have to be consistent in order not to create interference in the long-term memory of the operator.

Another important aspect is the mental workload and the attention. The attention is the cognitive process of selectively concentrating on one aspect of the environment while ignoring other things. The mental workload is critical not per se but it is critical whether the operator can perform his/her tasks, with any margin of attention for unforeseen circumstances, stress, or complexities which may be infrequent but certainly do arise from time to time. Performing a teleoperation task is usually heavy in terms of mental workload, with the effect that the attention decreases with time. It is important then to minimize the mental workload created by the GUI, and all the attention have to be put in the robot operation. The Graphical User Interface have to interfere as less as possible with the operator while operating, for example avoiding popups and windows which open automatically, and interrupt the robot operation because they have to be handled. Important messages have to be clear, direct and rapid, in order not to create stress and useless workload to the operator.

Fig. 5. Example of Robot Control Interface.

The attention of the user is on the big camera view on the center of the screen. Warning messages are shown in the bottom left part, which can be seen by the peripheral vision of the user, but they don't interrupt the operation. A secondary camera to control better the robot position can be added on a corner of the main camera. The more the objects are on the sides of the window, the less they are in the center of the attention of the user.

There are two ways to measure the mental workload. The first proposes a single-dimensional subjective mental workload scale (Wierwille, 1983),

while the second proposes a three-dimensional subjective mental workload scale (Reid, 1981).

The Graphical User Interface must be able to react to slips and lapses. Slips and lapses occur in skilled behavior, during the execution of tasks and procedures that the user has already learned. Slips distinguish from lapses by the source of the failure: a slip is a failure during the execution of a procedure, while a lapse is a failure of the memory. In critical scenarios like radioactive scenarios, lapses and slips can be critical.

A capture slip occurs when a person starts executing one sequence of actions, but then veers off into another (usually more familiar) sequence that happened to start the same way. A description slip occurs when two actions are very similar. The user intends to do one action, but accidentally substitutes the other.

For example, the lapses can be reduced managing carefully the operator memory. Lapses can also happen because of interruptions, which disrupt short-term memory and make you lose track of your place in the interrupted procedure. Another common lapse happens when your goal is actually satisfied in the middle of the procedure. The remaining steps are cleanup or shutdown subtasks, which you may forget because you've already discharged your original intention. The attention of the operator must be kept on the system until the robot is in a safe position (for example the charging station).

2.3 Validation and test

Once an HMI has been implemented, a user test is mandatory to establish the performance of it. User testing is the process of having the users evaluating the developed interface prototypes. There are several typologies of user testing.

Three common kinds are:

- Formative evaluation, aimed at finding problems for the next iteration of design.
- Field studies, aimed at finding problems in context.
- Controlled experiments, aimed at testing a hypothesis in a controlled environment.

Since user testing involves human subjects participating to experiments ethical issues are relevant and need to be taken into account. User testing puts psychological pressure on the user and Research involving human

subjects must be addressed very carefully and is subject to close scrutiny (Regulations and Ethical Committees).

3 Conclusions and Outlook

In this work, a review of the steps that have to be taken into account when developing a HMI system have been proposed. Most of the ideas and feedbacks presented are coming from the robotic teleoperators of the CERN accelerator facilities.

References

A. Baddeley. 1992. "Working memory." Science 255.5044: 556-559.

Association for Computing Machinery - ACM http://www.acm.org/

Hewett, Baecker, Card, Carey, Gasen, Mantei, Perlman, Strong and Verplank. 1992. ACM SIGCHI Curricula for Human-Computer Interaction

MacKenzie, I. Scott. 1992. Fitts' law as a research and design tool in human-computer interaction. Human-computer interaction 7.1

Reid, Gary B., Clark A. Shingledecker, and F. Thomas Eggemeier. 1981. Application of conjoint measurement to workload scale development. Proceedings of the Human Factors and Ergonomics Society Annual Meeting. Vol. 25. No. 1. Sage Publications.

Wierwille, Walter W., and John G. Casali. 1983. A validated rating scale for global mental workload measurement applications. Proceedings of the Human Factors and Ergonomics Society Annual Meeting. Vol. 27. No. 2. Sage Publications

Zhang, Z., F. Vanderhaegen, and P. Millo. 2004. Uncertainty analysis in the prediction of human operator violation using neural networks." WSEAS Transactions on Circuits and systems 3.2

CHAPTER 9

A MODULAR PASSIVITY FRAMEWORK FOR MULTILATERAL TELEOPERATION APPLICATIONS

M. PANZIRSCH[1], J. ARTIGAS[1] and M. FERRE[2]

[1]German Aerospace Center (DLR), Institute of Robotics and Mechatronics, Wessling, Germany; [2]Centre for Automation and Robotics (CAR) UPM-CSIC, Universidad Politécnica de Madrid, Madrid, Spain

In the past few years multilateral teleoperation systems that enable the interaction and coupling of several robotic devices gained in importance as this concept promises especially an increase of ergonomics and precision in teleoperation systems. The challenge in the control of such multi-robot setups is the generalization of the stability proof independent of the number of robotic agents involved. Particularly in the presence of time delay in the communication channel the use of passivity control methods are widely used in bilateral as well as multilateral systems. In literature it was shown that the passivity concept also provides a modular framework that allows for the generalization of stability proofs rendering a frequency-based analysis unnecessary. This paper provides an overview on the existing framework modules and their application to different bilateral communication architectures.

1 Introduction

The application of teleoperation setups in medical or harmful environments, for the maintenance of oil platforms and in underwater scenarios underlines the importance of the teleoperation concept itself but also the need of ergonomic and highly precise robotic systems. The with respect to the long history of robotics novel concept of multilateral teleoperation promises to provide benefits e.g. in the training of novel users (Feth,

2009), the accurate control of robot configurations by professional operators (Malysz, 2011) and through cartesian task allocation to two input devices (Panzirsch, 2015). In such multilateral systems an arbitrary number of agents can be virtually connected with each other in a way that each agent receives information on the position or the environmental interaction of one or more agents. An agent can be a human operator with the master input device, a slave with its environment or an artificial intelligence. The interconnection of the agents is mostly guaranteed by a virtual spring damper system that punishes the position deviation of the agents.
In order to allow interaction from a distance the use of passivity based approaches that were developed for bilateral control (Niemeyer, 1997, Hannaford, 2002) can be applied also to multilateral systems. A setup based on the wave variables transformation (WVT) has been presented by Kanno et al. (Kanno, 2012) and the time domain passivity approach (TDPA) has been employed by Panzirsch et al. (Panzirsch, 2012). Both concepts act on the communication channel which is a purely active component in a way that the passivity of this subsystem can be achieved.
Multilateral systems that consider passivity concepts to tackle the effects of time delay require the passivity of the overall teleoperation architecture since a system is only passive if every subsystem is passive. Still, this is in terms of effort not a drawback since passivity guarantees stability in the sense of Lyapunov and thus, no additional stability proof for a complex multilateral system in the frequency domain is necessary. Panzirsch et al. (Panzirsch, 2013) showed that the passivity of a generalized multilateral system can be easily proven and that the resulting passive framework which can be combined with TDPA and WVT does not reduce the system performance despite consideration of passivity. The framework in this work is based on the tool called network representation proposed by Anderson et al. for the use in teleoperation systems (Anderson, 1992).
This paper is organized as follows: Section 2 introduces the modular concept based on the network representation. The different modules for the assembly of a multilateral system are presented in section 3. The paper content is summarized to a conclusion in section 4.

2 Modular Framework

The network representation is used as it provides energy related ports at each network subsystem that allow the observation of energy flow in a teleoperation system. At first the signal flow diagram (compare Fig. 1) has to

be transduced into its network representation (see Fig. 2). The system can be split up into agent and track subsystems. For simplicity the time delay which would be part of the track subsystem is at first not considered in the network representation. At each port the velocity and force can be measured to observe the power with respect to the flow direction from master to slave (L2R) or from slave to master (R2L):

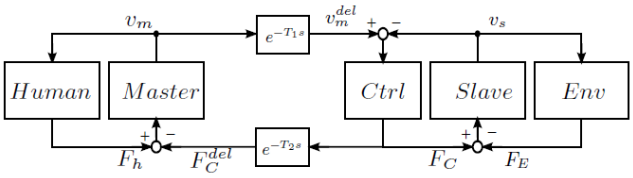

Fig. 1. Signal Flow diagram of a $PF_{computed}$ architecture with communication channel delay.

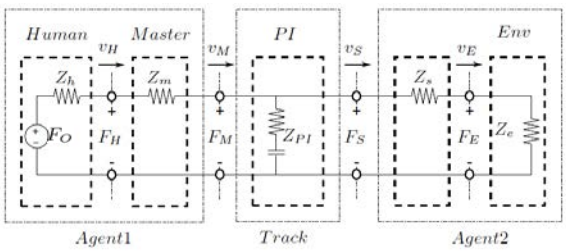

Fig. 2. Network representation of a $PF_{computed}$ architecture without communication channel.

Depending on the chosen architecture and the related force feedback ($PF_{computed}$, $PF_{measured}$, 3Channel or 4Channel) different tracks can be applied in the system. As the widely accepted assumption holds that the agents behave passive in their interactions only the passivity of the track subsystem has to be proven. In a multilateral system (compare Fig. 3) an arbitrary combination of tracks can be straight forwardly used to connect the agents. Panzirsch et al. designed a power control unit (PCU) that represents the sum of forces sent to a device via the tracks.

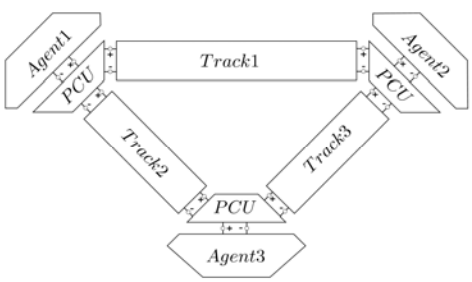

Fig. 3. Network representation of a trilateral teleoperation system (Panzirsch, 2016).

This sum of forces behaves passive as the same velocity is flowing at each port of the PCU (Panzirsch, 2013).

3 Track Design

In the next step the track is divided into its main modules to enable the analysis of their compositions depending on the type of communication channel architecture. Due to space constraints 2-Channel architectures will be focused in the following. Only the time domain passivity control applied to time delay and the measured force feedback are visualized in detail as they depend on the type of architecture chosen.

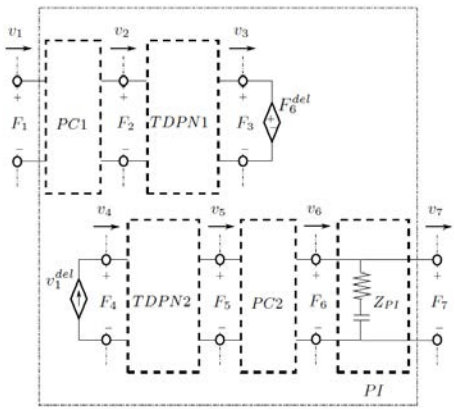

Fig. 4. TDPA applied on the time delay in a $PF_{computed}$ architecture.

The TDPA for a $PF_{computed}$ architecture is presented in Fig. 4. Two passivity controllers PC1 and PC2 dissipate energy generated by the time delay in R2L and L2R direction respectively. The track is split up into those two directions of energy flow and the communication is represented by time domain power networks (TDPN; Artigas, 2011). The dependent velocity (flow) source v_1^{del} injects the energy sent from the master in L2R direction on the slave side whereas the dependent force (effort) source F_6^{del} injects energy from the slave on the master side. The PI Controller is located on the slave side to improve the stability of the system. In contrast to this two PI controllers are considered in the PP architecture (compare Fig. 5). As the additional PI controller is located on the master side of the communication channel the force source of Fig. 4 is replaced by a velocity source v_8^{del}. The force

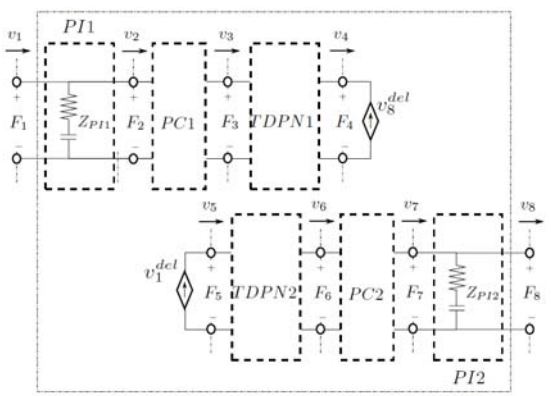

Fig. 5. TDPA applied on the time delay in a PP architecture.

feedback sent to the master is generated by the PI controller on the master side.

In the following the combination of all modules are presented for different 2-Channel architectures. Besides the time domain passivity control of time delay, scalings $_i$ of the feedback forces (e.g. for training purposes) and pose projection modules PR are integrated in the following. These passive PR modules serve e.g. the implementation of virtual grasping points (Panzirsch, 2015). As the pose projection does not depend on the communication channel architecture the PR modules are always the outermost modules on each side of the track. The gain $_1$ scales down the force feedback in R2L direction to the master and the gain $_2$ in direction to the slave respectively. Thus, the scaling behaves passive in the relevant flow direction of the track. Energy that is flowing from master to slave is reduced by the gain $_1$ whereas energy that is generated by that gain $_1$ in opposite direction is dissipated by the force source F_{10}^{del} (see Fig. 6). Note that the gain on the side of a slave robot is mostly one and can then be neglected.

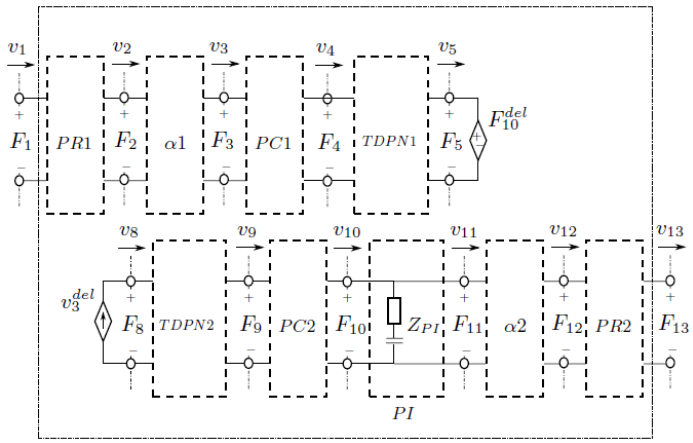

Fig. 6. Combination of modules in a $PF_{computed}$ architecture.

The wave variables transform can be integrated in the network of Fig. 6 by replacing the force and velocity source, the TDPN and PC subsystems with the WVT structure. Fig. 7 presents the composition of all relevant network subsystems in a PP architecture track. The PR and scaling subsystems are located analogously to the $PF_{computed}$ architecture. To the best of the author's knowledge no WVT has been presented for PP architecture yet.

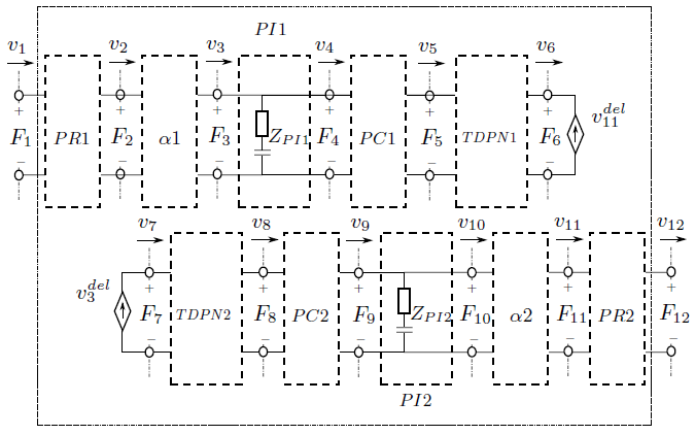

Fig. 7. Combination of modules in a PP architecture.

In literature (Panzirsch, 2016) it was shown that the approach guaranteeing passivity of measured force feedback in bilateral systems proposed by Willaert et al. (Willaert, 2009) cannot be applied to multilateral systems. Panzirsch et al. proposed two passivity controllers PC_L and PC_R (see Fig. 8) that dissipate excessive power introduced by the measured force feedback to achieve passivity. Fig. 9 presents the combination of the two pairs of time domain passivity controllers that consider time delay and measured force feedback respectively.

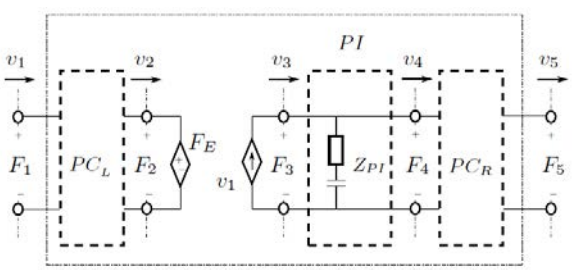

Fig. 8. Passivity of a track with measured force feedback (Panzirsch, 2016).

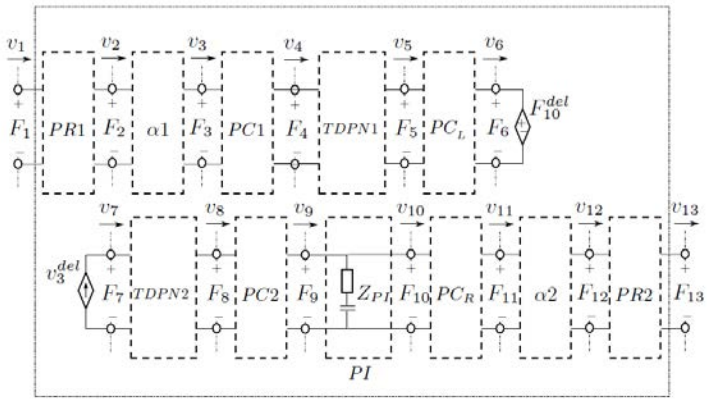

Fig. 9. Combination of modules in a $PF_{measured}$ architecture.

4 Conclusion

The latest results in the developments of new track modules of a passivity based framework for multilateral teleoperation have been summarized in the present work. It was shown that the time domain passivity control architecture can be integrated in the track design for the computed as well as the measured force feedback and the position-position architecture. The wave variables transformation concept can be easily integrated in the computed force feedback architecture, but the aptitude to the measured force feedback architecture has to be investigated. Future work has to focus the development of new tracks for the 3-Channel and 4-Channel control architectures.

References

Anderson, R.J., and Spong, M.W., 1992, Asymptotic Stability for Force Reflecting Teleoperators with Time Delay. The International Journal of Robotics Research, 11, 2, pp. 135-149.

Artigas, J., and Ryu, J.H., and Preusche, C., and Hirzinger, G., 2011, Network representation and passivity of delayed teleoperation systems. International Conference on Intelligent Robots and Systems, pp. 177–183.

Feth, D., Tran, B. A., and Groten, R., and Peer, A., and Buss, M., 2009, Shared-control paradigms in multi-operator-single-robot teleoperation, Human Centered Robot Systems, Springer Berlin Heidelberg, pp. 53-62.

Hannaford, B. and Ryu, J.-H. , 2002, Time-domain passivity control of haptic interfaces, IEEE Transactions on Robotics and Automation, 18, 1, pp. 1–10.

Kanno, T., and Yokokohji, Y., 2012, Multilateral teleoperation control over timedelayed computer networks using wave variables, Haptics Symposium, pp. 125–131.

Malysz, P., and Sirouspour, S., 2011, Trilateral teleoperation control of kinematically redundant robotic manipulators, The International Journal of Robotics Research, vol. 30, pp. 1643–1664.

Niemeyer, G., and Slotine, J.-J., 1997, Using wave variables for system analysis and robot control, IEEE International Conference on Robotics and Automation, pp. 1619–1625.

Panzirsch, M., and Artigas, J., and Tobergte, A., and Kotyczka, P., and Preusche, C., and Albu-Schaeffer, A., and Hirzinger, G., 2012, A peer-to-peer trilateral passivity control for delayed collaborative teleoperation, Haptics: Perception, Devices, Mobility, and Communication. Springer Berlin Heidelberg, pp. 395-406.

Panzirsch, M., and Artigas, J., and Ryu, J.H., and Ferre, M., 2013, Multilateral control for delayed teleoperation, International Conference on Advanced Robotics, pp. 1–6.

Panzirsch, M., and Balachandran, R., and Artigas, J., 2015, Cartesian task allocation for cooperative, multilateral teleoperation under time delay, International Conference on Robotics and Automation, pp. 312–317.

Panzirsch, M., and Hulin, T., and Artigas J., and Ott C., and Ferre M., 2016, Solving the problem of measured force feedback in passive multilateral teleoperation systems, Eurohaptics, London, England, accepted

Willaert, B., and Corteville, B., and Reynaerts, D., and Brussel, H.V., and Poorten, E.B.V., 2009, Bounded environment passivity of the classical position-force teleoperation controller, International Conference on Robots and Systems, pp. 4622–4628.

CHAPTER 10

ANALYSIS OF HAPTIC RESOLUTION ON TORSO FOR THERMAL AND VIBROTACTILE ACTUATORS IN A VIRTUAL REALITY VEST

G. GARCIA, J.C. RAMOS, J. BREÑOSA and M. FERRE

Centre for Automotion and Robotics (UPM-CSIC), Universidad Politécnica de Madrid, gonzalo.gvalle@upm.es, jcramar9@gmail.com, jose.brenosa@upm.es, m.ferre@upm.es

This paper is oriented to present the first steps in the development of a haptic vest, using several types of tactile stimuli. It is been intended to achieve touch-based communication through vibration motors and thermal effects through thermoelectric actuators, doing test to improve perceived sensations by users into virtual reality environments. Initial research like analyse vibration and thermal resolution are performed to place both actuators in vest areas in order to achieve real haptic sensations.

1 Introduction

In the last years, haptic technology has had a great boost and several investigation groups have studied it as a way to obtain enhanced results in human-machine interaction (Jarillo Silva, 2009) (Kuschel, 2010), bringing haptics to a broad range of applications (industrial, training or entertainment applications (Schmidt, 2010)). On the other hand, virtual reality is another emergent technology with, once again, a wide range of applications. One of that is “serious games”, that are games designed for a non-entertainment purposes. Combining both technologies it is possible generate systems where haptic technology produces a significant improvement in immersion and realism of virtual environment (Galiana Bujanda, 2013).

The work presented is being developing in the context of European Project H2020 AUGGMED, oriented to create a serious game platform for multi-agent counter terrorist training in mixed reality environments. In this

context, Universidad Politécnica de Madrid (UPM) is in charge of creation a haptic vest to improve immersion and realism in the virtual environment.

The aim is to develop a vest to generate several haptic effects (vibration, thermal) in the members of a training team. Haptic vest creates different feedback types on the skin to increase immersion and realism of virtual interaction through the torso trainee.

In this paper, it is shown the first steps on the vest development: actuator selection, virtual reality-vest interaction approach and a previous analysis of haptic interaction with skin.

1.1 Related Works

Both haptic technology and virtual reality systems have been amply investigated during last two decades. Moreover, in last years has been a considerable improvement in development of haptic devices related to virtual reality systems (Bau, 2012). Some developments of haptic vests have been already done, like TactaVest (Lindeman, 2004), a tactile vest for astronauts (Van Erp, 2003) or a vest developed that use different actuation methods distributed by several trunk areas (Jones, 2004).

Since one of the most known applications on virtual reality systems is "serious games", there are a lot of developed serious games oriented from military training to medical rehabilitation, going through other applications as education or information (Michael, 2005).

Finally, there are no studies about two-point discrimination distance with vibration or thermal actuators. There is only a study about vibration distances at back but it is not useful in this case (Eskildsen, 1969).

1.2 Research Objectives

The main aim is the development of a vest with haptic stimuli, allowing an increment in immersion and realism into a virtual reality environment. On the design, actuators have to be distributed by the entire torso. Thus, each actuator generates a different stimulus in a specific area.

Distribution of vibration and thermal actuators is organized as follows: tactile actuators will be placed on shoulders, upper back and upper chest, since these areas are commonly used by people to conduct touch-based communication among members inside the same trainee team. Furthermore, thermal effects will be placed on lower back and abdomen because is an area where thermal sensations are more easily perceived during the movements in the trials.

The first step is carrying out a test to determine the two-point threshold for discriminating vibratory and thermal stimuli on the chosen areas where actuators will be placed, establishing what is the minimum distance to place actuators in order to feel sophisticated haptic patterns.

2 Haptic Actuation

Two different actuation methods are going to be used to generate both types of haptic stimuli through the vest: vibration motors to create touch-based communication and Peltier cells to create hot/cold thermal feedback. Other options were evaluated but the two previous methods were chosen by their ability to generate real haptic sensations.

2.1 Vibrotactile Actuation

Two small vibration motors were selected among 10 analyzed motors through several performance tests: both are made by Precision Microdrives Ltd. and are shown in Fig. 1.

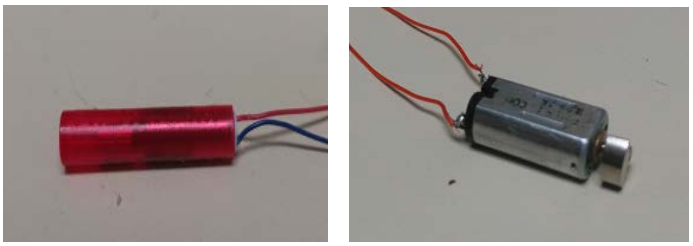

Fig.1. 304-116 Motor (left). 308-102 Motor (right)

The motors have been chosen because of their electrical characteristics (rated voltage and rated current are low) and due to rated vibration frequency. Since skin receptors need high frequencies (between 30 and 500 Hz, approximately) in order to appreciate vibrotactile effects and communicate sensations to nervous system. Motor characteristics are resumed in table 1.

Table 1. Characteristics of both vibration motors.

Characteristics	304-116 Motor	308-102 Motor
Rated Voltage (V)	3	4.5
Rated Frequency (Hz)	255	330
Rated Current (mA)	44	145

Although electrical characteristics are different, just a unique control circuit is needed to manage both motors. Moreover, distinct frequencies involve more options to achieve sophisticated vibration patterns.

2.2 Thermal Actuation

Peltier cells have been chosen to generate thermal feedback because of its capability to create hot and cold sensations with a single device. Other methods, as resistors, only can generate hot sensations on the skin. Finally, Peltier cells are easily controllable using a microcontroller and a circuit to control the current flowing by the cell.

After several tests (maximum and minimum temperature reachable, cold sensation time) performed with 7 different Peltier cell models, one was chosen to carry out first iterations of the vest development, shown in Fig. 2. Its characteristics can be seen in table 2.

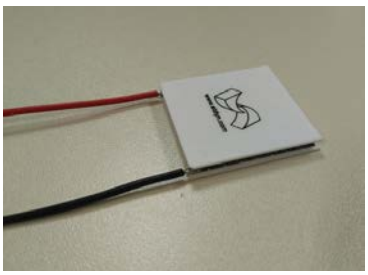

Fig. 2. Peltier cell used during experiments

Table 2. Characteristics of Peltier cell used during experiments

Characteristics	Peltier cell
Maximum Cooling Power (W)	21.4
Maximum Voltage (V)	4
Maximum Current (A)	9
Maximum Temperature Difference (K)	77

The Peltier cell manage average power but allowing to reach low temperatures in one of the faces. This maximum temperature difference can produce temperatures sufficiently high to be noticed by human skin and its size allows a correct integration in a wearable device.

3 Virtual Reality Environment

Vest integration inside a virtual reality environment is another of the goals in this development, in this matter and oriented for security forces training in a serious game, users can wear the vest and feel the virtual reality touch, receiving all stimuli that the avatar they are controlling is experimenting, improving immersion and realism during training.

For serious game environment, a software tool for videogames is being used, Unity 3D: this tool allows the creation of interactions with external devices like the vest. Moreover, Unity 3D is being used to create the virtual environment during the development of AUGGMED project, making the most appropriate to this purpose.

4 Resolution Experiment

The experiment is looking to obtain distances between vibration motors or thermal actuators for user can feel two different sensations (two motors vibrating or two cells heating). Distribution in areas previously chosen on the vest will be obtained with experiment results.

4.1 Vibration Patterns

First, vest areas chosen for vibrotactile feedback (shoulders, upper chest and upper back) are subdivided in 7 areas. On each area is placed two rows of motors (10 motors for 304-116 model and 6 motors for 308-112 model). Tests are done with both meshes obtaining two different discrimination distances. Fig. 3 shows a participant during the experiment.

Fig. 3. Participant during vibration experiment

The test procedure consists on a vibration sequence (1-second vibration and 3-second break off) and the user has to tell how many motors are working in that vibration second. Two motors vibrate in each sequence phase. Values are obtained (1 or 2 motors) for every possible distance, establishing discrimination distance for each participant. Sequence is random and user does not know in any moment the order of the generated patterns.

Tests are done with two motors type to find out if discrimination distances vary depending on the actuator, since two actuators have different rated frequency values and are not noticed on human skin in a similar way.

4.2 Thermal Patterns

Two vest areas has been chosen for thermal feedback: lower back and abdomen. Both areas are subdivided in 3 sub-areas where the test is performed. During the test, two Peltier cells are placed at different distances (5, 10, 15 and 20 cm). Users have to tell how many hot spots appreciate in each moment (1 or 2 points). Depending on when the user feels one or two points, the discrimination distance for thermal stimuli can be obtained.

4.3 Participants

24 subjects participated in the test (15 males and 9 females), from 22 to 35 years old. Most of them are from Universidad Politécnica de Madrid (UPM).

4.4 Vibration Experiment Results

Once all experiments are finished, two-point discrimination distance can be determined from the results. The resolution values obtained can only take ten-by-ten values (10, 20, 30…90) between 10 and 90 mm since these are minimum and maximum distances between two consecutive motors in the mesh.

Later, a statistical analysis of the data is done to identify non-valid or atypical values and erase them. Distance results are obtained for each analysed area. The distance between vibration motors can be determined in order to create sophisticated vibrotactile patterns on the vest. The data is divided by areas it is shown in table 3. Analysed areas are shown in Fig. 4.

Table 3. Resolution vibration distance for each analyzed area.

Areas	304-116 Motor Distance (mm)	308-102 Motor Distance (mm)
Upper Left Torso	40	40
Left Acromial Zone	40	---
Upper Left Back	50	40
Central Back Zone	50	---
Upper Right Torso	60	60
Right Acromial Zone	50	---
Upper Right Back	50	60

Fig. 4. Analysed areas during vibration experiment

4.5 Temperature Experiment Results

In the same way that vibration experiment, two-point discrimination distances for temperature are used in different areas of the abdomen area.

These values can only take values some values: 5, 10, 15 and 20 cm, since are separation distances between Peltier during different tests phases.

Finally, a statistical analysis (interquartile range) is done to erase atypical or non-valid data. Values obtained are used to determine distribution of Peltier cells on chosen areas. Data can be seen in table 4.

Table 4. Resolution temperature distance for each analyzed area.

Areas	Discrimination Distance (cm)
Right Abdomen	15
Lower Back	15
Left Abdomen	12.5

5 Discussion

Two experiments have been performed to determine two-point discrimination distance values for vibration and temperature on several areas at the human torso. With these values, resolution distances are obtained. These distances are used for distributing actuators over the vest.

In case of vibration motors, maximum resolution values are 60 mm, approximately. Therefore, motors must be placed at a distance larger than 60 mm to ensure correct vibration patterns in order to distinguish between different vibrations. To achieve generalized vibration sensations, actuators must be placed at minor distances (between 40 and 50 mm).

Regarding thermoelectric actuators, a high percentage of users can distinguish between two different temperature sensations by placing them at 15 cm, while if the purpose is a generalized sensation, like a wide area at the same temperature, Peltier cells must be placed at 10 cm between them.

6 Conclusions and Future Work

In this paper, first steps to develop a haptic vest have been proposed, selecting actuators and the method to interacting with a virtual reality environment.

Vibrotactile and thermoelectric actuators have been selected. These actuators create sensations on user skin. Preliminary test have been conducted to determine the actuator that will be integrated in the vest.

Next step has been the determination of two-point discrimination distance for vibration and temperature, obtaining results that allow the distri-

bution of actuators on the vest in order to create sophisticated haptic patterns.

As a future work, actuators will be integrated in the vest, assisted by obtained results. Moreover, an interface will be created to generate an interaction between haptic system and virtual reality environment.

References

Bau, O. 2012. REVEL: Tactile Feedback Technology for Augmented Reality. ACM Transactions on Graphics (TOG), 31(4): 89, 2012.

Eskildsen, P. 1969. Simultaneous and Successive Cutaneous Two-Point Thresholds for Vibration. Psychonomic Science, 14(4): 146-147.

Galiana Bujanda, I. 2013. Design and Control of Multi-Finger Haptic Devices for Dexterous Manipulation. PhD Thesis, Industriales.

Jarillo Silva, A. 2009. Phantom Omni Haptic Device: Kinematic and Manipulability. In Electronics, Robotics and Automotive Mechanics Conference, pages 193-198.

Jones, L.A. 2004. Development of a Tactile Vest. In Haptic Interfaces for Virtual Environments and Teleoperator Systems. Proceedings, 12th International Symposium on, pages 82-89.

Kuschel, M. 2010. Combination and Integration in the Perception of Visual-Haptic Compliance Information. Haptics, IEEE Transactions on, 3(4): 234-244.

Lindeman, R.W. 2004. The Design and Deployment of a Wearable Vibrotactile Feedback System. In Wearable Computers. Eighth International Symposium on, vol. 1, pages 56-59.

Michael, D.R. 2005. Serious Games: Games that Educate, Train and Inform. Muska&Lipman, Premier-Trade.

Schmidt, H. 2004. Hapticwalker: A Novel Haptic Device for Walking Simulation. In Proc. Of EuroHaptics.

Van Erp, J.B.F. 2003. A Multi-Purpose Tactile Vest for Astronauts in the International Space Station. In Proceedings of EuroHaptics, pages 405-408. Dublin, Ireland, ACM Press.

CHAPTER 11

PEOPLE POSITIONING SYSTEM WITH LOW COST 3D CAMERAS AND WIRELESS DEVICES FOR INDOOR ENVIRONMENTS

J. DUQUE[1], C. CERRADA[1] and E. VALERO[2]

[1]Departamento de Ingeniería de Software y Sistemas Informáticos, ETSI Informática, UNED, C/Juan del Rosal, 16. 28040 Madrid, Spain, jaimeduque@amenofis.com ; [2] School of Energy, Geoscience, Infrastructure and Society, Heriot-Watt University, Edinburgh EH14 4AS, United Kingdom

Indoor Positioning has been a field of study of great interest during the last years. This work analyzes *WiFi Positioning System* (WPS) and presents a new *Indoor positioning system* (IPS) based on the combination of WPS *fingerprinting* and the use of RGB-D cameras with the aim of improving the location of people. The combination of both technologies allows improving, in a simple and economical manner, the efficiency of WiFi positioning. An overview of related works is presented, and an analysis of WPS performance with the help of RGB-D cameras is developed, showing the benefits of the presented method.

1 Introduction

This work presents a new *Indoor positioning system* (IPS), based on the combination of WiFi positioning and the use of RGB-D cameras. The proposed system just requires *smart-phones*, widely used, and the installation of RGB-D cameras, while other positioning systems force users to wear non-common devices or cards on their bodies. The obtained results significantly increase the effectiveness with respect to common WiFi positioning.

WiFi Positioning System (WPS) is a well-established indoor positioning technique that works with wireless devices, such as mobile phones, for measuring the signal level they receive from the different access points

(A.P.), i.e. WiFi routers. At the beginning WPS was based on a similar technique to GPS, but using the triangulation of the signals devices received from the A.P., like the system RADAR (Bahl & Padmanabhan, 2000). However, these signals have a high variability because of the walls and obstacles and none equation works properly to transform this signal into distance.

In (Subbu, et al., 2014), three types of IPS based on WiFi are presented: *Fingerprinting*, which uses the signals obtained from the wireless device such as WiFi, sound, light or magnetic fields; *Crowdsensing*, an extension of *fingerprinting* that continuously collects data from the wireless devices in order to update the positioning data base; and finally, *Dead Reckoning Systems*, which use the accelerometer sensor of the wireless device for obtaining the inertial movement and the magnetic field sensor for the direction. Most current WPSs use the technique named *fingerprinting* (Liu, et al., 2014). With this technique, a map is created by recording the different signals received at each point. The obtained values, named *Received Signal Strength Indication* (RSSI), deliver the position of a user in real-time, comparing the values received from its wireless device against the values stored on the map.

Other authors (Quan, et al., 2010) show how WPS based on maps works better than techniques based on triangulation. The improvement of the method using the trajectory of the user is also analyzed, considering two ways: the nearest neighbor (the last location where the user has been) and the probabilistic location by means of a Markov process, obtaining worse results with the last one. (Martin, et al., 2010) study the accuracy of different techniques with *fingerprinting*: *Closest Point*, *Nearest Neighbor in Signal*, *Average Smallest Polygon* and *Nearest Neighbor in Signal and Access Point averages*. According to the authors, the results are good when the user is located in different rooms (78%-87%). If the user is inside a room the precision is lower, obtaining less than 50% of success in cells of 2 meters.

Indoor positioning techniques have also been used in Robotics. A noteworthy example can be found in (Biswas & Veloso, 2014), where a robot is located using three different systems: a laser rangefinder, a depth camera, and RSSI values. Each system is used independently according to the zone where the robot is situated. The authors of (Mirowski, et al., 2012) analyze how to generate a fingerprint map with a robot that has installed a RGB-D camera. Using *Simultaneous localization and mapping* (SLAM), the environment is built saving at each point the RSSI measurements.

In the field of people and objects detection, RGB-D cameras have been used in different works. In (Ye, et al., 2013) three Kinect sensors are used to extract several overlapped people from a scene. The authors of

(Takizawa, et al., 2013) propose a *smart-cane* for the visually impaired that, with the help of a Kinect sensor, allows locating objects. Several SLAM methods are evaluated in (Schindhelm, 2012) for building maps using robots with continuous positioning. And finally, the method *Kinect Positioning System* (KPS), analyzed in (Nakano, et al., 2012), tries to obtain the user position with Kinect sensors.

2 The method for improving WPS

Indoor positioning can be improved with the combination of the technology WPS and RGB-D cameras. At the same time, RGB-D cameras allow measuring the effectiveness of WPS. The scenario depicted in Fig. 1 represents how the new method works. One or more users move freely in a room. Several access points are accessible and there is an RGB-D camera, Kinect v2, situated at one corner of the room. This camera is connected to a web server that processes the positioning and stores the data base.

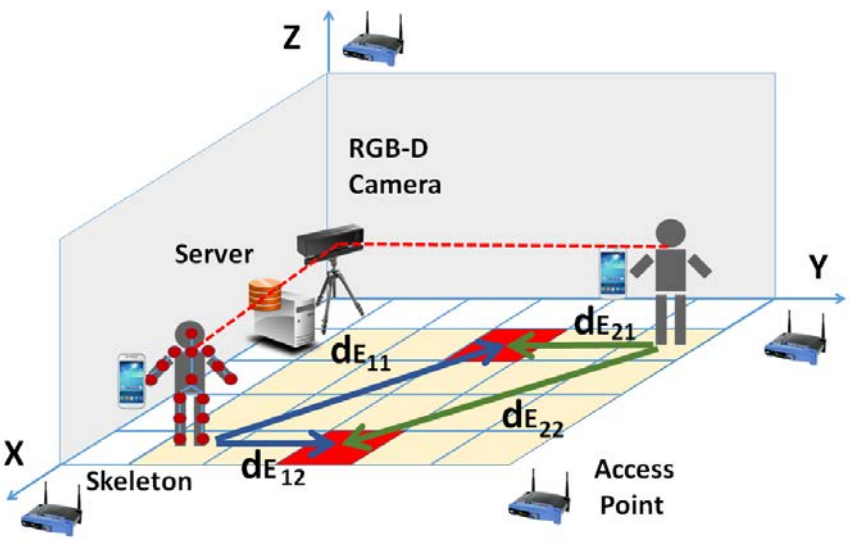

Fig. 1. Scenario of the system.

There are two different stages: *System Configuration* and *Positioning Operation.*

2.1 System configuration

During the *System Configuration* process, the system is initialized and, one user generates the WPS fingerprint map. This user moves around the environment and the system automatically records the RSSI values sent from their *smart phone*. This user has to cover the most part of the room to create a valid map. For each group of emitted RSSI values, a scan of the skeleton of the user is made with the RGB-D camera, saving the *x*, *y* and *z* coordinates of the user neck. *z* represents the height of the neck. Both scans, RSSI data and skeleton capture, have to be obtained synchronously at common time stamps.

The system records the RSSI measurements in a table and the skeleton coordinates in another one. For each time stamp and, linked for it, two types of data are saved: RSSI measurements and skeleton coordinates. The table for RSSI data includes the BSSID (*Basic Service Set Identifier*), the RSSI value and the time stamp. The BSSID is composed of the MAC (*Media Access Control*), unique for each access point.

When the configuration stage finishes, the maximum and minimum coordinates of *x* and *y* are obtained in order to divide the floor in different square cells. This cell division allows concreting RSSI measurements, reducing possible outliers. For each cell, a centroid is calculated for all the RSSI measures obtained. This centroid is composed of the average RSSI value of each access point, of the values measured in the cell.

2.2 Positioning operation

This is the usual operation mode of the system. The system provides the user their position in the scene. One or more users move freely around the room and each user carries a *smart phone*, which sends, synchronously with the rest of devices, RSSI data to the server, every second. When the web server receives these RSSI measurements from all the *smart phones*, a skeleton capture is made using the RGB-D camera.

In WPS, RSSI measurements are obtained from the *smart phone* and compared against the values kept in the fingerprinting map. This comparison is carried out against the centroids of different cells created during the system configuration. The RGB-D camera allows obtaining the real position of the user in order to obtain the error that is produced with WPS positioning. This error is based on the Euclidean distance between the measured RSSI vector and the RSSI vectors of the centroid of a cell.

If there is just one user in the room, it is assumed that the skeleton obtained with the RGB-camera is situated in their real position. The estimated position with WPS allows calculates the error produced with WPS.

When there are two or more users, several skeletons are obtained. At the same time, each user sends a group of RSSI measurements to the server. The system initially does not know what skeleton is linked to any particular RSSI data. The proposed method calculates the Euclidean distance between the RSSI data sent by *smart phones*, and the RSSI centroid of the cell where each skeleton is (see Fig. 1) and, looks for the best combination between each skeleton and the RSSI measures obtained from each *smart phone.* The best combination is the one where the sum of the Euclidean distances is lower. Finally, the system is able to relate each skeleton with a particular *smart phone*.

3 Experimentation and results

Two experiments have been developed: one for assessing the performance of WPS and a second one for evaluating the proposed method. One user created the initial fingerprint map moving through the most part of the room. The map was created with 1000 points, where each one had the skeleton and RSSI values. At the end of the system configuration, the floor was divided in 5 x 5 cells and the RSSI values were grouped for each cell calculating their centroids.

3.1 Evaluating WPS

WPS was evaluated in different scenarios. The first case was the detection of a user in a 9-room floor. The experiments showed that in 87% of the cases it was possible to detect in which room the user was. The second experiment consisted in evaluating the position of one user inside a room of 5 x 5 meters (the room of 5 x 5 cells depicted in Fig. 1). Results show that there is only a success of 14% detecting the cell where the user was situated. As seen in Fig. 2, RSSI values have a high variability that produces poor results when small cells are used. If the size of the cell was increased, the results were better, reaching 57% of success detecting the user in 2 x 2 meters cells.

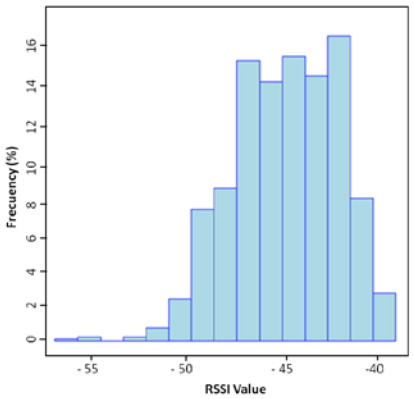

Fig. 2. Variability of RSSI measurements.

3.2 Combination of WPS and RGB-D cameras

When there is just one user inside the room, it is clear that their position is the one given by the skeleton, obtained with the RGB-D camera. Therefore, the success is 100% in locating the user.

When there are several users simultaneously, the Euclidean distances between their skeletons and WPS estimation help to determine the position as mentioned before. 250 tests have been performed, considering 2 or 3 users in the room. At the same time, the distance between the users has been taken into account. This distance has been calculated with the Euclidean distance between the skeletons. As shown in Table 1, when the distance is bigger, the results are better. If two users are situated at 2 meters, the proposed method obtains their correct position in 79% of the cases. For three users this percentage is lower but, in any case, is considerately better than the results produced with simple WPS.

Table 1. Results of different experiments.

Distance between users	Successes (2 users)	Successes (3 users)
0.5 meters	71%	41%
1.0 meters	73%	46%
1.5 meters	78%	53%
2.0 meters	79%	66%

4 Conclusions

This work illustrates a new method of indoor positioning based on the combination of WPS with fingerprinting and RGB-D cameras. The combination of both technologies, in a simple and economical manner, allows increasing the performance of WPS inside a room. The results show how this combination improves considerately the traditional WPS, obtaining successful rates close to 80% in some cases. The combination of WPS and RGB-D has a lot of advantages against other methods because the low cost, not having to wear special devices (only *smart phones*). At the same time, it is not an intrusive system because the identity of the users does not have to be known.

Acknowledgements

This work has been developed with the help of the research project DPI2013-44776-R of MICINN. It also belongs to the activities carried out within the RoboCity2030-III-CM project (Robótica aplicada a la mejora de la calidad de vida de los ciudadanos. Fase III; S2013/MIT-2748), funded by Programas de Actividades I+D en la Comunidad de Madrid and co-funded by Structural Funds of the EU.

References

Bahl, P. & Padmanabhan, V. N., 2000. RADAR: An in-building RF-based user location and tracking system. s.l., s.n., pp. 775-784.

Biswas, J. & Veloso, M., 2014. Multi-sensor mobile robot localization for diverse environments. In: RoboCup 2013: Robot World Cup XVII. s.l.:Springer, pp. 468-479.

Deak, G., Curran, K. & Condell, J., 2010. Filters for RSSI-based measurements in a Device-free Passive Localisation Scenario. Image Processing \& Communications, Volume 15, pp. 23-34.

Deak, G., Curran, K. & Condell, J., 2012. A survey of active and passive indoor localisation systems. Computer Communications, 35(16), pp. 1939-1954.

Feng, X., Gao, Z., Yang, M. & Xiong, S., 2008. Fuzzy distance measuring based on RSSI in Wireless Sensor Network. s.l., s.n., pp. 395-400.

Husen, M. N. & Lee, S., 2014. Indoor human localization with orientation using WiFi fingerprinting. s.l., s.n., p. 109.

Kornuta, C., Acosta, N. & Toloza, J. M., 2013. Posicionamiento WIFI con variaciones de fingerprint. s.l., s.n.

Lawson, C. T., Ravi, S. & Hwang, J.-H., 2011. Compression and Mining of GPS Trace Data: New Techniques and Applications, s.l.: s.n.

Liu, H., Darabi, H., Banerjee, P. & Liu, J., 2007. Survey of wireless indoor positioning techniques and systems. Systems, Man, and Cybernetics, Part C: Applications and Reviews, IEEE Transactions on, 37(6), pp. 1067-1080.

Liu, W. et al., 2014. Optimization of Sampling Cell Size for Fingerprint Positioning. International Journal of Distributed Sensor Networks, Volume 2014.

Martin, E., Vinyals, O., Friedland, G. & Bajcsy, R., 2010. Precise indoor localization using smart phones. s.l., s.n., pp. 787-790.

Mirowski, P., Palaniappan, R. & Ho, T. K., 2012. Depth camera SLAM on a low-cost WiFi mapping robot. s.l., s.n., pp. 1-6.

Nakano, Y. et al., 2012. Kinect Positioning System (KPS) and its potential applications. s.l., s.n., p. 15th.

Quan, M., Navarro, E. & Peuker, B., 2010. Wi-Fi Localization Using RSSI Fingerprinting.

Saputra, M. R. U., Widyawan, W., Putra, G. D. & Santosa, P. I., 2012. Indoor human tracking application using multiple depth-cameras. s.l., s.n., pp. 307-312.

Schindhelm, C. K., 2012. Evaluating slam approaches for microsoft kinect. s.l., s.n., pp. 402-407.

Shin, B.-J.et al., 2010. Indoor WiFi positioning system for Android-based smartphone. s.l., s.n., pp. 319-320.

Subbu, K., Zhang, C., Luo, J. & Vasilakos, A., 2014. Analysis and status quo of smartphone-based indoor localization systems. Wireless Communications, IEEE, 21(4), pp. 106-112.

Svecko, J., Malajner, M. & Gleich, D., 2015. Distance estimation using RSSI and particle filter. ISA transactions, Volume 55, pp. 275-285.

Takizawa, H. et al., 2013. Kinect cane: object recognition aids for the visually impaired. s.l., s.n., pp. 473-478.

Ye, G. et al., 2013. Free-viewpoint video of human actors using multiple handheld kinects. Cybernetics, IEEE Trans. on, 43(5), pp. 1370-1382.

CHAPTER 12

VISUAL ODOMETRY CORRECTION BASED ON LOOP CLOSURE DETECTION

L. CARAMAZANA, R. ARROYO and L. M. BERGASA

Robesafe Research Group, Department of Electronics, University of Alcalá (UAH), lidia.caramazana.zarzosa@gmail.com

An essential requirement in the fields of robotics and intelligent transportation systems is to know the position of a mobile robot along the time, as well as the trajectory that it describes by using on-board sensors. In this paper, we propose a novel approach focused on using cameras as perception sensors for visual localization in unknown environments. Our system allows to perform a robust visual odometry, where correction algorithms based on loop closure detection are applied for correctly identifying the location of a robot in long-term situations. In order to satisfy the previous conditions, we carry out a methodological improvement of some standar computer vision techniques. In addition, new algorithms are implemented with the aim of compensating the drift produced in the visual odometry calculation along the traversed path. According to this, our main goal is to obtain an accurate estimation of the position, orientation and trajectory followed by an autonomous vehicle. Sequences of images acquired by an on-board stereo camera system are analyzed without any previous knowledge about the real environment. Several results obtained from these sequences are presented to demonstrate the benefits of our proposal.

1 Introduction

In recent years, the estimation of an autonomous robot or vehicle pose using computer vision techniques has become a topic of great interest in the robotics community. This is due to the improvements in cameras features and to their reduced costs with respect to other sensors traditionally used for localization tasks, such as GPS, IMU, range-based or ultrasounds,

among others. Besides, the proliferation of visual SLAM systems (Bailey et al., 2006) has extended the application of camera-based approaches for determining the global location of a mobile robot in an unknown environment.

In this context, visual odometry (Nister et al., 2004) has the goal of estimating the position and orientation of a robot or vehicle by analyzing an image sequence acquired by cameras without previous information about locations. Each pair of images is considered to match their keypoints and calculate the translation and rotation between two poses of the vehicle. Unfortunately, visual odometry typically accumulates a drift when long periods of time are taken into account. This problem makes that the localization tasks could not be completely reliable in these cases. For this reason, in extended trajectories the information provided by standard visual odometry algorithms gives errors in long-term conditions.

According to the previous considerations, in this work we propose a novel approach based on loop closure detection using ABLE (Arroyo et al., 2014) for correcting the drift in visual odometry, which is initially processed by means of the LIBVISO library (Kitt et al., 2010). With the aim of solving the problems related to the drift, our system recognizes revisited places and recalculates a corrected pose. We contribute a method that uses this information to estimate the deviation between the revisited pose and the previous one. In order to validate our proposal, image sequences from the publicly available KITTI dataset (Geiger et al., 2013) are employed.

2 Method for visual odometry: the LIBVISO algorithm

The visual odometry algorithm provided by LIBVISO allows to determine the six degrees of freedom (rotation and translation) in a visual localization system. In our work, stereo cameras are employed in image acquisition. Due to this, intrinsic and extrinsic camera parameters are needed to correctly perform the matching between the stereo images. In our case, the tests performed in the KITTI dataset are carried out using the specific camera parameters defined in (Geiger et al., 2013). The application of a stereo camera approach provides a higher robustness to our global system, because it avoids the scale ambiguities that are common when monocular cameras are used for visual odometry computation.

The methodology behind our implementation derived from LIBVISO is mainly based on a trifocal geometry between the images. Initially, some keypoints are detected and their main features are extracted and matched for each two consecutive pair of images, as shown in the example present-

ed in Fig. 1. Taking into account the obtained matches, the movement of the autonomous robot or vehicle is estimated by processing a trifocal tensor that associates the keypoints between three frames of a same static scene.

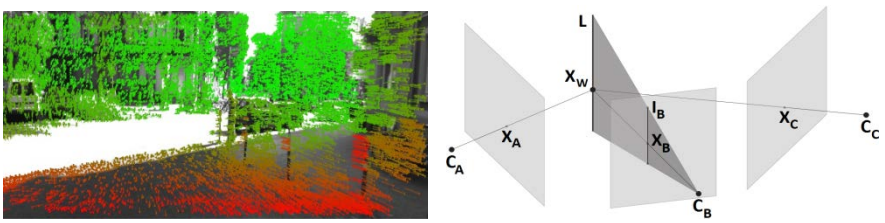

Fig. 1. A representation of the movement estimated over an example image using visual odometry, jointly with a diagram of the applied trifocal tensor.

In addition, the implementation of LIBVISO detects outliers using RANSAC (Scaramuzza et al., 2009), which allows to reject the atypical values obtained by erroneous matches and to improve the odometry results with respect to schemes without this filtering technique. However, this is not sufficient to avoid the drift along the time, as will be evidenced in the section of results. For this reason, we contribute a more robust approach based on a refined correction of the poses using loop closure information.

3 Method for loop closure detection: the ABLE algorithm

Some previous studies recently carried out by our research group in the topic of visual loop closure detection (Arroyo et al., 2014) are now applied to correct the drift derived from the previous visual odometry computation stage. The developed method for identifying when a place is revisited is named ABLE (Able for Binary-appearance Loop-closure Evaluation).

The main goal of this algorithm is to visually describe places in order to give similarity measurements between them for elucidating if a loop closure exists or not. Typically, ABLE computes global LDB binary features (Yang et al., 2012) for image description. In this case, disparity information obtained from the stereo images is also added to the descriptor. Apart from this, a variant of the description method initially designed in ABLE is contributed in this paper, where the recently proposed AKAZE features (Alcantarilla et al., 2013) are tested as core of the global description approach instead of LDB. We implement it to evaluate the robustness and efficiency of AKAZE, which adds gradient information in a nonlinear space to obtain a description invariant to scale and rotation.

After describing the images, the binary features (**d**) computed for each frame are matched to see if they are similar enough to consider a revisited place. In the case of binary descriptors such as LDB or AKAZE, the Hamming distance can be applied in matching, which provides a great efficiency, because it consists on a simple XOR operation ($\oplus$) followed by a basic sum of bits, as formulated in Equation (1). The obtained similarity values are stored on a distance matrix (M). These values are used to detect the loop closures when high similarity measurements are obtained.

$$M(i,j) = M(j,i) = \text{bitsum}(\mathbf{d}(i) \oplus \mathbf{d}(j)) \tag{1}$$

4 Our proposal for visual odometry correction

The information about the loops identified in the previous system stage is now used to correct the visual odometry. Here, we contribute the formulation of our method to perform these corrections. After a revisited place is detected in a specific frame, the drift of the pose currently estimated by the visual odometry algorithm is compensated by taking into account the pose obtained when the place was previously traversed. In this case, we consider corrections for the plane *xz*, where the deviation (Δ) between the current pose (i) and the previous one (j) is calculated as follows:

$$\Delta x(i) = |x(i) - x(j)| \tag{2}$$

$$\Delta z(i) = |z(i) - z(j)| \tag{3}$$

Then, the current poses are updated ($x(i)'$, $z(i)'$) in the x and z axes using the previously estimated deviation:

$$x(i)' = x(i) + \Delta x(i) \tag{4}$$

$$z(i)' = z(i) + \Delta z(i) \tag{5}$$

Besides, an average deviation (Δx_{avg}, Δz_{avg}) is subsequently computed after detecting the first pose corresponding to a loop closure. This information is employed to correct the poses in the rest of the trajectory, where m is the number of processed frames:

$$\Delta x_{avg} = \frac{\sum_{i=1}^{m} \Delta x(i)}{m} \tag{6}$$

$$\Delta z_{avg} = \frac{\sum_{i=1}^{m} \Delta z(i)}{m} \tag{7}$$

After calculating the average deviations in the loop zone, the poses in the remaining frames are updated according to the following equations:

$$x(i)' = x(i) + \Delta x_{avg} \tag{8}$$

$$z(i)' = z(i) + \Delta z_{avg} \tag{9}$$

The application of the formulated corrections in poses improves the accuracy initially obtained by only using a visual odometry without consider the progressive drift, as corroborated in the next section of results.

5 Evaluation and main results

Our proposal is evaluated in the KITTI Odometry dataset (Geiger et al., 2013). It contains 22 sequences recorded on different car routes around Karlsruhe (Germany). GPS ground-truth measurements are available. A ground-truth for loop closure was also defined in (Arroyo et al., 2014).

In Fig. 2, it can be seen how the visual odometry measurements obtained by LIBVISO without correction have a considerable drift with respect to the GPS ground-truth. The maps presented correspond to some significant sequences from the KITTI dataset, which are also presented in Fig. 3 to show the matches of the loop closures detected using ABLE.

In addition, Fig. 4 depicts some examples of distance matrices processed by means of ABLE using LDB and AKAZE descriptors as core. The detected loop closures correspond to the diagonals in the matrices. Besides, Fig. 5 introduces precision-recall results about ABLE performance in loop closure detection depending on the descriptor used as core. Apart from LDB and AKAZE, we also test other typical descriptors such as HOG (Dalal et al., 2005), SURF (Bay et al., 2008), BRIEF (Calonder et al., 2010) and ORB (Rublee et al., 2011). These results demonstrate the better performance of LDB and the new approach based on AKAZE.

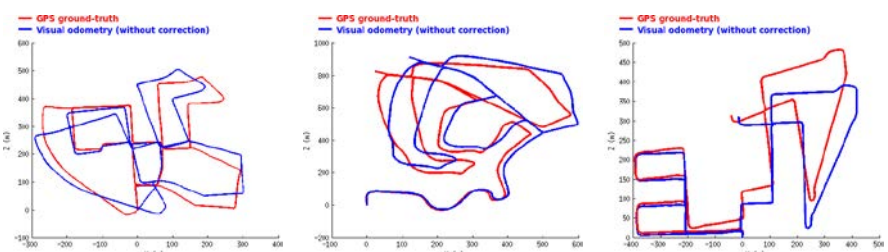

(a) Sequence 00 (b) Sequence 02 (c) Sequence 08

Fig. 2. Results for visual odometry without correction in the KITTI dataset.

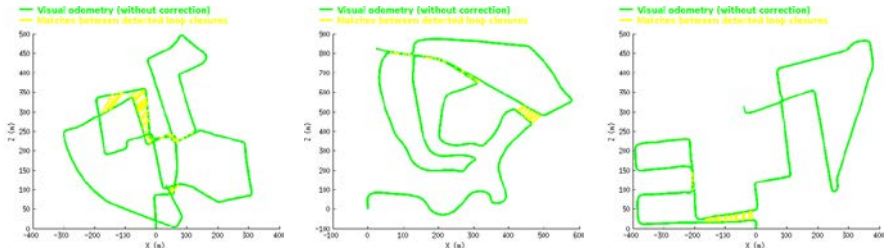

(a) Sequence 00 (b) Sequence 02 (c) Sequence 08

Fig. 3. Results for loop closure detection in the KITTI dataset.

Finally, Fig. 6 evidences the better accuracy of our proposal based on a visual odometry with loop closure corrections, where it can be seen how the drift is reduced with respect to the original visual odometry.

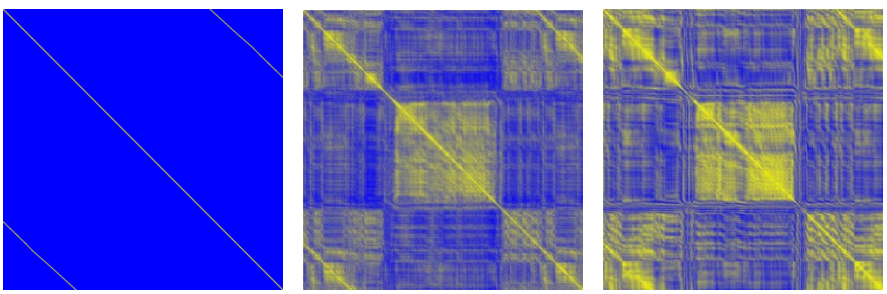

(a) M ground-truth (b) M using LDB (c) M using AKAZE

Fig. 4. Examples of distance matrices from the Sequence 06 of the KITTI dataset.

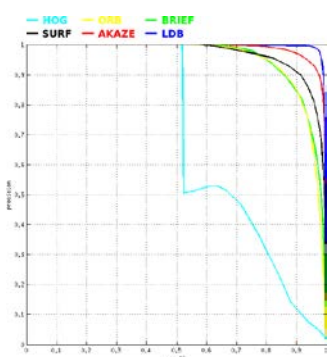

Fig. 5. Precision-recall curves obtained for the Sequence 00 of the KITTI dataset.

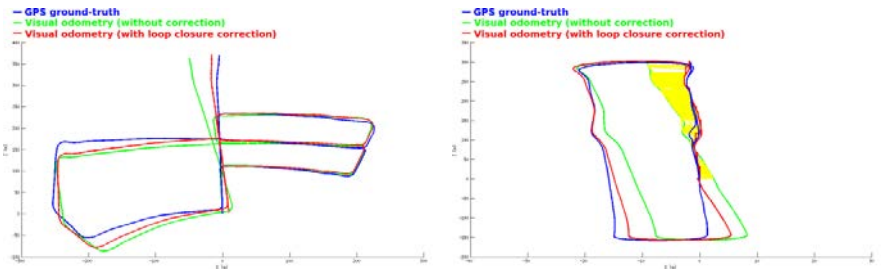

(a) Sequence 05 (b) Sequence 06

Fig. 6. Results for visual odometry with loop correction in the KITTI dataset.

6 Conclusions and future works

In this work, we have defined and validated our system based on a robust visual odometry estimation using loop closure corrections. The results exposed along the paper demonstrate the benefits of this proposal, such as the visible reduction of the progressive drift accumulated along the time.

The contributions presented can be divided into three main areas. First of all, the implementation of the initial stereo visual odometry system based on LIBVISO. Secondly, the application of ABLE for loop closure detection, including a new approach based on AKAZE features. Finally, the formulation of a complete method for correcting the visual odometry estimations using the information about the loop closures detected.

In future works, we plan to improve our visual odometry model using optimizations based on algorithms such as Levenberg-Marquardt.

Acknowledgements

This research has received funding from the Spanish MINECO through the project Smart Elderly car (TRA2015-70501-C2-1) and the RoboCity2030-III-CM project (Robótica aplicada a la mejora de la calidad de vida de los ciudadanos. Fase III; S2013/MIT-2748), funded by Programas de Actividades I+D en la Comunidad de Madrid and cofunded by Structural Funds of the EU.

References

Alcantarilla, P. F., Nuevo, J., and Bartoli, A., 2013, “Fast explicit difusion for accelerated features in nonlinear scale spaces," in British Machine Vision Conference (BMVC), pp. 1-13.

Arroyo, R., Alcantarilla, P. F., Bergasa, L. M., Yebes, J. J., and Bronte, S., 2014, “Fast and effective visual place recognition using binary codes and disparity information," in IEEE/RSJ International Conference on Intelligent Robots and Systems (IROS), pp. 3089-3094.

Bailey, T., and Durrant-Whyte, H., 2006, “Simultaneous Localisation And Mapping (SLAM): Part II State of the art,” IEEE Robotics and Automation Magazine (RAM), 13(3): 108-117.

Bay, H., Ess, A., Tuytelaars, T., and Van Gool, L., 2008, "Speeded-Up Robust Features (SURF)," Computer Vision and Image Understanding (CVIU), 110(3): 346-359.

Calonder, M., Lepetit, V., Strecha, C., and Fua, P., 2010, “BRIEF: Binary Robust Independent Elementary Features," in European Conference on Computer Vision (ECCV), pp. 778-792.

Dalal, N., and Triggs, B., 2005, "Histograms of Oriented Gradients for human detection," IEEE Conference on Computer Vision and Pattern Recognition (CVPR), vol. 2, pp. 886-893.

Geiger, A., Lenz, P., Stiller, C., and Urtasun, R., 2013, "Vision meets robotics: The KITTI dataset," International Journal of Robotics Research (IJRR), 32(11): 1231-1237.

Kitt, B., Geiger, A., and Lategahn, H., 2010, “Visual odometry based on stereo image sequences with RANSAC-based outlier rejection scheme," in IEEE Intelligent Vehicles Symp. (IV), pp. 486-492.

Nister, D., Naroditsky, O., and Bergen, J., 2004, "Visual odometry," in IEEE Conference on Computer Vision and Pattern Recognition (CVPR), vol. 1, pp. 652-659.

Rublee, E., Rabaud, V., Konolige, K., and Bradski, G., 2011, "ORB: An efficient alternative to SIFT or SURF," in International Conference on Computer Vision (ICCV), pp. 2564-2571.

Scaramuzza, D., Fraundorfer, F., and Siegwart, R., 2009, “Real-time monocular visual odometry for on-road vehicles with 1-point RANSAC,” in IEEE International Conference on Robotics and Automation (ICRA), pp. 4293-4299.

Yang, X., and Cheng, K. T., 2012, “LDB: An ultra-fast feature for scalable augmented reality on mobile devices," in International Symposium on Mixed and Augmented Reality (ISMAR), pp. 49-57.

CHAPTER 13

OBJECT PERCEPTION APPLIED TO DAILY LIFE ENVIRONMENTS FOR MOBILE ROBOT NAVIGATION

A. C. HERNÁNDEZ, C. GÓMEZ, J. CRESPO and R. BARBER

RoboticsLab, Universidad Carlos III de Madrid,
alejandracarolina.hernandez@alumnos.uc3m.es, claragobla@gmail.com,
jocrespo@ing.uc3m.es, rbarber@ing.uc3m.

To move around the environment, human beings depend on sight more than their other senses, because provides information about the size, shape, color and position of an object. The increasing interest in building autonomous mobile systems makes the detection and recognition of objects in natural environments is a very important and challenging task. In this chapter, a vision system to detect objects considering natural environments, able to work on real mobile robot is developed. This system is based on supervised algorithms of classification and as input, RGB and depth images are used. Different segmentation and feature extraction methods have been applied. The proposed system has been tested in a real mobile robot and the experimental results have demonstrated the usefulness of the system for detection and location of the objects in natural environments as well as to support navigation tasks in mobile robots.

1 Introduction

Robots need to have a set of capabilities that allows them to move and interact with a real environment. Among all the skills needed, perception constitutes one of the cornerstones. From the five different senses that humans have, vision is arguably the most important for safely moving and interacting with the world. Object detection is one important research topic in computer vision due to wide applications. Great advances have been made in the past decade, especially since the milestone work by (Viola et

al., 2001). Object recognition in real scenes is one of the most challenging problems in computer vision, as it is necessary to deal with difficulties such as viewpoint changes, occlusions, illumination variations, background clutter or sensor noise. Numerous methods for object recognition have been developed over the last decades. Some methods to object recognition are based on machine learning. Machine learning is a branch of computer science and applied statistics covering algorithms that improve their performance at a given task based on sample data or experience. Common algorithm types include supervised learning, where the algorithm generates a function that maps inputs to desired outputs. Support Vector Machines is a useful technique for data classification. The goal of SVM is to produce a model (based on the training data) which predicts the target values of the test data given only the test data attributes. Some researches like (Gupta et al., 2014) and (Lim et al., 2013) using SVM as classification algorithm combined with others.

On the other hand, among the most important stages of an object detection system are the image segmentation and feature extraction. There are many image segmentation techniques, some of them are based on colour as it does (Hernández et al., 2016) and (Hernández et al., 2012). There are approaches that use 3D information for point cloud segmentation (Meisner et al., 2011). Also, there are region growing techniques, as watershed (Beucher et al., 1979). In this work, segmentation techniques based on contours extraction and the watershed algorithm to segment the selected objects are implemented. Regarding feature extraction techniques, some researches shown the use of SURF (Bay et al., 2006) in object detection applied to indoor environment for mobile robot (Astua et al., 2014). Other techniques based on bag of words to object classification are presented in (Csurka et al., 2004).

2 Proposed system

In order to achieve the main goals of the work, a vision system to detect objects considering natural environments, it means without any modifications of the environment, and able to work on real mobile robot with the final goal to contribute with navigation tasks, place recognition and high level tasks of semantic navigation is developed. The proposed system is integrated into a real mobile robot, and a camera with specific characteristics as a sensor to images capture is used. The idea is to capture real-time images of natural environments, process, extract the features of the objects in the scene, then use a classifier to detect the object, to finally locate it in the

original scene. The proposed detection system is based on SVMs as algorithm classification. As input to this system RGB and depth images are used. The process implemented is depicted in Fig. 1, which is divided into three main stages: an offline stage to train the classifier, and two online stages, one for the preprocessing of the retrieved images and other where the object classification process is performed.

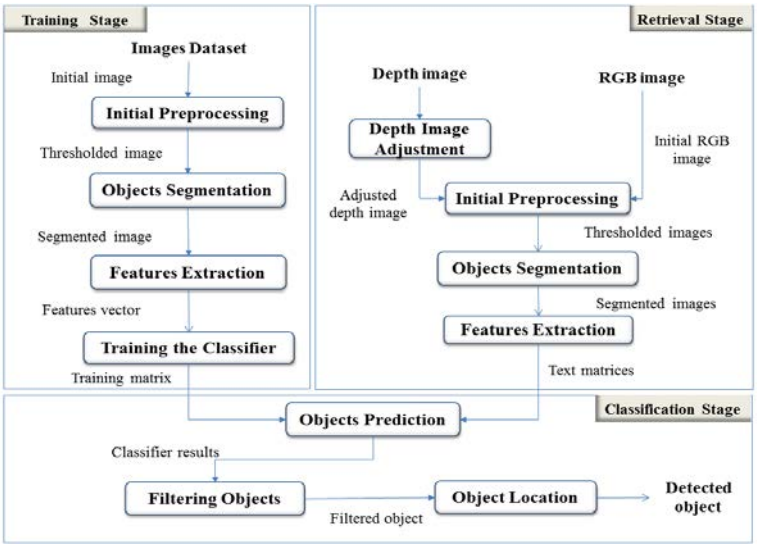

Fig. 1. Detailed diagram of the proposed system.

3 Image preprocessing

The first two stages of the proposed detection system are training stage and retrieval stage. The process begins with the preparation of a data set of images that contain the objects to be detected. This work focuses on the detection of three objects present in indoor environments: chairs, closets and screens. Fig.2 shows an example of the data set of images for closet object.

Fig. 2. Data set of class 1: Closets.

In the initial preprocessing different techniques as equalization, morphological operations, Gaussian filter and thresholding are used to get an image without noise, with better contrast and highlighted regions of interest. Regarding segmentation, the techniques are based on contours extraction, selection of regions of interest, Hough transform and an algorithm based on regions growing called watershed. Next, two alternatives to extract features of the objects are explored: geometric shape descriptors (solidity, extent, aspect ratio, circularity and a handle ratio) and bag of words. To complete this first stage, training matrices are created to train the classifier and the parameters of SVMs are defined.

In the retrieval stage, through the subscription to ROS topics camera/depth/image and camera/rgb/image, color real-time depth and RGB images are obtained. An adjustment process for depth images to remove noise and invalid pixels is performed. The same techniques for initial preprocessing, segmentation and features extraction in the training stage has been applied, with some variations to adapt them to the image preprocessing in real-time. In Fig. 3 segmentation process applied to RGB real-time image can be seen.

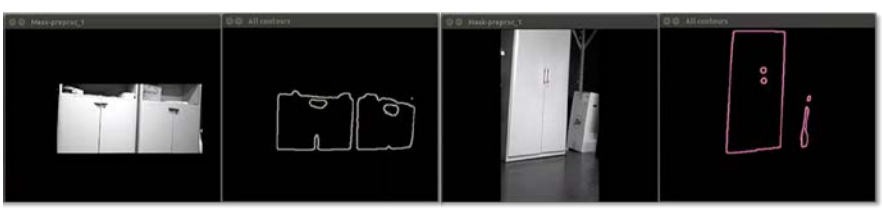

Fig. 3. Real-time RGB image segmentation.

4 Classification stage

The final stage consists of predicting the objects in the real-time images. The classification method used is Support Vector Machine. Two approaches for implementing the selected classification method are explored. The first using three SVMs for the prediction process one against all, and a second approach that uses a single SVM for the prediction process one against one. With the final results of each approach, the next step is the location of the object detected in the original image. To determine the distance to the detected object relative to the center of the camera, the coordinates of the center of mass are obtained from the RGB image to get corresponding distance in the depth image. The orientation relative to the center of the camera is computing by a simple linear interpolation. This information is encapsulated in a ROS message, which contains the name of

the detected object, distance from the center of the camera and the orientation angle. The name provides semantic information that supports higher-level reasoning and can be used for navigation decisions.

5 Experimental results

To evaluate the developed system, several tests have been performed to demonstrate its usefulness in the detection of the selected objects. Furthermore, through the comparison between the results obtained by applying two approaches in the prediction process and two features extraction techniques allows to determine which alternative offers better performance taking into account the proposed problem and the environment of the application.

The environment chosen for testing is a laboratory. The selected robot is a platform called TurtleBot. A camera ASUS Xtion Pro Live as a sensor for detection is used. To guarantee the hardware and software integration, the system is developed under the Robot Operating System (ROS), using C++ and OpenCV libraries. Additionally, to carry out the performance evaluation of the system, the concept of confusion matrix is used. Several measures can be obtained from this matrix. In this work, accuracy, misclassification, sensitivity and specificity are used.

First, preliminary tests for each object have been performed in order to determine the effective of the system separately. From the obtained results it can be concluded that the best accuracy is to closet object (78.07%), followed by chairs with 71.45% and finally, the screens with the lowest percentage of 65.47%. The findings of these tests have been taking into account to improve the proposed system to perform the successive tests.

The next test consists of the implementation of two approaches of classification. The method of features extraction based on shape descriptors is applied. Table 1 shows the evaluations performed applying one against all approach. The results of using a single SVM can be seen in Table 2.

Table 1. Evaluation of the system applying one against all approach.

Evaluations	Closets	Chairs	Screens
Model Accuracy	81.58%	72.79%	65.90%
Misclassification rate	18.42%	27.21%	34.10%
True positive rate	63.13%	66.10%	60.00%
True negative rate	100.00%	79.49%	71.79%

Table 2. Evaluation of the proposed system using a unique SVM.

Evaluations	Closets	Chairs	Screens
Model Accuracy	81.97%	76.56%	60.13%
Misclassification rate	18.03%	23.44%	39.87%
True positive rate	81.08%	100.00%	29.63%
True negative rate	82.81%	53.13%	90.63%

The results show that using a single SVM the model accuracy for closets and chairs improve slightly compared with using three SVMs. However, in case of the chairs, the sensibility reaches 100% and the specificity decreases from 79.49% to 53.13%. Regarding the screens, the misclassification rate increases from 34.10% to 39.87%.

Then, another test applying the method to features extraction based on bag of words in the proposed detection system has been performed. The results show that the model accuracy increases to the three selected objects, as following, from 81.58% to 85.42% closets, from 72.79% to 73.06% chairs and from 65.90% to 76.56% screens. The main reason for these results is the largest number of descriptors extracted on each image that makes the most robust classifier.

The last test consists of integrating the proposed detection system with a navigation system to evaluate the real-time functioning of both systems together. The navigation system receives the information of the detected object (name, distance and orientation angle), and in the case that this information corresponds to the desired one for the event, the robot moves towards that object. With this test, it can be said that the process of integration has been completed successfully and the navigation targets has been achieved. In Fig. 4 some results of this experiment are shown.

Fig. 4. Results of the integration of both systems.

6 Conclusions

In this work has been proposed to build a vision system able to detect and locate objects in natural environments that contributes to improving navigation system of mobile robots. To demonstrate the usefulness of the developed system, several experimental tests have been performed. From the results of the preliminary tests have been determined that the best accuracy is to closet object. Afterwards, results of experiments using different features extraction techniques and two approaches of classification show that using a single SVM the accuracy do not present major changes compared with using three SVM. However, this approach is not as suitable as when three SVMs are used. Probably to use a single SVM involves combinations of more robust features, especially in the case of the screen objects. The method to features extraction based on bag of words allows determine presence or absence of objects in the scene, nevertheless, for location is very difficult to find where the detected object is in the image. Furthermore, training stage is slower than using shape information due to higher number of features that are extracted. All the analysis conducted suggest that the best option for the detection of selected objects consists of three SVM, using shape descriptors such as feature extraction method. On the other hand, the integration process with a topological navigation system has been conducted successful and the navigation targets have been achieved. Finally, future works will be oriented to improve each object model through feature and integrating the developed system in a semantic navigation system.

Acknowledgements

The research leading to these results has received funding from the RoboCity2030-III-CM project (Robótica aplicada a la mejora de la calidad de vida de los ciudadanos. Fase III; S2013/MIT-2748), funded by Programas de Actividades I+D en la Comunidad de Madrid and cofunded by Structural Funds of the EU.

References

Astua C., Barber R., Crespo J. and Jardon A. 2014. Object detection techniques applied on mobile robot semantic navigation. Sensors 14(4):6734-6757.

Bay, H., Tuytelaars, T. & Van Gool, L. 2006. Surf: Speeded up robust features. In Computer vision - eccv 2006, pp. 404–417. Springer.

Beucher, S. & Lantuéjoul, C. 1979. Use of watersheds in contour detection. In International workshop on image processing, real-time edge and motion detection.

Csurka G., Dance C., Fan L., Willamowski J. and Bray C. 2004. Visual categorization with bags of keypoints. In Workshop on statistical learning in computer vision, ECCV, vol. 1, no. 1-22, pp. 1-2.

Gupta, S., Girshick, R., Arbeláez, P. & Malik, J. 2014. Learning rich features from rgb-d images for object detection and segmentation. In Computer vision. pp. 345–360. Springer.

Hernández, A. C., Gómez, C., Crespo, J. & Barber, R. 2016. A home made robotic platform based on theo jansen mechanism for teaching robotics. In Inted 2016.

Hernández-López, J.-J., Quintanilla-Olvera, A.-L., López-Ramírez, J.-L., Rangel-Butanda, F.-J., Ibarra-Manzano, M.-A. & Almanza-Ojeda, D.-L. 2012. Detecting objects using color and depth segmentation with kinect sensor. Procedia Technology, 3, 196–204.

Lim, J. J., Pirsiavash, H. & Torralba, A. 2013. Parsing ikea objects: Fine pose estimation. In Computer vision (iccv), pp. 2992-2999.

Meisner, P., Schmidt-Rohr, S. R., Lösch, M., Jäkel, R. & Dillmann, R. 2011. Robust localization of furniture parts by integrating depth and intensity data suitable for range sensors with varying image quality. In Advanced robotics, pp. 48–54.

Viola, P. & Jones, M. 2001. Rapid object detection using a boosted cascade of simple features. In Computer vision and pattern recognition, 2001. Vol. 1, pp. I-511.

CHAPTER 14

3D OBJECT RECOGNITION AND POSE ESTIMATION USING VFH DESCRIPTORS

A. LÁZARO, J. MORIANO, L.M. BERGASA, R. BAREA and E. LOPEZ

Robesafe group, Universidad de Alcalá, alberto2991lazaro@gmail.com

This paper presents the perception system involved in an application for grabbing objects in an industrial environment through a robotic arm by using 3D pointcloud images taken from a RGBD camera. This system recognizes and estimates the pose of the objects placed on the working area. It uses VFH descriptors and Kd-tree classifiers for the recognition and geometrical models and a RANSAC estimator for the pose estimation using this information. Some experimental results in a real environment validate our proposal.

1 Introduction

This work is focused on object recognition and pose estimation in industrial environments using a RGBD camera. This vision system is able to detect objects, recognize them and estimate their position offering the possibility of detecting important features which can be used to automate processes. This target can be achieved using RGB cameras but they have some drawbacks faced with depth cameras which will be explained hereafter. The stages that have to be completed by the vision system to provide the necessary data are segmentation, recognition, pose estimation and scene reconstruction. Segmentation identifies the interested objects to be grabbed. Once these objects are segmented they pass to the recognition algorithm. Shape estimator is used to recognize and obtain the position and orientation of the objects. Taking advantage of ROS communication facilities, the obtained data are published to be reconstructed thanks to RVIZ as it can be seen in Fig. 1.

Fig. 1. Captured environment and virtual reconstruction.

2 State of the art

Regarding to the topic of automatic objects classification, several projects have been carried out. Hereafter we show some of the most important. In (Bdiwi, 2012) a more complex classification process is developed, in this case the system is able to difference among books depending on their shapes and using alphanumeric codes. They use a CCD camera, it uses a rectangle to compare the different shapes. Another example for the object classification is included in (Li, 2014) using a depth sensor. In this work, a multilevel part-based object model was proposed using latent support vector machine as a core learning machine for training.

Our proposal, as difference with the above works, uses a depth camera for obtaining 3D Point Cloud images (Cruz,2012), (Rusu,2011) and then to recognize the shape of the different objects. It provides several advantages, the main ones are the use of an RGB-D camera and a better 3D reconstruction of the scene.

3 Object recognition method

The vision system must detect the objects placed in the working scene. So 3D pointcloud is clustered in foreground and background classes using depth. After that, foreground class is downsampled using Uniform Sampling algorithm named VoxelGrid filter before being clustered in objects.

The aim of clustering the foreground data is to divide an unorganized PCL into smaller parts, which contain the points that belongs to a same object (Muja, 2009). This clustering has been done relying on spatial decomposition techniques that find boundaries and subdivisions. The algorithm used is based on Euclidean distances.

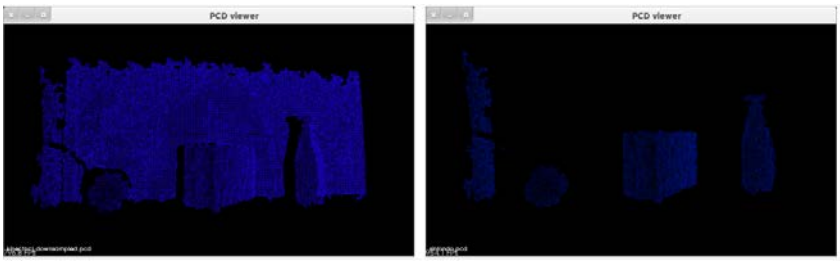

Fig. 2. Background extraction example: in the left image the original capture.

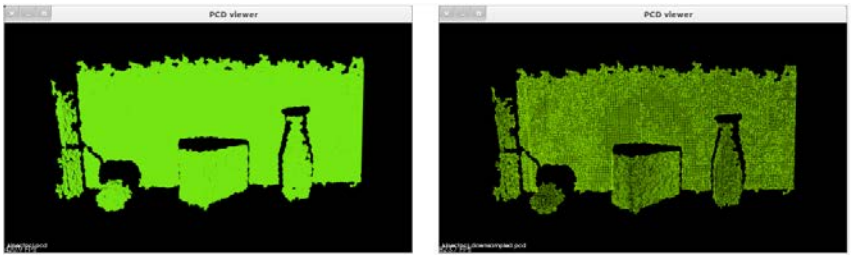

Fig. 3. Downsampling the captured scene example: the PCL depicted on the right.

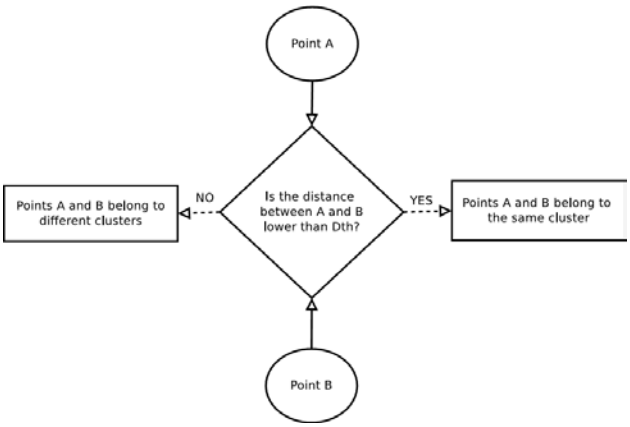

Fig. 4. Cluster extraction diagram: the algorithm works out the distance between two points, depending on this value the evaluated points are considered as part of the same cluster or as part of two different clusters according to the diagram.

Once the scene is clustered, is time to tackle the object recognition of the different objects placed in the scene (Rusu, 2010; Rusu, 2009). To carry out this recognition VFH descriptors, which is based on the FPFH descriptor, are used (Rusu, 2009; Rusu, 2008). This recognition consists in two processes:

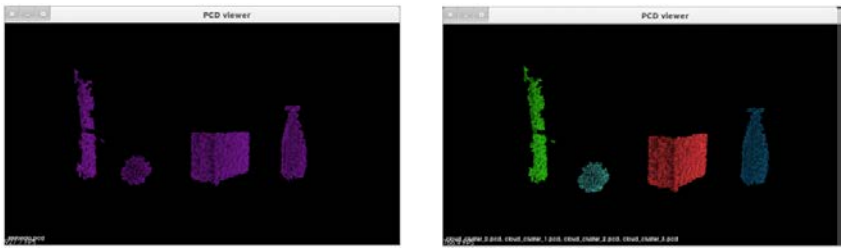

Fig. 5. Cluster extraction example: in the right image the points considered as part of the same cluster are represented in the same color.

3.1 Training process

The first step is to build a dataset that contains some captures (36 in our case) taken from different points of view for each object that is wanted to be recognized by the system and to calculate their VFH descriptor. This dataset is used to train the object recognition system. The training process builds a space-partitioning data structure that stores a set of K-dimensional points in a tree structure that enables efficient range searches and nearest neighbor searches called Kd-tree (Rusu, 2008), (Salti, 2011).

Fig. 6. Objects employed to build the dataset. Each object represents a sample of the three classes needed in this work: ball can and milk (from left to right).

3.2 Testing process

This process compares VFH descriptors for each of the segmented objects extracted from the captured scene and the ones that are saved in the training dataset through K-Nearest neighbors algorithm(k-NN) (Muja, 2011). The result of this comparison is a set of index which values are inversely proportional to the likeness between the analyzed cluster and each element of the dataset (Bariya, 2010). These index are provided to a voting method to determine the class among the trained classes which belongs to the unknown object if the analyzed object belongs to one of the trained classes. If so, the voting system classifies it.

Fig. 7. Example of the testing process: the input used in this working example is one of the PCLs of the dataset.

4 Pose estimation method

Once each of the elements placed in the working scene are recognized, the coefficients that determine their position and orientation are recovered by using RANdom SAmple Consensus (RANSAC). RANSAC algorithm is usually employed to carry out in objects recognition approaches when the set of objects to be distinguished have different shapes (Schnabel, 2007), (Papazov, 2010), but in this work it has been used just for estimating the pose of the objects and their dimensions.

Three models (sphere, cylinder, plane) jointly with their RANSAC estimators are used to estimate the parameters that defines the pose and the dimensions of the different objects (balls, cans, milk cartons) (Aldoma, 2012), (Mishra,2011). To estimate the dimensions of the carton box once the different planes have been estimated geometric constraints are applied.

5 Perception system experiments

The following tests have been carried out to measure the power of the designed vision system evaluating different aspects such as time costs or percentage success. Hereafter we present the different tests carried out to evaluate our vision system performance regarding the processing time an object recognition results. The first experiment tests the performance of our objects recognition system for 5 different objects of each class not

used in the training process. As it can be seen in Table 1 the correct recognition ratio is close to 100%.

Table 1. Object recognition results: index shown are the returned by the system.

Object/Candidate	Ball	Can	Milk carton
Ball	100%	0%	0%
Can	1%	95%	4%
Milk carton	1%	5%	94%

The object recognition system runs in a computer with Intel Core i7 CPU 860 @ 2.8GHz x8} processor. Table 2 evaluates the different processing time depending on the recognized elements

Table 2. Object recognition processing times.

Object	No. balls	No. cans	No. Cartons	Time costs
Test 1	1	0	0	190ms
Test 2	2	0	0	275ms
Test 3	3	0	0	410ms
Test 4	0	1	0	345ms
Test 5	0	2	0	650ms
Test 6	0	0	1	890ms
Test 7	1	1	0	515ms
Test 8	1	1	1	1345ms

Fig. 7 shows the results extracted from all tests to determine the dimension, position and orientation errors through the mean and the deviation for the different primitive shapes measured in meters.

6 Conclusions and future work

This paper has addressed the object recognition, pose estimation and dimensions appraisal. Due to the real time constraints geometric restrictions, VFH descriptors and a Kd-tree classifier have been applied over the 3D point cloud images. Object pose estimations are precise enough for a robot to interact with them. The vision system algorithm could provide a robotic system the information needed to move or avoid objects. Although we have presented a real time solution for the addressed problem we will go

on working on reducing the processing time in order to make our system able to recognize objects faster than a human.

Acknowledgements

This work was supported in part by the MINECO SmartElderlyCar (TRA2015-70501-C2-1-R) project and by the RoboCity2030 III-CM project (S2013/MIT-2748) funded by Programas de I+D en la Comunidad de Madrid and cofunded by Structured Funds of the UE.

References

Aldoma, A., Marton, Z.-C., Tombari, F., Wohlkinger, W., Potthast, C., Zeisl, B., Rusu, R.B., Gedikli, S., Vincze, M., 2012. Tutorial: Point Cloud Library: Three-Dimensional Object Recognition and 6 DOF Pose Estimation. IEEE Robot. Automat. Mag.

Bariya, P., & Nishino, K. (2010, June). Scale-hierarchical 3d object recognition in cluttered scenes. In Computer Vision and Pattern Recognition (CVPR), 2010 IEEE Conference on (pp. 1657-1664). IEEE.

Bdiwi, M., & Suchý, J. 2012. Robot control system with integrated vision/force feedback for automated sorting system. In Tech. for Practical Robot Applications (TePRA), 2012 IEEE Int. Conf. on (pp. 31-36). IEEE.

Cruz, L., Lucio, D., & Velho, L. 2012. Kinect and rgbd images: Challenges and applications. In Graphics, Patterns and Images Tutorials (SIBGRAPI-T), 2012 25th SIBGRAPI Conference on (pp. 36-49). IEEE.

Li, K., & Meng, M. 2014. Robotic object manipulation with multilevel part-based model in RGB-D data. In Robotics and Automation (ICRA), 2014 IEEE International Conference on (pp. 3151-3156). IEEE.

Mishra, A. K., & Aloimonos, Y. (2012). Visual segmentation of “simple” objects for robots. Robotics: Science and Systems VII, 1-8.

Muja, M., & Lowe, D. G. 2009. Fast Approximate Nearest Neighbors with Automatic Algorithm Configuration. VISAPP (1),2, 331-340.

Muja, M., Rusu, R. B., Bradski, G., & Lowe, D. G. (2011, May). Rein-a fast, robust, scalable recognition infrastructure. In Robotics and Automation (ICRA), 2011 IEEE Intern.l Conference on (pp. 2939-2946). IEEE.

Papazov, C., & Burschka, D. (2010). An efficient RANSAC for 3D object recognition in noisy and occluded scenes. In Computer Vision–ACCV 2010 (pp. 135-148). Springer Berlin Heidelberg.

Rusu, R. B., Blodow, N., & Beetz, M. 2009. Fast point feature histograms (FPFH) for 3D registration. In Robotics and Automation, 2009. ICRA'09. IEEE International Conference on (pp. 3212-3217). IEEE.

Rusu, R. B., Bradski, G., Thibaux, R., & Hsu, J. 2010. Fast 3d recognition and pose using the viewpoint feature histogram. In Intelligent Robots and Systems (IROS), 2010 IEEE/RSJ Intern. Conf. on (pp. 2155-2162). IEEE.

Rusu, R. B., Holzbach, A., Beetz, M., & Bradski, G. 2009. Detecting and segmenting objects for mobile manipulation. In Computer Vision Workshops (ICCV WS), 2009 IEEE 12th Int. Conf. on (pp. 47-54). IEEE.

Rusu, R. B., Marton, Z. C., Blodow, N., & Beetz, M. 2008. Learning informative point classes for the acquisition of object model maps. InControl, Automation, Robotics and Vision, 2008. ICARCV 2008. 10th International Conference on (pp. 643-650). IEEE.

Rusu, R. B., Marton, Z. C., Blodow, N., & Beetz, M. 2008. Persistent point feature histograms for 3D point clouds. In Proc 10th Int Conf Intel Autonomous Syst (IAS-10), Baden-Baden, Germany (pp. 119-128).

Rusu, Radu Bogdan and Cousins, Steve. 2011. 3D is here: Point Cloud Library (PCL). ICRA.

Salti, S., Tombari, F., & Stefano, L. D. 2011. A performance evaluation of 3d keypoint detectors. In 3D Imaging, Modeling, Processing, Visualization and Transmission (3DIMPVT), 2011 Intern. Conf. on (pp. 236-243). IEEE.

Schnabel, R., Wahl, R., & Klein, R. (2007, June). Efficient RANSAC for point-cloud shape detection. In Computer graphics forum (Vol. 26, No. 2, pp. 214-226). Blackwell Publishing Ltd.

CHAPTER 15

INERTIAL-VISUAL ODOMETRY ON MOBILE DEVICES

R.S. NUÑEZ CRUZ and J.M. IBARRA ZANNATHA

Automatic Control Department CINVESTAV, rnunez@ctrl.cinvestav.mx, jibarra@cinvestav.mx

On this paper we present a novel and simple approach to estimate ego-motion using inertial sensors and monocular cameras included on mobile devices. The presented algorithm uses inertial measurements to estimate camera's position and attitude on a defined time interval. This movement is used to calculate an initial estimation of the Fundamental Matrix, then guided feature matching is performed and resulting information is used to optimize the initial motion estimation by minimizing the reprojection error. The difference of motion before and after optimization is used to correct inertial sensor's drift over time. The experimental results show acceptable performance on drift compensation and scale estimation on real time implementations.

1 Introduction

Data fusion of information from digital cameras and inertial sensors has become very popular in robotics with applications on autonomous navigation (Tkocz, 2014) and mapping (Tanskanen, 2013), due to the small size and weight of the sensors, as well as its low energy requirements, these algorithms are the preferred option on GPS-denied environments, successful implementations are often more common on humanoids, MAV's (Anderse, 2007) and UAV's.

Visual-Inertial data fusion is motivated by the complementary properties of these two kind of sensors (Martinelli, 2014): Visual information produces good estimation at low speed motion but its accuracy decays on high speed motion due to blur effects, on the other hand inertial sensors offers

good estimations on high speed motions but they tend to accumulate drift due to offset integration. The selected data fusion algorithm should consider these deficiencies in order to produce a useful and accurate solution.

Nowadays commercial smart phones are provided with these two sensors on board, becoming an attractive platform for new applications such as people tracking and 3D reconstruction. On the other hand the short memory and process capability of these devices limit the complexity of the algorithms that can be implemented on line.

In this paper we propose a visual-aided inertial odometry algorithm for a wide variety of mobile devices, like a humanoid, MAV or a smart phone. Then, we consider an architecture including a monocular camera and an Inertial Measurement Unit (IMU) with a 3-axis accelerometer and a 3-axis gyroscope.

We consider that the IMU's frame rate is high enough compared with the camera's frame rate so it is possible to have enough inertial samples to estimate motion in the time interval between successive images.

The rest of the paper is organized as follows: we discuss the proposed algorithm overview on section 2 including a calibration step, data fusion, and offset compensation. On section 3 we discuss motion estimation using inertial measurements which involves the estimation of gravity direction and magnitude to extract linear acceleration values from IMU data. We also define the method used to calculate Fundamental Matrix (FM) from motion estimation.

Section 4 describes how to use the FM to define a search window in order to reduce the time used to match points. We also present the use of the Reprojection Error to refine the initial motion estimation and to calculate the offset of inertial sensors. Section 5 presents experiments results obtained of our implementation on an Android device. Finally conclusions and future work are presented on section 6.

2 Algorithm Overview

The proposed algorithm estimates the movement of a device incrementally by using IMU signals and visual information. Here the IMU is the main sensor where, by integration is possible to estimate the device pose, while the visual information is used to refine the initial estimation and to adaptably calculate the IMU offsets (Fig. 1).

For each iteration the input of the algorithm is a pair of images and the IMU signals recorded during the time interval used to get the images. An

iteration starts by calculating the change of position X and attitude θ of the device.

The Fundamental Matrix F_0 is then calculated by using the position of the device at the time the pair of images was taken. Using the epipolar restriction is possible to define a search window in the process of find matches $\{x_i \leftrightarrow x_i'\}$ which reduces computation time and false correspondences. Optionally a RANSAC block can be added to eliminate possible outliers.

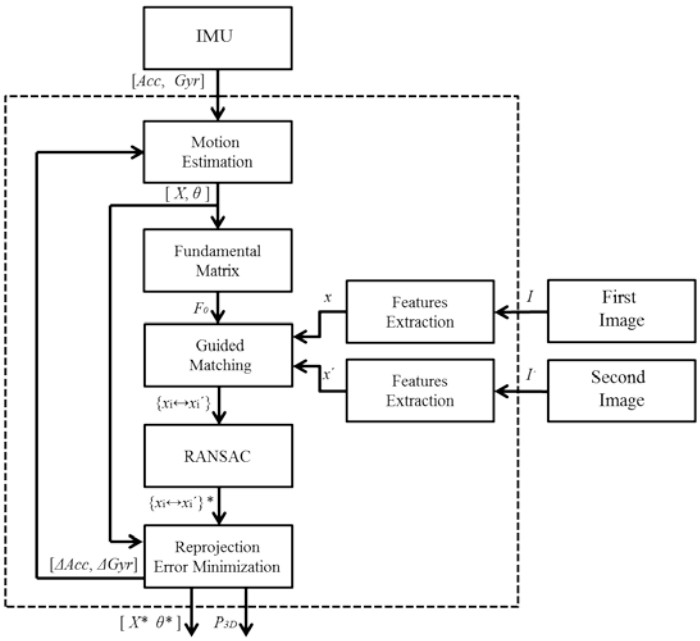

Fig. 1. Algorithm Flow Chart.

Sensor Fusion is accomplished by minimization of the reprojection error which is the difference between the coordinates of each feature on the image and the projection of the 3D position of the feature to the image plane. The reprojection error can be described in function of the position of the cameras so by using the initial estimation [X θ], and from the inertial measures is possible to obtain a refined [X^* θ^*] estimation.

By using the difference between the initial and the final estimation of the pose of the device is possible to estimate the bias of the IMU sensors in order to correct offset values.

The output of each iteration is the refined position estimation and the 3D position of the detected features.

2.1 Calibration step

As we choose IMU as the main sensor on our application, it is important to identify the corresponding offset values to obtain a robust approximation. We began with a calibration step to get an initial estimation of these values. The user will be asked to align the screen of the Android device to each one of the 3 axis and remain steady for some seconds (Fig. 2), the samples recorded under this process will be used to identify the average value of the offsets for the six variables of the IMU.

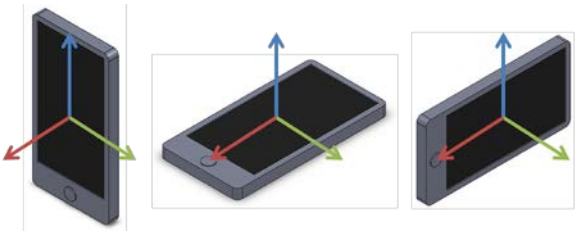

Fig. 2. Calibration step.

3 Motion from Inertial Measurements

IMU signals are generally perturbed by noise η and offset Δ values that produce drift when integrated, we represent this as follows:

$$\begin{aligned} Acc &= \ddot{X} + \Delta Acc + \eta Acc + G \\ Gyr &= \dot{\theta} + \Delta Gyr + \eta Gyr \end{aligned} \tag{1}$$

Must of the current algorithms deals with noise by using some sort of filter, usually these filters use the current measure and the value previously calculated (low pass filter or Kalman filter) in order to produce a filtered value for each new measure produced by the sensor.

In our implementation the movement is calculated only after a new image frame is available, at that time is possible to access a vector of several IMU samples, all this information can be used to eliminate noise at the same time by using a curve fitting algorithm.

Offset can be difficult to compensate in IMU signals, because it depends on time and temperature of the sensor, when using Kalman filters the offset can be estimated on each iteration, only if an accurate model of uncertainty is available (Aksoy, 2014). On our implementation offset values are

calculated as a function of the difference between the initial pose, obtained using IMU signals, and the correct pose, using visual information.

In the case of accelerometer signals it is also necessary to compensate gravity vector *G*, which can be found by rotating the gravity vector in the global frame to the IMU frame according to the device attitude. By using the next expression:

$$G = \left(R_x(\theta_1)R_y(\theta_2)R_z(\theta_3)\right)^T g\hat{z} \tag{2}$$

Where $R_i(\theta)$ represent a rotation matrix of an angle θ in the *i* axis, *g* is the magnitude of gravity and $\hat{z}$ is a unitary vector in the *z* axis. After this considerations position and attitude can be found by integrating the signals $\ddot{X}$ and $\dot{\theta}$.

3.1 Fundamental Matrix from camera pose

The fundamental matrix is the algebraic representation of the epipolar geometry which relates the coordinates of corresponding features from two different images. The fundamental matrix can be estimated in different ways, for example by using the normalized eight-point algorithm or by using the camera positions.

In the latter case we consider the first camera to be located at the origin so the position of the second camera is defined by *X* and the rotation matrix is $R(\theta) = R_x(\theta_1)R_y(\theta_2)R_z(\theta_3)$, then the fundamental matrix *F* is described as follows:

$$F = \left[X\right]_x R(\theta) \tag{3}$$

Where the operator $\left[v\right]_x$ represents the 3x3 skew symmetric matrix of vector *v* used to represent cross products as matrix multiplications.

4 Refinement using Visual Information

The relation between the homogenous image coordinates *x* and x' of a point correspondence and the fundamental matrix is described as follows:

$$x'^T Fx = 0 \tag{4}$$

Here *Fx* describes the epipolar line on which the corresponding point x' on the other image must lie, so it is possible to define a search window based on the intersection of a window centered at the coordinates of the point x with area r^2 and the region constructed for all the pixel whose distance to the epipolar line is $\leq d_{\min}$.

On this region, correspondence points will be selected based on the similarity of their descriptors.

4.1 RANSAC

Although the use of guided matching reduces the occurrence of outliers by spatial restrictions it is recommended to add a RANSAC step to eliminate false correspondence caused by occlusion or change of luminosity.

It is important to ensure outliers elimination so it is possible to assume that the difference between the pose estimations before and after refinement is caused by the error in offset estimation.

4.2 Reprojection Error Minimization

The proposed algorithm in this section is used to refine the pose estimation obtained from IMU signals by considering the restriction of the epipolar geometry. The method is based on the *Gold Standard* (Hartley, 2004) algorithm but the reprojection error is minimized over the relative position of the cameras.

Objective

Given an initial approximation of the relative pose of the cameras [X_0 θ_0] and correspondence points $\{x_i \leftrightarrow x_i'\}$ find the refined approximation [X^* θ^*] which minimize reprojection error:

$$r_e = \sum_i d(x_i, \hat{x}_i)^2 + d(x_i', \hat{x}_i')^2$$

Algorithm

(i) Define camera matrices $C = [I \mid 0]$ and $C' = [R(\theta) \mid X]$

(ii) Using $\{x_i \leftrightarrow x_i'\}$ and matrices *C*, *C´* find 3D Points P_i^{3D} by triangulation.

(iii) Calculate the reprojected points: $\hat{x}_i = CP_i^{3D}$, $\hat{x}_i' = C'P_i^{3D}$

(iv) Minimize r_e using Levenberg-Marquat algorithm over the posem $[X_k \quad \theta_k]$

Algorithm. 1. Sensor Fusion.

The 3D coordinates of the matched points $P^{3D}*$ can be used to provide a map of the environment seeing during the trajectory, also the pose correction can be used to update offset estimation by using the following rule:

$$\begin{aligned} \Delta Acc^{k} &= \Delta Acc^{k-1} - \alpha\left(X* - X_0\right) \\ \Delta Gyr^{k} &= \Delta Gyr^{k-1} - \alpha\left(\theta* - \theta_0\right) \end{aligned} \tag{5}$$

Where $\alpha > 0$ is a constant used as a feedback gain to regulate the offset values of the IMU model.

5 Experiments

The proposed algorithm was implemented on a commercial Android device, the camera was set to provide frames at 1fps and the IMU provide information 20 times faster, the algorithm was programed using threads which allow the system to record new measurements while processing the information of the previous iteration.

The experimental results (Fig. 3.) were obtained by moving the Android device over a textured scene, the plot shows the estimated trajectory of the device which error measurement is below 5% of the total trajectory length. These results were obtained at relative low speeds because the presence of blurring effects the estimation of the IMU offset causing divergence of the algorithm.

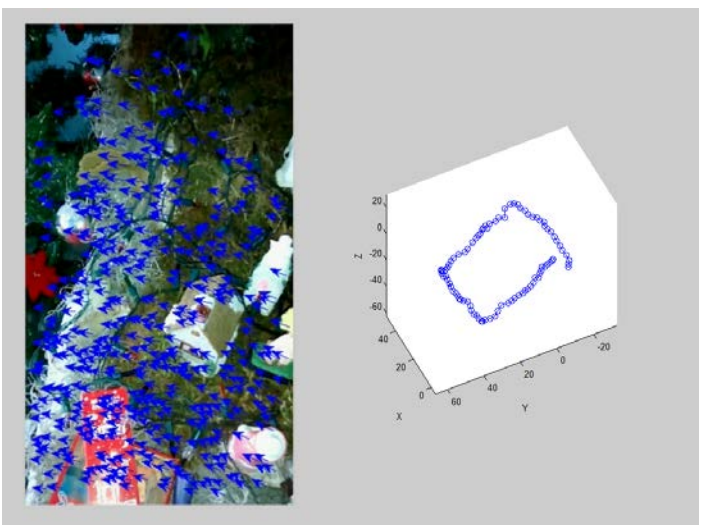

Fig. 3. Experiment Results.

6 Conclusions and Future Work

The proposed algorithm shows a novel alternative to filters in the process of fusing information from IMU sensors and cameras, although the algorithm works fine some optimization can still be made to increase the processing speed, it is also necessary to detect blurring to prevent error to be transmitted to offset estimations. Another improvement will be to add Magnetometer measurements to improve attitude estimation (Tian, 2013) We are also working on the construction of the map by using the estimated 3D localization of the features. To increase the image rate we must optimize de algebraic operations like in our previous applications.

References

Aksoy, Y., Aydin, A. 2014. Uncertainty modeling for efficient visual odometry via inertial sensor on mobile devices, in Proc. Int Conf. on Image Processing, Paris, France, pp. 3397-3401.

Anderse, E.D., Taylor, C.N. 2007. Improving MAV Pose Estimation Using Visual Information, in Proc. Int. Conf. on Intelligent Robots and Systems ,San Diego, CA, USA, pp. 3745-3750.

Hartley, R., Zisserman. 2004. Multiple View Geometry in Computer Vision. Cambridge University Press, New York.

Martinelli, A. 2014. Visual-inertial structure from motion: observability vs minimum number of sensors, in Proc. Int Conf. on Robotics & Automation, Hong Kong, China, pp. 1020-1027.

Tanskanen, P., K. Kolev. 2013. Live Metric 3D Reconstruction on Mobile Phones, in Pro. Int. Conf. on Com. Vis, Sydney, Australia, pp. 65-72.

Tian, Y., J. Zhang. 2013. Adaptive-Frame-Rate Monocular Vision and IMU Fusion for Robust Indoor Positioning, in. Proc. Int. Conf. on Robotics and Automation, Karlsruhe, Germany, pp. 2257-2262.

Tkocz, M., K. Janscheck. 2014. Closed-Form Metric Velocity and Landmark Distance Determination utilizing Monocular Camera Images and IMU Data in the Presence of Gravity, in Proc. Int. Conf. on Auto. Robot Sys. and Competitions, Espinho, Portugal, pp. 8-13.

CHAPTER 16

A NEW GENERATION OF ENTERTAINMENT ROBOTS ENHANCED WITH AUGMENTED REALITY

D. ESTEVEZ, J. G. VICTORES and C. BALAGUER

RoboticsLab, Universidad Carlos III de Madrid, destevez@ing.uc3m.es

While robots have been recently introduced in domestic environments to perform household chores, few robots are being used for entertainment, partially due to the lack of infrastructures for this purpose. In this paper, we propose an architecture that enables integrating interactive virtual elements in a robot-based gameplay. Several robot game concepts that may be enhanced with Augmented Reality are presented as guidelines toward the future of robot entertainment.

1 Introduction

Robotics and automation have been traditionally aimed towards improving our daily lives. From the static regime of industrial production, the past decade has seen these mechanisms subtly make their move towards our domestic environments, from motorized blinds to more sophisticated devices such as cooking helpers or robotic vacuum cleaners. While the original focus of these mechanisms has been to partially or fully automate difficult or tedious everyday tasks and chores, a subset of current household robots has been developed with a very different concept in mind: some for education, and some others for pure entertainment.

Robotics is capable of making difficult areas more appealing, even to the youngest and the elder. In entertainment, robotics has the potential to attract and engage players, entertaining in ways never dreamed of before. However, due to the intrinsic complexity of robotic systems, practical issues arise. Gameplay quality dramatically decreases as real-world issues such as sensor noise, actuator failure, and communication lag intervene. To

fill this gap, researchers and developers have been experimenting with Augmented Reality (AR) to present useful gameplay information, or even overlaying this on a transmission of the robotic systems' vision of the world, thus providing enhanced interaction and playability in entertainment.

2 Related work

This section will be dedicated to describe the state of the art of games that involve Augmented Reality (AR), and AR games that involve robots.

2.1 AR games

The first examples of AR games appeared in the context of research projects. One of the first examples of these games was developed by Ohshima et al., called AR2 Hockey (Ohshima, Satoh, Yamamoto, & Tamura, 1998). In this game, two players can play simultaneously in real-time a game of air hockey. A multiplayer AR racing game was presented by Oda et al. in (Oda, Lister, White, & Feiner, 2008). Fiducial markers define the game area, where several players can interact with the virtual racing car or the track, either by driving the car or by adding obstacles and waypoints.

Using techniques such as Parallel Tracking and Mapping (PTAM) to register the virtual objects over the real world, markerless AR games can be achieved, such as Ewok Rampage (Klein & Murray, 2007). This game can be played over any flat surface, both indoors and outdoors. The objective is to destroy the enemies before they reach the player. Other methods for makerless AR use 3D sensors and light projectors to overlay the virtual elements over the real world, and remove the need for the user to wear any display. Some applications exist using this method, such as IllumiRoom, which improves the game experience of existing games (B. Jones et al., 2014), or RoomAlive, an immersive game experience that projects a virtual world on top of the room (B. R. Jones, Benko, Ofek, & Wilson, 2013).

Due to the increase in performance of mobile devices such as smartphones and portable game consoles, the amount of commercial AR games available in the market has increased in the last years. They typically lack publications explaining their inner workings, apart from scarce online resources. Some examples of these games, that usually require one or more fiducial markers to achieve the augmentation, are Invizimals[1],

[1] http://invizimals.eu.playstation.com/, last accessed: May 16, 2016

Wonderbook[2] or AR Games[3]. The HoloLens[4], a Head-Mounted Display (HMD) being developed by Microsoft, is another development that, according to the information provided by the company, can work without fiducials for several applications such as games, designing art and engineering, and remote conferences.

2.2 AR robot games

A limited number of developments exist that achieve interaction between the AR-generated virtual elements and the real world elements. Even less mix AR with robots. Similar AR game developments to the concept presented in this work are the Parrot Drone quadcopter[5] and Sphero (Carroll & Polo, 2013) games. These games allow the user to teleoperate the robots from a mobile device, that overlays enemies or waypoints (depending on the game) on top of the video stream obtained from the on-board camera.

Our previous work, Robot Devastation (Estevez, Victores, Morante, & Balaguer, 2015) introduced the idea of multiplayer AR games with robots as the physical avatars of the players. It describes an AR game in which the player fights with a robot against other robots with virtual weapons, acquiring the robot's Point of View (POV) for the combat.

Lupetti et al. present a system in which people and a robot physically interact in a game (Lupetti, Piumatti, & Rossetto, 2015). Virtual elements are projected onto the playground to avoid the need for screens. The robot perform different roles (e.g. companion, adversary, avatar for a remote player) along each game.

3 Proposed architecture

In our previous work we envisioned an architecture in which the player has a First Person View of the world through a camera present in the robot. In this situation, the player can perceive the environment as if a miniature version of him was onboard in the robot. In this work we extend the existing architecture with a more general one, suitable for more kinds of game.

2 http://wonderbook.eu.playstation.com/, last accessed: May 16, 2016
3 http://www.nintendo.com/3ds/ar-cards, last accessed: May 16, 2016
4 https://www.microsoft.com/microsoft-hololens/, last accessed: May 16, 2016
5 http://ardrone2.parrot.com/usa/apps/, last accessed: May 16, 2016

The proposed system has three main parts, as seen in Fig. 1. One or several robots provide an interface for physical interaction with the world and other players. Virtual elements are created in the Player's PC using a Game Engine that uses an AR engine to calculate how the virtual elements are overlaid on top of the real world view. Cloud communications between robots and player PCs coordinate the game.

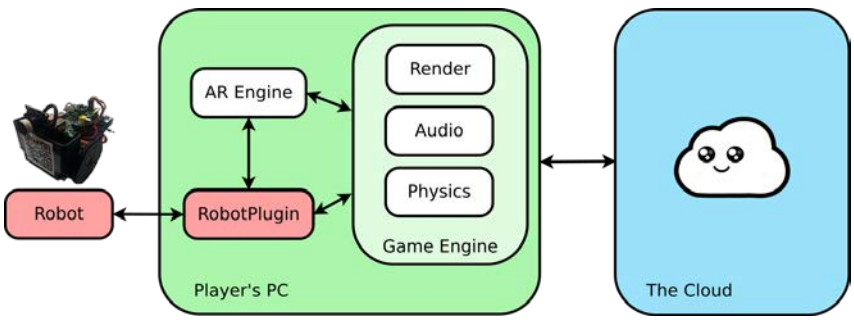

Fig. 1. The proposed architecture incorporates robot components (red).

3.1 Robots

The most basic robot architecture suitable for AR gaming includes one camera, wireless network hardware and some kind of motor to allow movement. Fig. 2 shows an example of basic robot platforms.

Fig. 2. Example of robots: current generation of Robot Devastation robots.

The camera obtains a view of the real world from the robot's POV, which is streamed wirelessly to the player. More than one cameras (or an RGB-D sensor) can be incorporated to the robot so that 3D information about the environment can be obtained, which also allows to provide a stereo video stream, which increases game immersion. The wireless connection is also used to teleoperate the robot and to send different commands.

Finally, the robot needs some means of achieving locomotion, that can be wheels, legs or just a pan-tilt mechanism.

With the recent increase in miniaturization and reduction in size of modern dedicated GPUs (e.g. NVIDIA Jetson[6]) and VPUs (Vision Processing Units) the robot could perform most of the computations related to detection and tracking of other robots, elements of the environment and, in general, to leverage the amount of processing required at the player's PC, allowing the use of smartphones as game interfaces.

3.2 Player's PC

AR games require virtual objects the user can interact with, which are displayed on top of the real environment. They also need to manage the interaction between the real elements, the virtual elements, and the user. To generate and manage these virtual elements, current existing game engines can be used, as they can render high-quality graphics and have physics engines able to simulate physical interactions between virtual elements.

In order to perform convincing registration between the real and virtual elements, an AR engine needs to be added to the game engine. The purpose of this AR engine is to locate and model the real environment and robots. Different techniques are available for performing this registration, including classical techniques, such as using fiducial markers, or more advanced markerless techniques, such as Parallel Tracking And Mapping (PTAM).

3.3 Cloud communications

Cloud communications, depicted in Fig. 3, are managed at the different levels: between the robot and the player, between robots, and between players. Communication between the robot and player include, as described in the previous section, one or more video streams and some channel to send commands and receive telemetry from the teleoperated robot. Communication between players allows sharing scores, placement of players, environment maps, actions, virtual NPCs, etc. Communication between robots manages different interactions between robots (e.g. hits, power-ups…).

6 http://www.nvidia.com/object/embedded-systems-dev-kits-modules.html last accessed May 16, 2016

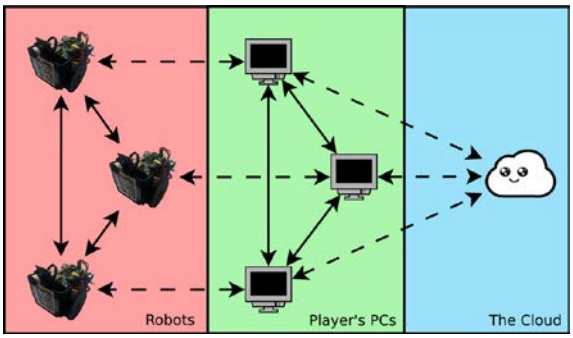

Fig. 3. Cloud communications share information across different layers.

4 Proposed games

The proposed architecture is general enough to allow different types of games. Some example games of combat, racing and sports are proposed in this section.

4.1 Robot Devastation (2.0)

Robot Devastation is an AR game that emulates robot combats (Fig. 4).

Fig. 4. Conceptual image of Robot Devastation 2.0 gameplay.

The player assumes the role of the robot pilot, as if he were sitting inside the robot cockpit, and battles against other robots. Weapons and projectiles, as well as bullets, fire, explosions and damage inflicted to the robots are simulated using AR. This prevents damage to the player, other people

around the robots, or the robots themselves, and at the same time it provides engaging gameplay. Virtual Non-Playing Character (NPC) autonomous robots can be added to balance teams or to increase game difficulty.

4.2 Augmented reality robot racing

Similar to the previous setting, where the player assumes the role of the racing robot pilot as if he were sitting inside the robot cockpit. Fiducial makers or elements from the environment can be set as waypoints to mark the race track. Augmented reality allows this track to be shown on top of the real world, and to include different power-ups or obstacles along the race. The player can race against other physical robots, against virtual robots, or against a mix of them, in different environments (land, water, air).

4.3 Augmented reality robot sports

This type of game allows the player to play a sport against other robot. Different sports may require more complex robot configurations, e.g. a mobile robot could play curling, whereas a humanoid robot would be required for playing volleyball or basketball. Popular robot competitions such as RoboCup could additionally benefit from incorporating AR, providing power-ups and secret items to unlock new features.

5 Conclusions

Most current AR games lack an embodiment of the agent. In practice, this leaves the environment physically "disconnected" from the virtual agents, and vice-versa. Certain AR games that involve robots have been recently developed. However, they are typically single or two player games, and present no multiplayer agenda. The authors believe that a new generation of entertainment robots, enhanced with augmented reality similar to the ones presented in this paper, will mark the future trends of robotics and entertainment.

Acknowledgements

This work has been supported by RoboCity2030-III-CM project (Robótica aplicada a la mejora de la calidad de vida de los ciudadanos. Fase III;

S2013/MIT-2748), funded by Programas de Actividades I+D en la Comunidad de Madrid and cofunded by Structural Funds of the EU.

References

Carroll, J., & Polo, F. (2013). Augmented reality gaming with sphero. In ACM SIGGRAPH 2013 Mobile (p. 17).

Estevez, D., Victores, J., Morante, S., & Balaguer, C. (2015). Robot Devastation: Using DIY Low-Cost Platforms for Multiplayer Interaction in an Augmented Reality Game. EAI Endorsed Transactions on Collaborative Computing, 15(3), 1–5.

Jones, B. R., Benko, H., Ofek, E., & Wilson, A. D. (2013). IllumiRoom: peripheral projected illusions for interactive experiences. In Proceedings of the SIGCHI Conference on Human Factors in Computing Systems (pp. 869–878).

Jones, B., Sodhi, R., Murdock, M., Mehra, R., Benko, H., Wilson, A., … Shapira, L. (2014). RoomAlive: magical experiences enabled by scalable, adaptive projector-camera units. In Proceedings of the 27th annual ACM symposium on User interface software and technology (pp. 637–644).

Klein, G., & Murray, D. (2007). Parallel Tracking and Mapping for Small AR Workspaces. 2007 6th IEEE and ACM International Symposium on Mixed and Augmented Reality, 1–10.

Lupetti, M. L., Piumatti, G., & Rossetto, F. (2015). Phygital Play. Intelligent Technologies for Interactive Entertainment (INTETAIN), 2015 7th International Conference on, 17–21.

Oda, O., Lister, L. J., White, S., & Feiner, S. (2008). Developing an Augmented Reality Racing Game. Proceedings of the 2nd International Conference on INtelligent TEchnologies for Interactive enterTAINment.

Ohshima, T., Satoh, K., Yamamoto, H., & Tamura, H. (1998). AR 2 Hockey: A case study of collaborative augmented reality. In Virtual Reality Annual International Symposium, 1998. Proceedings., IEEE 1998 (pp. 268–275).

CHAPTER 17

COMPARISON OF COLOR-BASED AND DEPTH-BASED VISION TECHNIQUES IN SURFACE DETECTION FOR HAND TRACKING

D. BAUTISTA, V. GARCÍA, J. M. COGOLLOR, J. M. SEBASTIÁN, M. FERRE and R. ARACIL

Centre for Automation and Robotics CAR (UPM-CSIC), José Gutiérrez Abascal 2, 28006 Madrid, Spain. E-mails: anabelle.bloza@alumnos.upm.es; victor.garciaver@alumnos.upm.es; jm.cogollor@upm.es; jose.sebastian@upm.es; m.ferre@upm.es; rafael.aracil@upm.es

This article focuses its objective in presenting the results obtained in the research done for surface detection using non-invasive vision-based techniques. Two different algorithms based on color and depth information, respectively, are compared to obtain the most optimal and accurate solution for the detection of a table surface. This detection will act as first stage to create a workspace for the monitoring of hands movement and object manipulation during handmade daily activities. The research has been carried out at the Centre for Automation and Robotics by using OpenCV libraries for image processing and sensor Kinect™, as a camera device. The main idea is to evaluate how a table can be properly detected and positioned in order to provide reliable information about the relative position of hands while preparing drinks or even food. Continuous and robust data of hands attitude is essential to analyze trajectories, even more considering cognitive rehabilitation techniques of those people who suffer from brain injuries. First of all, a short introduction to other works related in the field is done and the importance of hand kinematics in cognitive rehabilitation is also highlighted. Later, the current solution adopted is described to finally present the methodology followed, results and final conclusions.

1 Introduction

The detection, and even tracking of surfaces are a continuous field of research and reliable real-time solutions have been proposed up to now, moreover, in the robotics field (Pomares et al., 2008). Detection and tracking complement each other since motion trackers require an initialization stage for calibration. In addition, researchers have also worked on the tracking of deformable surfaces or objects, even considering self-occlusion (Pizarro and Bartoli, 2012). However, detecting non-rigid objects still lags behind and proposed methods are not convincing enough to be implemented in real-time applications.

In our case, the detection of a rigid surface such as a table additionally is used to support the tracking and monitoring of human hands movements for assessment of the execution of handmade tasks. More specifically, deep research has been also done on the skills for manipulating objects (Ferre, 2011). A wide range of methods for hand tracking have been created and need the presence of markers or cables to be attached to the body (glove-based devices). Moreover, there are systems based on the skin color and shape feature (Manresa, 2005). As these methods don't offer robustness enough when working with complex environments**,** vision-based techniques are chosen which are quite common nowadays.

The work presented here aims to make a decision on what kind of vision technique use, color based or depth based, for table detection. This detection means to know the position of the table thanks to the information about corners coordinates, edges recognition and consequently, the centre of the table.

The paper introduces the relevance of the hands movement capture in cognitive rehabilitation and the experimental platform used in Section 2 and 3, respectively. The methodology used and assessment of results obtained are shown in Section 4. Finally, Section 5 wraps up the main conclusions derived from this work.

2 The added value of hand tracking for cognitive rehabilitation purposes

The main difficulties people who suffer from stroke find in everyday tasks are related to sequence actions and recognise the tools usage so the level of dependence on caregivers or healthcare systems is so high they are not able to enjoy independent lives (Sunderland & Shinner, 2007).

Interpreting data on a patient’s movement in order to recognize the action and to determine if an action is correct, can be critically affected by

more elementary deficits of the patients in performing goal-directed movements.

The interpretation of attitude data of this kind of patients in order to recognize and determine the level of success of the execution of actions depends totally on the devices used for the capture of that data and the quality of it. Due to the behaviour of stroke patients, it is preferable not to influence the patients movements during the execution of the rehabilitation tasks so the use of a non-invasive (for example, vision based) technique is mandatory.

3 Experimental platform

3.1 Hardware architecture

The set up used for the experiments is shown in Fig. 1:

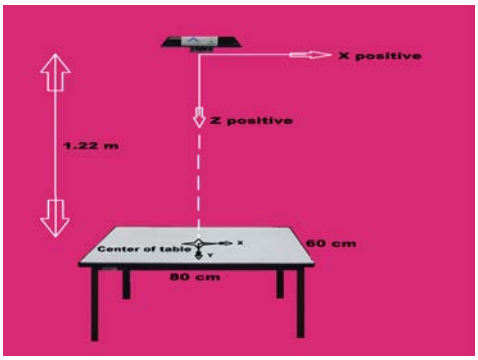

Fig. 1. Set up for evaluation.

The height of Kinect™ is optimal in order to make effective the detection and recognition stages. However, this height has a maximum value of 1.8 m to maintain the effectiveness of the software focused on the recognition. Anyway, Kinect™ must have the whole table always in the field of view so as bigger the table is as higher Kinect™ has to be located but at cost of resolution.

3.2 Software description

The development of the software based on OpenCV libraries has been implemented, as well as the tests performed, using Python 2.7 over a Linux

platform (Ubuntu). So, Libfreenect software from OpenKinect community has been used as drivers to manage the information provided by Kinect™.

3.2.1 Depth based processing

In order to have a structured environment to work and carry out a valid hand tracking, the first step is to make a proper table detection using the image of disparity provided by the IR sensor.

Kinect™ provides a 480x640 depth image where each pixel stores a measure of disparity in a raw format of 11 bits. So, bearing in mind that the table will occupy the majority of the space in the initial image, the first step has been to analyze the depth histogram in order to obtain the most common value. This value will be used as a mask to find where the table is placed. This first step makes possible to find flat square surfaces of different sizes and shapes in the picture.

To reduce the noise in the image, a filtering stage is performed. A Gaussian filter is used to smooth and reduce the detail in the image, whereas erosion and dilation filters are used to remove the smallest objects.

Finally, to get the figure of the real table, a filtering by size is performed according to a minimal area obtained by experimental results. The four corners of the square shape and the center of this have been found and represented in real time. Also the distances of these points have been calculated according to this post «Color/Depth Mapping».

3.2.2 Color based processing

In this case, a RGB frame captured by Kinect™ is transformed in HSV color space to obtain the histogram of the Hue component and later, the information of a greater amount of pixels corresponding to the same hue is extracted. Previously, a range of 20 values has been established as acceptable values for a flat color. From these values, a discrimination by color is carried out to segment the table from the rest of the scene. (Fig. 2A).

Once segmented, 3 erosions and 4 dilatations are applied, and a Gaussian filter for blurring and a canny detector to find the edges were also implemented. (Fig. 2B, Fig. 2C).

The next step was to find the contour, the area and perimeter of the space found, restricting it to a value greater than 1000 in the case of perimeter and more than 10000 for the area. This ensures that the space to be calculated is large enough and correspond to the table.

To verify that the procedure has the expected result, the outline of the table is drawn, the center and the corners are highlighted too. (Fig. 3B).

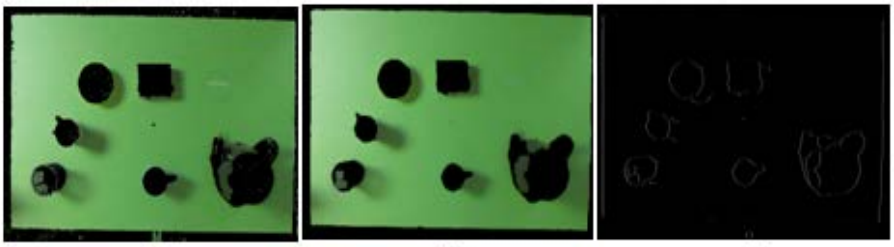

Fig. 2. Color processing. A) Color discriminate; B) Noise filters; C) Edges detection.

4 Experiments and results

The points that belong to the corners and the center of the table can be observed in Fig. 3. First of all, regarding the detection based on depth information, the original points obtained by the use of the IR camera have not an exact correspondence in the RGB image (due to the different calibration parameters: focal distances, distortion coefficients, the center of the image and the rotation and translation parameters). To make a mapping between depth and color pixels, initially, a re-projection has been done (Fig. 3A).

Fig. 3. Comparison of vision-based techniques for table detection. A) Depth-based algorithm; B) Color-based algorithm.

Also, through this calibration, the dimensional measures of any corner obtained have been evaluated. The variation of the corners measures and the real measure in 100 trials, can be observed in the Fig. 4, getting a typical deviation with respect to the real corner of 2,67 cm.

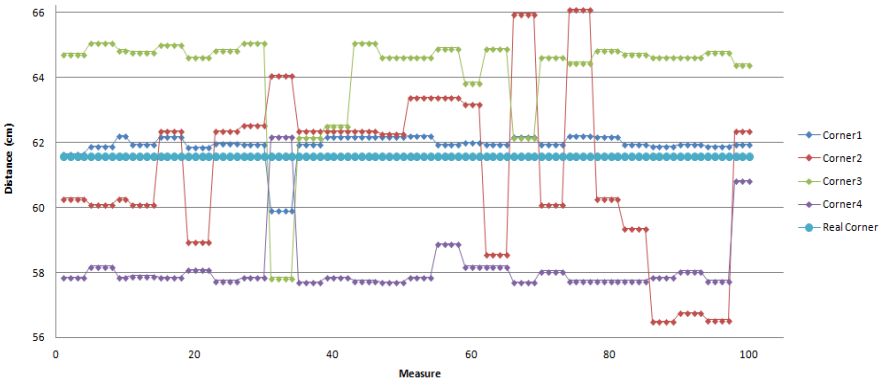

Fig. 4. Dimensional measures of corners.

In relation to assess the robustness of the discrimination technique by color, several tests have been carried out. The first one by holding and varying the positions of different colored objects over the table to observe the small variation of the area detected, whose average value is indicated in Fig. 5.

Fig. 5. Table detection with presence of colored objects.

Another test performed is focused on the color variation, with the aim of checking that the algorithm is able to recognize the surface regardless its color, orientation and light conditions. (Fig. 6)

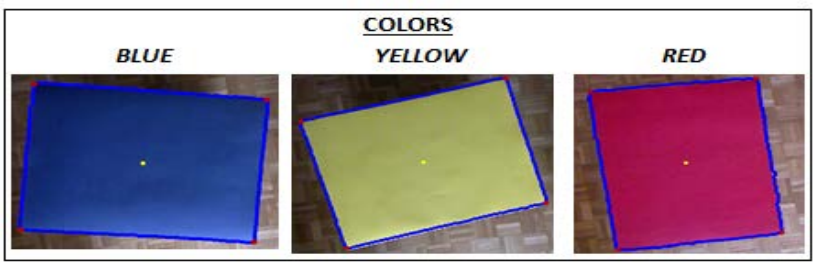

Fig. 6. Table detection with variance in color, orientation and lighting.

A final test has also been done to evaluate the permanence of pixels. For that purpose, a percentage of active points, maintaining the light conditions, is calculated. This value expresses the amount of active pixels detected in all the images that compose the sample, with respect to the pixels detected in, at least, one image. The results obtained in a sample of 100 images are presented in Fig. 7 and the value corresponds to 88.06%.

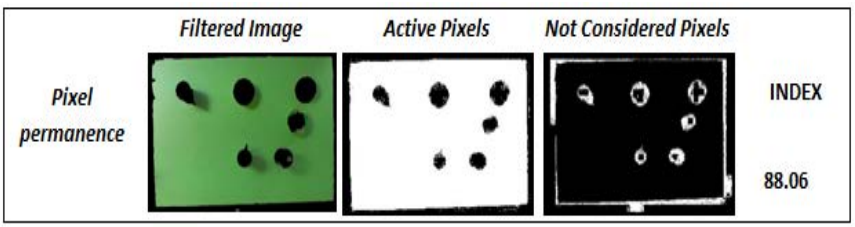

Fig. 7. Permanence of pixels and percentage of active points.

5 Conclusions

The aim of this paper has been to assess different vision-based techniques to detect the surface of a table containing certain objects, to serve as first step for a future hand tracking while manipulating them. This information could be used for user monitoring purposes, for example, in cognitive rehabilitation techniques.

Regarding the technique focused on color data processing, the area value detected practically remains the same when different colored objects are present over the table. Moreover, their position does not affect the detection.

As the color is very sensitive to light conditions, tests based directly on the pixel information are sensitive to changes, hence the dominant color variance reaches 11.8 in yellow, having the possibility of higher variance in red, for example.

Finally, the evaluation of permanence has resulted in a value of 88%, which means that 88% of pixels belonging to the table will be detected at each execution of the algorithm. Points having greater permanence are edges.

Meanwhile, the treatment of depth images is more robust to changes in lighting and provides good corners detection. However, it must be taken into account possible changes in the camera orientation, movements of the table or even curve surfaces for the quality of the detection.

As a future work, it is interesting to combine both techniques so that the shadows of objects and color sensitivity could be overridden by detecting depth, and likewise, the low height of objects and closer to the actual position of the corners could be reinforced by the color detection.

Acknowledgements

The research presented in this article has been supported by the European The Active Hands Project, from EIT Health-Call 2015 "Innovation by Ideas" and has received funding from the RoboCity2030-III-CM project (S2013/MIT-2748), funded by Programas de Actividades I+D en la Comunidad de Madrid and cofunded by Structural Funds of the EU.

References

«Color/Depth Mapping». [Online]. Available: https://openkinect.org/wiki/Imaging_Information. [Accessed: 20-apr-2016].

Ferre, M., Galiana, I., Wirz, R., and Tuttle, N. 2011. Haptic device for capturing and simulating hand manipulation rehabilitation, *IEEE/ASMET Trans. Mechatronics*, vol. 16, no 5, pp.808-815, Oct. 2011.

Manresa, C., Varona, J., Mas, R., Perales, F. 2005. Hand Tracking and Gesture Recognition for Human-Computer Interaction. Electronic letters on computer vision and image analysis 5(3), 96–104.

Pizarro, D. and Bartoli, A. 2012. Feature-based deformable surface detection with self-occlusion reasoning. Intl. J. of Computer Vision, 97(1):54–70.

Pomares Baeza, Jorge; García Gómez, Gabriel Jesús; Gil Vázquez, Gil Vázquez; Sebastian y Zuñiga, Jose Maria y Torres Medina, Fernando. 2008. Improving detection of surface discontinuities in visual-force control systms. "Image and Vision Computing", v. 26 (n. 10); pp. 1435-1447.

Sunderland, A. & Shinner, C. 2007. Ideomotor apraxia and functional ability. *Cortex,* 43*,* 359-367.

CHAPTER 18

WEB TECHNOLOGIES IN JDEROBOT FRAMEWORK FOR ROBOTICS AND COMPUTER VISION

A. MARTÍNEZ and J. M. CAÑAS

RoboticsLab, Universidad Rey Juan Carlos, josemaria.plaza@urjc.es

This paper presents a new development in the robotic software platform JdeRobot. Four web tools have been created to access to cameras, RBGD devices, wheeled robots and drones from any web browser. They use last generation web technologies like WebGL, WebWorkers and WebSockets to provide real time communication with robots and sensor devices. The sensors can be monitorized and the robot teleoperated from any computer, smartphone or laptop, regardless their operating system.

1 Introduction

In the last years, several robotic frameworks (also named SDKs or middlewares) have appeared that simplify and speed up the development of robot applications. They offer a simple and more abstract access to sensors and actuators than the operating systems of the robot. The SDK Hardware Abstraction Layer (HAL) deals with low level details of accessing to sensors and actuators, releasing the application programmer from that complexity.

They provide a particular software architecture for robot applications, a particular way to organize code, to handle code complexity when the robot functionality increases. In addition, robotic frameworks usually include simple libraries, tools and common functionality blocks, such as robust techniques for perception or control, localization, safe local navigation, global navigation, social abilities, map construction, etc.. This way they shorten the development time and reduce the programming effort needed to code a robotic application as long as the programmer can build it by re-

using the common functionality included in the SDK, focusing in the specific aspects of the application.

Some tools of the JdeRobot robotic SDK (JdeRobot, 2016) let the human user to teleoperate robots (Kobuki wheeled robot, drone) and monitor the data from camera or RGBD sensors like Kinect. They are desktop applications in Linux that connect to the robot or sensor device and show a graphical user interface to the human user.

This paper presents the recent development of the web version of such tools. They provide the same functionality as the desktop equivalent but now from a web browser, so they are truly multiplatform. This way the robots can be teleoperated from any operating system (Windows, MacOs, Android, IOS...) and from any computer, even smartphones and tablets.

2 JdeRobot software platform

JdeRobot is a software development suite for *robotics* and *computer vision* applications. These domains include sensors (for instance, cameras), actuators, and intelligent software in between. It has been designed to help in programming such intelligent software. It is mostly written in C++ language and provides a *distributed component-based programming environment* where the application program is made up of a collection of several concurrent asynchronous components. Components may run in different computers and they are connected using ICE communication middleware (ZeroC, 2016). Components may be written in C++, Python, Java... and all of them interoperate through explicit ICE interfaces.

JdeRobot simplifies the access to hardware devices from the control program. Getting sensor measurements is as simple as calling a local function, and ordering motor commands as easy as calling another local function. The platform attaches those calls to remote invocations on the components really connected to the sensor or the actuator devices. Several *driver components* have been developed to support different physical sensors, actuators, both real and in simulation. They are ICE servers. Currently supported robots and devices include cameras, RGBD sensors (Kinect and Kinect2 from Microsoft, Asus Xtion), Kobuki (TurtleBot) from Yujin Robot and Pioneer from MobileRobotics Inc., ArDrone quadrotor from Parrot, laser scanners, Nao humanoid and Gazebo simulator.

JdeRobot includes several robot *programming tools and libraries*. For instance: viewers and teleoperators for several robots, its sensors and motors; a camera calibration component and a tunning tool for color filters; VisualHFSM tool for programming robot behavior using hierarchical Fi-

nite State Machines. In addition, it also provides a library to develop fuzzy controllers, a library for projective geometry and computer vision processing.

JdeRobot is *open-source software*, licensed as GPL and LGPL. It also uses third-party software like Gazebo simulator (OSRF, 2016), ROS, OpenGL, GTK, Qt, Player, Stage, GSL, OpenCV, PCL, Eigen, Ogre. It is ROS compatible.

3 Web tools

Four web tools have been developed using last generation web technologies like HTML5, JavaScript, CSS, WebGL, WebWorkers and WebSockets. All of them are ICE clients that run in the web browser and connect to the corresponding JdeRobot driver using ICE and Websockets.

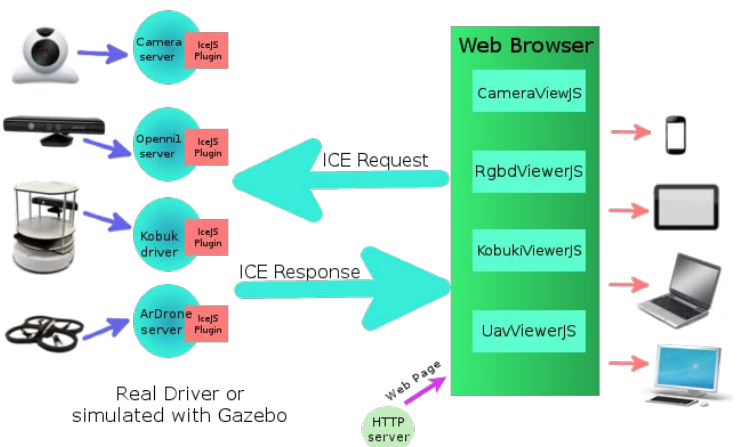

Fig. 1. Architecture of web tools in JdeRobot

As can be seen in Fig. 1. The new release of ICE library supports WebSockets so the drivers have been used without source code modification, just a change in configuration to set WebSockets protocol instead of TCP or UDP.

Each client is divided into three distinct parts: (a) *Connectors*, where it internally creates a thread (WebWorker) that connects to the ICE server; (b) *Core*, that handles the inner workings of widgets; (c) *Graphic inter-*

face, that organizes the appearance of the widgets within the webpage. In depth details and explanations can be found in (Martínez, 2016).

3.1 CameraViewJS

This client connects to the JdeRobot CameraServer which is the driver for real cameras. As can be seen in Fig. 2, CameraViewJS shows the images in a HTML5 Canvas and the number of FPS (Frames per second) received.

Fig. 2. Appearance of CameraViewJS webtool

It uses the API.Camera connector, which creates a WebWorker. The *connect* function establishes a JavaScript promise that is resolved when the WebWorker indicates that the connection has been established.

Like all the sensors, the WebWorker starts a stream with the JdeRobot ICE server, the driver. It constantly requests sensor data to the driver and passes them to the main thread. Fig. 3 shows this dialogue.

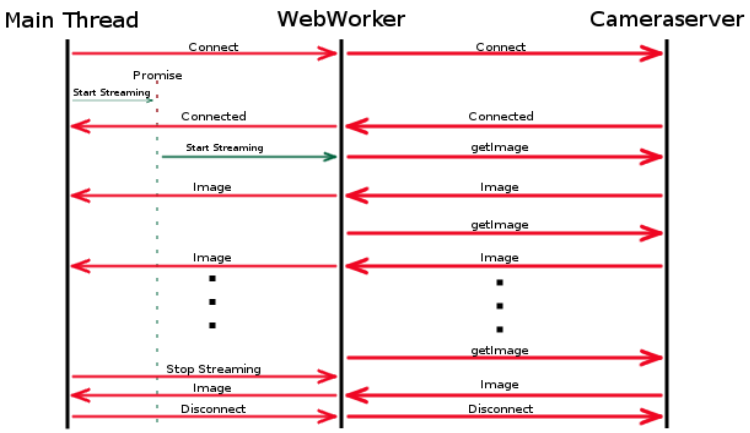

Fig. 3. Message exchange for CameraViewJS webtool

3.2 RGBDVieerJS

This web client connects to the JdeRobot server *Openni1Server* which provides information from RGBD sensors. As can be seen in Fig. 4, it shows the color and depth images in two HTML5 canvas and their FPS. A third canvas shows with WebGL the 3D scene, made of color points in 3D.

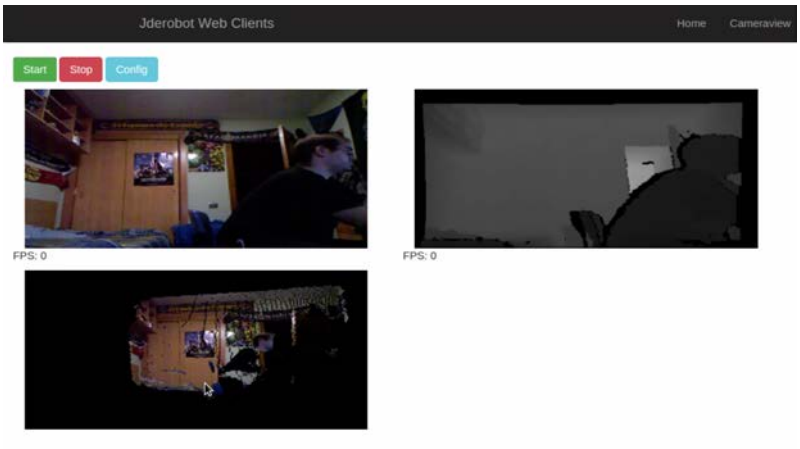

Fig. 4. Appearance of RGBDViewerJS webtool.

RGBDViewerJS uses two API.Camera connectors, one for the RGB image and one for the distance.

To create the 3D scene, a 3D point is computed for each pixel in the depth image using the camera calibration parameters (pin hole model). The color is taken from the corresponding pixel in the RGB image, which is registered with the depth image.

3.3 KobukiViewerJS

This web client connects to JdeRobot *KobukiDriver* and is used to teleoperate a Kobuki wheeled robot from the browser. As seen in Fig. 5, it shows the images from the robot stereo pair and the data from the onboard laser sensor. Another canvas displays the 3D scene using WebGL.

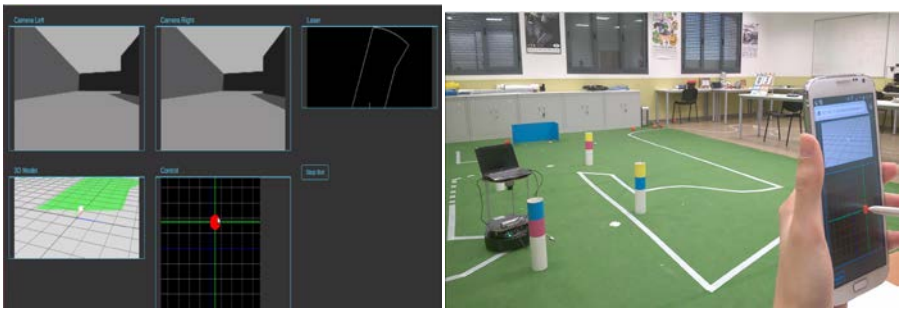

Fig 5. Appearance of KobukiViewerJS both with a simulated Kobuki robot and a real one

Regarding sensors, KobukiViewerJS uses two API.Camera connectors to connect with cameras, an API.Laser to get laser information and an API.Pose3D for robot position and orientation. Every time it receives laser data, the 2D-laser canvas and the 3D WebGl canvas are updated (green layer). When it receives a new Pose3D (encoders) data the orientation and position of the 3D model robot is updated too.

Regarding actuators, this webtool client has an API.Motors connector to send orders to the robot motors. When the control widget is moved then speed orders are sent to the robot. As seen in Fig. 6 the exchange of messages for the actuators is in the opposite way to that of sensors.

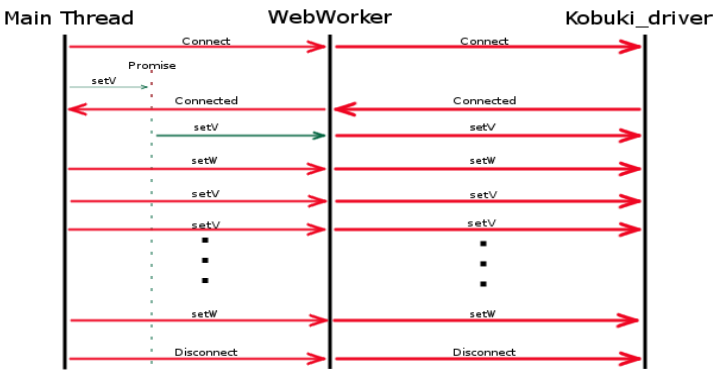

Fig 6. Message exchange for motors in KobukiViewer.JS

3.4 UAVViewJS

This client connects to JdeRobot *ArDroneServer* and allows to teleoperate a Parrot ArDrone quadrotor. As shown in Fig. 5, it shows the drone on

board camera images. 3D scene is shown in other canvas. In addition it provides two touch joysticks to control the drone movement. It also has flight indicators and buttons for takeoff, landing and camera change.

Fig 7: UAVViewerJS with a simulated drone a with a real one from a smartphone.

UavViewerJS has API.Camera and API.Pose3D connectors to communicate with the drone driver for sensors. For actuators it uses API.ArdroneExtra and API.CMDVel to send motion commands.

5 Experiments

Several experiments have been performed to test the web tools functionality, as was shown in the previous images. In addition, we measured the framerate for the CameraViewJS web tool in different network scenarios. In good connectivity settings the web tools performs similar to the local desktop tool, about 8 fps. In poor connectivity scenarios the performance slows down to 4, 2 or 1 fps, depending on the bandwidth limitations.

6 Conclusions

Four webtools have been created in JdeRobot that allow multiplaform tools to teleoperate wheeled robots or drones and to monitor cameras and RGBD sensors from any browser, including those in smartphones. They use advanced web technologies like WebSockets, WebGL and WebWorkers. They have been included in the last official JdeRobot release.

Acknowledgements

This research has received funding from the RoboCity2030-III-CM project (Robótica aplicada a la mejora de la calidad de vida de los ciudadanos. Fase III; S2013/MIT-2748), funded by Programas de Actividades I+D en la Comunidad de Madrid and cofunded by Structural Funds of the EU.

References

OSRF, Gazebo simulator web page, 2016 http://gazebosim.org/

JdeRobot web page, 2016 http://jderobot.org

Martínez, A., Final Degree Project "Tecnologías web en la plataforma robótica JdeRobot". Esc.Téc.Sup.Ing. Telecomunicación, URJC, 2016.

ZeroC ICE middleware, 2016 https://doc.zeroc.com/display/Ice35/Home

CHAPTER 19

STEREOVISION MATCHING BASED ON COMBINING NEURAL NETWORKS FOR OUTDOOR IMAGES

P.J. HERRERA[1], F. MONTES[2] and G. PAJARES[3]

[1]ETS de Ingeniería Informática, UNED, Madrid, Spain, pjherrera@issi.uned.es; [2]Centro de Investigación Forestal, INIA, Madrid, Spain, [3]Dpto. Ingeniería del Software e Inteligencia Artificial, Facultad de Informática, UCM, Madrid, Spain

We present a strategy for stereovision matching using pixels as features in images obtained from outdoor environments. The image segmentation process identifies textures out of interest through a Fuzzy Clustering scheme. Then, we present an approach to the stereovision matching problem. Based on six attributes we compute a matching probability between pairs of pixels of the stereo pair. The probability value is a weighted sum of the attributes. We use two combined ADALINE neural networks to compute the weight for each attribute. The proposed approach is compared favorably against five combined decision making strategies.

1 Introduction

In a practical stereo vision system, both left and right images are obtained at different positions or angles, and thus even the corresponding features in both images may display different values. A correspondence is established between features when such differences in feature values are assumed to be small, but the differences are sometimes too large to be considered, and matching is then rejected on this assumption. This may lead to incorrect matches. In order to avoid such problems, a stereo vision system with two basic components may be designed. These components are *image segmentation* and *stereo-matching process* (see Fig. 1). The function of the image segmentation is to extract information (features and attributes) from the

scene and to make this information available to the stereo-matching process.

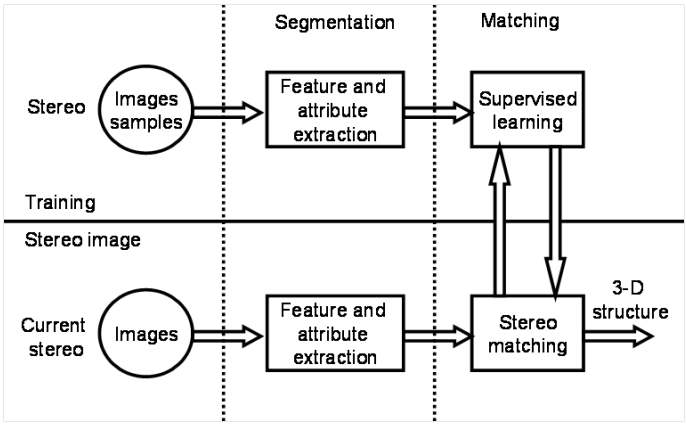

Fig. 1. Diagram of the stereo vision system.

The stereovision matching process works in two mutually exclusive ways: Training (*T*) and Stereovision (*S*), see Fig. 2. In *T* mode, a weight vector is estimated to be used in *S* mode. If access to *T* mode is done from *S* mode, the weight vector is recalculated with the correct matches obtained in the current stereovision mode. In the *S* mode, true matches are established with a view to the ADALINE (ADAptive LINear Element) neural network (Patterson, 1996).

The images analyzed in this work belong to forest environments and the interest is focused on the trunks of the trees. The first step (image segmentation) consists on the identification of the textures out of interest to be excluded during the matching process. This is carried out through a segmentation process which combines methods for texture analysis (Gonzalez & Woods, 2007) and the well-known Fuzzy Clustering strategy (Zimmermann, 1991). The first one tries to isolate the leaves based on statistical measures and the second one classifies the other two kinds of textures: sky and grass.

Once the above textures have been identified, now the goal is to match the tree trunks of each stereo pair. With such purpose we exclude the pixels identified as belonging to one of the three kinds of textures mentioned above. The remaining pixels are the candidates to be matched, where those belonging to the trunks are found.

The main contribution of this paper is the combination of a segmentation approach and a matching process through the application of the epipolar, similarity and uniqueness constraints under the ADALINE neural network for obtaining a disparity map.

This work is organized as follows. In section 2 we describe the procedures applied for the image segmentation. Section 3 describes the design of the matching process. In section 4 a test strategy is designed and a comparative analysis is performed. Finally, the conclusions and future work are presented in section 5.

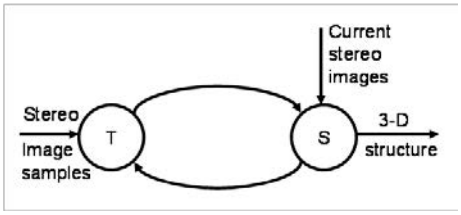

Fig. 2. Operation nodes of the stereo matching system.

2 Image segmentation

The image segmentation extracts features and attributes of the images. A variety of techniques have been used for texture identification (Trias-Sanz et al., 2008). The textures produced by the leaves of the trees under analysis do not display spatial distributions of frequencies nor textured patterns; they are rather high contrasted areas without any spatial orientation (Wang & Boesch, 2007). Hence, we have verified that the most appropriate texture descriptors are those capturing the high contrast, i.e. statistical second-order moments (Gonzalez & Woods, 2007). One of the simplest is the *variance*. It is a measure of intensity contrast defined in our approach as in (Gonzalez & Woods, 2007).

As mentioned before, in our approach there are other two relevant textures that must be identified. They are specifically the sky and the grass. For a pixel belonging to one of such areas the variance should be low because of its homogeneity. Nevertheless, this is not sufficient because there are other different areas which are not sky or grass fulfilling this criterion. Therefore, we apply a classification technique based on the Fuzzy Clustering (FC) approach, which is selected because it is a well-tested method (Zaixin et al., 2014). In this work the application of FC is as in (Herrera et al. 2011).

3 Stereovision matching process

Once the image segmentation process is finished, we have identified pixels belonging to three types of textures out of interest. The exclusion of these

textures is useful because the errors that they could introduce during the correspondence can be considerably reduced.

As mentioned above, in our approach we apply three stereovision constraints: epipolar, similarity and uniqueness. The epipolar allows restricting the search space for correspondence. The similarity and uniqueness, which are based on the ADALINE approach allows computing the disparity map. Our stereo matching system is designed with parallel optical axis geometry and is composed of two basic modules, Fig. 2: (1) *training* (*T*) and (2) *current stereo matching* (*S*). In the *T* mode the system updates, through the corresponding training process, the synaptic weight vectors attached to each ADALINE. This is a supervised learning process because an unknown set of weights is estimated from known input and output samples as in (Pajares & Cruz, 2001). During the *S* process, an incoming pair of features with their associated attributes is presented and processed by the system. The updated synaptic weight vectors are used to decide if it is a true or a false match. We base our approach on the Widrow-Hoff *delta rule* for learning (Patterson, 1996) which is applied to two single-layer feed forward linear networks, with two real-valued outputs (see Fig. 3). Each single neural network model is an ADALINE.

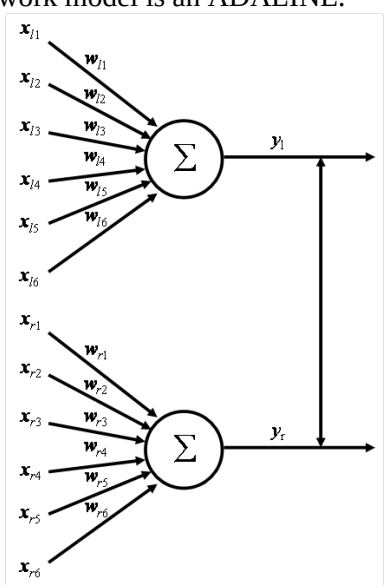

Fig. 3. Two ADALINEs applied to stereovision matching.

The inputs of each neuron are the components of the six-dimensional $\boldsymbol{x}_l$ and $\boldsymbol{x}_r$ vectors, respectively (hereafter written as $\boldsymbol{x}_m$ where the sub-index *m* denotes either *l* or *r*). The input vectors in a neural network are the training samples to perform the updating process. Each component $\boldsymbol{x}_{li}$ or $\boldsymbol{x}_{ri}$ is an

input attached to a synapse. Each element has six synapses, as we are processing pairs of features with six attributes. As usual, a weight is associated to each synapse. Hence, in our approach we also define the corresponding six dimensional synaptic weight vector as $\boldsymbol{w}_{\mathrm{m}} = \{\boldsymbol{w}_{\mathrm{m1,\ldots,}}\ \boldsymbol{w}_{\mathrm{mn}}\}$, $n = 1,\ldots 6$ which is updated during the training process. The sub-indices 1, 2, 3, 4, 5 and 6 in the components of $\boldsymbol{x}_{\mathrm{m}}$ and $\boldsymbol{w}_{\mathrm{m}}$ are associated to the correlation, color, texture, gradient magnitude, gradient direction and Laplacian, respectively. With this convention, our model consists of two ADALINEs and performs two weighted sums as an inner product between each input vector and the corresponding synaptic weight vector to compute the analogue output, y_{m}, as

$$y_{\mathrm{m}} = x_{\mathrm{m}} w_{\mathrm{m}}^{\mathrm{t}} = \sum_{i=1}^{n=6} x_{\mathrm{m}i} w_{\mathrm{m}i} \tag{1}$$

For a given ideal pair of true matches with their corresponding $\boldsymbol{x}_{\mathrm{l}}$ and $\boldsymbol{x}_{\mathrm{r}}$ attribute vectors, we can assert that $\boldsymbol{x}_{\mathrm{l}}$ and $\boldsymbol{x}_{\mathrm{r}}$ are equal (i.e. the two features of a pair of true matches have identical attribute values). Hence, we can initially choose the weight vectors $\boldsymbol{w}_{\mathrm{m}}$ as unit vectors in Equation (1).

Under the hypothetical ideal case, it is assumed that y_{l} is equal to y_{r}, so we give proper form to this fact: "for an input sample vector $\boldsymbol{x}_{\mathrm{l}}$ the desired or target analogue output value is y_{r} but y_{l} is the actual value computed by the neuron and vice versa". The vertical double arrow in Fig. 3 represents this output relation. This is the supervised concept: a known output for a given input. But as such input/output relation is an ideal case, this assertion will not be truth and we must assume $y_{\mathrm{l}} \neq y_{\mathrm{r}}$ and $\boldsymbol{w}_{\mathrm{m}} \neq 1$. Hence, the goal is to learn each $\boldsymbol{w}_{\mathrm{m}}$, so that the differences between y_{l} and y_{r} are minima for a given number of training samples.

To do that, we apply the *delta rule* as in (Pajares & Cruz, 2001), where the training samples are pairs of true matches with their corresponding attribute vectors. When the *T* is completed, the specific weight for each attribute is updated and is available for the *S*.

The stereo matching is a process in which the contents of a pair of new stereo images are to be matched. As mentioned before, the image analysis system extracts pairs of features and determines their corresponding six dimensional associated attribute vectors $\boldsymbol{x}_{\mathrm{l}}$ and $\boldsymbol{x}_{\mathrm{r}}$. Once this information is obtained, the updated $\boldsymbol{w}_{\mathrm{s}}$ vector is used. This vector becomes available after a previous training process.

To measure the similarity between a pair of pixels under correspondence we use the matching probability, in Equation (2), taken from the classical work of (Kim & Aggarwal, 1987).

$$p_{lr} = \sum_{j=1}^{n} w_{sj} \frac{1}{1+\left|av_{1j} - av_{rj}\right|}, \quad \text{where} \quad \sum_{j=1}^{n} w_{sj} = 1; \quad 0 \le w_{sj} \le 1 \tag{2}$$

where *av* denotes the *attribute value* corresponding to each pixel; the subscripts *l* and *r* denote pixels belonging to the left and right images, respectively, in the pair of features to be matched; w_{sj} is the associated specific weight for each attribute *j* and *n* is the number of attributes. The choice of this matching probability is because it considers the relative importance of each attribute and this is a key issue in our approach.

The decision about the best match is made by selecting the maximum matching probability p_{lr} among all candidates.

4 Results

The tests have been carried out with twenty pairs of stereo images. The total number of pairs of pixels extracted from these images is 131724100. This number of pairs of pixels is representative of the forest environment where the measurement device works. We use four pairs of them for the training involved in the FC approach and also for extracting initial inputs vectors in the ADALINE approach. At a second stage, for the remainder sixteen stereo pairs we obtain each disparity map by applying the ADALINE approach pixel by pixel.

The tests consist on the computation of the errors obtained in the disparity maps. For such purpose we have available the *ground truth* disparity maps for the tree trunks of each stereo pair, provided by the end users. Thus, for each pixel in a trunk we know its correct disparity value according to this expert knowledge; which allows us to compute the percentage of error. For each one of the sixteen pairs of stereo images used for testing, we compute the disparity error for the pixels belonging to the trunks and then average these errors among the sixteen pairs of stereo images.

Based on Equation (2), we compute the matching probabilities between pixels. These probability values allow us to compare the effectiveness of our stereovision system against the combined decision making strategies YAG, CFI, SFI, DES and MCDMF (Herrera et al., 2011).

From results in Table 1 one can see that the strategies that combine the simple attributes improve the results. Although the ADA method corresponds to a different matching strategy, their results are similar. This allows us to validate ADA against the other five methods. It is very difficult to surpass the percentages obtained with the ADA method by using only the epipolar, similarity and uniqueness constraints.

Table 1. Averaged percentage of errors and standard deviations obtained for the ADA approach against the combined decision making strategies.

Category	Methods	%	σ
Decision making strategies	*YAG*	13.3	1.9
	CFI	11.2	1.3
	SFI	11.2	1.3
	DES	11.2	1.6
	MCDMF	9.3	0.9
	ADA	9.1	1.1

5 Concluding remarks

The stereovision matching process is based on the application of three stereovision matching constraints. For each pixel in the left image, a list of possible candidates in the right one is obtained for determining its correspondence. This is carried out through the ADALINE working as a stereo matching learning approach where the measurement vectors are used for updating the synaptic weight vectors.

The proposed ADALINE strategy outperforms the combined decision making methods: YAG, CFI, SFI, DES and MCDMF. Some optimization approaches could be used, such as simulated annealing or Hopfield neural networks, where global matching constraints are applied under an energy minimization based process.

Acknowledgements

This work has been developed with the help of the research projects 979S/2013 of the MAGRAMA (Organismo Autónomo Parques Nacionales) and DPI2013-44776-R of the MICINN. It also belongs to the activities carried out within the framework of the research network CAM RoboCity2030 S2013/MIT-2748 of the Comunidad de Madrid.

References

Gonzalez, R.C., Woods, R.E. 2007. Digital Image Processing, Prentice Hall, Upper Saddle River, NJ.

Herrera, P.J., Pajares, G., Guijarro, M. 2011. A segmentation method using Otsu and fuzzy k-Means for stereovision matching in hemispherical images from forest environments. Applied Soft Computing 11(8): 4738−4747.

Kim, Y.C., Aggarwal, J.K. 1987. Positioning three-dimensional objects using stereo images. IEEE Journal of Robotics and Automation 3(4): 361−373.

Pajares, G., Cruz, J.M. 2001. Local stereovision matching through the ADALINE neural network. Pattern Recognition Letters 22: 1457−1473.

Patterson, D.W. 1996. Artificial Neural Networks, Prentice-Hall, Singapore.

Trias-Sanz, R., Stamon, G., Louchet, J. 2008. Using colour, texture, and hierarchical segmentation for high-resolution remote sensing. ISPRS Journal of Photogrammetry & Remote Sensing 63: 156−168.

Wang, Z., Boesch, R. 2007. Color- and Texture-Based Image Segmentation for Improved Forest Delineation. IEEE Trans. Geoscience and Remote Sensing 45(10): 3055−3062.

Zaixin, Z, Lizhi, C, Guangquan, C. 2014. Neighbourhood weighted fuzzy c-means clustering algorithm for image segmentation. IET Image Processing 8(3). 150−161.

Zimmermann, H.J. 1991. Fuzzy set theory and its applications, Kluwer Academic Publishers, Norwell, MA.

CHAPTER 20

MINI EYE-IN HAND VISION SYSTEM FOR LANDMINES DETECTION TASKS

J. GAVILANES, R. FERNÁNDEZ, H. MONTES, and M. ARMADA

Centro de Automática y Robótica CAR (CSIC-UPM),
roemi.fernandez@car.upm-csic.es

This chapter presents the design, implementation and testing of a mini eye-in hand vision system intended to be used in a robotic arm for mapping the terrain and detecting landmines during close-in detection tasks. Results of preliminary experimental tests show the potential of the proposed approach.

1 Introduction

The most recent report from the Landmine & Cluster Munition Monitor organization indicates that in 2014 a total of 3678 mine/ERW casualties were recorded, making an average of 10 casualties per day and a 12% increase from 2013. From this total, the 80% were civilians, and 39% were children. Taking into account that in many states and areas, numerous casualties go unrecorded, it is possible to affirm that the true casualty figure is significantly higher (International Campaign to Ban Landmines, 2015). The process of detection and deactivation of these devices represents a complex problem that includes several operational stages. From these activities, the close-in detection is one of the most dangerous and tedious tasks, since it is performed by human operators who inspect every centimetre of terrain equipped with prodders and metal detectors.

Wheeled, tracked or legged robots, endowed with a robotic arm and proper array of sensors for mines detection, constitute a good solution for automating this risky and time-consuming task. Mobile robots are capable of operating continuously during long periods of time without losing repeatability of movements and avoiding, in case of accidents, the injury of

operators or the loss of human lives. Consequently, several prototypes have been proposed in the last years (Hirose et al., 2005; González de Santos et al., 2007; Colon et al., 2007; Fukushima et al., 2008; Freese et al., 2010; Doroftei and Baudoin, 2012; Balta et al., 2014).

In order to improve the autonomy of these robotic systems during close-in detection tasks, a mini-eye in hand vision system is proposed in this work. The information provided by this system will be crucial for controlling the movements of a robotic arm, which is responsible of keeping the mine detection system as closer as possible to the ground, as well as for detecting and discriminating characteristics of interest that may be present in the field during the demining operations.

2 Mini eye-in hand vision system

The proposed mini eye-in hand vision system is composed of a mini-TOF (Time-Of-Flight) camera and two mini-RGB cameras (see Fig. 1).

The mini-TOF camera is characterized by emitting an infrared signal, which is then received by each pixel on the sensor. Thus, each pixel measures the time the infrared signal has taken to travel from the illumination unit to the object and back to the focal plane array. In this way, the mini-TOF camera provides a pseudo-image of distances in which each pixel in the scene has a value that represents the distance of the corresponding point on the space, measured with respect to the sensor. This information, provided by the mini-TOF camera, will allow keeping the metal detector at a constant height from the ground, whereas the colour information provided by the mini-RGB cameras will be very useful for the detection and discrimination of objects present in the field.

Fig. 1. Close-up view of the mini eye-in hand vision system.

The proposed mini eye-in hand vision system is installed on a robotic arm that has 5 DOF in elbow-up configuration, three of them for positioning the metal detector in the Cartesian space, and the other two, located at the wrist of the manipulator, for adapting the metal detector attitude in case of terrain inclinations. In turn, the robotic arm is installed on-board of a six-legged robot that acts as mobile platform. By means of a joint coordination of both systems it is possible to achieve an accurate positioning of the metal detector on the terrain. The proposed robotic arm configuration provides sufficiently mobility for positioning and orienting the metal detector with respect to the ground and reduces possible undesirable contacts with other parts of the robot or objects in its environment.

3 Pre-processing algorithms

This Section presents the pre-processing algorithms that have been implemented for the mini eye-in hand vision system.

3.1 Image registration

The image registration is essential not only for obtaining the RGB image mosaic from the two images acquired with the mini-cameras, but also for combing this resulting RGB panoramic image with the point cloud provided by the mini-TOF camera. In both cases, we will require finding a precise point to point correspondence between the images of interest. For the first case, the automatic method based on characteristics to compute the homography between the two images can be summarised in the following steps:

- Compute interest point features in each image to subpixel accuracy.
- Compute a set of interest point correspondences.
- RANSAC robust estimation.

For the second case, in which it is desired to register the resulting RGB image mosaic with the data acquired by the mini-TOF camera, we assume that the configuration of the set-up is fixed, i.e. it will not experience any variation in the relative positioning of the cameras that make it up. Therefore, the RANSAC algorithm can be used to find the rotation and translation *(R,T)* that allows the transformation of the data acquired by the mini-TOF camera into the reference frame of the RBG mosaicking image.

For that, N pairs of control point matches between Frames F_1 and F_2 are selected, where F_1 and F_2 correspond to mini-TOF reference frame and the

reference frame of the RGB mosaicking image, respectively. The extraction of these control points is done manually in Matlab, using a calibration pattern. In this way, the transformation given by (*R*, *T*) may be applied to any image acquired with the mini-TOF camera, obtaining quickly and efficiently the registered data and it won't be necessary to recalculate this transformation as long as the mini eye-in hand vision system is not modified.

3.2 Image mosaicking

The main objective of this part is to combine two partially overlapped views of a scene to produce a single image with an extended field of view, known as image mosaic. The three basic steps for the construction of an image mosaic are (Capel, 2001):

- Image registration: the aim is to register each image into a global coordinate frame containing the entire scene. For convenience, it is chosen to be aligned with the axis of one of the input images.
- Re-projection: After the registration procedure, it is necessary to specify a transformation *Tr* that maps the image points into points in the global frame. *Tr* is referred as the rendering transformation. In principle, *Tr* could be any one-to-one mapping, but in practice it is usually determined by the choice of the re-projection manifold (plane – planar projection, cylinder – cylindrical projection, sphere – spherical projection, etc.). In the proposed case, a planar projection is selected due to its simplicity and common use. In the planar projection, the rendering transformation is a homography.
- Blending: when choosing the value of a pixel in the rendered image, it is possible to draw on information from several input images. Therefore, the final stage is to combine input images in their overlapping portions. The blending algorithm has the following steps:
    - To transform the pixel coordinates into each input image by using the rendering transformation and the computed homographies.
    - For each image in which the transformed pixel lies inside the image boundary, sample the intensity value using a bilinear interpolation.
    - Combine the set of intensity values obtained into a single value by using an averaging function. Therefore, the value of the output pixel is simply obtained by calculating the average of the values extracted from the input images.

4 Experimental results

Several preliminary experimental tests have been conducted in order to validate the proposed mini eye-in hand vision system and the pre-processing algorithms described in Sections 3.1 and 3.2.

The colour images acquired with the mini-RGB cameras are shown in Fig. 2. Note that the mini-RGB cameras have been previously calibrated in order to ensure a correct white-balance in both acquired scenes. Since the incident light affects differently to each mini-RGB camera depending on the angle from which the light is projected, most of their parameters are calibrated automatically by the internal microprocessor of the mini-RGB cameras. Fig. 3 displays the amplitude image and the z-axis range data acquired with the mini-TOF camera.

Fig. 2. Colour images acquired with the two mini-RGB cameras.

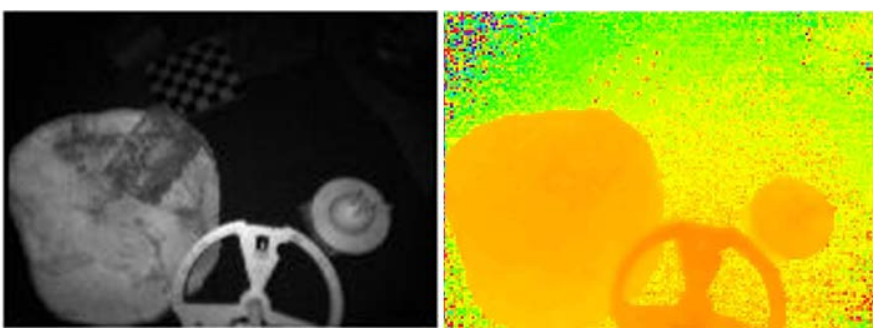

Fig. 3. Amplitude data (left-hand size) and Z-axis range data (right-hand size) acquired with the mini-TOF camera.

Fig. 4 presents the resulting RGB image after mosaicking the two images acquired by the mini-RGB cameras. This resulting image is then utilised together with the amplitude image from the mini-TOF camera for conduct-

ing the registration procedure. Fig. 5 illustrates the result obtained from this registration procedure. In this way, direct correspondence between the RGB information and the range data is achieved. The red asterisks shown in Fig. 4 represent the control points that have been selected in the RGB image resulting from the mosaicking algorithm, while in Fig. 5 red asterisks represent the corresponding points in the image resulting from the registration procedure. In this way, it is possible to get a visual idea of the registration error. Finally, Table 1 shows not only the maximum and minimum registration errors, but also the mean registration errors on the *x* and *y* axes for the analysed images.

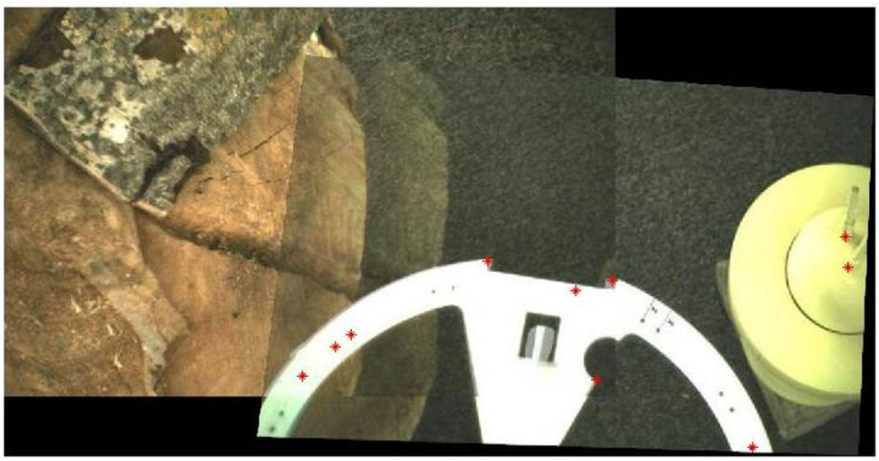

Fig. 4. Resulting RGB image after the mosaicking.

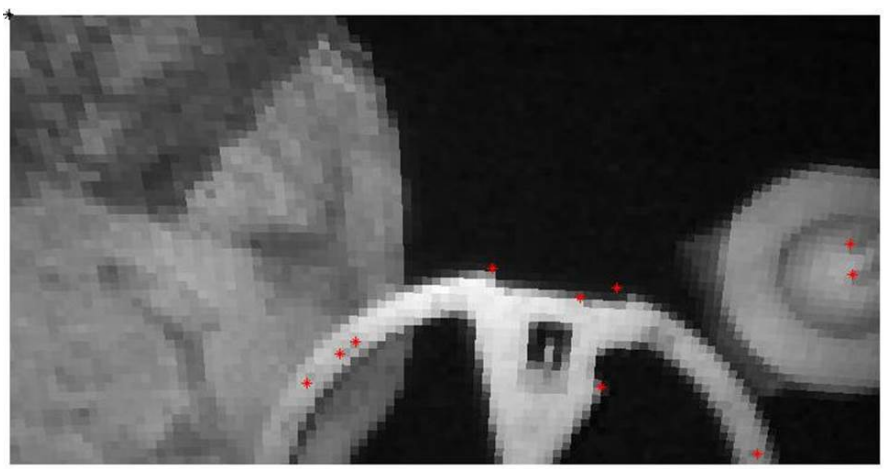

Fig. 5. Mini-TOF amplitude image resulting after the registration procedure.

Table 1. Registration errors for the proposed vision system.

Registration Error	Value (pixels)
Minimum and maximum errors on *x*-axis	[1-8]
Minimum and maximum errors on *y*-axis	[1-10]
Mean error on *x*-axis	4
Mean error on *y*-axis	4

5 Conclusions

A mini eye-in hand vision system composed of a mini-TOF and two mini-RGB cameras has been presented for improving autonomy of robotics systems during close-in detection tasks. The mini-TOF camera provides a point cloud of the terrain that will allow the robotic arm to keep the mines detector at a constant height above the ground and performing an efficient scanning of the contaminated terrain, whereas the mini-RGB cameras provide colour information that can be useful for detection and discrimination of objects on the terrain. Therefore, it is expected that the proposed mini eye-in hand vision system will contribute to improve the detection rate of antipersonnel mines.

Acknowledgements

The research leading to these results has received funding from the RoboCity2030-III-CM project (Robótica aplicada a la mejora de la calidad de vida de los ciudadanos. Fase III; S2013/MIT-2748), funded by Programas de Actividades I+D en la Comunidad de Madrid and cofunded by Structural Funds of the EU. Dr. Roemi Fernández acknowledges the financial support from Ministry of Economy and Competitiveness under the Ramón y Cajal Programme. Dr. Héctor Montes acknowledges support from Universidad Tecnológica de Panamá.

References

International Campaign to Ban Landmines - Cluster Munition Coalition. 2015. Landmine monitor report.

Fukushima, E.F.; Freese, M.; Matsuzawa, T.; Aibara, T. and S. Hirose. 2008. Humanitarian demining robot gryphon - current status and an objective evaluation. International Journal on Smart Sensing and Intelligent Systems 1, 735-753.

Freese, M.; Singh, S.P.N.; Singhose, W.; Fukushima, E.F. and Hirose, S. 2010. Terrain modeling and following using a compliant manipulator for humanitarian demining applications. Field and Service Robotics, Springer Tracts in Advanced Robotics 62, 3.

Colon, E.; De Cubber, G.; Ping, H.; Habumuremyi, J-C; Sahli, H. and Baudoin, Y. 2007. Integrated robotic systems for Humanitarian Demining. International Journal of Advanced Robotic Systems.

Doroftei, I. and Baudoin, Y. 2012. A concept of walking robot for humanitarian demining. International Journal Industrial Robot 39, 441.

Hirose, S. and Kato, K. 1998. Quadruped walking robot to perform mine detection and removal task. Proceedings of the 1st International Symposium CLAWAR'98, Brussels, Belgium.

Hirose, S.; Takita, K.; Kato, K.; Torri, A.; Ogata, M. and Sugamuna, S. 2005. Quadruped walking robot centered demining system – development of TITAN-IX and its operation. Proceedings of the 2005 IEEE International Conference on Robotics and Automation ICRA'2005, Barcelona Spain.

González de Santos, P.; Cobano, J.; García, E; Estremera J. and Armada, M. 2007. A six-legged robot-based system for humanitarian demining missions. Mechatronics 17, 417.

Balta, H.; Wolfmayr, H.; Braunstein, J. and Baudoin Y. 2014. Integrated mobile robot system for landmine detection. Proceedings of the 12th IARP Workshop HUDEM 2014, Croatia.

Prado, J. and Marques, L. 2014. Energy efficient area coverage for an autonomous demining robot. ROBOT 2013: First Iberian Robotics Conference, Springer International Publishing 253, 459.

Capel, D. 2001. Image Mosaicing and Super-resolution. Ph.D. Thesis. University of Oxford.

CHAPTER 21

NEW TRENDS AND CHALLENGES IN THE AUTOMATIC GENERATION OF NEW TASKS FOR HUMANOID ROBOTS

R. FERNANDEZ-FERNANDEZ, J. G. VICTORES and C. BALAGUER

RoboticsLab, Universidad Carlos III de Madrid, rauferna@ing.uc3m.es

In this paper, the study and implementation of a task generation system that uses the information obtained from the user and already known cases is presented. One of the main objectives of the system is to introduce a new approach in robotics that takes into account the physical limitation of teaching and learning time, and thus the amount of knowledge that a robot can obtain of a given environment (tasks, objects, user preferences…), as a critical bottleneck of any robotic system. For this, the study of the Case Based Reasoning (CBR) problem is presented. Additionally, Base Trajectory Combination (BATC), a novel trajectory combination method based on a simplified CBR structure, using trajectories instead of high-level tasks, is proposed and explained. Finally, this system is tested with Move-it! as the simulation environment, using the humanoid robot TEO from Universidad Carlos III de Madrid as the robotic platform. The results of these experiments are also presented with the corresponding conclusions and future research lines.

1 Introduction

The goal of this work is the design of a system capable of the automatic generation of new tasks, using both the information stored from old cases and from user interaction. This idea started since the first studies in human memory (Ebbinghaus, 1885), when the scientific community started to see how the knowledge stored in memory was used as a support for the generation of new tasks and even as a tool for predicting the future (Ingvar 1985), (Schacter, Addis, and Buckner 2007).

On the other hand, roboticists have yet to find a solution for most of the challenges that imply working in a real environment. However, in current systems, there is a tendency to use the knowledge of a robot as an infinite resource that contains all the knowledge already adapted to all the different circumstances that can occur. This leads us to highly knowledge dependent systems, which can only correctly within the specific domain for which they were designed. Therefore, one of the purposes of this work is to design a system able to work with a limited knowledge database. This means, a database with scarce knowledge that sometimes is not even related to the context where the system needs to work. This scenario is pretty similar to the case of the children during their first steps of learning, where their knowledge is quite limited. In turn, they use help of a constant interaction, habitually with their parents, for learning and executing new tasks (Wells, 2009). This is the reason why our objective will be to study and propose a system able to generate new tasks using the information retrieved from a limited knowledge database and user interaction.

2 State of the art

One of the base problems to solve is the CBR problem. This means, the idea of using previous cases to help with the achievement of new tasks. This idea started with the publication of (Schank and Abelson 1975), and in a relatively small time, some systems based on this idea started to appear. An example of this is CHEF (Hammond, 1986), which uses recipes as cases, or ISAC (Bonzano, Cunningham, and Meckiff 1996), a system to support air-traffic controllers. The basic overall structure used in CBR systems was presented in (Kolodner 1992), and can be seen in Fig. 1.

Fig. 1. Overall scheme of all the process involved in a CBR system.

Since the proposal of this structure, some papers have appeared with the objective to solve some specific CBR problematics presented in this structure. This is the case of PARADYME (Kolodner, 2014), a case retrieval method for the retrieval of old cases. However, the number of this kind of publications is quite low in comparison with the ones oriented to applications. The reason is because the problems presented in CBR systems are

complex high level problems of which most are not yet solved. This is especially notable in the reasoning stage. This stage concerns solving problems like the adaptation of high level tasks and the evaluation of the tasks generated, problems that presents a huge challenge for the implementation of a CBR system.

In addition to this, there are some similar projects that face similar problems to the ones presented in this paper. In (Beetz, 2011) a system designed to generate new tasks using the information from pages like *wikihow.com* or *ehow.com,* and the information stored in a KnowRob[1] ontology database is presented. Another example is (Ramirez-Amaro, 2015), in this case the system is focused in the design of semantic rules that allow the conceptual definition of tasks from user demonstration. The goal is to later use this conceptual definition to allow the robot to perform the task under different circumstances, and to make the process of learning a new task easier at the same time, using for this the information from known cases for the generation of the new ones. In (Morante, 2014) the idea was to design a task generalization method based on the idea of using the information about the changes that an action produces in the environment. This means instead of working with tasks defined as robot movements, to work with tasks defined as changes in the environment.

3 BATC

The idea of BATC[2] is to use the trajectories that define the tasks, before attempting to directly use the tasks themselves. The goal of this is triple. First, since BATC uses trajectories, it can be later used for the implementation of a high level CBR system. Second, since BATC uses low level cases, most of the problems presented in a CBR system become easier to solve. Finally, the last reason is because the implementation of BATC would be solving a not solved problem in robotics, which is the combination of known trajectories for the generation of new ones.

3.1 The idea behind BATC

The idea behind BATC consists in using a mathematical method, since trajectories are mathematical functions, for the combination of these trajec-

1 http://www.knowrob.org/

2 https://github.com/roboticslab-uc3m/teo_batc

tories, in this case a weighted sum. This way, in BATC a feature vector is assigned to every trajectory in order to compare them (Fig. 2).

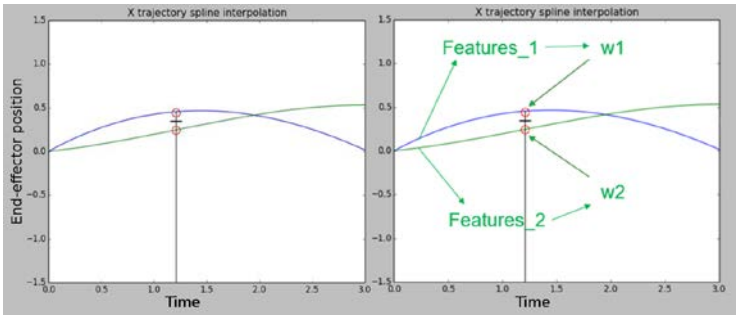

Fig. 2. In BATC the new point is defined using the points in the database (left), and a weighted sum with the weights assigned using features vectors (right).

3.2 The BATC algorithm

Using the feature vector and the Euclidean distance, the two best trajectories (the ones closer to the goal trajectory) are selected. Then, the base one weights are assigned using the Euclidean distance between the base trajectories and the goal one. The new trajectory will be then the spline defined by the succession of points presented in the equation 1, where *Sp1(t)* and *Sp2(t)* are the values of the trajectories splines at the instant *t*, w_1 and w_2 are their respective weights, and the difference between *t* and *t+1* is the time step used to define the new trajectory. This way, changing the weights, we can adapt the trajectory generated to the needs of the user.

$$Tr = \left[Sp_1(t) * w_1 + Sp_2(t) * w_2, Sp_1(t+1) * w_1 + Sp_2(t+1) * w_2 ...\right] \quad (1)$$

In the case of orientation, since BATC works with quaternions (nonlinear units), the SLERP method for the interpolation of quaternions is used instead of the weighted sum. The new orientation can be defined as the succession of quaternions obtained using equation 2. Where, $q_1(t)$ and $q_2(t)$ are the two quaternions of the base trajectories in the instant *t*. The value w_1 is the weight of $q_1(t)$, obtained the same way as in the case of SPLINES.

$$NewOri = SLERP(q_1(t), q_2(t), w_1) \quad (2)$$

The CBR structure in Fig. 1 was used as the base structure for the implementation of BATC: First, the trajectories are stored in a database with its features vector. Next, there is an interaction step where the user specify the features of the goal trajectory. Then, the BATC reasoning system gen-

erates the new trajectory, using the trajectories in the database and the information from the user. Finally, the new trajectory can be executed.

4 Experiments

For the implementation of the BATC system, Moveit![3] and ROS were used as the simulation software, with TEO the humanoid robot (Martinez, 2012) from the Universidad Carlos III de Madrid, as the robotic platform. Results obtained are shown in Fig. 3. Here, two base trajectories stored in the robot database ("arm to the front" and "arm up") were used for the generation of the new one, defined with its final position.

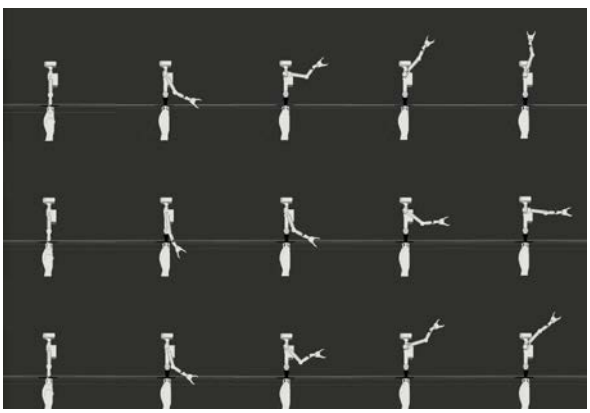

Fig. 3. The first row corresponds to the "arm up" trajectory, the second one is "arm to the front", and the last one is the generated one "arm to the diagonal".

The experiment performed to test BATC consisted in changing the number of trajectories in the database, and studying how the system behaves with a set of random goals. The results of these tests can be seen in Table 1. The error obtained is the sum of the final position error, bounded in *[0.0 , 1.5]* in Moveit! units, plus the orientation error *[0.0 , 0.1]*. The first conclusion we can extract, is that adding just one more trajectory "arm to the back" the mean error, is now decreased by almost the half. One of the reasons of this is because the new trajectory is the opposite of "arm to the front" in the "x axis". This implies that we are maximizing this defined space, and therefore the performance obtained by BATC. On the other hand, in the third scenario the new trajectory is "arm to the x diagonal", a

3 http://moveit.ros.org/

variation of "arm to the front". The results this time, are quite similar to the ones obtained in the last experiment. This leads us to the conclusion that the more different are the base trajectories, the more information the BATC system has, and the better the performance.

Table 1. Experimental results with BATC.

Experiment Number	Configuration error 2 base trajectories	Configuration error 3 base trajectories	Configuration error 4 base trajectories
1	0.746	0.279	0.256
2	0.315	0.432	0.774
3	0.508	0.565	0.464
4	0.732	0.489	0.616
5	0.328	0.253	0.172
6	0.473	0.372	0.686
7	0.687	0.263	0.236
8	0.676	0.303	0.521
9	0.194	0.174	0.095
10	0.668	0.447	0.366
Mean error	0.492	0.337	0.351

5 Conclusions and future ideas

The overall idea of this work was to present a new approach in the area of robotics, using the knowledge as another limitation of the system. To do this, the study of the resolution of the CBR problem in a limited knowledge scenario was presented. Several contributions have been made:

- The presentation of the Base Trajectory Combination (BATC) system, a novel method for the automatic generation of new trajectories using the information from already known trajectories and user interaction. This method is designed to be able to work in scenarios where the robot's knowledge (set of trajectories in robot memory) is scarce.
- The integration of BATC and TEO in the ROS environment has been presented, using Moveit! as the trajectory planning software. This integration opens the possibility of future works that can make use of this state of the art software and TEO.
- The BATC implementation and behavior has been tested, using different experiments and scenarios, with the main goal to study how this system behaves when having to cope these different situations.

Furthermore, the ideas presented in this paper and the implementation of BATC have given us some ideas about future trends in the area of robotics:

- The design of new systems that are able to work using a generic database with limited knowledge.
- The generation of robotic systems that are able to learn new concepts and tasks using the interaction with the environment, the user, and the information stored from already known cases.
- New approaches that take into account the physical limitation of teaching and learning time, and thus the amount of knowledge that a robot can obtain of a given environment, as a crucial bottleneck of any robotic system.

Acknowledgements

This research has received funding from the RoboCity2030-III-CM project (Robótica aplicada a la mejora de la calidad de vida de los ciudadanos. Fase III; S2013/MIT-2748), funded by Programas de Actividades I+D en la Comunidad de Madrid and cofunded by Structural Funds of the EU.

References

Beetz, M., U. Klank, I. Kresse, A. Maldonado, L. Mosenlechner, D. Pangercic, T. Ruhr, and M. Tenorth. 2011. 'Robotic Roommates Making Pancakes'. In 2011 11th IEEE-RAS International Conference on Humanoid Robots (Humanoids), 529–36.

Bonzano, Andrea, Pádraig Cunningham, and Colin Meckiff. 1996. 'ISAC: A CBR System for Decision Support in Air Traffic Control'. In Advances in Case-Based Reasoning, edited by Ian Smith and Boi Faltings, 44–57. Lecture Notes in Computer Science 1168. Springer Berlin Heidelberg.

Hermann Ebbinghaus. 1885. 'Memory: A Contribution to Experimental Psychology'.

Ingvar, D. H. 1985. '"Memory of the Future": An Essay on the Temporal Organization of Conscious Awareness'. Human Neurobiology 4 (3): 127–36.

K. J. Hammond. 1986. ‘CHEF: A Model of Case-Based Planning’. In Proceedings of the Fifth National Conference on Artificial Intelligence (AAAI-86).

Kolodner, Janet L. 1992. ‘An Introduction to Case-Based Reasoning’. Artificial Intelligence Review 6 (1): 3–34.

Kolodner, Janet L. 2014. ‘Selecting the Best Case for a Case-Based Reasoner’. In 11th Annual Conference Cognitive Science Society Pod. Psychology Press.

Morante, S., J.G. Victores, A. Jardon, and C. Balaguer. 2014. ‘Action Effect Generalization, Recognition and Execution through Continuous Goal-Directed Actions’. In 2014 IEEE International Conference on Robotics and Automation (ICRA), 1822–27.

Ramirez-Amaro, Karinne, Michael Beetz, and Gordon Cheng. 2015. ‘Transferring Skills to Humanoid Robots by Extracting Semantic Representations from Observations of Human Activities’. Artificial Intelligence, August.

Schacter, Daniel L., Donna Rose Addis, and Randy L. Buckner. 2007. ‘Remembering the Past to Imagine the Future: The Prospective Brain’. Nature Reviews Neuroscience 8 (9): 657–61.

Schank, Roger C., and Robert P. Abelson. 1975. ‘Scripts, Plans, and Knowledge’. In Proceedings of the 4th International Joint Conference on Artificial Intelligence - Volume 1, 151–57. IJCAI’75. San Francisco, CA, USA: Morgan Kaufmann Publishers Inc.

S Martinez, CA Monje. 2012. “TEO: Full-Size Humanoid Robot Design Powered by a Fuel Cell System.” Cybernetics and Systems 43 (3): 163–80.

Wells, C. Gordon. 2009. The Meaning Makers: Learning to Talk and Talking to Learn. 2nd ed. New Perspectives on Language and Education. Bristol, UK; Buffalo, NY: Multilingual Matters.

CHAPTER 22

HUMANOID ROBOTS FOR UNDERWATER WORKS

G. EJARQUE, R. SALTAREN, R. ARACIL, G. POLETTI and C. GARCIA

Centro de Automática and Robótica-CSIC-UPM, rsaltaren@etsii.upm.es

This chapter addresses recent developments of human-like robots designed to work as robotic divers, assuming hazardous activities currently carried out by human divers in hostile underwater environments. The risks involved in the most dangerous branches of the professional diving industry are highlighted. Current devices for underwater operations are described i.e., manned and unmanned vehicles, and recent developments of robotic divers are addressed. Finally, a functional prototype of an underwater anthropoid robot developed at CAR (CSIC-UPM) is presented.

1 Introduction

The underwater works carried on submerged structures require devices for moving and handling equipment and tools. Remotely operated vehicles (ROV) have been used for decades on tasks requiring inspection and manipulation, in both offshore and inland applications. However, when the complexity of the task is elevated, human intervention is needed.

There are a number of associated risks to the works realized in underwater environments, that expose divers to harmful phenomena and lethal risks. There exists a strong necessity of underwater works. However, there is no device combining the capabilities of ROV and divers, to perform these tasks without need human immersion.

This chapter is structured as follows. Section 2 describes the risks implied in professional diving activities. Section 3 presents current technologies to assist divers in underwater operations. Section 4 collects recent advances on underwater humanoid robots developed in the academic and

industrial world. A novel underwater anthropoid robot is presented in Section 5. Finally, the conclusions are summarized in Section 6.

2 Risks associated with diving operations

Apart from the health hazards derived from diving activities *e.g.,* decompression illness, pulmonary barotrauma, nitrogen narcosis (WHS Council, 2009), there exist several risks associated with the works performed by human divers. The professional diving sector include several dangerous activities, some of them are presented in the following sections.

2.1 Offshore diving

The offshore oil and gas industry as well as the prominent offshore wind power sector, require commercial divers to perform underwater operations for construction and maintenance of submerged structures.

Saturation divers can perform several operations at more than 300m depth using a mixture of oxygen and inert gases, wearing hard helmets and full body suits to protect against abrasion, puncture, or debris.

When working on cold waters, tethered divers controls its temperature by means of drysuits outfitted with warm water circulation (Gerwick, 2007). Further, they have fiber optic communication and hydraulic lines to power several tools. Some examples are shown in Fig. 1.

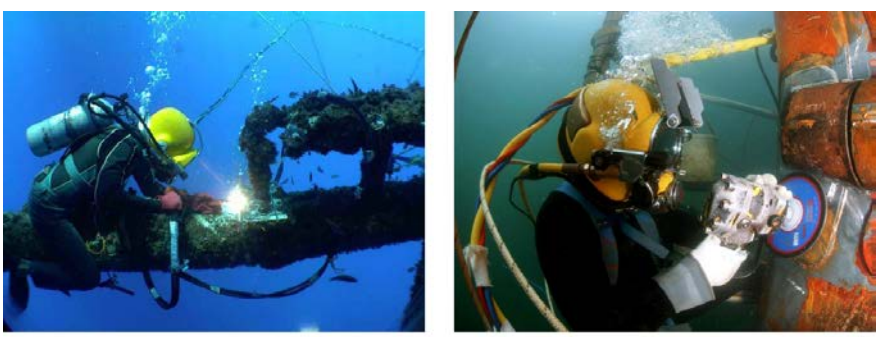

Fig. 1. Typical offshore diving operations: pipeline welding (left) and abrasive cleaning (right). Source: Professional Diving Academy and US Navy.

One important limitation of commercial divers is the difficulty in determining its own position, because water pressure affects human sensory and

reasoning capabilities, and produces disorientation and loss of reference planes. Also, speaking intelligibility is reduced due to the breathing gas mixture. All this facts increase the risk of physical fatigue and stress.

Besides, marine currents tend to displace the divers away from their working position, while marine growth can rip their suits. Commercial divers are exposed to noise, electrical shocks, and also accidents related with the use of tools *e.g.,* water jetting, hydraulic cutting, or welding.

Fig. 2. Hazardous material diving activities: sewage diving (left) and nuclear diving in power reactors (right). Source: NEDCON Internaltional LLC.

2.2 Hazardous materials diving

As shown in Fig. 2, hazardous material (HazMat) divers deals with diving operations in highly contaminated environments, such as sewage treatment plants, septic tanks or polluted waters. Nevertheless, are highly exposed in such environments (U.S. Navy, 2008).

HazMat divers perform critical tasks, such as installation and maintenance of gates and valves, inspection of areas with zero visibility, pollution control, measurements, and sampling activities.

For instance, sewage divers risk to contract diseases through cuts and punctures due to the presence of sharp objects in the raw sewage, such as broken glass and hypodermic needles.

Due to the turbidity of water, light levels are low and the divers must rely on its touch sense to be guided. Furthermore, full decontamination equipment is required when the operation is completed, emergency procedures must be planned, and equipment and personnel must be in place to recover the diver in case of accident.

Within the HazMat diving activities, nuclear diving is probably between the most dangerous. Nuclear divers work at the water-filled fuel pools of

nuclear power reactors performing several operations, such as replacing sensors into the fuel transfer canals, recover lost items which could damage the fuel rods, or welding on cracked steam dryers (Sheafer, 2011).

To control the radiation exposure, nuclear divers have to use special equipment. Several electronic dosimeters, which are monitored, are used to record the received radiation at different parts of the body. Also, a portable dosimeter allows the diver to detect radiation sources during the dive.

Once the operation is completed, an exhaustive cleaning process is needed using demineralized water, and the personnel must ensure there is no imperceptible irradiated material using radiation meters.

3 Current devices for underwater operations

Beyond certain depth underwater works become impossible for humans without using machines. Several underwater vehicles have been developed in the last decades to supplement divers in their underwater activities. The following sections present two of the most extended technologies.

3.1 Remotely operated vehicles

A remotely operated vehicle is an unmanned underwater vehicle connected to a mothership through an umbilical cable and controlled by a pilot (Moore et al., 2010). The umbilical transmits power and commands to the propulsion system, and sends back data, such as audio and video signals or sensor readings, to the control station placed in the mothership.

The size of an ROV can range from small vehicles of a few kilograms to large units weighing many tons. Observation class ROVs are mainly used for scientific purposes and inspection tasks, while the work class ROVs are preferred when underwater works are required (Gerwick, 2007).

The offshore oil and gas industry implements large work class ROVs, which are usually outfitted with two manipulators with multiple DOF and interchangeable tools *e.g.,* jet cleaning equipment or sampling devices.

Nevertheless, divers are more flexible for completing tasks, and sometimes more economical. Moreover, for certain tasks an ROV has limited dexterity, whereas a diver can be pretty dexterous (Lay, 2015).

3.2 Atmospheric diving suits

An atmospheric diving suit (ADS) is a pressure resistant suit made with rigid hulls articulated with special watertight joints, to protect the diver from exposure to high pressures. These rigid suits can attain up to 600m depth, while keeping the internal pressure close to one atmosphere.

The ADS systems are equipped with thrusters for independent mobility and two grippers operated by the diver, using its arms to perform underwater tasks. These special suits are used for deep-water operations in the offshore oil and gas fields, and also for military purposes worldwide.

The main advantage of the ADS is the absence of physiological hazards produced by water pressure (Lay, 2013). However, a diver using an ADS loses the human sense of touch and the grippers provide only 75% of the dexterity of a traditional diver. ADS are bulky and may cause maneuverability problems for accessing confined spaces (Thornton, 2000).

4 Recent developments of robotic divers

Despite of the extensive development of human-like robots for land (Cass, 2013), (Sakagami et al., 2002) and space applications (Diftler et al., 2011), humanoid robots for underwater applications are scarce and almost all the available records refers to conceptual ideas not yet realized. The following sections describe the state of the art of human-like robots, designed specifically for operation in underwater environments.

4.1 Red sea robotic explorer

Stanford University and King Abdullah University of Science and Technology (KAUST), together with Meka Robotics (currently acquired by Google) are collaborating since 2012, on the development of a new underwater robotic diver to help marine scientists in the exploration of the fragile ecosystem of the Red Sea (http://www.redsearobotics.net/).

The underwater robot, depicted in Fig. 3, is still under development and combines a thruster-actuated vehicle with two lightweight arms and compliant hands, to perform fine and dexterous tasks (Khatib, 2015).

The robot arms have 7-DOF each, and are almost like the human arm in terms of mobility. The hands, provided with tactile sensing, allow the operator to detect slippage and texture of the manipulated object.

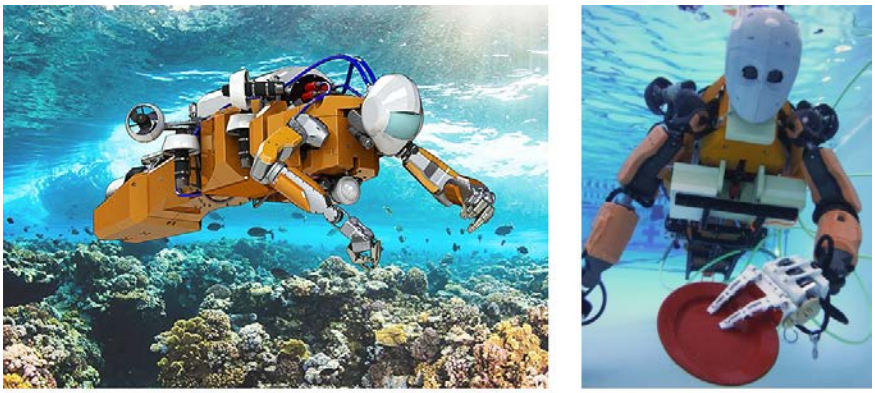

Fig. 3. The Red Sea Robotic Explorer: concept design (left) and first underwater manipulation tests. Source: KAUST and Stanford University.

4.2 Robotic divers in Japanese patents

The patent document in (Hirabayashi et al., 1986) describes an underwater working robot to operate in narrow spaces by means of a head, having sensors and a manipulator for handling objects, which is installed on the end of a neck, extendable along the body of the robot.

Another antecedent can be found in (Nagaoka et al., 1996), where a humanoid robot for operation in underwater structures is described. The invention claims a device in which an underwater inspection and working apparatus are integrated into a single humanoid robot.

5 Underwater anthropoid robot CAR (CSIC-UPM)

A novel underwater robot, named DiverBot, has been developed at the Group of Robots and Intelligent Machines of the Centre for Automation and Robotics (CSIC-UPM), since 2011.

The robot, shown in Fig. 4, was designed with the proportions of chimpanzees, and the capability to change between two different functional configurations i.e., anthropoid and vehicle mode. These particular features have led to an invention patent (Ejarque et al., 2016).

DiverBot is fitted with electrical thrusters, two hydraulic arms and two hydraulic legs. The prototype is capable to transform into an ROV or a humanoid robot, thus combining the advantages of both systems.

Hydraulic technology allows DiverBot to reach high depths due to the intrinsic waterproof features and force ratio of its actuators. The electric thrusters enable motion through the water under vehicle mode.

The hydraulic arms and legs allow obstacle avoidance, underwater walking and climbing, and underwater manipulation of materials and tools to perform complex tasks (*e.g.,* welding and assembling). Additionally, its hydraulic legs allow to fasten its body on submerged surfaces.

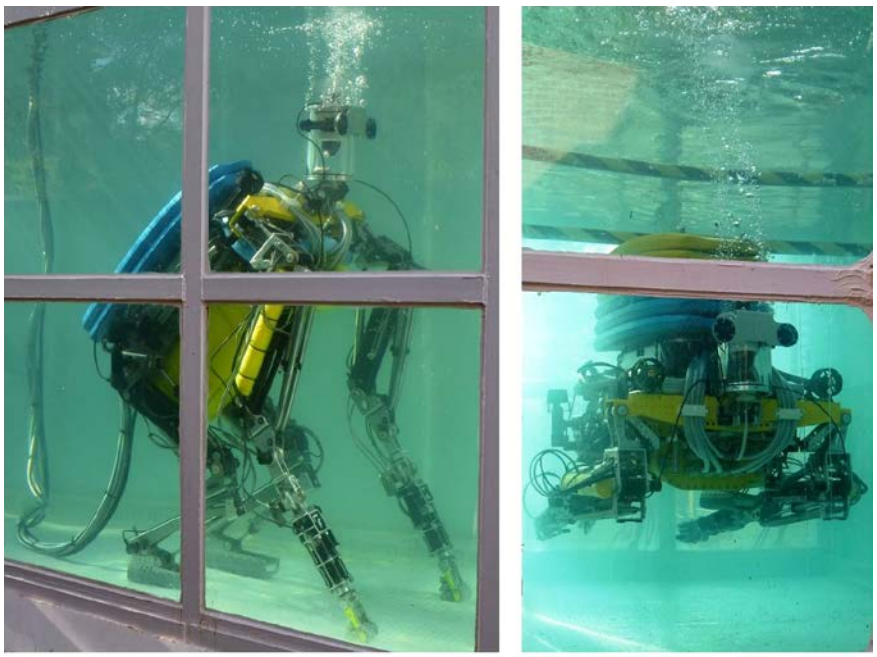

Fig. 4. Functional prototype of an underwater anthropoid robot: anthropoid mode (left) and vehicle mode (right). Patent No: ES2544007B2.

6 Conclusion

The aim of this chapter has been to contextualize the necessity of novel underwater robots for works requiring physical interactions. These robots are designed to assume the risks associated with some diving activities, carried out by human divers in hostile underwater environments.

There is a strong necessity of underwater works, but most of the available tools are prepared just for inspection tasks. ROV and ADS have already had decades of evolution and have proven to be useful technologies

for working at greater depths. Nevertheless, they lack human dexterity, which is very important for performing complex tasks.

Humanoid robotics can broadly contribute to this problem, providing human-like robots for underwater works.

The Red Sea Robotic Explorer is currently under development and promises interesting results, while there is no evidence that the underwater robots of the patents proposals have been materialized so far.

The potential applications of the presented DiverBot prototype, open new horizons in the applied research of underwater robotics. Thus, robotic divers could be the next generation of machines for underwater interventions, and the development of underwater humanoid robots will be certainly one of the challenges of applied robotics in the coming years.

Acknowledgements

The research leading to these results has received funding from the Spanish Government CICYT project Ref. DPI2014-57220-C2-1-P, DPI2013-49527-EXP, the Universidad Politécnica de Madrid project Ref. AL14-PID-15, and the RoboCity2030-III-CM project (Robótica aplicada a la mejora de la calidad de vida de los ciudadanos. Fase III; S2013/MIT-2748), funded by "Programas de Actividades I+D en la Comunidad de Madrid", and cofunded by Structural Funds of the EU.

References

Cass, S. 2013. DARPA Unveils Atlas DRC Robot. IEEE Spectrum.

Diftler, M.A., Mehling, J.S., Abdallah, M.E. 2011. Robonaut 2 - The First Humanoid Robot in Space. In 2011 IEEE International Conference on Robotics and Automation (ICRA), pp. 2178-2183.

Ejarque, G.E., Saltaren, R.J., Poletti, G.A., and Aracil, R. 2016. Robot submarino humanoide transformable. Patent No. ES2544007B2, Universidad Politécnica de Madrid. Spanish Patents and Trademarks Office.

Gerwick, B. 2007. Construction of Marine and Offshore Structures (Third Edition). CRC Press, Taylor & Francis Group: USA.

Hirabayashi, K., Ikeda, T., Shibata, Y., and Tsugaki, S. 1986. Underwater Work Robot. Patent No. JPS6116192, Japan Patent Office.

Khatib, O. 2015. The Red Sea Robotic Exploratorium: Enabling Intuitive Underwater Telemanipulation. Stanford University. Retrieved from: http://cs.stanford.edu/group/manips/projects/redsearobotics.html.

Lay, A.M. 2013. Hardsuit Atmospheric Diving Systems. UnderWater Magazine, 26(4): 14-23.

Lay, A.M. 2015. State of the Art: Remotely Operated Vehicles do it all. UnderWater Magazine, 28(1): 16-22.

Moore, S.W., Bohm, H., and Jensen, V. 2010. Underwater Robotics: Science, Design and Fabrication. MATE Center: USA.

Nagaoka, E., Inoue, M., and Maruyama, T. 1996. Submerged Inspection and Working Robot. Patent No. JPH08240689, Japan Patent Office.

Sakagami, Y., Watanabe, R., Aoyama, C., et al. 2002. The Intelligent ASIMO: System Overview and Integration. In IEEE/RSJ International Conference on Intelligent Robots and Systems, volume 3, pp. 2478−2483.

Sheafer, W.L. 2011. The Life of a Nuclear Diver, Nuclear Diving. Retrieved from: http://www.divingheritage.com/nuclear.htm.

Thornton, M.A. 2000. A Survey and Engineering Design of Atmospheric Diving Suits. Master thesis, Texas A&M University: USA.

U. S. Navy 2008. Guidance for Diving in Contaminated Waters. Retrieved from: http://www.supsalv.org/pdf/Contaminated.

WHS Council 2009. Technical Advisory for Inland/Inshore Commercial Diving Safety and Health. Workplace Safety and Health Council, Singapore. Retrieved from: http://www.asmi.com/download.cfm?dobjid=288.

CHAPTER 23

CABLE DRIVEN ROBOT TO SIMULATE LOW GRAVITY AND ITS APLICATION IN UNDERWATER HUMANOID ROBOTS

M. BAYAS, A. BARROSO, D. PEÑA, R. SALTARÉN, R. ARACIL, A. VERONESI, G. LIBERT

Centre for Automation and Robotics CAR (UPM-CSIC) C/ José Gutiérrez Abascal 2, 28006 – Madrid, rsaltaren@etsii.upm.es

This chapter addresses the main results obtained during the design and analysis of a cable-driven robot able to simulate the dynamic conditions existing in underwater environment. This work includes the kinematic and dynamic modeling as well as the analysis of the tension of the cables along different trajectories. The low-gravity simulator application is novel in the context of cable-driven robots and it is aimed to be implemented in an underwater humanoid robot. Therefore, this works can be seen as a test case of the complementary research contributions of the group of Robotics and Intelligent Machines at CAR in the recent years.

1 Introduction

In the past few years, cable-driven parallel mechanism have been increasingly studied since they are low-cost, light-weight robots that have all required physical features in industry regarding the load capacity or the workspace size. The application addressed in this work involves the design and analysis of a cable-driven robot as well as the implementation of different paths to be followed by the end effector. These results have been implemented in a CAE software to simulate the multibody dynamic of the system and obtain useful values like the variation of the strain of the cables along a trajectory or the position, speed and acceleration of the end-effector at any time.

A desired purpose of these developments is to manage the dynamic of an underwater humanoid robot attached to the end effector. With this cable-robot as a testing bench, it will be possible to simulate the usual forces that would appear when the robot is submerged like the buoyancy, which implies a vertical upwards force equivalent to a reduction of the gravity force. It can be possible also the application of lateral forces in order to simulate underwater currents or the effect of the waves on the surface of the sea.

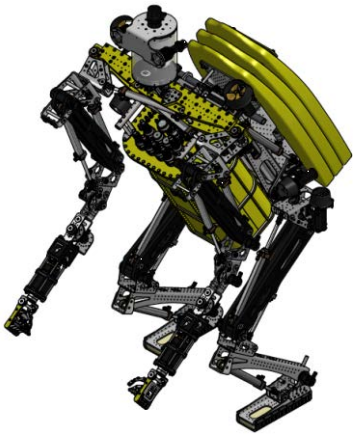

Fig. 1. The underwater humanoid robot, DiverBot.

This chapter shows the main results obtained with analytic procedures in order to obtain the models and with the simulations in a multibody dynamics software. In section 2 of this chapter is described the inverse kinematic analysis of the cable robot and the obtaining of the Jacobian of the system. Afterwards, section 3 shows the dynamic expressions obtained for the model. The implementation in the CAE software is presented in section 4 and finally, a short conclusion can be found in section 5.

2 Kinematic expressions

Once the position of the end effector is defined in its 6 degrees of freedom (position and orientation), we want to obtain all the values of the joints. This problem can be solved with an inverse kinematic analysis of the mechanical model. In the general case, this problem is reduced to solving all the algebraic equations of a multivariable system.

The dimensions chosen for the cable robot structure to develop the path planning and force analysis, considering the load of the humanoid robot is conformed by four pillars of 10m high with a square section of 50cm side.

These pillars are at the corners of a square of 10m on each side. There are eight actuators on the top of the pillars (two actuators per pillar) with their eight cables connected to them which can move the load along all the workspace. To relieve the strain on the engines, counterweights are attached at the opposite end of each cable.

The kinematic model has a central moving platform constrained by the eight cables with their length L_i variable with time and their orientation defined by unitary vectors u_i. These cables are connected to the pillars in the points B_i and connected crossed in the in points P_i in order to avoid singularities in the central position (i = 1, 2… 8)

When the platform moves, the position of its center of mass, P_G, linked to the moving coordinate system, K_P, varies respect the fixed coordinate system, K_B.

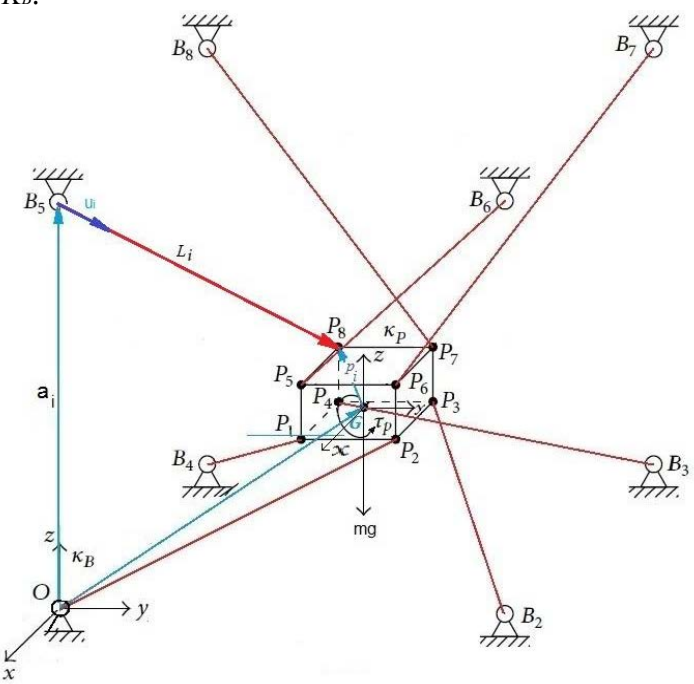

Fig. 2. Kinematic scheme of the cable robot of 6 DOF.

Following the kinematic notation (Fig. 2) the position of the end effector can be written as:

$$L_i = P_G - a_i + p_i \tag{1}$$

Where a_i is the position of each actuator in the fixed reference system and p_i is the position of P_i in the reference of the end effector. The Jacobian

matrix can be obtained in order to know the relation between joint speeds ($\dot{L}_i$) and the velocities of the moving platform in 6 degrees of freedom ($\dot{T}_i$) by the following expression:

$$\dot{L} = J^T \dot{T} \tag{2}$$

To obtain the Jacobian matrix, (1) must be derived respect time. It is non-symmetric matrix of dimension 8x6:

$$J^T = \begin{pmatrix} u_1 & p_1 \times u_1 \\ u_2 & p_2 \times u_2 \\ \cdots & \cdots \\ u_8 & p_8 \times u_8 \end{pmatrix} \tag{3}$$

3 Dynamic analysis

The dynamic model relate all the movements of the robot with the forces involved on it in order to make multibody simulations and obtain the dynamic values like forces and accelerations.

When all cables are tensioned, Newton-Euler laws can be used in order to obtain the moving equations respect a vector of generalized coordinates, $\mathbf{x} = [P_{Gx}, P_{Gy}, P_{Gz}, \alpha, \beta, \gamma]$. The vector $\theta = [\alpha, \beta, \gamma]$ defines the Euler angles (yaw, pitch and roll) of the platform and it is related with angular speed by:

$$\omega = S\dot{\theta} = \begin{pmatrix} \cos(\beta)\cos(\gamma) & -sin(\gamma) & 0 \\ \cos(\beta)\sin(\gamma) & cos(\gamma) & 0 \\ -\sin(\beta) & 0 & 1 \end{pmatrix} \begin{pmatrix} \dot{\alpha} \\ \dot{\beta} \\ \dot{\gamma} \end{pmatrix} \tag{4}$$

The forces of the actuators (τ) can be obtained from the forces applied to the end effector (F) by using the Jacobian matrix:

$$F = J\tau \tag{5}$$

The expression for the movement of the platform is:

$$M(x)\ddot{x} + C(x,\dot{x})\dot{x} + G(x) = -\tilde{J}\tau \tag{6}$$

Where:

$$M(x) = \begin{pmatrix} mI & 0 \\ 0 & S^T I_G S \end{pmatrix} \tag{7}$$

$$C(x, \dot{x}) = \begin{pmatrix} 0 & 0 \\ 0 & S^T I_G \dot{S} + S^T (S\dot{\theta}) \times I_G S \end{pmatrix} \tag{8}$$

$$G(x) = \begin{pmatrix} -mg \\ 0 \end{pmatrix} \tag{9}$$

$$\tilde{J}^T = J^T \begin{pmatrix} I & 0 \\ 0 & S \end{pmatrix} \tag{10}$$

The Inertia matrix, I_G, expressed in the reference system of the platform and is expressed in the fixed reference system by the similarity transformation: $S^T I_G S$. In a similar way, the Jacobian matrix has been referenced in the fixed system.

In order to have a better comprehension of the movement, a dynamic model of the electric actuators has been implemented and incorporated to the general dynamic equations.

4 Simulations with MSC ADAMS

With the multibody dynamics software MSC ADAMS, the model of the cable-driven parallel robot is developed following the structure detailed in section 2. In the end effector, the underwater humanoid robot has been attached adding an additional load of 150Kg. For these simulations the cables have considered rigid links with their corresponding mass.

As the inverse kinematics of the model is known, the length of all cables can be identified in any position or orientation of the moving platform. With this information, a path planning has been developed to set different trajectories for the end effector and study the behavior of the load, its varying dynamic parameters, the tension of the cables or the force needed by the actuators in any time.

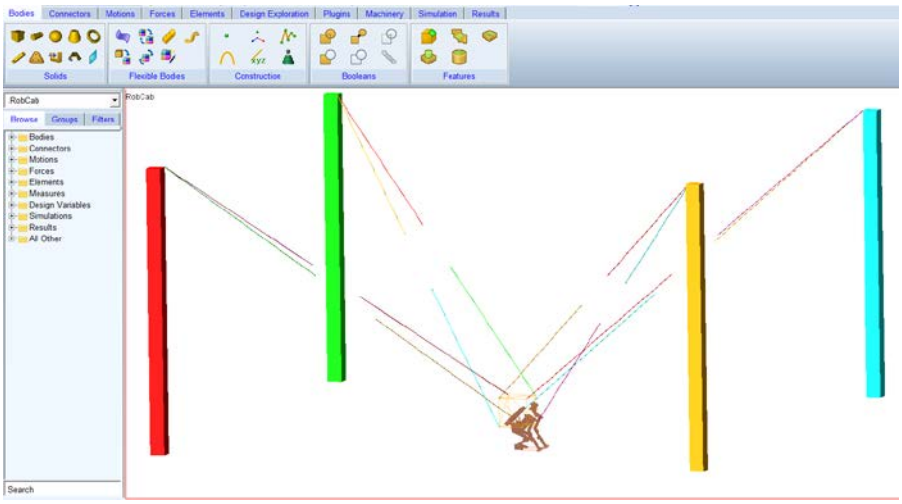

Fig. 3. Simulation of the model with the humanoid robot attached.

The workspace of the load is bounded not only by the geometric limits of the pillars but the maximum strain that cables can support, this is the wrench-feasible workspace (WFW).

In order to know the maximum forces that the cable robot has to manage during the working of the cable robot, the load is moved towards several singularity points situated on the frontier of the static workspace. A vertical trajectory has been defined in order to obtain the curves of tensions in the cables when the load is elevated 3 meters from the ground.

The dynamic values and the force in the cable under greater tension are presented in Fig. 4. At the beginning of the movement, it is needed a high effort of the actuators which generates high tensions in the cables. When underwater robot is situated in a higher position, actuators have to generate higher force in order to hold it in that static position. Tensions of the cables, will be bounded above by 5500N taken into account a situation where the robot is totally suspended. To maintain these boundary, top speed will be about 1 m/s with accelerations until 1m/s^2.

Another trajectory is shown in Fig. 5. Where a rotation of -30º is applied to the end effector respect to the vertical axis. Measures are taken in the cable under greater tension.

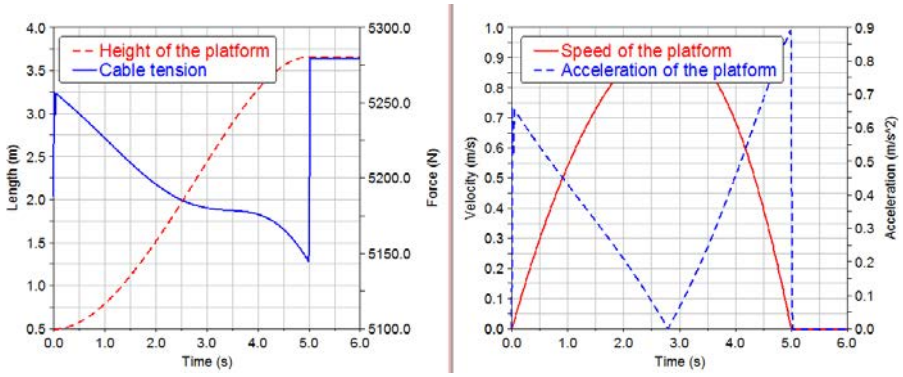

Fig. 4. Dynamic values of the vertical displacement of the load.

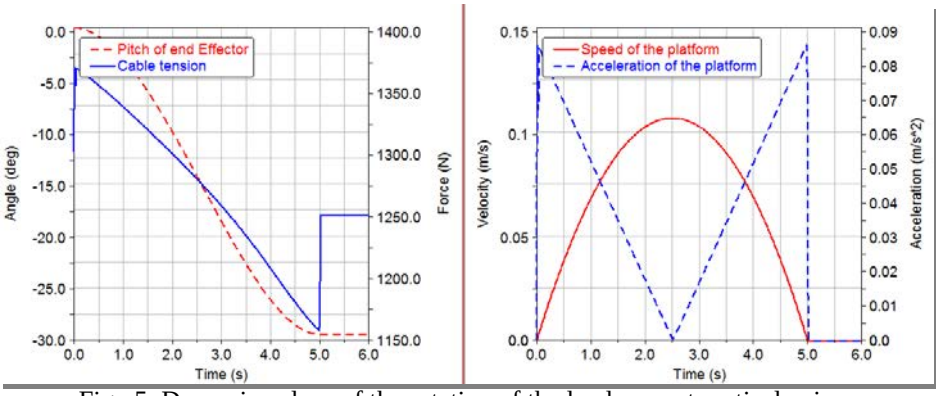

Fig. 5. Dynamic values of the rotation of the load respect vertical axis.

5 Conclusions

With the knowledge acquired with the dynamic model of this cable-driven parallel robot it is possible to size the components, define the feasible workspace of the end effector or set different trajectories. The next steps to follow can be the implementation in a real prototype that enables deeper research on the behavior of 6 degrees of freedom cable robots and the direct application in the simulation of low gravity and underwater environments on the previous prototypes developed by the group of investigation in CAR.

Acknowledgements

The research leading to these results has received funding from the Spanish Government CICYT project Ref. DPI2014-57220-C2-1-P, DPI2013-49527-EXP, the Universidad Politécnica de Madrid project Ref. AL14-PID-15, and the RoboCity2030-III-CM project (Robótica aplicada a la mejora de la calidad de vida de los ciudadanos. Fase III; S2013/MIT-2748), funded by Programas de Actividades I+D en la Comunidad de Madrid and cofunded by Structural Funds of the EU.

References

Tempel P. Schnelle F. Pott A. Eberhard P. 2015 “Design and Programming for Cable-Driven Parallel Robots in the German Pavilion at the EXPO 2015” Machines, 3, pp 223-241.

Avello A. 2014. “Teoría de máquinas”, Tecnum-Universidad de Navarra, Segunda Edición.

Lau. D.T.M. 2014. “Anthropomorphic Cable-Driven Robot”. Institutional Repository of The University of Melbourne.

T.Bruckmann, A Pott. 2013. “Cable-Driven Parallel Robots”, Proceedings of the Second International Conference on Cable-Driven Parallel Robots. Springer-Verlag Berlin Heidelberg. Springer.

Khosravi M. A., Taghirad H. D. 2013. “Experimental Perfomance of Robust PID Controller on a Planar Cable Robot”, Cable-Driven Parallel Robots Mechanisms and Machine Science Volume 12, pp 353-370.

Gouttefarde, M., Merlet, 2006 J-P, Daney D., “Determination of the wrench-closure workspace of 6 DOF parallel cable-driven mechanisms” Advances in Robot Kinematics INRIA, France, pp 315-322.

Riechel, A.T., Ebert-Uphoff, I. 2004 “Force-feasible workspace analysis for undersconstrained pointmass cable robots. Proceedings of the 2004 IEEE International Conference on Robotics and Automation, pp. 4956-4962.

CHAPTER 24

WAITER ROBOT: ADVANCES IN HUMANOID ROBOT RESEARCH AT UC3M

J. LORENTE[1], J. M. GARCÍA[2], S. MARTÍNEZ[3], J. HERNÁNDEZ[4], C. BALAGUER[5]

RoboticsLab, Universidad Carlos III de Madrid.
[1]jlorentemonzo@gmail.com, [2]juanmiguel.garcia@uc3m.es, [3]santiago.martinezlacasa@uc3m.es, [4]juanhernandezvicen@gmail.com, [5]carlos.balaguer@uc3m.es

Multiple robotic system are used to develop new tasks as a waiter robot. The most complex kind of robots devoted for these tasks are humanoid ones. This paper is focus on presenting the evolution of the control system applied on the humanoid robot TEO at the Carlos III University of Madrid. There are two main goals to be achieved by this research. The first one is to learn how a humanoid robot can manipulate objects without physical grasping, maintaining the object balance and its own whole-body balance, and to develop an appropriate control system to deal with this specific service application. The operation of the system is supported in the proposal of one simplified robot model that joins both the robot balance and manipulation model and the simplified object balance model. The second objective is to suggest new complex strategies related to balance control taking into account stronger external disturbance.

1 Introduction

The actual world is deeply adapted to humans, as we are the ones living in it. This is why the development of humanoid robots is such a relevant matter, getting rid of the need for adapting the environment. This has other advantages. A robot is mechanically similar to a human and it can carry out similar tasks. However, there are also disadvantages in designing a humanoid robot, apart from the obvious complexity of its building. This is to

say, the more resemblance between the humanoid and the human, the more the problems of the later become the problems of the former. One of these problems to be solved is equilibrium.

In this paper we go through the equilibrium control in a waiter robot. Not only do we control the equilibrium of the robot itself, but also the equilibrium of the objects being carried on a tray. This becomes a complex task since it is a non-grasping manipulation. On the one hand, the robot has the ability of sensing if it is losing stability and falling. On the other hand, it has the ability of avoiding the fall of the transported objects. These abilities are intrinsic and instinctive in human beings, but not in robots.

When it comes to equilibrium, we must take into account any influences in the system. It can suffer two types of disturbances (Petrović et al., 2014): the ones caused by the system itself and the external ones. Both types influence the locomotion equilibrium as well as the manipulation equilibrium. It is our job to analyze how they affect the system.

2 Waiter robot

The 'waiter robot application' simulates the movement behaviour of a waiter while trying to transport bottles/cups on a tray. There are two tasks for achieving the main target of this application. The first task is focused on keeping the balance of the transported object. During the execution of the application, the objects are disturbed by forces caused by the own movement of the waiter robot. The second task is to control the stability of the waiter robot. During its movement, the humanoid robot ought to be able to avoid falling while it walks. Both tasks, body balance and object balance, must be accomplished in the same control period, imposing a strict manipulation and locomotion coordination (Fig. 1).

The waiter task is bio-inspired in the real world. To define this application, the morphological aspects related with a human waiter were taken into account. So, like human beings use their own proprioceptive sensors to detect their equilibrium state, a robot also uses its sensor for locomotion tasks. These sensors are inertial, position and force/torque sensors. Besides, the sensors are necessary to develop manipulation tasks. Then, it is important to sense the arm's state to control the pose of the drink tray.

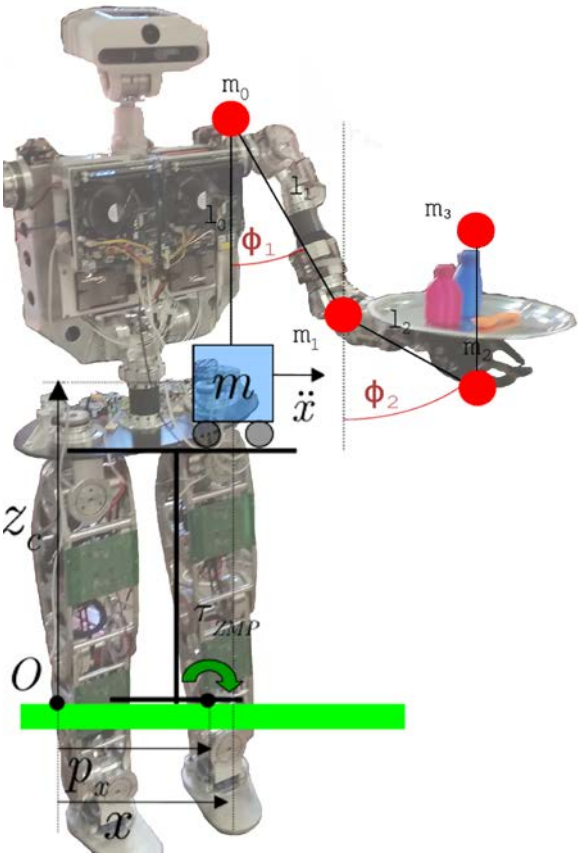

Fig. 1. Simplified mathematical model generated for balance control.

3 Locomotion equilibrium control

Several authors have been researching balance in bipedal robots since years ago, and this topic has suffered major development in recent years. Some of them have studied the forces acting on humanoid robots (Sardain & Bessonnet, 2004) and others have even developed balance strategies (Stephens, 2011). The stability control can be designed in so many different ways. For instance, using the Zero Moment Point as the reference point for stability, and implementing a ZMP balancing control (Vadakkepat & Goswami, 2008).

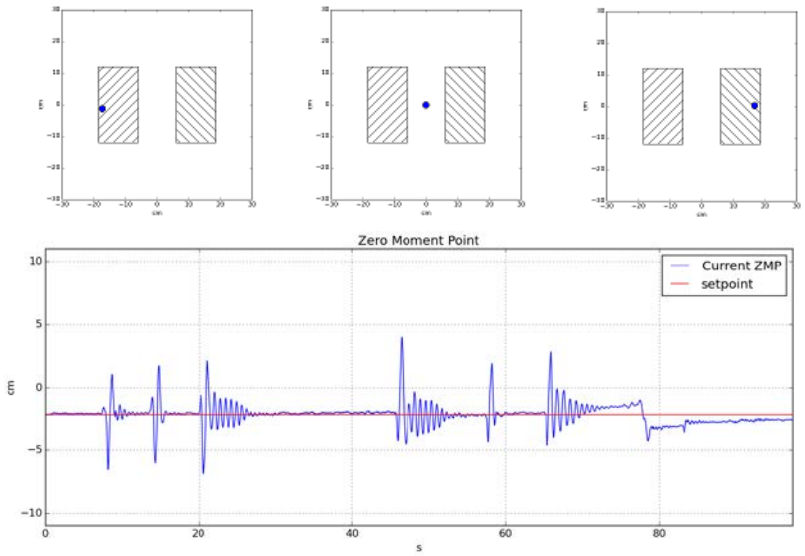

Fig. 2. Computation of ZMP for different situations and results of the stabilization control applying ankle strategy.

In the humanoid robotics research group, it is currently developing an equilibrium control for our humanoid robot TEO, using inertial and force/torque sensors, and based on the same principle regarding the ZMP. First of all, we use the data obtained through the sensor to compute the Zero Moment Point (Fig. 2) using the cart-table model (Kajita & Espiau, 2008). Then, the current ZMP and the desired ZMP are compared in a PID controller, which consequently offers an output. This output is used as the velocity input, in deg/s, to be sent to the motors of the robot's ankles. Finally, thanks to this velocity command, the rotation of the ankles counteracts the leaning of the robot avoiding its fall.

This strategy is implemented both in the sagittal and the frontal plane. However, it is slightly different for the frontal plane, as the system becomes a double-support inverted pendulum instead of a single-support one. For this case, the same procedure is followed but the velocity command is sent to the ankles and to the hip joints, trying to maintain the torso straight and then returning to the stability position.

4 Manipulation equilibrium control

To model the behaviour of the bottle or drinks on the tray, a linear inverted pendulum model (LIMP) is used. In this case, the goal is to maintain stability and the pendulum model is a good option because there is a large friction force between the bottle and tray. Due to a non-slip material in the tray, it is possible to affirm that there is no linear movement between the bottle and the tray. Only, rotational movements will be generated. For this reason, the LIPM model was chosen and not the cart-table as in the case of the stability of the whole-body humanoid robot. Therefore, the control algorithm mainly is focused on variations of the rotation's angle of the bottle to indicate its stability.

In this case, the bottle does not rest on a single point, i.e., the bottle rests on a surface. Then, it is possible to use the same balancing robot strategy to define the state of stability for the bottle. That means ZMP can be used as indicative. Thus, when the projection of the sum of the forces/torque in the centre of mass of the bottle exceeds the support surface with the tray, this one will fall. Therefore, it is important to develop a complex 3-D kinematics configuration with a special non-grasping device to keep the balance of the bottle over the tray (Balaguer et al., 2006).

5 Advances on the development of the waiter robot

We aim to achieve a equilibrium control during locomotion. Nevertheless, currently we are focusing on static equilibrium, not involving locomotion yet. That will be the next step once the static control is successfully implemented. On the other hand, static equilibrium is related to manipulation as they influence each other, so it has to be taken into account.

The already implemented equilibrium control works correctly when counteracting small disturbances. However, when a strong disturbance affects the robot, the ankles reaction is not enough for avoiding the fall. Here is when the hip and step strategies come into action. Firstly, the limits of the ankle strategy must be determined. We can set these limits mathematically or by experimentation and the aim is to be able to anticipate if the ankles reaction will be enough for avoiding the fall or not. Once this is achieved, the same must be done in order to check if the hip strategy is enough or the system needs to jump into the last option: the step.

The hip strategy is based on the same principle as the ankle strategy, with the slight variation that the velocity command is also sent to the hip joint. The motion of the whole torso provides a stronger counteraction,

which increases the options of stabilization. The step strategy can be implemented in many different ways (Assman, 2012), but the gist of it is to perform a step in order to change the support region and thus recover stability. Sometimes the gait planning is done according to the ZMP (Arbulu & Balaguer, 2007), which is a big advantage in order to join the locomotion process and the step strategy.

Furthermore, if more effective ways of keeping balance are wanted, we can dig into more complex strategies. The control of many other joints of the robot can add an extra point in the equilibrium control. Bending the knees, for instance, is useful for this purpose. Moreover, moving the arms back or forth helps keeping balance by changing the center of gravity, but this can be implemented only in one arm as the waiter robot is using the other one to carry bottles or cups.

Finally, we must also consider the influence of the manipulation process in the equilibrium control and viceversa. The motion required to avoid the fall of the objects being carried on the tray provokes instability in the body balance as well as the whole body equilibrium control affects the manipulation control. This is to say, the manipulation process must be taken into account in the equilibrium control and the effects of this equilibrium control will influence the manipulation system.

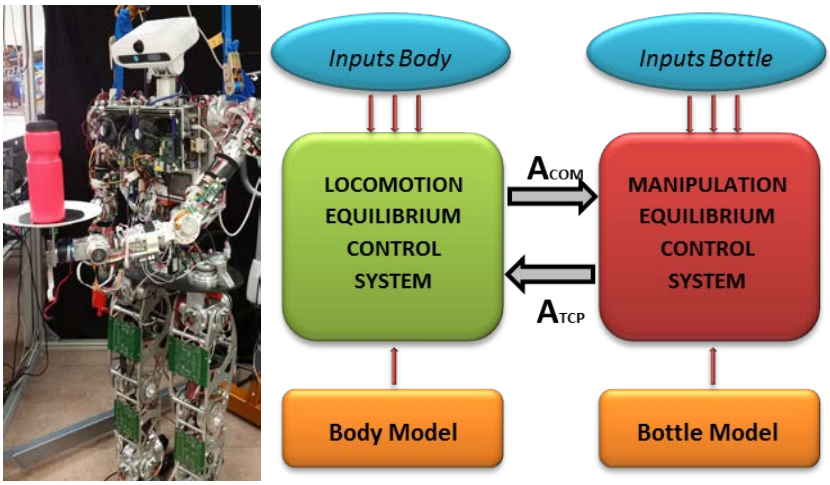

Fig. 3. Control and coordination scheme of the whole body balance.

6 Conclusions

The development of applications of the real world in humanoid robots implies the integration of basic research topics in this field of robotics. Gait planning (Arbulu & Balaguer, 2007) or multi-contact body balance (Vukobratović & Borovac, 2004) are examples of this basic research used to develop more complex tasks regarding equilibrium and locomotion. In the case of manipulation, classic research is focused on how objects can be grasped. In this paper the application of a waiter humanoid robot has been presented. This application combines classic equilibrium control techniques with a special case of manipulation. Non-grasping manipulation of objects implies to face the treatment of the problem in a different way. In this case, the main problem is to keep the object in equilibrium on a tray. So, all parameters related with body balance have been translated to determine the object balance. Thus, facing both balance problems in an integrated way increases exponentially the complexity of balance control in this application.

Acknowledgements

The research leading to these results has received funding from the RoboCity2030-III-CM project (Robótica aplicada a la mejora de la calidad de vida de los ciudadanos. Fase III; S2013/MIT-2748), funded by Programas de Actividades I+D en la Comunidad de Madrid and cofunded by Structural Funds of the EU.

References

Arbulu, M., Balaguer, C. 2007. Real-Time Gait Planning for the Humanoid Robot Rh-1 Using the Local Axis Gait Algorithm. International Journal of Humanoid Robotics (6:1): 71-91.

Assman, T. M. 2012. Humanoid push recovery stepping in experiments and simulations. Technische Universiteit Eindhoven: Eindhoven, Holland.

Balaguer, C., Virk, G., Armada, M. 2006. Robot applications against gravity. IEEE Robotics & Automation Magazine (13:1): 5-6.

Kajita, S., Espiau, B. “Legged Robots”, in Springer Handbook of Robotics, edited by B. Siciliano and O. Khatib, Germany: Berlin, pp. 361-389, 2008.

Petrović, V., Jovanović, K., Potkonjak, V. 2014. Influence of External Disturbances to Dynamic Balance of the Semi-Anthropomimetic Robot. Serbian Journal of Electrical Engineering (11:1): 145-158.

Sardain, P., Bessonnet, G. 2004. Forces acting on a biped robot. Center of pressure - Zero moment point. IEEE Transactions on Systems, Man, and Cybernetics - Part A: Systems and Humans (34): 630-637.

Stephens, B. J. 2011. Push Recovery Control for Force-Controlled Humanoid Robots. Carnegie Mellon University: Pittsburgh, USA.

Vadakkepat, P., Goswami, D. 2008. Biped Locomotion: Stability, Analysis and Control. International Journal on Smart Sensing and Intelligent Systems (1): 187-207.

Vukobratović, M., & Borovac, B. (2004). Zero-moment point—thirty five years of its life. International Journal of Humanoid Robotics, 1(01), 157-173.

CHAPTER 25

MANIPULATION BALANCE CONTROL SYSTEM BY COMPUTER VISION TOOLS

J. HERNÁNDEZ [1], J. M. GARCÍA[2], S. MARTÍNEZ[3], J. LORENTE[4], C. BALAGUER[5]

RoboticsLab, Universidad Carlos III de Madrid.
[1]juanhernandezvicen@gmail.com, [2]juanmiguel.garcia@uc3m.es, [3]santiago.martinezlacasa@uc3m.es, [4]jlorentemonzo@gmail.com, [5]carlos.balaguer@uc3m.es

Nowadays, new functions for humanoid robots are required. One of these functions can be an application in which the robot is able to serve drinks or cups over a try. Therefore, the goal of this paper is to show a research related to waiter robots and settles the bases of manipulation balance. To accomplish a manipulation balance oriented to transported object tasks, the control system and equilibrium of the object over a tray has been developed. Normally, the movement features come from the position of the motors or the inertial sensors. However, the novelty of this control system is to obtain these characteristics by computer vision tools.

1 Introduction

Throughout history, human beings have dreamt about a machine able to help us with our daily obligations or even to do them by itself. This desire, added to the advances which are taking place during the last years in different fields of the robotic and the technology available, have leaded to the need of developing new applications for humanoid robots to help people in the accomplishment of different tasks. In hospitals, museums, or office buildings/department stores, where they perform janitorial services, deliver, educate, or entertain. (Jardon, 2006) (Kulyukin, 2005) (Engelberger, 1999).

At the Carlos III University of Madrid, the humanoid robotics group "RoboticsLab", we have started to develop an autonomous mobile humanoid robot, which should be inserted as assistance robot or a personal robot in an office or a workshop environment as a waiter robot. The main component of such a robot for handling objects is its hand which carries out a tray.

The goal of this research is to investigate in the area of compliant control of humanoid robots with focus on the design and execution of complex manipulation skills. In particular, we must address the important subject manipulation control based on computer vision control. In essence, it is described the following aims: waiter robot application, kinematic and dynamic model for service tasks, and manipulation balance oriented to object transport tasks.

To control the stability of drinks or cups over the tray, methods related to artificial vision have been used. The inclination angle will be obtained to detect if it is in an equilibrium position or otherwise, if the humanoid robot's arm should make a correction in the tray position to avoid the bottle falling.

2 Robot model for manipulation balance application

To achieve a good balance control, it is needed to model the behavior of the bottle or drinks over the tray. Therefore, as the linear inverted pendulum model (LIPM) is the one whose performance is nearest to the reality, it has been chosen (Fig. 1) (Bugmann, 2015). The robot's hand corresponds to the car of the LIPM, whereas the bottle is the inverted pendulum which we want to maintain stabilized. Therefore, it is important to develop a complex 3-D kinematics configuration with a special non-grasping device to keep the balance of the bottle over the tray (Balaguer et al., 2006).

$$(I + ml^2)\ddot{\theta} - mgl\theta = ml\ddot{x}$$
$$(M + m)\ddot{x} + b\dot{x} - ml\ddot{\theta} = u$$

From these equations of the LIPM model can be deduced that the information needed to control the inverted pendulum, among others, comes from the angular acceleration. Therefore, the angular position of the bottle in each moment will have to be obtained by computer vision.

The decision of using this pendulum model is due to large friction force between the bottle and tray, as far as there is a non-slip material in the tray, there will be no linear movement between the bottle and the tray. Only, ro-

tational movements will be generated. Therefore, the main characteristic employed in the control algorithm to indicate its stability, will be focused on the variations of the rotation's angle of the bottle, as said before. In addition, we can disregard the viscosity in the mathematical pendulum model. This allows us to simplify further our model and thus, to reduce the computing load during the control of the bottle.

Since the bottle rests on a surface, the strategy of Zero Moment Point (ZMP) employed in Fig. 1, can be used to define its balance (Suleiman, 2011). With the projection of ZMP, which will be obtained by computer vision tools, the stability state can be established. If the ZMP has overtaken the bottle resting surface, this one will fall from the tray.

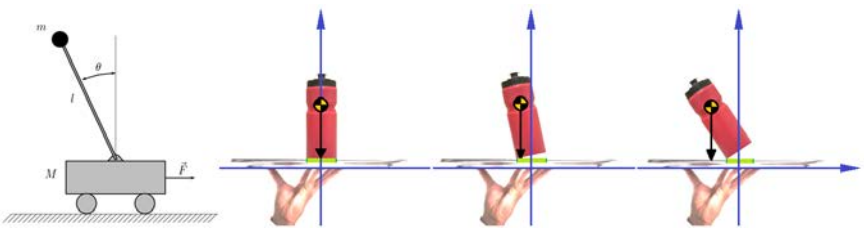

Fig. 1. Different degrees of stability applied to the linear inverted pendulum model.

3 Object characteristics obtained by computer vision

To accomplish the bottle balance by manipulation techniques following the LIPM, a wide range of features have to be obtained. These characteristics to close the control loop have been acquired mainly by computer vision. In this section, the way to obtain these features is explained.

To control the bottle equilibrium it is needed first to localize it in the space of the image, knowing the situation in which it is in each moment. The inclination angle will be also obtained, to detect if it is in an equilibrium position or otherwise if the humanoid robot must make a correction in the tray to avoid the bottle falling. Once the tilt angle has been acquired, the angular speed and the angular acceleration will be calculated. These properties will be the inputs to control the robot arm position, closing the feedback loop in order to achieve the bottle balance (Milighetti, 2011).

To localize the bottle in the image, after having differenced it from the other objects in the image, the geometrical center has been chosen based on a good reason: As it is geometrically symmetric, its center of mass is the same as its geometrical center. We also have to take in account that by

computer vision we are not able to know the content inside the bottle, so we consider it is filled up with water having constant density. Therefore, we have an advantage in knowing each time the position in the image corresponding with both, the COM and the geometrical center of the bottle.

To obtain the inclination angle of the bottle (Fig. 1), based on experiments carried in (Cholewiak, 2015), in which the estimated future positions obtained by vision of an object in a non-equilibrium state, were related with the real position demonstrating that error committed was near to zero, have confirmed our choice of obtaining the inclination angle by computer vision. To achieve that aim, the bottle has been introduced in a rectangular box which comprehends the whole bottle. At the beginning it has been set as a totally straight position in which the value is 90 degrees, being zero degrees when the bottle is lying on the right side and 180 degrees when it is lying in the other side.

Finally, the angular speed and acceleration have been obtained. To obtain the speed we can use the optical flow and the histograms to estimate the speed and the disparity (Okada, 1996). However, to be able to calculate the angular speed and acceleration of the bottle in the image, it is needed to know an initial angle position, a final angle position and the time used to move from one position to the other one, as seen in next equations:

$$\omega = \lim_{\Delta t \to 0} \frac{\Delta \theta}{\Delta t} = \frac{d\theta}{dt} \qquad \alpha = \frac{\Delta \omega}{\Delta t} = \frac{\omega_1 - \omega_0}{t_1 - t_0}$$

A problem appears when we want to implement these equations by artificial vision techniques. As far as the data obtained are discrete, we have to work with this limitation and take in account that in the first iteration we will not have enough information. Since the second iteration, enough data from past and present position/speed will be available. With these values obtained and taking in account the time of this process we can obtain the angular speed/angular acceleration of the bottle (Fig. 2).

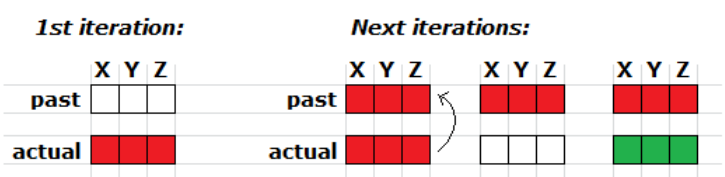

Fig. 2. Scheme for speed and acceleration discrete calculations.

4 Experiments performed

As the aim of this investigation is to set the bases for a service robot able to maintain the equilibrium of a bottle over a tray, is very important to evaluate the information obtained by computer vision techniques, to confirm that we have achieved a robust acquisition system. Therefore, several trials related to the bottle position and inclination have been performed.

First trials were made to acquire the position coordinates (x, y) of the geometrical center of the object among the image. As a result, a robust system to acquire the position of the bottle in the image has been obtained. This step was critical because its influence in the linear speed acquisition is high. From this point on, knowing the previous and the current position, linear velocity and acceleration have also been obtained.

The second experiment was related to the tilt angle of the bottle in relation to the horizontal plane. The program was configured in such a way that when the bottle was totally straight the bounding box appeared in a green color. When the bottle was bend no more than five degrees, the bounding box color is yellow (in this position, it still would be able to recover the equilibrium by its own weight), and lastly if this five degrees were overtaken, the bounding box changed its color to red meaning that the bottle was going to fall if corrective techniques were not applied. To set the inclination angle, the support surface and the position of the ZMP have been taken in account and the bottle has been modeled following the linear inverted pendulum model. We have to realize that once the ZMP has overtaken the support surface, the bottle is not any more in a position in which it can recover the equilibrium by itself without any external force.

After the acquisition of the tilt angle, we have obtained the angular position in each moment, allowing as calculating angular speed and acceleration. With this experiment we have confirmed that we are obtaining right the inclination angle of the bottle (Fig. 3).

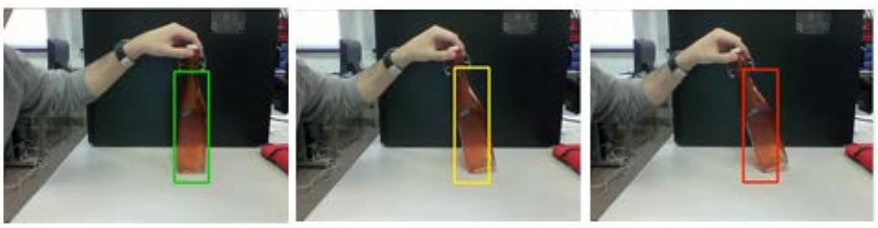

Fig. 3. Balance evaluation of the bottle applying to the LIMP model.

5 Future works

The experiments performed before, were developed with the aim of achieving a final complex system in which the humanoid robot is capable to assist people, by serving them drinks in a try. Therefore, the next step done in the research carried will be directed to reach a control system based on the position of the head in function of the direction of the movement of the bottle, in order to maintain through artificial vision techniques, the geometrical center of the bottle in the center of the image. The answer desired would be that once the bottle starts moving the robot also starts to move its head and to follow it (Fig. 4).

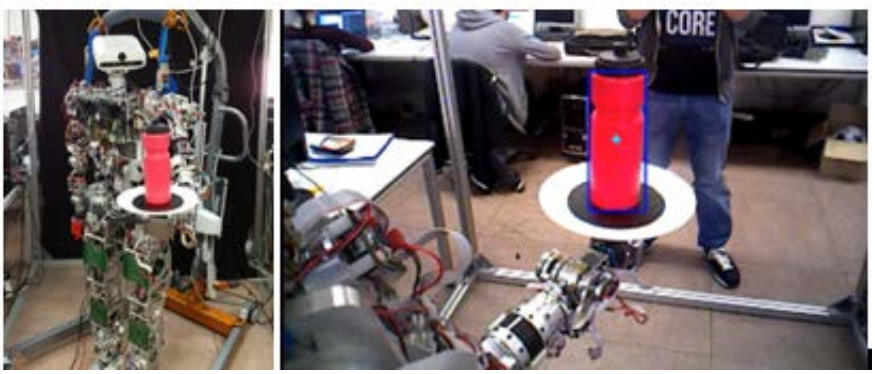

Fig. 4. Head movement to maintain the bottle centered in the image.

As the objective is to reach a full robust system, once the head control would be done, an arm position control will have to be integrated by using the angular speeds and accelerations obtained by computer vision, in order to rectify the tilt angle of the bottle and maintain it straight as a waiter would do to avoid the falling of the drinks over the tray.

Furthermore, once the bottle equilibrium over the tray has been achieved, an improvement in the application will be made in such a way that the arm can respond to an external stimulus such us a push force made for example by a human interaction, avoiding the falling of the bottle.

6 Conclusions

Manipulation tasks are not limited to grasping. There are manipulation applications in which physical interaction with objects is need but without grasping. The application exposed is one of them. The research performed

is based on the knowledge from balance research and its application for maintaining equilibrium of an object on a tray. The visual perception has been used to determine the parameters related to the movement of the object and, then, compute the equilibrium indicators. Thanks to the use of a LIMP model balance control will be implemented based on visual information. The next step will be the integration with the manipulation controller in order to keep object balance through arm movement, counterbalancing any king of disturbance.

Acknowledgements

The research leading to these results has received funding from the RoboCity2030-III-CM project (Robótica aplicada a la mejora de la calidad de vida de los ciudadanos. Fase III; S2013/MIT-2748), funded by Programas de Actividades I+D en la Comunidad de Madrid and cofounded by Structural Funds of the EU.

References

Balaguer, C., Virk, G., Armada, M. 2006. Robot applications against gravity. IEEE Robotics & Automation Magazine (13:1), p.5-6.

Bugmann, G. (2015). Joint Torques and Velocities in a 3-mass Linear Inverted Pendulum Model of Bipedal Gait. In Towards Autonomous Robotic Systems (p.82-93). Springer International Publishing.

Cholewiak S A, Fleming R W, Singh M., 2015. Perception of physical stability and center of mass of 3-D objects. Journal of vision, vol. 15, no 2, p.13-13.

Engelberger, G. Nof, S. Y. (1999). Handbook of industrial robotics (Vol. 1). John Wiley & Sons, 2nd ed, p.1201-1212.

Jardon, A., Gimenez, A., Correal, R., Cabas, R., Martinez, S., & Balaguer, C. (2006). A portable light-weight climbing robot for personal assistance applications. Industrial Robot: An International Journal, 33(4), p.303-307.

Kulyukin, V., Gharpure, C., & Nicholson, J. (2005). Robocart: Toward robot-assisted navigation of grocery stores by the visually impaired. In Intel-

ligent Robots and Systems, 2005. (IROS 2005). 2005 IEEE/RSJ International Conference on (p.2845-2850). IEEE.

Milighetti, G., Vallone, L., & De Luca, A. (2011). Adaptive predictive gaze control of a redundant humanoid robot head. In Intelligent Robots and Systems (IROS), 2011 IEEE/RSJ International Conference on (pp. 3192-3198). IEEE.

Okada, R, Shirai, Y, Miura, J., 1996. Object tracking based on optical flow and depth. En Multisensor Fusion and Integration for Intelligent Systems. IEEE/SICE/RSJ International Conference on. IEEE, 1996. p.565-571.

Suleiman, W., Kanehiro, F., Miura, K., & Yoshida, E. (2011). Enhancing zero moment point-based control model: system identification approach. Advanced Robotics, 25(3-4), p.427-446.

CHAPTER 26

MOVIDIS: FIRST STEPS TOWARD HELP THE MOBILITY OF PEOPLE WITH VISUAL DISABILITY IN PANAMA

H. MONTES[1, 2], I. CHANG[1], G. CARBALLEDA[1], J. MUÑOZ[1], A. GARCÍA[1], R. VEJARANO[1] and M. ARMADA[2]

[1]Universidad Tecnológica de Panamá; [2]Centro de Automática y Robótica-CSIC-UPM, hector.montes1@utp.ac.pa; hector.montes@csic.es

The autonomous mobility of visual disability people is a problem that must be solve in any part of the world. In this work is described the first steps that will be carried out to help the mobility of these people in public transport system in Panamá. Two different systems are proposed to achieve this purpose. The first is the design of apps for smartphones, and the other is a RF system with different communication protocols. These prototypes will be worn by the visually impairment people, and their easy-use will be intuitive.

1 Introduction

The World Health Organization (WHO) defines disability, including visual impairment, as a complex phenomenon reflecting an interaction between the characteristics of the human organism and the characteristics of the society in which he lives (WHO, 2011). Disability is part of the human condition, where almost everyone will suffer some form of temporary or permanent disability at some point in their lives, and the people who reach the senility will experiment increasing difficulties in their functioning. Disability is complex, and interventions to overcome the disadvantages associated with it are many and systemic, and vary according to context (WHO, 2011).

According to the WHO Fact Sheet No. 282 of 2014 entitled "Visual impairment and blindness" (WHO, 2014), in summary, states the following:

- 285 million people are estimated to be visually impaired worldwide: 39 million are blind and 246 have low vision.
- About 90% of the world's visually impaired live in low-income settings.
- Globally, uncorrected refractive errors are the main cause of moderate and severe visual impairment; cataracts remain the leading cause of blindness in middle- and low-income countries.
- 80% of all visual impairment can be prevented or cured.

In 2006, in the Republic of Panama, the First National Survey on Disability (PENDIS 2006) was performed, whose results were published in the report entitled "Study on the prevalence and characterization of disability in the Republic of Panama" (SENADIS, 2006). This report indicates that there are 370,053 persons with disabilities representing 11.3% of the population in 2006. Of them 83,757 people have visual impairment, which it is the second disability most prevalent in the population of Panama preceded by the multiple disabilities.

There are important technological solutions and results of interesting research projects to help people with visual disabilities in their autonomous mobility for different environments. A good example is the application Georgie awarded by Google in 2012 as the "Best Smartphone application for blind people" in Europe (Wilson-Hinds, 2015). This application is intended to help blind people navigate through daily obstacles such as taking the bus, read printed text and know where they are at all times.

However, this is a problem that still needs to be resolved. Therefore, there are several studies related to barrier-free mobility of visually impaired people in the use of public transport services, where they have to overcome numerous problems and specific obstacles (Fürst, 2010; Fürst and Vogelauer, 2013). Other studies suggest equip to bus stops and trams with fixed communications equipment, and visually impaired people with portable devices based on integrated voice synthesis able to communicate between them by means of Wi-Fi connection (Baudoin et al., 2005).

Other researchers have developed applications on smartphones based on MoBraille, which is a system that connects an Android phone with any Braille display with Wi-Fi. This allows a Braille reader benefit from many of the features of an Android phone efficiently and privately (Azenkot et al., 2011). In addition, other technologies based on mobile phone have been used, that consist of the Global Positioning System (GPS), Global System for Mobile Communications (GSM) and Bluetooth technology for purposes of location and communication installed in public transport at pilot cities (Markiewicz and Skomorowski, 2011).

Some concepts of these studies will be considered for the development of the MOVIDIS project, adapting to the particular characteristics of the public transport in Panama, which differ noticeably of the public transport system in Europe.

2 MOVIDIS project conceptualization

Improving the mobility of visually impaired people in the public transport in Panama will do the interaction of these people with the society and the environment becomes more tolerable and less dangerous, increasing the sense of integration into society. This is one of the main ideas proposed in this project, where it will use the technology to contribute these benefits to the people with visual disabilities in Panama.

The solutions proposed in this project are of technological nature, which will carry a hard work to be validated. However, these tasks are also related directly within the social field, starting with the visually impaired people, with the environment where they must interact (bus stops, streets, sidewalks, etc.), with those with whom they must interact (on the street, at bus stops, on the bus), and with the transport system itself (driver, bus types, types of routes, schedules).

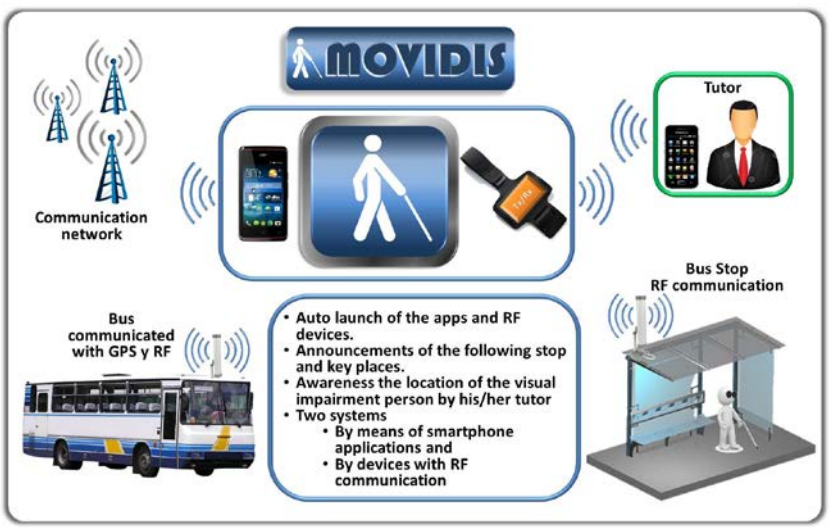

Fig. 1. Conceptual diagram of the MOVIDIS project.

Fig. 1 shows the conceptual diagram of the MOVIDIS project, where in its centre is represented a visually impairment person with two devices, a

smartphone and a RF device. Both devices will be used by these people in order to mobilise themselves within public transportation and its environment. In order to carry out these tasks, will be designed some specific applications for smartphones based on android (apps), and electronic prototypes using RF devices to connect (communicating between them) the visual disability people with the bus stops, with the bus, with the bus driver. Besides, the tutor of the visually impairment people will always have access to their location, with the purpose of the safety of themselves. On the other hand, the project members have the necessary expertise regarding smartphone apps design, RF communication device design, and in automatic control of buses (Montes et al., 2010; Montes et al., 2011; Montes et al., 2013).

3 Description of the smartphone apps design

One of the systems that will be developed to support the mobility of visually impaired people is focused on the use of android phones with capacity for monitoring the geographical location of these people. The applications that will be developed have the following general requirements: (a) to serve as guidance in public transport, and (b) to assist in the autonomous mobilization in environments that allow access to bus stops, for the visually impaired people. These applications will be integrated into a user-friendly format.

These apps must comply with the following:

- Detect the correct bus stop and the specific route.
- Geographical location of the visually disability people (ViDis) with the support of Google maps, GPS, and satellite coordinates.
- Emit voice messages of the place-name or geographic location, for both the ViDis and their Tutor.
- Simulation as a GPS device in the android phones of the bus drivers.
- Positioning and location in indoor of the ViDis in order to direct them toward the bus stops.

In Fig. 2 the functional diagram of the smartphone apps that will be designed within MOVIDIS project is shown. The interaction between the ViDis with the bus (and bus stop) and with the tutor is represented on the diagram. Besides, the ViDis must interact in indoor in order to know how to access to the exit to move toward the bus stop. For this purpose, several devices and communications signals will be used in the design of this system (RFID, NFC, Smart Beacon, WiFi, Bluetooth, XY Find-it, voice).

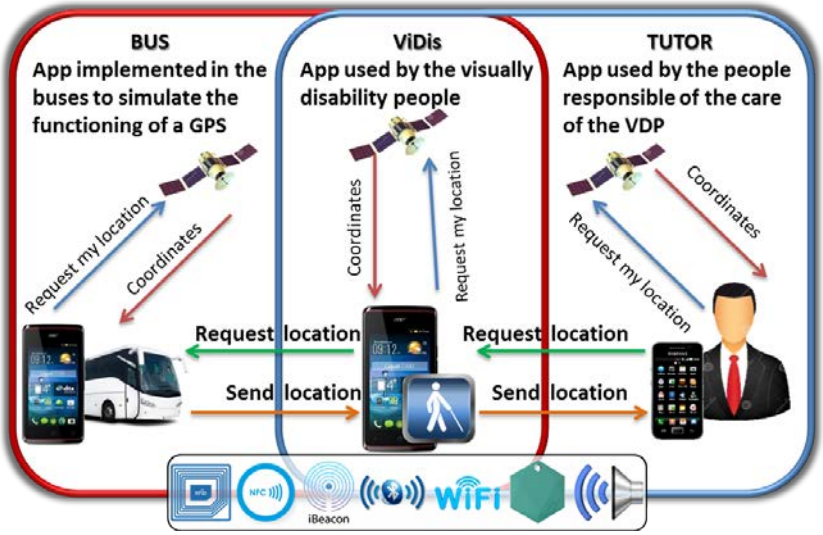

Fig. 2. Functional diagram of the smartphone apps in MOVIDIS project.

4 Description of the RF system design

The RF system that will design in MOVIDIS project will be based on Electronic Travel Aids (ETA) devices, which transform information about the environment that would normally be relayed through vision into a form that can be conveyed through another sensory modality (Dakopoulos and Bourbakis, 2010). This concept is very useful to assist in the mobility to visually impaired people, e.g., in the public transport system in cities of Panama. In order to achieve this objective, the RF system must have the following devices and/or characteristics:

- ETAs device for guiding of the ViDis through the outdoor environment.
- RF transceiver devices installed in the bus stops in order to communicate with the ETAs and with other transceiver devices in the bus.
- RF transceiver devices installed in the bus in order to communicate with the ETAs and other transceiver devices.
- RF transceivers installed in the bus station in order to communicate with the transceiver in the buses to acquire the stored data and to modify the patterns of new route of the bus.

The nomenclature that will be used for the design of RF system devices in the MOVIDIS project are presented below:

- MOVI-ETA: the device responsible for sending/receiving information from/to the ViDis to/from other modules of the RF system.
- MOVI-bus: the transceiver device that will be installed in buses of the public transport system.
- MOVI-stop. The transceiver device that will be installed on the bus stops.
- MOVI-master. The transceiver device to be installed at the bus station of the public transport system.

In Fig. 3 the coverage areas of the different subsystem that compose the RF system for MOVIDIS project are shown. Besides, the communication protocols between these subsystems, which have been considered for MOVIDIS, are presented in the legend of Fig. 3.

The range and power of RF signals transmission are important variables that are considered during the design, implementation and validation of the prototypes in order to have a good efficiency in the signals quality.

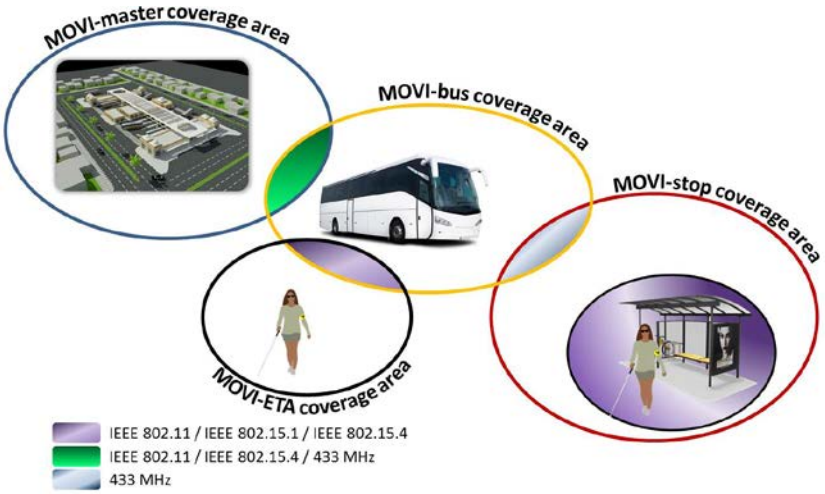

Fig. 3. Coverage areas and wireless communications protocols in MOVIDIS.

5 Conclusions

MOVIDIS is a project funded by SENACYT (*Secretaría Nacional de Ciencias y Tecnología*) from Panama for assist the mobility of people with

visual disability in this country. MOVIDIS is the first project of technological nature that will be developed in Panama, therefore will have a positive impact in the citizenship.

Two different communication systems are proposed, one is apps for smartphones with android and the other is a RF system with different protocols, in order to provide the required data/information to the ViDis for their mobilization in autonomous way within the public transport system of Panama. It should be noted that the public transport system in Panama is not very efficient if it is compared with the public transport system from Europe. Therefore, the challenge in this project is huge.

Acknowledgements

This work has been developed within the framework of the MOVIDIS Project, funded by SENACYT under Contract Nº 109-2015-4-FID14-073. Dr. Héctor Montes also acknowledges support from the RoboCity2030-III-CM project (Robótica aplicada a la mejora de la calidad de vida de los ciudadanos. Fase III; S2013/MIT-2748), funded by Programas de Actividades I+D en la Comunidad de Madrid and cofunded by Structural Funds of the EU.

References

Azenkot, S., Prasain, S., Borning, A., Fortuna, E., Ladner, R.E., and Wobbrock, J.O. 2011. Enhancing independence and safety for blind and deaf-blind public transit riders. In: Proc. of the SIGCHI conference on Human Factors in computing systems. Vancouver, Canada, pp. 3247-3256.

Baudoin, G., et al. 2005. The RAMPE Project: Interactive, Auditive Information System for the Mobility of Blind People in Public Transports. In: Proc. of the 5th Intl. Conf. on ITS Telecom. ITST 2005, Brest, France.

Dakopoulos, D. and Bourbakis, N. G. 2010. Wearable Obstacle Avoidance Electronic Travel Aids for Blind: A Survey. IEEE Trans. on Systems, Man, and Cybernetics, Part C: Applications and Reviews, 40, (1) 25–35.

Fürst, E. 2010. Mobility barriers in urban transport for the sight or hearing impaired: Solutions help all passengers. In: Real Corp 2010: Cities for Everyone. Live., Healthy, Prosperous. Vienna, 18-20 May, pp. 437-444.

Fürst, E. and Vogelauer, C. 2013. Best and bad practices in public transport: approaches to a barrier-free design for the visually and hearing impaired. European Transport Conference 2013. 29p.

Markiewicz, M., and Skomorowski, M. 2011. Public transport information system for visually impaired and blind people. In Transport Systems Telematics. Springer, pp. 271-277.

Montes, H., Salinas, C., Sarria, J., and Armada, M. 2011. High-Accuracy measurements system for secure steering of large vehicles. In Proc. Field Robotics, CLAWAR2011, Sept. 6-8, Paris, France, pp. 455-462.

Montes, H., Salinas, C., Sarria, J., Armada, M. 2010. Lateral and Longitudinal Control System for the Automation of an Articulated Bus. In: Proc. Emerging Trends Mobile Robotics, Sept. 3, Nagoya, Japan, pp. 793-800

Montes, H., Salinas, C., Sarria, J., Reviejo, J., Armada, M. 2013. Automatic Control of a Large Articulated Vehicle. In: Proc. ROBOT2013: First Iberian Robotics Conf., 28-29 Nov., Madrid, Spain. Advances in Intelligent Sys. & Computing, Ed. Springer, Vol. 253, 2014, pp 427-441.

SENADIS. 2006. Estudio sobre la prevalencia y caracterización de la discapacidad en la República de Panamá. Informe Final. Grupo para la Educación y Manejo Ambiental Sostenible GEMAS.

WHO. 2011. Word report on disability. Published by the WHO and the World Bank. Available in: http://whqlibdoc.who.int/publications/ 2011 /9789240685215_eng.pdf?ua=1

WHO. 2014. Visual impairment and blindness. Fact Sheet Nº 282, August of 2014. Available in: http://www.who.int/mediacentre/factsheets/ fs282/en/

Wilson-Hinds, G. 2015. Screenreader-Supporting blind and visually impaired users. UK. Available in: http://www.screenreader.net/

CHAPTER 27

FACIAL EXPRESSIONS AND VOICE CONTROL OF AN INTERACIVE ROBOT

P. ENCALADA, B. ALVARADO, F. MATÍA

Centro de Automática y Robótica, Universidad Politécnica de Madrid,
b.alvarado@alumnos.upm.es, fernando.matia@upm

There are different types of interfaces for human-robot interaction (HRI), but in the case of social robots, few have been developed. Doris is a new interactive social robot designed to work in indoor environments where the exchange of information with people is the main goal, which justifies that part of the research focused on HRI. Speech is the main method for interaction and has been performed based on visemes lip syncing to solve this problem. The lip syncing performed consists in the union of two channels, visual and auditory, with parallel coordination between mouth movements of the robot consisting of 6 degrees of freedom and where the audio text synthesized is predefined by the user, so the robot can communicate with the environment demi-naturally. The audio synthesis is performed with a Text To Speech (TTS) electronic card, containing a configuration set for tone, speech pronunciation, frequency, language, etc. The position of the robot lips are preset coordinates for each viseme to pronounce syllables in the Spanish language, stored in a coded database acceded by the synchronization algorithm which sets the mouth position interactively and ends with the syllables of the string analyzed.

1 Robot architecture

Doris is a half-humanoid robot. Its base consists of a differential drive PatrolBot robot in which the upper body and the mechanical head are installed. It has an onboard computer, with Ubuntu 12.04 and Robotic Operative System (ROS). A scheme of the robot's architecture is shown in Fig.

1, where the implementation leads to a Server-Client application, being the server the robot itself.

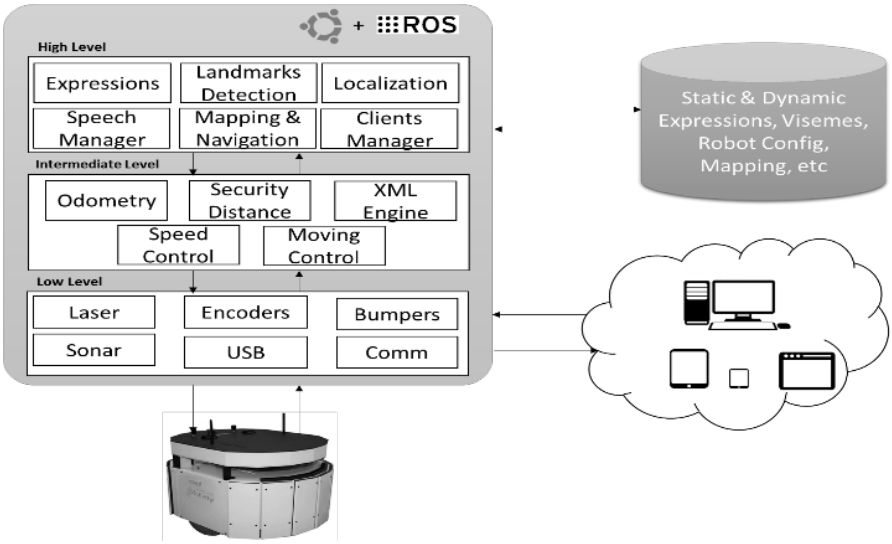

Fig. 1. Doris architecture.

Clients like a mobile, desktop and web applications, can connect to the robot wirelessly to request information or perform certain task. This architecture allows reading different sensors such as laser, encoders, bumpers, etc. transform that data from low level to an intermediate level so it can be processed for odometry, motion, etc. In this level there is the XML engine, which serves to the higher level to perform database tasks.

In this High level section, the main important subtasks for this project are the Expression and the Speech Manager. Their connection with the robot is shown in Fig. 2.

The hardware expressed in the figure, shows the cards connected into the robot. The face movements (Hernández, 2014) are controlled with a Master Pololu card (Pololu Maestro Servo Controller User's Guide, 2016), which connects via USB, while the audio synthesis (Encalada, 2016) uses an Emic2 Parallax card (Parallax, 2016), which connects via RS232.

In social robotics, the most important thing is related with the HRI aspect, so that the user can feel comfortable when interacting with the robot. Robots have different ways to communicate with humans, such as voice, facial expressions, language, gestures and movements, personality, etc.

In the latest years different prototypes had been designing and developed for different areas as entertainment, museum guiders, hospital helpers (Encalada, 2016), having in mind to avoid the uncanny valley.

This is a coefficient measuring the rejection or of robots with human-like appearance, which is an important aspect to be considered when designing and developing a robot. This phenomenon was studied by Masahiro Mori, and named by Sigmud Freud.

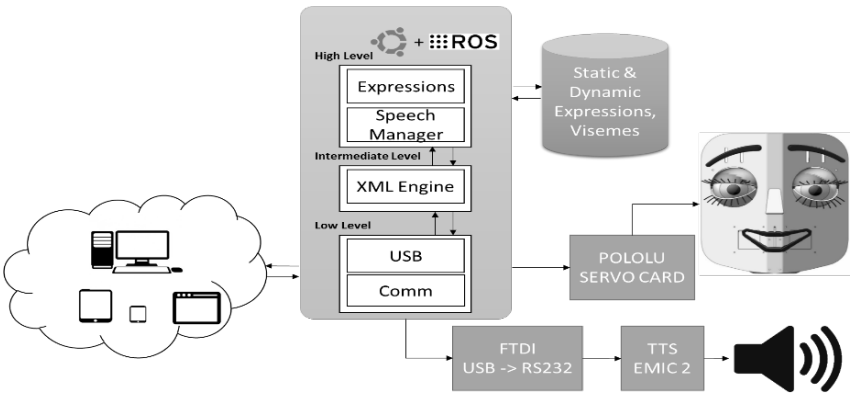

Fig. 2. Expressions and Speech Manager Architecture in Doris.

The level of acceptance or rejection is shown in Fig. 3, where an expectation of this phenomenon is obtained from examples, from an industrial robot to a human itself with excellent health conditions (Mori, 1970). It can be appreciated that this acceptance level is not a linear trajectory, having a big drop down when the robot starts being more human-like.

In the speech synchronization with the mouth movement there is an acoustic unit named viseme, which is the visual representation of the generated sound and the exact position of the mouth.

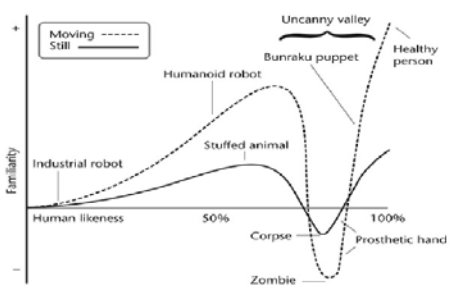

Fig. 3. Expressions and Speech Manager Architecture in Doris.

2 Lip syncing

In order to improve the speech bimodal perception, a lip sync algorithm has been developed, which consists in the hardware shown in Fig. 2.

Doris' lips are composed of six degrees of freedom, commanded by the servomotor itself, which are manipulated in order to emulate the speech. These lips were inspired in a female human anatomy.

Table 1. Description of the muscles implied when speaking.

N	Muscle	Functionality
1	Upper elevator lip	Lifts up the upper lip
2	Orbicularis	Opens and closes the lips forward and backward movements
3	Lower depressor lip	Depress de lower lip
4	Mentalis	Lifts up the skin chin and influences the lifting of the lower lip
5	Risorius	Retracts the lip commissure (smiling)
6	Zygomaticus major	Rise up the lip commissure abductor
7	Zygomaticus minor	Lifter and abductor of the upper lip mid part

The six degrees of freedom of the Doris' lips are equal to the movement described in the Table 1. A comparison is made in Table 2 from the female human lips to Doris' lips (Fig. 4).

Table 2. Doris and human lips comparison table.

N	Muscle	Corresponding degree of freedom
1	Upper elevator lip	1
2	Orbicularis	1, 2, 3, 4, 5, 6
3	Lower depressor lip	2
4	Mentalis	2
5	Risorius	3,4
6	Zygomaticus major	4
7	Zygomaticus minor	1

The steps to achieve the lip syncing are shown next:

Insert Text: the robot operation is responsible for configuring the system from any client. The algorithm receives the information to be transmitted through the robot in a string based format.

String analysis: the string must be normalized before moving to the next block. This means that it should remove some characters, symbols and spaces nor required to proceed with the hyphenation.

Hyphenation: it is done by taking into account Spanish language division rules.

Comparison with visemes database: each syllable is compared with the encrypted database, where each element has the syllable and the viseme code to which it belongs. Simple or compound visemes exist.

Select motion: each viseme has specific coordinates, which means that the robot actuators are placed in a specific position for visual effect in the corresponding syllable pronunciation and these data are sent to the Pollolu card alongside while the audio synthesis is being undertaken

Text to speech converter configuration: in this block commands to the Emic2 card are sent to set variables such as pitch, speed, amplitude and language.

Converting text to speech: commands are sent from the Doris Kernel to Emic2 card which is responsible of synthesizing the audio character string requested by user.

The Spanish language has 27 letters which combined make 2479 syllables, each one written in a XML Database. The syllables database was arranged so it can have a distribution for different visemes, resulting in 52 visemes groups.

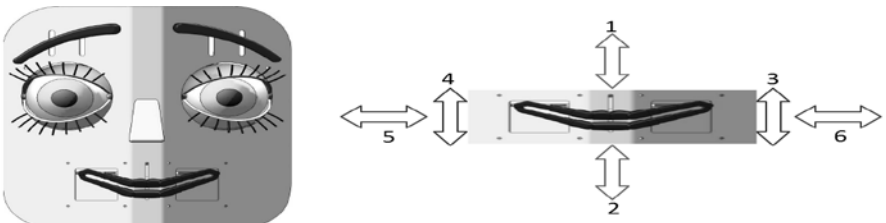

Fig. 4. Doris's lips.

The 2479 syllables are coded in such form that the codification header represent the group which the viseme belongs, shown in Fig. 5. The classification with this database and the viseme assignation was realized by checking each syllable and comparing to the corresponding viseme.

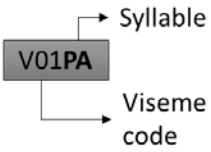

Fig. 5. Syllable and viseme code.

3 Test and results

Several tests had been made to the system. The text to say is “Master en Automática y Robótica”, the Fig. 6 shows the acoustic result synced with the servo movements, in this case with servo_0.

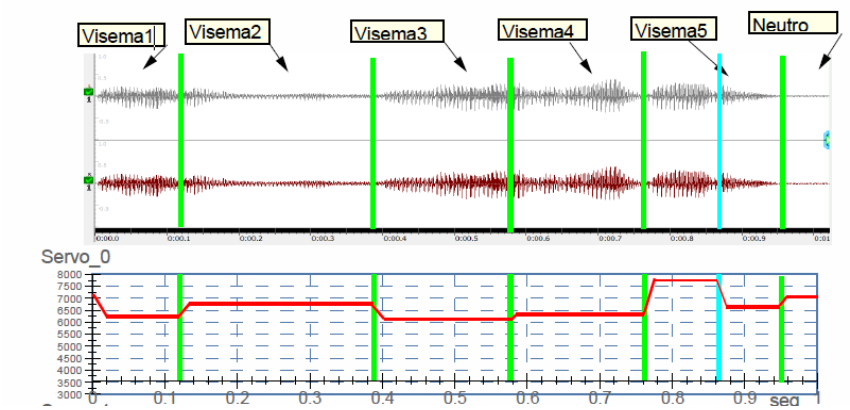

Fig. 6. String conversion to Audio synchronized with servo movements.

3 Conclusions

It has been created a coordinated movement sequence from the analysis of the text features to synthesize, improving the bimodal reception of speech, the audio and visual robot lips movement channels are synced, increasing its own level of compression or robot-human information exchange.

The string division used to synthesize acoustic units like syllables, corresponds to movements (viseme). A specific XML database was created for the Spanish language syllabic division. This database with quick access has the six servomotors positions for the main seven visemes taken into account.

An embedded circuit was used for text to voice synthesis. Having its own microprocessor makes easier the task, while the robot is performing other tasks like moving the lips.

Acknowledgements

The research leading to these work has received funding from the NAVEGASE project (*Navegación Asistida Mediante Lenguaje* Natural, DPI 2014-53525-C3-1-R), funded by Spanish *Ministerio de Economía y Competitividad*, as well as from the RoboCity2030-III-CM project (Robótica aplicada a la mejora de la calidad de vida de los ciudadanos. Fase III; S2013/MIT-2748), funded by Programas de Actividades I+D en la Comunidad de Madrid and cofunded by Structural Funds of the EU.

References

Masahiro Mori (1970). The Uncanny Valley. Energy 7(4) pp. 3335, translation by Karl F. MacDorman and Takashi Minato.

M. Álvarez, R. Galán, F. Matía D. Rodriguez-Losada A. Jiménez (2010), An Emotional Model for a Guide Robot, IEEE. Transactions on Systems, Man, and Cybernetics Part A, 40(5) pp. 982-992. Systems and Humans, USA.

B. Hernández (2014) "Control de Gestos de una Cara Robotizada". Final Bachelor Degree Dissertation. Universidad Politécnica de Madrid, Spain.

P. Encalada (2016) "Control de Voz y Expresiones Gestuales en un Robot Interactivo". Final Master Degree Dissertation. Universidad Politécnica de Madrid, Spain.

Personal Robot Group, "Leonardo", [Online].
http://robotic.media.mit.edu

UPF, "iCub_, [Online].
http://www.upf.edu/enoticies/es/0910/0803.html.

C. Breazeal, "Designing Social Robots", The MIT Press, Cambridge, 2001.

Parallax, “Emic 2 Text-to-Speech Module”, [Online]. https://www.parallax.com/product/30016.

Pololu, “Pololu Maestro Servo Controller User's Guide”: https://www.pololu.com/docs/0J40/all#5

CHAPTER 28

TOWARDS COMPLEX HUMAN ROBOT COOPERATION BASED ON GESTURE-CONTROLLED AUTONOMOUS NAVIGATION

J. DE LEÓN, M. A. GARZÓN, D. A. GARZÓN, J. DEL CERRO and A. BARRIENTOS

Centro de Automática y Robótica-CSIC-UPM, jorge.deleon@upm.es

This paper presents a new approach for human robot co- operation, where a mobile ground robot is provided with the ability of following a person that has been detected with a Kinect sensor. It can plan a trajectory to follow the person and avoid obstacles that appear in the environment in an autonomous way. It has been developed to work in coordinated tasks where the person needs to exchange data and take advantage of the sensors, communications and other capabilities of the robot, in order to accomplish a collaborative labor with a situation of proximate interaction. The UGV is controlled by reading some predefined gestures of the person, and the autonomous navigation is based on a well established navigation scheme. A set of initial experiments demonstrate the feasibility of the system.

1 Introduction

A new generation of service robots has emerged. Robots are moving out from factories, and entering our houses and every day lives. The spread of these robotic systems and the frequent interaction with humans in these scenarios led to the broadening of another subject area: human-robot interaction, also known as HRI.

Human-robot interaction is dedicated to understanding, designing, and evaluating robotic systems to be used by or with humans and involves a continuous communication between humans and robots, where communications are implementable in different ways. We can distinguish two general categories of interaction:

- Remote interaction: humans and robots do not share the same physical workspace, being separated spatially or even temporally (e.g. the Mars Rovers are separated from the Earth both in space and time);
- Proximate interaction: humans and robots are located within the same workspace (for example, service robots may be in the same room as humans).

We have focused on a proximate interaction where the human was in charge of the guidance of the collaboration task. In the experiment, the person walks randomly through the obstructed scenario while he gives positioning orders to the robot by body gestures. Then, the robot follows his partner by autonomous navigation, at the same time that it must achieve a specific relative position to the person in response of the given gestures. At this point, our proposal starts to differ to other research works by not only using the gesture control to simple teleoperation, even more, getting a team joint formation by human and robot. This formation is maintained meanwhile they are avoiding the obstacles on their way.

Until there, two levels of interaction are entailed: gesture guidance and autonomous tracking. But our work goes further and presents a novel approach to the HRI that includes a third level of interaction. It involves a collaborative task simulation where one UGV and one human have to continuously exchange information to accomplish a joint labor.

2 Related work

Gesture control for robots is not a novel idea, in fact, (Waldherr et al., 2000) gives a good approach to a human tracking, task assignment and navigation control for a mobile robot using gesture recognition techniques. Their system follows the operator arm with a camera and a computer vision system in order to identify preconceived configurations and movements; information related to different actions. Nonetheless, their tracking module is unable to follow people who do not face the robot and the distance between the robot and the operator has to be maintained constant.

Nowadays, there has been a lot of research works addressing the RHI through gesture or posture identification using Kinect®. Most of the ap-

proaches are oriented to the study of humanoids and articular robots motion. (Igorevich et al., 2011) controls the arms of the humanoid Huno Robot. (Quian et al., 2013) gives three kinds of tasks to a pair of articular robotic arms. (Yang et al.) have developed a system to achieve the simulation and the NAO robot control using the skeleton representation of the human posture. (Lei et al.) goes further and uses the joint angles representation of the skeleton for giving to the system an easy operator exchange. (Chang, Nian, Chen, Chi, & Tao, 2014) studies the RHI language through the semaphore alphabet recognition.

This kind of HRI has been also explored using mobile robots. Perhaps, the closest study to our approach is (Bonanni, 2011). He also integrates a gesture recognition module with a people tracking system in a follow people task for a UGV. Nevertheless, their robot is not available to make a full navigation labor and it has no other function but to follow the operator.

It can be appreciated that none of the works listed above achieves the full operational requirements needed for the task that we are intending. Even more, everyone approaches to the HRI only from the technical view, but not from a collaborative goal like our proposal.

3 The mobile platform

The platform is based on the Summit XL® platform by Robotnik® (Fig. 1). It has skid-steering kinematics. The robot can move autonomously or it can be teleoperated using video feed from an on-board camera. Furthermore, it is equipped with a small form factor PC which allows deploying all the data processing and navigation algorithms in a fully autonomous manner.

Various sensor modalities are also present. The odometry is provided by an encoder on each wheel and a high precision angular sensor assembled inside the chassis. One Hokuyo UTM-30LX-EW laser rangefinder is mounted on the platform, it can scan a 270º semicircular field, with a guaranteed range that goes from 0.1 to 30 meters. A Novatel OEM-4 GPS engine is also used; it can offer centimeter level positioning accuracy. The MicroStrain 3DM-GX3 25 which is a high-performance, miniature Attitude Heading Reference System (AHRS) is mounted inside the robot. Additionally PTZ camera is placed in the front of the robot and provides video in real-time.

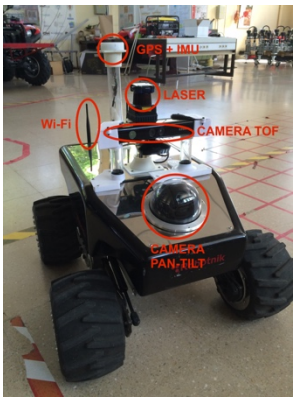

Fig 1. Summit Robot.

4. Finding and tracking people

The system presented in this paper aims to build a robotic system that firstly looks for a person to interact with, then initiates interaction, and uses hand gesture recognition to detect a pointing gesture and the depth value to follow the person. Gestures detected by the robot are analyzed and compared with a database of gestures to perform the corresponding action (stop, turn on itself, move aside, etc). Meanwhile, the value of the distance obtained between the person and the robot is continuously analyzed to always keep a safe distance from the person. It also ensures that wireless communication being using by the robot sensors is not interrupted.

4.1 Detecting people

Traditionally, robotics systems need special marks that stand out of the environment to conduct a robust tracking. However, with the use of Kinect, procedures have changed and it is capable of detecting people almost automatically. The package that OpenNI offers for ROS performs automatic detection of persons. It has several strengths, such as automatic detection of people entering the scene and removing them when they leave it. Another feature that facilitates the task, is that when a person is placed in the position of Psi (which can be seen in Fig. 2(a)), it creates a relationship with the person and starts the tracking of the person. Fig. 2(b) shows the flowchart for setting a target on a person.

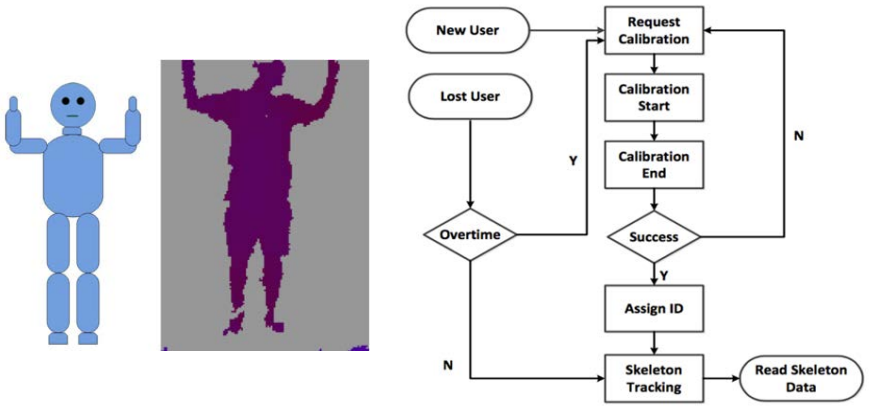

Fig 2. (a) Psi pose for detecting the tracking objective (left). Person in psi pose detected by the Kinect (right). (b) Flowchart for setting a target on a person.

4.2 Control strategy

As far as we know, for the Summit XL robot, linear motion X and angular rotation Z are useful for control strategy. In the coordinate, positive X axis is toward the front of robot, positive Y axis is along the right side of robot, and positive Z axis points to sky. The Robot Control module converts some signals generated from other modules into the linear and angular velocity of the UGV. The Skeleton Tracking module can generate and send six different signals through identifying some simple motions and events done by the person. The signal for obstacle avoidance is generated and sent by the laser module and the Kinect depth camera. Then the mobile robot will make different reactions according to different signals (Table 1), the distance of the person and the obstacles detected in the scene.

Table 1. Movement detect by the Summit XL.

Person pose	Summit Action
Arms Down	Follow me
Left Arm Up	Position at my left
Right Arm Up	Position at my right
Arms Up	Stop
Left Arm on Head	Twist on its self
Ducking	Abort mission

Arms Down: This pose makes the mobile robot follow the person through tracking the position of the person's center of mass. If the center of mass position is in the center of coordinate system and the distance between the person and the mobile robot is appropriate, the mobile robot will keep still. Otherwise, the mobile robot will take some actions to maintain the person's center of mass in center of its view sight and the distance between them within the specified range. When the robot detects more than one person in the scene, it will follow always the person that has identify himself with the Psi pose and ignore the rest.

- **Left Arm Up**: This pose will send to the robot the order to pose it at the left of the person.
- **Right Arm Up**: This pose will send to the robot the order to pose it at the right of the person.
- **Arms Up**: This pose will send to the robot the order to stop moving.
- **Left Arm Head**: This pose will send to the robot the order to twist on its self.
- **Ducking:** This pose will send to the robot the order to stop moving, abort the mission and desvinculate the person.

Furthermore, if the robot detects an obstacle (with laser or ToF camera) during the trajectory, it is able to find an alternative path to avoid the obstacle and get to the objective point. Once the point is reached if the person continues there, the robot will follow him, otherwise, will wait until it detects again the person.

5. Experimental results

In order to evaluate the behavior of the HRI collaborative task, the person walked randomly around an indoor scenario with obstacles. The robot should follow him while it was receiving orders through the gestures listed above. Also, the person was constantly streaming arbitrarily data to the robot wirelessly. The purpose of this was simulate the information that would be collected by sensors in the aim of this work. If the robot loosed completely the target or stopped receiving data, the trail would be considered failed. The test results show the good performance of the implemented system. The robot achieves an 88% of efficiency in the gesture recognition and it had not problems to follow the target with obstacle avoidance; this fact can be extracted from the zero collisions obtained in the ten trials.

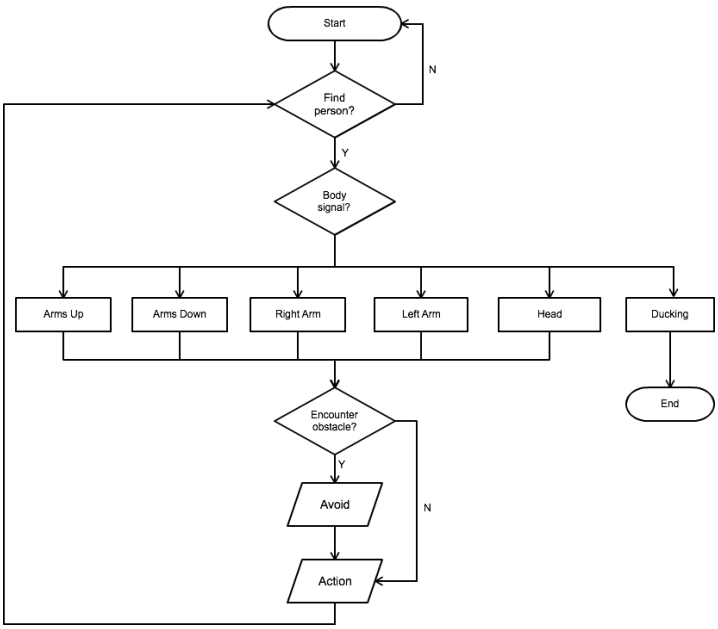

Fig 3. Algorithm to track a person and avoid obstacle.

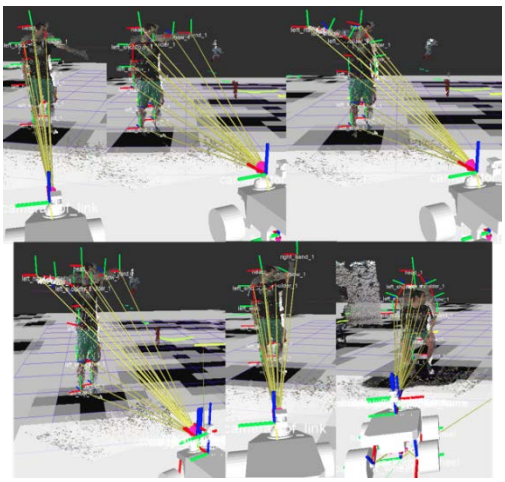

Fig 4. Poses detected by the robot.

6 Conclusions

In this article a novel approach to HRI is described. It proposes collaborative tasks between human and robot with three different kind of interac-

tion. The first one was a direct control of the robot movements using a gesture recognition system. The second one was a following behavior using tracking techniques including obstacle avoidance navigation. The third one was a continuous exchange of information which implies the ability of the robot to work in a collaborative task. This work went further of previous ones adding the interaction factor over the technical needs for the development of the labor.

Acknowledgements

This work was supported by the Robotics and Cybernetics Group at Universidad Politécnica de Madrid (Spain), and funded under the projects: PRIC (Protección Robotizada de Infraestructuras Críticas; DPI2014-56985-R), sponsored by Spanish Ministry of Economy and Competitiveness and RoboCity2030-III-CM project (Robótica aplicada a la mejora de la calidad de vida de los ciudadanos. fase III; S2013/MIT- 2748), funded by Programas de Actividades I+D en la Comunidad de Madrid and co-funded by Structural Funds of the EU.

References

Bonanni, T. M. (2011). Person-tracking and gesture-driven interaction with a mobile robot using the Kinect sensor. Universita di Roma, Faculty of Engineering.

Chang, C. W., Nian, M. D., Chen, Y. F., Chi, C. H., & Tao, C. W. (2014). Design of a Kinect Sensor Based Posture Recognition System (pp. 856–859). IEEE. http://doi.org/10.1109/IIH-MSP.2014.216

Igorevich, R. R., Ismoilovich, E. P., & Min, D. (2011). Behavioral synchronization of human and humanoid robot. In 2011 8th International Conference on Ubiquitous Robots and Ambient Intelligence (URAI) (pp. 655–660). http://doi.org/10.1109/URAI.2011.6145902

Qian, K., Niu, J., & Yang, H. (2013). Developing a gesture based remote human-robot interaction system using kinect. International Journal of Smart Home, 7(4).

Waldherr, S., Romero, R., & Thrun, S. (2000). A gesture based interface for human-robot interaction. Autonomous Robots, 9(2), 151–173.

CHAPTER 29

A REVIEW ON HOW TO EASILY PROGRAM ROBOTS AT HIGH SCHOOL

V. GÓNZALEZ, F. R. CAÑADILLAS, R. PÉRULA-MARTÍNEZ, M.A.SALICHS, and C. BALAGUER

RoboticsLab, University Carlos III of Madrid. veronica.gonzalez@uc3m.es, felix.rodriguez@uc3m.es, raul.perula@uc3m.es, salichs@ing.uc3m.es, balaguer@ing.uc3m.es

In this paper we analyze some of the most used programming methodologies but in the Spanish high school level. There are two main trends in high school programming, blocks and text code. Although there are some relevant studies that show block programming is an easy way to learn the fundaments, when it has to be applied to a field like robotics sometimes may be very limited. Programming by blocks is not a very mature methodology based on structural programming. Some tools for this kind of programming are Ardublockly, Bitbloq, Scratch4Arduino, or Lego software. Nevertheless, programming by text code has been used since almost the beginning of computer science. The most common programming languages for this kind of methodologies are C++ through using Arduino, or Python. Thus, we show the main features for these programming tools providing a general vision on which to choose depending on what you pretend to teach.

1 Introduction

In the last few years technology has evolved exponentially, being this one of the most influential factors in our society. More and more, new generations have to adapt to this great evolutionary leap in order to meet the challenges of technology.

Nevertheless, these new generations have been growing surrounded of the new technologies, acquiring new knowledge about computer science and engineering. This makes it essential the incorporation of specific branches in science within the educational contents.

Nowadays, educational robotics is one of the most emerging disciplines for learning and reinforcing knowledge about computer science, electronics, programming, mechanics, etc. (Mubin, 2013), (Benitti, 2012). Robots are used as "edutainment" platforms, generating a good learning atmosphere. In this way, a greater interest and curiosity are generated in the student (Eguchi, 2010).

In Spain, this discipline has been integrated within the educational system by means of a new subject called “Technology, Programming and Robotics” (Spain, 2015), representing an important evolution of education.

Nevertheless, within educational robotics, there are different basic skills where the programming is highlighted. To teach programming improves many skills of students, such as logical thinking and resolution process, understanding better the world around them. A successful learning causes an increase in the motivation of the student (Hirst et al., 2003), (Pásztor, 2013), as well as the self-confidence is reinforced (Yamazaki et al., 2015) when the desired objective is achieved. Communicative and social skills are also reinforced (Pap-Szigeti, 2007), since students work collaboratively to solve all the problems raised.

In order to confront the challenge of the programming teaching, teachers need support with different tools and methodologies. A review of some the most used programming tools for the educational field in the Spanish secondary schools are presented in this work. A description of the tool is provided, as well as the methodology used and its main features.

This paper is structured as follows. Section 2 presents a description of the selected programming tools. And Section 3 presents the preliminary conclusions and future works related to this paper.

2 Programming tools

In this section we present some but not all of the most actual and usually used software to teach programming oriented to robotics at Spanish high school. For each, we show a general description to place the reader in a specific context. Next, we briefly present the methodology used, and finally the main features they offer to young programmers and teachers.

2.1 Arduino

Arduino software (Fig. 1) is one of the most used in the world for programming low-cost microcontrollers, very often used in robotics. It has been used mostly to teach basic programming or real-time projects.

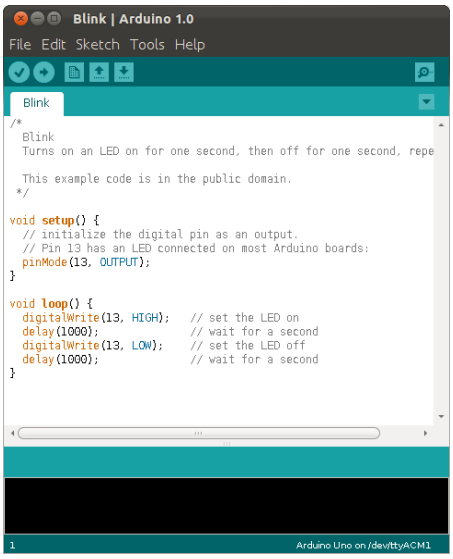

Fig. 1. Integrated Development Environment (IDE) for Arduino software.

Arduino can be programmed directly in C or C++ languages (Arduino, 2016). These kind of languages usually are very difficult to learn if the students do not have previous knowledge in programming. Nevertheless, Arduino uses a simplified version to try to help non-professional programmers.

Distinguished features are, for instance, the ***setup*** and ***loop*** functions. The first has the particularity to be called at the beginning of any program. It usually contains initializations and the assignment for the analog or digital inputs/outputs. On the other hand, the second function must contain the main code, but with the particularity that is continuously executing.

2.2 Bitbloq

Bitbloq (Bq, 2016) is an IDE developed by the company Bq. Bitbloq can be used to create programs using blocks or code (Fig. 2).

The methodology used by Bitbloq is based on creating some pieces of code by blocks which contain a specific functionality. Moreover, it is possible to visualize the source code auto-generated by those blocks. In addition, it is also possible to program electronic objects like sensors or actuators – common elements in robotics.

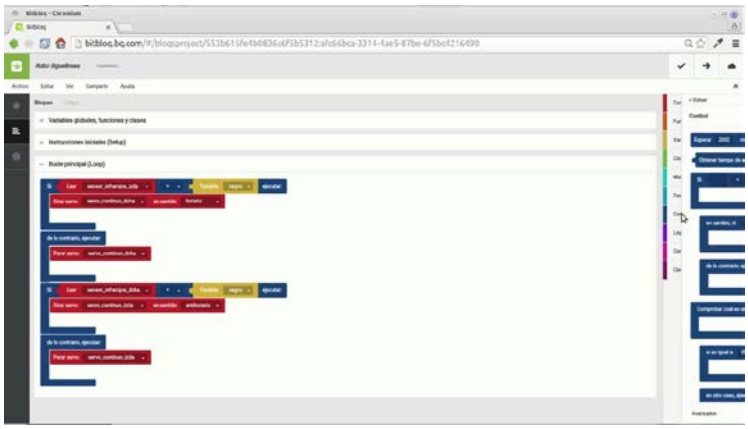

Fig. 2. Bitbloq online IDE.

Finally, Bitbloq is specially designed to using its own microcontroller board called ZUM Core. But it also allows using a generic Arduino UNO or a derived like the Freaduino UNO.

2.3 Lego Labview

Lego Mindstorm kit has different ways to be programmed. Nevertheless, the easiest and most affordable software is usually the software Lego provides in its website, EV3 Software (LEGO, 2016).

This software is compatible with the last version of Lego Mindstorm (EV3) and it can be installed in a PC/MAC or tablet. For the previous versions of Lego Mindstorm, there is also available the corresponding software.

This software is based on National Instruments LabVIEW (National Instruments, 2016). It is a software which uses an icon-based drag-and-drop programming interface (Fig. 3). In this way, the user can create your own programs by blocks flowcharts, without the need in order to create large lines of code. Each of the sensors and motor that compose the kit has a block, which can be configured with different variables. The user can control and read sensor data by Bluetooth, WI-FI or mini-USB port.

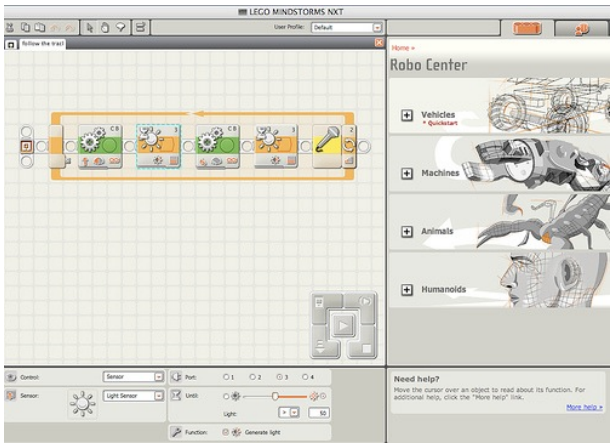

Fig. 3. Lego Labview IDE.

The software is conceptually very simple and together with the simplicity of the interface is ideal for children and professors with little programming experience. But, this type of programming has one inconvenience: the creation of complex actions can be complicated, since the blocks programming does not offer great freedom. Also, unlike other software, this software has a home edition, which is free, and an education version, which has to be paid.

2.4 Scratch4Arduino

Scratch4Arduino (S4A) has been developed at Citilab by the Edutec Research Group (Citilab, 2015). This software is based on the software Scratch, developed originally by the MIT.

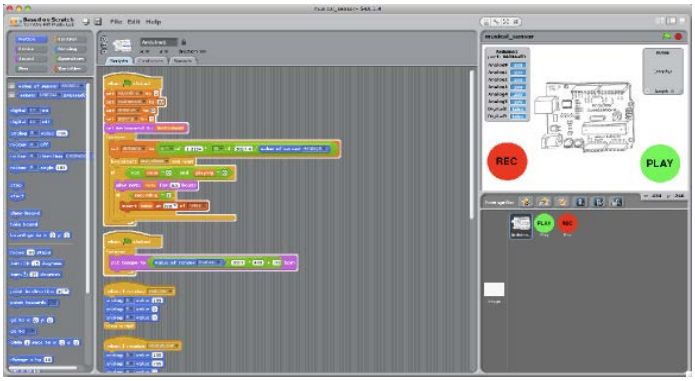

Fig. 4. Scratch4Arduino IDE.

S4A programming uses blocks that represent the same as the elements available for Arduino and Scratch. It has many types of general blocks like events, loops, conditionals, operators, etc. Furthermore, it has specific blocks for the input/output of analog and digital signals, useful for an Arduino board. Finally, it has also available all Scratch blocks for creating graphical and sound elements.

S4A is distinguished by its simplicity (Fig. 4). Thanks to that, it is an ideal tool to start programming. Through a connection to an Arduino board, it can use electronic components for controlling graphic elements. Moreover, it allows to program mobile robots, but being permanently connected by USB, a very important disadvantage.

2.5 Visualino

Visualino (Visualino, 2016) is a software with a visual programming environment for Arduino, which is composed of different work environments where the different elements used for programming of the board are distributed. This software allows you to create code via block diagram. This software is Open Source and multi-platform, requiring the version 1.6 of the Arduino IDE.

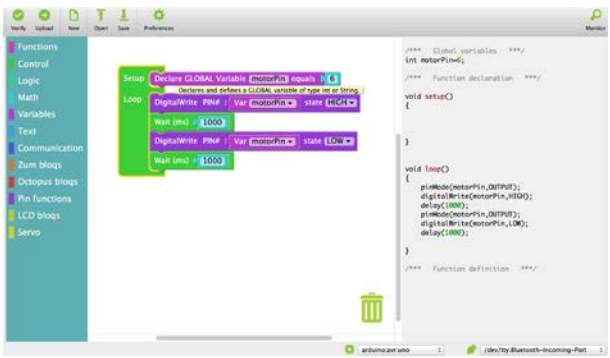

Fig. 5. Visualino IDE.

The programming is done by block flowchart, whose programming is based on Blockly of Google (Google developers, 2016) and Bitbloq of Bq (Bq, 2016). The different elements are organized in work environments: variables, mathematics fields, control blocks, pin functions, etc., in addition to having environments for the ZUM board and Octopus components of Bq. The program can be loaded to the board via USB or Bluetooth.

The interface of Visualino (Fig. 5) is very visual and simple, which contains the basic functions that Arduino IDE has. Unlike other software as Bitbloq, Visualino is very practical, since inside the code editor you can see and edit the block flowchart, and in parallel, the native code of Ar-

duino is shown. Also, it lets you organize the elements of the code in the different functions, ***setup*** and ***loop***.

3 Conclusions and Future Work

As we have discussed, it is easy to see that software is an important part for teaching robotics and may be a hard task to select which one to use. For that reason, we can reaffirm that software based on blocks is the best option for students who do not have a previous experience but it may be limited when trying to develop more complex tasks. Nevertheless, traditional programming software like Arduino IDE may be the best option for students with previous knowledge using blocks.

As a future work, we will do an essay with students. In this essay, we will compare the difference between two groups of students. The first one will learn to program using only blocks and the second group will use only the traditional methodology. The final goal will be to obtain some metrics useful to test new software systems.

Acknowledgements

The research leading to these results has been obtained in collaboration with CREA Robótica Educativa and the RoboCity2030-III-CM project (Robótica aplicada a la mejora de la calidad de vida de los ciudadanos. Fase III; S2013/MIT-2748), funded by Programas de Actividades I+D en la Comunidad de Madrid and cofounded by Structural Funds of the EU.

References

Arduino, 2016. Arduino Guidelines and Tutorials. < https://www.arduino.cc/en/Tutorial/HomePage >. [Online. Last access: 17/04/2016].

Benitti, F. B. V. 2012. Exploring the educational potential of robotics in schools: A systematic review. Comput. & Educ., 58(3): 978-988.

Bq, 2016. Bitbloq. < http://bitbloq.bq.com/ >. [Online. Last access: 17/04/2016].

Citilab, 2015. Scratch4Arduino. < http://s4a.cat/ >. [Online. Last access: 20/04/2016].

Eguchi, A. 2010. What is educational robotics? Theories behind it and practical implementation. In Proc. Soc. Inform. Technology & Teacher Educ. Int. Conf., Chesapeake, VA: AACE, pp. 4006-4014.

Evans, B., 2011. Arduino Programming Notebook, Ardumania.

Google developers, 2016. Blockly. <https://developers.google.com/blockly/>. [Online. Last access: 17/04/2016].

Hirst, J. A., et al. 2003. What is the best programming environment/language for teaching robotics using Lego Mindstorms?. Artif Life Robotics, 7: 124-131.

LEGO, 2016. Aprende a programar. < http://www.lego.com/es-es/mindstorms/learn-to-program >. [Online. Last access: 17/04/2016].

Monk, S., 2015. Fritzing for Inventors. Mc Graw Hill Education.

National Instruments, 2016. Software de Desarrollo de Sistemas NI LabVIEW. <http://www.ni.com/labview/esa/>. [Online. Last access: 17/04/2016].

Pap-Szigeti, R., "Cooperative strategies in teaching of web-programming," in Practice and Theory in Systems of Education, pp. 51-64, 2007.

Pásztor, A. 2013. Mobile Robots in Teaching Programming for IT Engineers and its Effects. Int. J. Advanced Comput. Sci. and Applicat., 4(11): 162-168.

Spain. 2015. Decreto 48/2015, de 14 de mayo, del Consejo de Gobierno, por el que se establece para la Comunidad de Madrid el currículo de la Educación Secundaria Obligatoria. Boletín Oficial de la Comunidad de Madrid *(BOCM)*, no. 118, pp. 10–309.

Visualino, 2016. Visualino. <http://www.visualino.net>. [Online. Last access: 20/04/2016].

Yamazaki, S., et al. 2015. Comparative Study on Programmable Robots as Programming Educational Tools. In Proc. 17th Australasian Computing Educ. Conf. (ACE 2015), Sydney, Australia, pp. 155–164.

CHAPTER 30

TOWARDS A TELEOPERATED SYSTEM BASED ON ELECTRONIC NOSE FOR ODORS TRACKING: FIRST PROTOTYPE

C. D. GALÁN, JOSÉ M. COGOLLOR and R. GALÁN

Centre for Automation and Robotics CAR (UPM-CSIC), José Gutiérrez Abascal 2, 28006 Madrid, Spain. E-mails: danielgalanv@alumnos.upm.es; jm.cogollor@upm.es; ramon.galan@upm.es

This paper presents the research done by the Intelligent Control Group from the Centre for Automation and Robotics focused on the design and implementation of a teleoperated system proposed to be used to perform tracking tasks based on odor recognition. The teleoperated system is composed by: an Unmanned Ground Vehicle, which turns out to be the slave robot that executes the task in the remote environment, and the master device, which is used by the operator to generate the commands for the navigation and guidance purposes. Additionally, the master can be used for additional check of the sensors evolution thanks to an easy-to-use interface. An electronic nose with sixteen chemical sensors, from Figaro Inc., was especially designed and integrated in the slave robot as the main component for the objective pursued. Moreover, four temperature sensors, a relative humidity sensor and an atmospheric pressure sensor were also fitted to the electronic nose. The final objective of the prototype is to support help in the localization of disaster victims in areas where the rescue personnel have difficulties to come in.

1 Introduction

For decades, unmanned vehicles have been an useful tool for military missions, mainly in the area of strategic and tactical reconnaissance. More than 30 nations have developed or produced more than 250 models of

these vehicles and more than 40 countries operate more than 80 different types of the same.

An important year along the developments of unmanned vehicles was 2000, when the market reached the order of a billion on a constant growth rate of about 7% for subsequent years, whereas today, approximately 90% of these vehicles are a direct result of requests by the national government to its civil and military programs.

For the next few years, the development of unmanned vehicles in Europe, both in civil and military applications, is one of the most important challenges at the same time a great opportunity for the European Community and for their industries to settle down in the technological limit and commercial industry.

Considering applications focused on odor tracking, the use of mobile robots in this area has generated a variety of researches, which can be grouped into:

- Multirobots. Considerable progress has been done by Stewart R.L. et al, Hannawati A. and Russell R.A., Cui X, Jatmiko W., and others (Hayes A.T. 2002).
- Robots that use computer vision. Pyk P., Broxvall M. and others (Loufti A. 2004).
- Robots that use electronic noses in a stereo architecture, where the sensors are located in both sides of the robot. Lilienthal A. and Duckett T., Martinez D., and others.

The very first results of our proposed prototype show sensor activation in acetone, ammonia, carbon dioxide and isoprene when humans are near so alive people detection can be achieved (Moreno,. 2009) (Galan, 2011) (Galan, 2012). But the conditions of pressure and temperature have a strong influence. Therefore, the prototype has been designed to facilitate the replacement of sensors. It is the operator's experience what allows a quick localization of the victims.

The paper briefly describes the architecture of the system in Section 2 in order to explain more in detail the electronic nose and its usage in Section 3. Section 4 focuses on the sensors implemented for odor recognition to finally, wrap up the main conclusion in Section 5.

2 General Architecture of the system

Fig. 1 shows a representation of the hardware architecture designed.

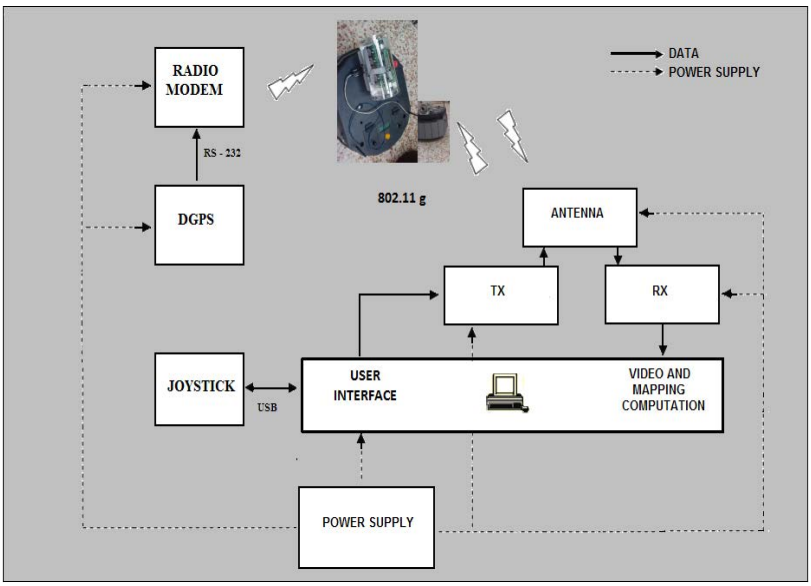

Fig. 1. Architecture of the teleoperated system.

On the one hand, the master commander is further equipped with:

- An antenna (TX/RX) in order to receive the navigation data and transmit the control movements commands.
- A joystick with a vibration motor as haptic device for the control of the movements and force reflection to the operator.
- The central processor focused on the general computation of: the mapping of the area, the generation of the visual guidance to the operator based on the odors detected by the electronic nose and the generation of errors.
- A display for user interface.
- The power supply.
- A Differential GPS (DGPS) and radio modem in order to generate and send the corresponding corrections for the GPS signals to the robot.

On the other hand, the slave robot is further equipped with:

- An on-board antenna to send the navigation/video/odors data signals to the master commander and to receive the movement commands provided by the pilot.
- Batteries focused on the power supply.
- Video and infrared cameras in order to obtain information of the environment.
- An electronic nose, to detect odors, which is described in more detail in the next section.
- A radio modem in order to receive the GPS corrections provided by the DGPS located in the master commander.
- The corresponding motion servo-actuators.
- The corresponding processor for the on-board computing.
- Converters from RS 232 and PCI to CAN bus.

Meanwhile, the communications system is divided into two ways: communication between the master commander and the robot, and communication between GPS's.

The first one is achieved thanks to a pair of antennas which transmit and receive data through a wireless connection based on the protocol 802.11 g. This protocol presents lots of advantages including high bandwidth at 54 Mbps and low frequency (2.4 GHz) so the clarity of the signal makes the system quite adequate for urban missions due to that possible obstacles don't interfere the performance and communications.

The communication between GPS's is achieved by radio modems installed in both vehicle and master commander. The last one in conjunction with a Differential GPS sends to the vehicle the corrections for the correct calculation of the robot position and velocity, which are sent back to the master commander by the on-board antenna to inform the operator about the localization of the vehicle.

The connection between all the on-board devices installed in the robot is ensured thanks to a CAN bus which offers a wide range of advantages including its capacity of detecting errors and its tolerance to failures.

Finally, regarding software distribution, the platform presents:

- A monitoring stage for: analysis of emergency events, robot performance, communication between devices and historical files creation.

- Bilateral control software to ensure the correct exchange of information between the operator and the robot for its positioning and force reflection using the haptic device. (Position - Position scheme)

3 Electronic nose, odors representation and tracking

The electronic nose (Fig. 2) comprises three modules: chemical, electronic and software.

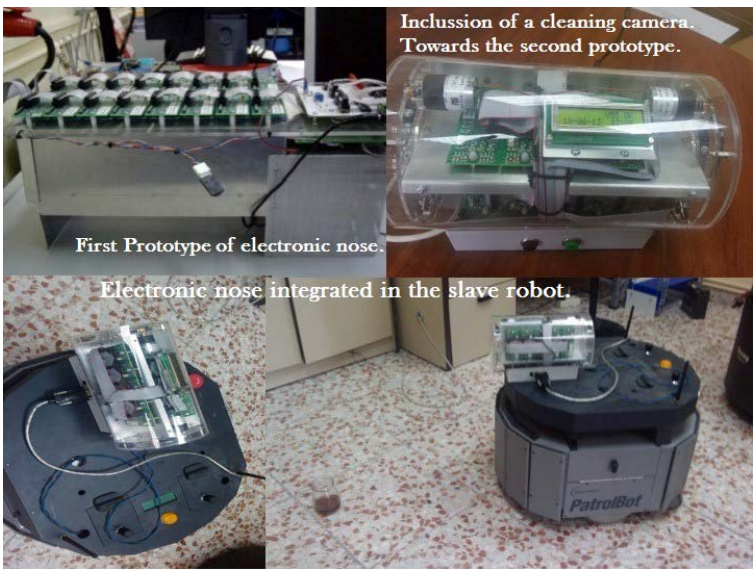

Fig. 2. Electronic nose designed and tested.

The different components chosen for the design and construction of the electronic nose have been selected based on the type of chemical odor sensors chosen for the sensor array. Moreover, it is small to facilitate the integration on a mobile robot.

The chemical module of the electronic nose consists of one chamber where the sensors are located. It contains a simple acquisition system for sampling the volatile components of the sample. The sensor chamber and the sample are separated by a cover, that can be open, and a small ventilation unit that draws the odor sample gas molecules from the sample chamber into the sensor chamber.

After the sensors are exposed to the odor samples, this chemical signal is transferred, as an analog signal, to the next module, in this case, the electronic module, where the signal is amplified, filtered and converted into digital values; these will be used in the final module, where several algorithms have been developed to classify the odor that has been detected by the electronic nose and to obtain the direction the odor comes from in order to be represented in the computer of the master commander and let the operator to track it by making the robot move to that direction.

When the sample has been taken the nose open a backdoor and active another ventilation for cleaning the chamber.

Each sensor is mounted on a separate card so that they can be easily removed or changed by the operator. The algorithms focused on obtaining the direction of the odor make the robot measures in semicircles (-60, -30, 0, 30, 60 degrees) and calculate the samples mean square error. The goal is to know in what direction that error is minimum. For the cases were local minimums are found it has been used the relaxation technique. To reduce the time to find the source location the algorithm has been modified to ensure progress without checking the smell of 60 ° and -60 ° when the error decreases.

Once the direction of the odor is clear, both the classification of the odor and its direction are sent to the master commander in order to represent them over a navigation map created by the SLAM algorithm implemented using the video image data. Finally, the type of the odor is associated with a color and a colored beam pointing to the source direction of the odor is drawn based on a predefined angle α. (Fig. 3)

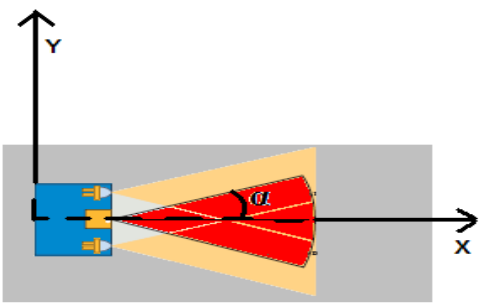

Fig. 3. Visual representation of the odor.

4 Sensors for odor recognition

Odor sensors used in this design are manufactured by the Japanese company Figaro Group. The selection was based on the following reasons: low cost, availability in the market and commonly used applications.

The manipulation of the sensor response with respect to its base line is the first stage of preprocessing. Considering the dynamic response of the sensor, three techniques are commonly used: Differential, Relative and Fractional.

The second stage of the preprocessing is to compress the response of the sensor array to create a feature vector or olfactory fingerprint. According to the procedure used to generate the fingerprint olfactory, dynamic transient compression methods can be grouped into three classes: sub-sampling methods, parameter extraction methods and methods of system identification.

Standardizations are the final stage of digital preprocessing and normalization techniques can be grouped into two classes: local and global methods.

Finally, the data obtained from the previous stage, are analyzed by pattern recognition techniques, which act as a system for signal processing. The sensor array produces a matrix, where the columns represent a vector response associated with a particular odor, and the rows are the individual sensor response to different measure.

5 Conclusion

The electronic nose is a device that emulates the human olfactory system, as it is able to identify different smells. Its performance is largely determined by the sensor array, as in identifying odors, the chosen sensors decisively affect the type of odor that can be identified. Another feature that also influences the selection of the type of sensor used in the electronic nose is the technology used in the manufacture of chemical sensors. Most gas sensors of artificial olfactory systems used in the researches described here are the tin oxide semiconductor, the QCM, SAW and the conductive polymers.

At the stage of pattern recognition, methods used are the statistical accompanied by neural networks, because of its self-learning ability. It is important to note that a good odor localization system is critical for improving the effectiveness of these mobile olfactory systems. So far, the be-

havior of this type of robots, in general terms, is based on imitation of the behavior of insects.

Finally, the accomplishments achieved with electronic noses leave no doubt that this is a device whose application will have a great scope in the future, due to all the benefits that have and could have, especially in the field of medicine and security.

Acknowledgements

The research leading to these work has received funding from the NAVEGASE project (*Navegación Asistida Mediante Lenguaje Natural*, DPI 2014-53525-C3-1-R), funded by Spanish *Ministerio de Economía y Competitividad*, as well as from the RoboCity2030-III-CMproject (*Robótica Aplicada a la Mejora de la Calidad de Vida de los Ciudadanos. Fase III*;S2013/MIT-2748), funded by *Programas de Actividades I+D en la Comunidad de Madrid* and cofounded by Structural Funds of the EU.

References

Galán D., Galán R.; Martinez A.L. et al. "Learning Odors for Social Robots: The URBANO experience". 3rd International Conference on Advanced Cognitive Technologies and Applications, COGNITIVE 2011, September 2011, Rome Italy.

Galán D., Galán R.; Martínez A.L. et al. "The sense of smell in social robots". 7th IEEE Conference on Industrial Electronics and Applications (ICIEA 2012). Singapur. Pp. 1429-34.

Hayes A. T., Martinoli A. and Goodman M. R. (2002). Distributed Odour Source Localization. *IEEE Sensors Journal*, Volume 2, Number 3.

Loufti A., Coradeschi S., Karlsson L. and Broxvall M., (2004). Using an Electronic Nose on a Multi-Sensing Mobile Robot. Intelligent Robots and Systems, (IROS 2004). Proceedings, 2004 IEEE/RSJ International Conference.

Moreno, I.; Caballero R.; et al. "La nariz electrónica: Estado del Arte" Revista Iberoamericana de Automática e Informática Industrial RIAI, Volume 6, Issue 3, July 2009, Pages 76-91.

CHAPTER 31

"SHOULD I STAY OR SHOULD I GO?" – ENABLING AUTONOMOUS MOBILE DEVICES TO OPTIMIZE DATA COLLECTION PERFORMANCE

H. HILDMANN[1] and E. KOVACS[2]

[1] Universidad Carlos III de Madrid Madrid – hanno.hildmann@uc3m.es;
[2] NEC Research Labs Europe – ernoe.kovacs@neclab.eu;

In this chapter we present a novel technique that can be used to empower semi-autonomous devices to have a larger degree of self-determination in the context of improving the efficiency of data collection related tasks. The approach presented has been conceived in the context of an environmental monitoring project using a swarm of UAVs and is currently the subject of a patent application (PCT/EP 2015/067850 – pending), however, no empirical validation of the performance is provided here. This chapter is intended as the initial presentation of the approach to the community.

1 Introduction

There are numerous scenarios where the continuous / repeated monitoring of large areas is required. Such scenarios can occur in the context of risk assessment and / or risk-assessment driven resource allocation in changing environments such as environmental protection activities (e.g. illegal logging operations, poaching in national parks or assessment of air pollution (Andrews, 2014), (Goodyer, 2013), bio-security measures (e.g. continuous health monitoring of herds of roaming animals or defense against invasive flora) or for public safety and civil security (e.g. monitoring environmental conditions, controlling crowd movement in major public events or disaster response and mitigation, specifically, large scale evacuations (Tanzi, 2014), (Rossi, 2014).

1.1 Using autonomous devices for wide area monitoring

The rapid increase in reliability and performance of autonomous devices, combine with the decreasing costs associated with their production, operation and maintenance suggests the use of non-human assets for such monitoring tasks. Specifically, and in the context of the research within which the presented approach was conceived, swarms of relative low-cost – and potentially expendable – devices are increasingly considered as semi-autonomous mobile sensing devices for surveillance and monitoring operations such as the ones mentioned above.

Typically, the areas to be observed are orders of magnitude larger than the sum of the areas each individual device can observe at any given time or, conversely, the required level of monitoring (and in many cases the amount of available funding) does not warrant the deployment of a swarm large enough to provide continuous data collection capabilities for an entire area. This leads to the need to coordinate and schedule the members of a swarm, much like police cars patrol the streets.

The basic rule of thumb normally involves ensuring that the last observation for each sub area is fresher than a threshold maximum age. Naturally, this leads to inefficiencies, since not all areas exhibit the same risks or change dynamics. To palliate this, it is common to use domain knowledge and manual adjustments to ensure that critical areas are observed more regularly or even continuously (Chen, 2012).

Traditional monitoring techniques for large areas using mobile sensors are based on periodically checking on the different sub-areas. This guarantees a maximum age of the observation, but is likely to be sub-optimal for most scenarios, where the rate of change for the observed variable can greatly differ from location to location and change over time. Due to this we investigated a *projected information gain*-based approach to empower the individual devices to improve the efficiency of their monitoring activities. We propose a method to optimally schedule mobile sensors with the aim to maximize the collected information for a limited sensor fleet size.

1.2 Example scenario

Let’s consider an application scenario to better illustrate these points: a city council uses a fleet of UAVs with zenithal cameras to estimate traffic volumes and people counts in different parts of the city, with the aim to improve emergency response times and efficiency. One would expect that a proportionally larger number of devices is allocated to the downtown areas on weekdays, however, this poses at least two critical problems:

- manual UAV allocation based on domain knowledge is likely to be biased. This can lead (over time) to situations where drones over-examine areas deemed important, while under-examining exactly the areas most likely to suffer from a shortage in response resources should a problem occur.
- the system evolves slowly: an area will only gain importance once events of interest have been repeatedly observed in it. Specifically in the context of crowd movements during massive public events such as New Year's celebrations it is not feasible to prepare incident responses on the basis of past experiences and failures. In other words: *sometimes you have to get it right the first time!*

2 Wireless Sensor Networks (WSN) going mobile

Our approach assumes that the mobile sensors are sensing a physical, numerically expressible magnitude. This is true for most scenarios, including traffic and people flows, environment measures (thermal, humidity, CO2), pollution, deforestation, water salinity, and many others.

In such case, one can consider each observable area as a time series of values provided by an arbitrarily complex sensor. Specifically, one might consider the fleet of sensors as a traditional wireless sensor network (WSN), with the exception that the sensors are mobile.

Because our approach borrows from ideas developed in WSN, we'd like to take a break to describe a WSN specific problem: power consumption. WSN devices are typically low power optimized and meant to last in the field for long periods. As such, their main power drains comes not from their normal operations (including sensing), but from actually transmitting the collected information over a wireless link.

To ease the power burden of communication, WSN have developed a plethora of techniques. We focus on lossy data compression: by learning from values sensed up to the present time, a sensor may attempt to derive a model that explains future values in a variety of ways including sensing the parameters that govern a stochastic process mimicking the observed data, or transmitting expected values together with its expected validity.

Mobile sensing networks, as opposed to their WSN counterparts, do not suffer from the same constraints: typically, the energy required to physically move the UAV far outweighs the communication costs. Their constraint is much more subtle: by measuring at a location, the system sacrifices its knowledge about other locations.

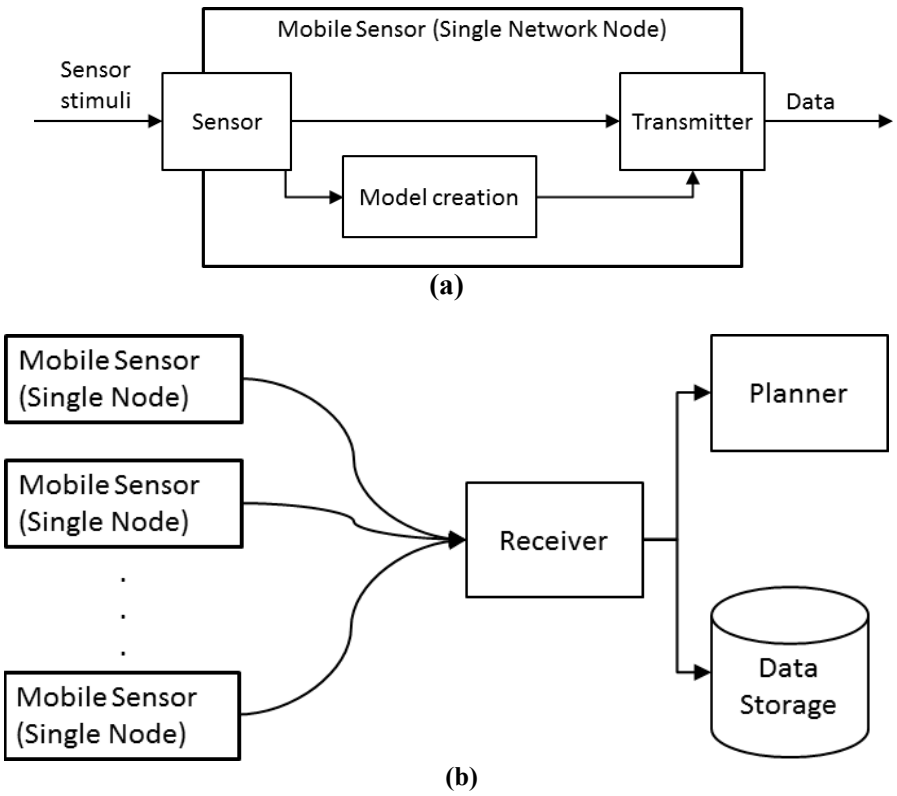

Fig. 1. (**a**) Our model for a UAV based node in our mobile wireless sensor network. The model creation module uses standard techniques to derive a model predicting the information gained when remaining at the current location. (**b**) An illustration of a UAV based swarm of mobile sensor nodes feeding a back-end data handler with the ability to use the transmitted models in a planner.

We propose to apply algorithms developed for the purpose of power saving in the area of WSN to semi-autonomous mobile sensors with the aim of maximizing the information collected for a large surveilled area.

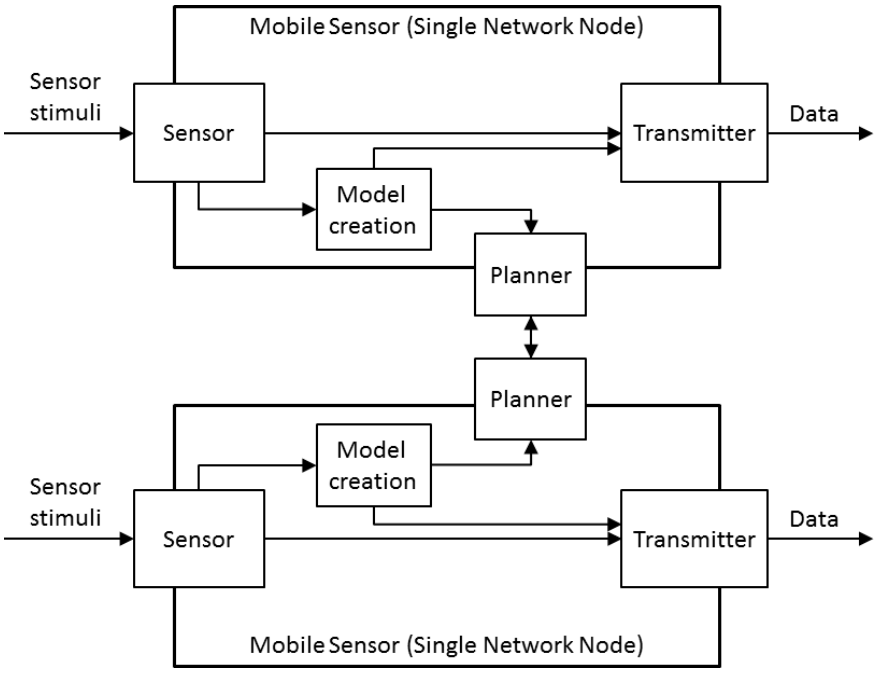

Fig. 2. Network nodes like the one described in Fig. 1, but with the ability to perform its own planning. Empowering UAVs in mobile sensing swarms to self-determine the time they will spend on a specific location allows us to move the entire planning process into the swarm and let it operate in a decentralized set-up. The above illustrates a distributed version of the sensing swarm, where the individual UAVs communicate with each other and potentially have the ability to exchange locations allocated to them with another UAV in order to increase the overall efficiency of the swarm. A distributed task allocation algorithm to facilitate this has previously been presented in (Hildmann, 2014), (Hildmann, 2015).

3 Using predicted information gain to improve the efficiency of a UAV across all locations it is covering

Mobile sensors like UAVs with e.g. on-board CO2 sensors (Rossi, 2014) can be understood as mobile devices that can receive some sensory input, transform it into some data format and use on-board communication to transmit the collected data to a data sink that collects all the information.

In addition to the traditional set-up, our mobile sensors create a model that can be used to predict future values, as well as their uncertainty. This model is sent along with the data to the receiving data handler.

The receiving end can use this information model to determine whether it is more advantageous to have the mobile sensor remain at the location or whether more can be gained from sending it to another destination.

Of course it is possible (and indeed, intended in the context of our work) to enable the UAV to do its own planning (Hildmann, 2015). The example on the following pages illustrates this with a simple example.

3 Example

The times series coming from a mobile sensor node can be evaluated using off-the shelf prediction algorithms such as e.g. Kalman Filters. These can be used to predict future values, and will yield not only an estimation, but also a confidence interval (e.g. the temperature will be 5C +/- 1C). Typically confidence intervals expand the further away we attempt to predict. We therefore know that while temperature will be within +/- 1C in the next 5 minutes, we would expect it to be, for instance, +/- 5C in an hour.

For the purpose of mathematical analysis, let's assume a simplified model that estimates confidence interval width as a function of time that increases proportionally with a factor α:

$$\text{uncertainty}(t) = abs(|\max val(t) - \min val(t)|) = \alpha(t - t_0) \quad (1)$$

Here, α indicates how much uncertainty will increase the further away the considered time t is from t_0. Note that α is the modeled parameter (for this very simple model), and depends on the surveyed area, i.e. the position of the mobile sensing platform. With this, we are now able define the goodness of our surveillance using the following cost function J:

$$\text{J}(t) = \sum_{\substack{i \in areas \\ d \in sensors}} \text{P}d \times \text{uncertainty}i(t) \quad (2)$$

P_d is 1 or 0 depending on whether sensor d is located at location i at time t. If the sensor is in the location, the P_d is 0, meaning the uncertainty is 0. If it isn't, P_d is 1, and uncertainty is determined as per the above formula.

Once we fix t, we can use traditional optimization algorithms (e.g. gradient descent) to find the combination of locations of sensor nodes that minimizes the uncertainty.

The main factor affecting the solution will be α, which indicates how quickly uncertainty increases for an area over time:

- At t=0, we place a sensor in location 1 and none in 2 (P_1=0, P_2=1). The uncertainty (J) is therefore 0*3 + 0*1
- At t=1 and t=2, we do not move the sensors, so the uncertainty remains that of area 2: i.e.: 0*6 + 1*2 (at t=1), 0*9 + 1*3 (at t=2)
- At t=3, however the uncertainty coming from area 2 would be 4, while the uncertainty from area 1, monitored until now, would be 3 (α1*(3-t_0) for t_0=2. Therefore, we move the sensor from area 1 to area 2, and manage to maintain an uncertainty of 3.

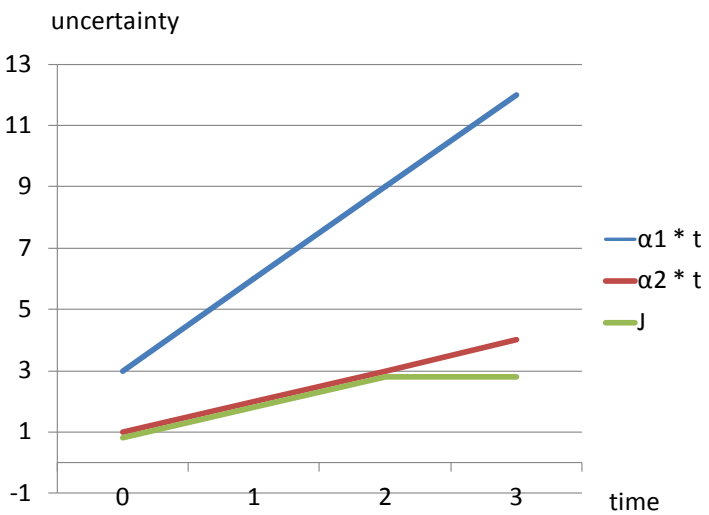

Fig. 3. In our simplified scenario, we have α1=3 and α2=1 for locations 1 and 2.

Using this method, the information gathered from the sensor is optimized for the available sensors. Had we used a traditional system and sampled areas periodically, uncertainty would increase because we monitor area 2 (which changes slowly or predictable) while letting area 1 rapidly evolve and increase the uncertainty of the collected information.

Acknowledgements

The presented work was undertaken at NEC Research Labs Europe in the context of the *Mobile Sensing Platforms for Public Safety* Project, funded by the Global Safety Division of NEC. The authors further acknowledge the contributions of their former colleague and lead inventor of the presented approach, M. Martin, as having been substantial.

References

Andrews, C. 2014. UAVs in the wild. Engineering Technology 9(7): 33-35

Camara, D. 2014. Cavalry to the rescue: Drones fleet to help rescuers operations over disasters scenarios. 2014 IEEE Conf. on Antenna Measurements Applications (CAMA), Antibes Juan-les-Pins , France

Chen, X. 2012. Fast Patrol Route Planning in Dynamic Environments. IEEE Trans. Systems, Man, and Cybernetics - Part A: Systems and Humans – 42(4): 894-904.

Goodyer, J. 2013. Drone Rangers. Engineering Technology 8(5): 60-61

Hildmann, H. and Martin, M. 2014. Adaptive scheduling in dynamic environments. 3rd Workshop on Information Technologies for Logistics (IT4L'14), Warsaw, Poland

Hildmann, H. and Martin, M. 2015. Resource allocation and scheduling based in emergent behaviors in multi-agent scenarios. 4th Int. Conf. on Operational Research in Enterprise Systems (ICORES), Lisbon, Portugal

PCT/EP 2015/067850 (pending). Distributed scheduling under uncertainty for mobile multi-agent systems. Martin M. and Hildmann H. (inventors)

Rossi, M. and Brunelli, D. and Adami, A. and Lorenzelli, L. and Menna, F. and Remondino, F. 2014. Gas-Drone: Portable gas sensing system on UAVs for gas leakage localization. 2014 IEEE Sensors, Valencia, Spain

Tanzi, T. and Apvrille, L. and Dugelay, J.-L. and Roudier, Y. 2014. UAVs for humanitarian missions: Autonomy and reliability. San Jose, USA

CHAPTER 32

MULTIPLE ROBOTS, SINGLE OPERATOR: CONSIDERATIONS ABOUT INFORMATION AND COMMANDING

J.J. ROLDÁN, J. DEL CERRO and A. BARRIENTOS

Centre for Automation and Robotics (CSIC-UPM), jj.roldan@upm.es, j.cerro@upm.es, antonio.barrientos@upm.es

Multiple robot, single operator scenarios suppose a challenge in terms of human factors. Two relevant issues are keeping the situational awareness and managing the workload of operators. In order to address these problems, this work analyses the management of information and commands in multi-robot missions. About the information, this paper proposes a selection based on mission and operator states. Regarding the commands, this work reflects about the levels of automation and the methods of commanding.

1 Introduction

In recent years, multi-robot missions have been applied in multiple areas. The teams of robots may be homogeneous or heterogeneous and include ground, marine, submarine or aerial robots. The arguments that support the use of multiple robots are diverse: e.g. to cover larger areas, to reduce the duration of mission or to perform simultaneous tasks.

Robot fleets present obvious advantages over single robots. First of all, they have a wider range of application, since they can carry out complex missions that require coordinated tasks. Additionally, they can perform missions more efficiently because they have multiple resources to properly assign to the tasks. Previous works quantify these advantages in terms of targets reached and time consumed (Garzón, 2015).

Nevertheless, multi-robot missions pose a series of challenges related to human factors (Cummings, 2008). The main ones are keeping the situa-

tional awareness and managing the workload of operators. Currently, the operators have to do an effort to perceive information, understand the mission, make decisions and control the robots.

This paper analyses the management of information and commands in multi-robot missions, in order to address the mentioned human factors problems.

2 Multi-robot missions

Multi-robot missions can be addressed as complex systems or various single robot missions (Roldán, 2015). In the first perspective, the mission is a set of resources that are assigned to a series of tasks to achieve a set of objectives. In the second one, the mission is a set of tasks that are simultaneously performed by single robots and consist of sequences of actions.

A review of the multi-robot scenarios covered by the literature leads to the tasks collected in table 1. Most of the missions can be split into these basic tasks. For instance, fire detection and extinguishing is a sequence of begin, surveillance (to find the fires), reconnaissance (to check them), capture (for taking the water), release (for throwing it) and finish tasks.

Table 1. Tasks of multi-robot missions.

Task	Description
Begin	Preparation and deployment
Surveillance	Covering area to detect targets
Reconnaissance	Visiting points to check targets
Tracking	Following mobile targets
Capture	Picking a resource
Release	Placing a resource
Maintenance	Performing maintenance operations
Finish	Collection and shutdown

Other important issue about multi-robot missions is the control and coordination architecture (Roldán, 2016). This architecture determines the roles of operator, interface and fleet and the communication among them. There are three paradigms: centralized (mission planning, task allocation and path planning are performed by the control station), distributed (these functions are performed by the robot fleet) and hybrid (compromise between centralized and distributed).

3 Information

Multi-robot missions generate huge amounts of data: e.g. robot telemetry, payload data, resources, targets, camera images... This volume of data depends on the number of robots and may exceed the attention span of operator. For this reason, the interface must search the relevant information within the whole data. As seen in Fig. 1, the proposal of this work is selecting the information according to mission and operator states.

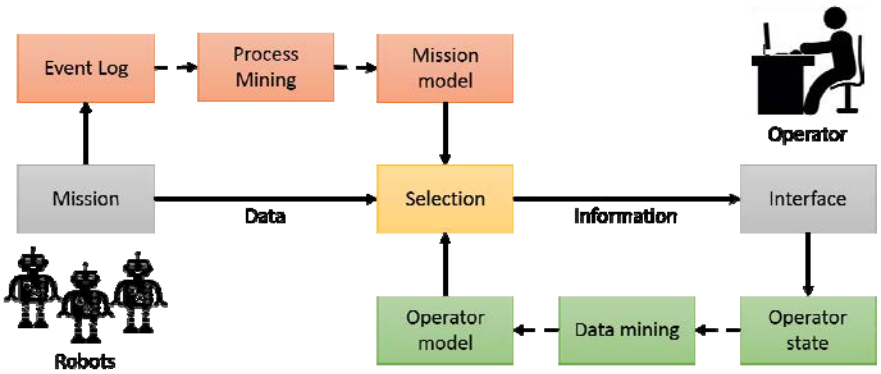

Fig. 1. Selection of information.

3.1 Selection according to the mission state

This selection of information requires a mission model to determine its state and describe its evolution. This model can be obtained by means of mission analysis or through the experience of previous similar missions.

Process mining (Van Der Aalst, 2011) is an emerging discipline that allows automatic discovery of process models through event logs. An example of application of this discipline in the context of multi-robot missions is shown in Fig. 2.

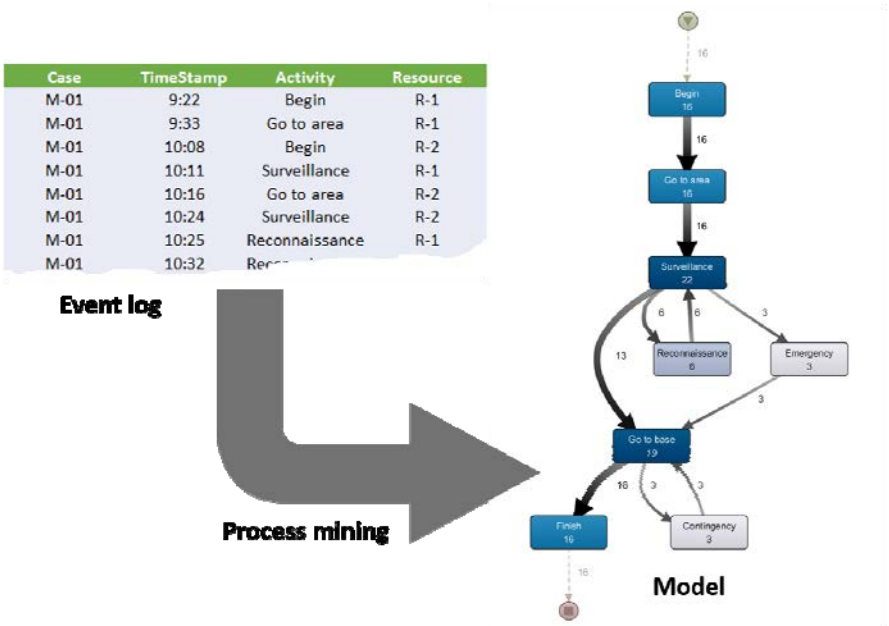

Fig. 2. Process mining applied to multi-robot mission.

3.2 Selection according to operator

This selection of information uses an operator model to predict his behavior during the mission. This model has to integrate operator state and preferences and can be obtained by means of data mining.

In this way, the information should be adapted to the physical and psychological state of operator. For instance, when the operator is stressed, tired or bored, the system should reduce the amount of data, in order to prevent saturation and errors.

In addition, the information should be adapted to the preferences of the operator. For example, if the operator usually asks for a specific information in a certain moment of the mission, the interface should anticipate the operator request and provide him with this information.

4 Commanding

Commanding is the other relevant issue for multi-robot missions. Choosing the correct commanding method can lead to save time and reduce er-

rors. In this sense, two relevant issues are the level of automation and the kind of commands.

4.1 Level of automation

(Beer, 2014) recapitulates the literature about levels of automation; from the ten levels defined by (Sheridan, 1979) to the four levels proposed more recently by (Ruff, 2002) and other authors. This last case is considered simpler and more useful, so it is shown in table 2 and explained below.

Table 2. Levels of automation.

Number	Name
1	Full manual control
2	Management by consent
3	Management by exception
4	Full automatic control

In the first level, the operator selects and launches the tasks and the role of computer is restricted to support. The second level is management by consent, which means that the computer selects the action and the operator accepts or rejects them. The third level is management by exception, where the computer selects the tasks and launches them if the operator does not cancel them. In the fourth level, the computer selects and launches the tasks and the role of operator is limited to supervision.

A question widely discussed in literature is "which is the best level of automation?" A consensus answer is that it depends on multiple factors, such as the specific mission, fleet and operator. For instance, (Parasuraman, 2000) distinguishes among different functions (information acquisition, information analysis, task selection and execution) and proposes the use of different levels of automation for each of them.

4.2 Method of commanding

If the level of autonomy is full automatic control, defining a method of commanding is not required. This is because the computer makes decisions and executes actions and the operator does not have to manage them. Nevertheless, if the level of autonomy is management by exception, management by consent and, specially, full manual control, choosing an adequate method of commanding is relevant. In fact, it has influence not only on the

time required for sending the commands but also on the performance of control and monitoring.

This section addresses the methods of commanding in low autonomies systems (levels between 1 and 2). In these modes, the operator creates and controls the tasks and the computer only shows the possibilities or suggests one or more of them.

The lowest level is the direct control of the robots to perform the tasks. In this case, the operator uses a device to command the robots (e.g. keyboard, mouse, joystick, joypad or remote control). This control is based on speed commands of translation (x, y and z axis) and rotation (roll, pitch and yaw). This method has the restriction that the operator only commands a robot at time, remaining the rest as not used.

The next method is the definition of path through waypoints. In this case, the operator sends goals to the robots that they have to reach. These waypoints contain at least the target position and orientation, but also can include information such as speed, time, and actions to be performed when reached. There are two ways to define the waypoints: doing path planning before mission, and generating each waypoint when the previous one is reached. This method allows the operator to move multiple robots at the same time, but it still require an effort to command and supervise them.

In the highest level, the operator directly sends the tasks to the robots. Therefore, the robots have to split the high level tasks into low level actions. An example is shown in Fig. 3, where the operator commands the surveillance of an area and the robot generates the coverage path and follows the waypoints.

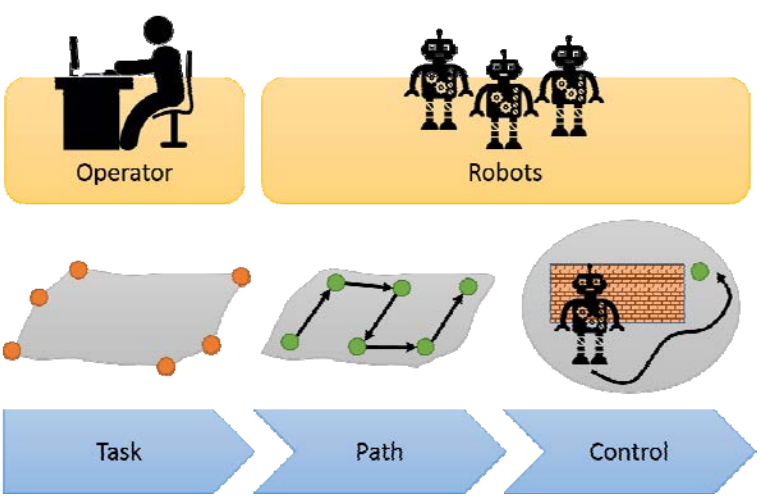

Fig. 3. High-level commanding.

The structure of these task commands is explained in table 3. The station and robot fields define the sender and receiver of command respectively. Task field determines the task: e.g. surveillance, reconnaissance, tracking, etc. Point list can contain not only one or more points but also an area defined by its vertices. Finally, target and resource lists define respectively the goals and the means of the task (e.g. in fire detection and extinguishing, the target is the fire and the resource is the water).

Table 3. Command structure.

Name	Description
Station	Station that sends the command.
Robot	Robot that must receive the command.
Task	Name of the task.
Point list	Area, path or point of the task.
Resource list	Resources of the task
Target list	Objectives of the task.

5 Conclusions

This paper analyses the multiple robot, single operator scenarios. These systems present challenges related to human factors, such as the situational awareness and the workload of operators. On the one hand, this paper proposes a selection of information based on mission and operator states. On the other hand, it proposes the use of high-level commands from the operator to the robots.

Acknowledgements

This work is framed on SAVIER (Situational Awareness Virtual EnviRonment) Project, which is both supported and funded by Airbus Defence & Space. The research leading to these results has received funding from the RoboCity2030-III-CM project (Robótica aplicada a la mejora de la calidad de vida de los ciudadanos. Fase III; S2013/MIT-2748), funded by Programas de Actividades I+D en la Comunidad de Madrid and cofunded by Structural Funds of the EU, and from the DPI2014-56985-R project (Protección robotizada de infraestructuras críticas) funded by the Ministerio de Economía y Competitividad of Gobierno de España.

References

Beer, J., Fisk, A. D., Rogers, W. A. 2014. Toward a framework for levels of robot autonomy in human-robot interaction. Journal of Human-Robot Interaction, 3 (2), 74.

Cummings, M.L., Mitchell, P.J. 2008. Predicting controller capacity in supervisory control of multiple UAVs. Systems, Man and Cybernetics, Part A: Systems and Humans. IEEE Transactions on, 38 (2), 451-460.

Garzón, M., Valente, J., Roldán, J. J., Cancar, L., Barrientos, A., Del Cerro, J. 2015. A Multirobot System for Distributed Area Coverage and Signal Searching in Large Outdoor Scenarios. Journal of Field Robotics.

Parasuraman, R., Sheridan, T. B., Wickens, C. D. 2000. A model for types and levels of human interaction with automation. Systems, Man and Cybernetics, Part A: Systems and Humans, IEEE Transactions on, 30 (3), 286-297.

Roldán, J. J., del Cerro, J., Barrientos, A. 2015. A proposal of methodology for multi-UAV mission modeling. In Control and Automation (MED), 2015 23th IEEE Mediterranean Conference on, 1-7.

Roldán, J. J., Lansac, B., del Cerro, J., Barrientos, A. 2016. A Proposal of Multi-UAV Mission Coordination and Control Architecture. In Robot 2015: Second Iberian Robotics Conference, Springer International Publishing, 597-608.

Ruff, H. A., Narayanan, S., Draper, M. H. 2002. Human interaction with levels of automation and decision-aid fidelity in the supervisory control of multiple simulated unmanned air vehicles. Presence: Teleoperators and virtual environments, 11(4), 335-351.

Sheridan, T. B., Verplank, W. L. 1978. Human and computer control of undersea teleoperators. Technical report, DTIC Document.

Van Der Aalst, W. 2011. Process mining: discovery, conformance and enhancement of business processes. Springer Science & Business Media.

CHAPTER 33

A DEVELOPMENT PLATFORM FOR THE EVALUATION AND VALIDATION OF ALGORITHMS FOR SELF-ORGANIZATION IN HYBRID SWARMS

M. ALMEIDA[1] and H. HILDMANN[2]

[1] NEC Research Labs Europe – miguel.almeida@neclab.eu;
[2] Universidad Carlos III de Madrid – hanno.hildmann@uc3m.es;

The presented development platform is part of an NEC internal research project using swarms of UAVs (acting as Mobile Sensing Platforms (MSPs)) for public safety applications such as environmental monitoring and disaster response. Besides the used quadcopters, a variety of devices is considered and functionality for including e.g. rovers or fixed wing drones is available. This sets the stage for future projects and the collaboration with other research groups focusing on inter-swarm collaboration.

1 Introduction & Motivation

The process of designing and implementing algorithms for the control of swarms poses the challenge of evaluating and testing them in the real world, that is, using actual hardware and letting it operate in a physical environment. By their nature (i.e. distributed, intended for swarms and aiming to facilitate self-organization) the algorithms under evaluation require a substantial number of devices in order to show the intended benefit.

Especially when targeting swarms of devices capable of flight – often called *drones* (a class of devices that has recently received enormous interest from the public) – poses practical, financial as well as ethical and legal challenges as these devices are subjected to a variety of different legal requirements depending on where (location) and under which circumstances (commercial, non-commercial, etc.) they are operated (Coopmans, 2014), (Wilson, 2014), (Schneider, 2014), (Ogan, 2014).

The development (and demonstration) platform presented in this chapter addresses these issues by (a) facilitating the use of hybrid swarms as well

as (b) allowing the forming of a swarm from devices physically located at different locations and legally owned and operated by different labs.

By *hybrid swarms* we mean non-homogeneous swarms, that is, swarms consisting of different classes or types of devices, but also of devices at different levels of physical embodiment. The architecture for our devices (Fig. 4) consists of three, physically separate components: the computing platform (CP), the mobile platform (MP) and the sensing platform (SP). Together, these components form a Mobile Sensing Platform (MSP). The CP, executing the swarm algorithms, is interacting with its environment in a closed control loop with the MP (and, application and SP-hardware dependent, receive additional input from the SP). We can connect the CP to either the physical MP or to a *simulated MP* with the CP unable to tell the difference (functionality to use *simulated SP*s is included in the development platform as well). Due to this we can form swarms of CPs (typically low cost and expendable) connected to either type of MP.

This setup makes it possible to operate large swarms in which not all devices are actually completely functional and airborne UAVs (the same holds for other devices types). Furthermore, we can connect devices operating (simulated) MPs even if these devices are not physically co-located.

The benefits of this are:

- We can operate large swarms without having to own MPs for all of the members of the swarm or having obtained legal permits to operate these MPs (some countries require individual permits per UAV).
- Devices can be shared between labs, enabling the forming of large swarms of physically not-collocated CPs.
- We can subject a swarm to simulated extreme environmental conditions and test the performance of the swarm and the individual CPs even if these conditions exceed the MPs' operational limits and conditions or violate operating procedures of the MPs.
- We can intentionally harm devices (reduce their functionality or impair their capabilities) to evaluate the swarm's performance and its ability to mitigate the impact of attacks and critical device failures.
- We can operate a swarm of e.g. simulated surveillance drones (i.e. CPs with simulated MPs) over territories where flight operations are highly regulated (e.g. nuclear power plants) or where device malfunction would potentially cause disruptions (e.g. near airports).

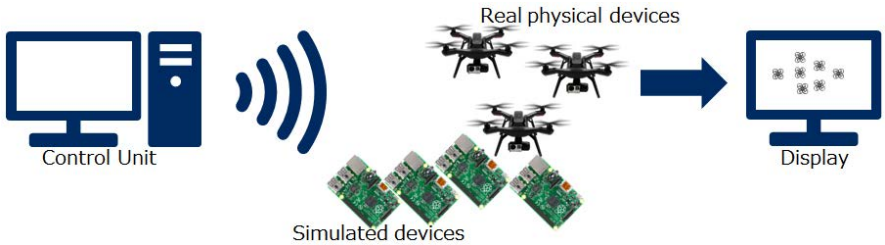

Fig. 1. The 4 components of the platform: (1) control interface (2) physical devices, (3) simulated devices and finally (4) a visualization module.

Fig. 1 shows the 4 components of the platform: (1) a control interface to run the simulation, (2) physical devices (possibly in a number of different locations), (3) simulated devices and finally (4) a visualization module showing the scenario (using e.g. google maps). In case of a (homogeneous) swarm of physically realized and fully functional UAVs the visualization would offer additional view-points and -angles but the swarm could – of course – be observed in the traditional way from e.g. a viewing platform.

2 Hardware & Software

It should be noted that the platform is intentionally designed to be able to handle a number of different device types, i.e. it is not restricted to our quadcopters or, for that matter, to UAVs in general. Specifically the use with fixed-wing drones as well as rovers (unmanned ground vehicles) is possible and simulations could even use all of these device types together.

Our drones are quadcopters with a maximum power demand of 500W (the demand when hovering is approx. 70W) supplied through a battery (11,1v 3000mAh). Their approximate weight is 600g with additional load capacity of around 300g. The projected flight time for use in demos (i.e. outside and subjected to environmental conditions but without additional load) is 15 minutes. The dimensions are 177mm x 177mm x 192mm.

The computing platform (the CP) is a Raspberry Pi 2 with the following specifications: a 900MHz quad-core ARM Cortex-A7 CPU, 1GB RAM, 4 USB ports, 40 GPIO pins, Full HDMI port, Ethernet port, Combined 3.5mm audio jack and composite video, Camera interface (CSI), Display interface (DSI), Micro SD card slot, VideoCore IV 3D graphics core.

The onboard computing platform (the Raspberry Pi 2) is running Linux (Raspbian) as operating system and ROS (BSD or LGPLv3 or GPLv3 License) over VPN to connect to other modules.

Fig. 2. A picture of the used hardware (UAV, serial number NEC.NLE-001).

The flight module (the hardware that takes care of implementing and realizing all the flight operations) is a Pixhawk. It has a 168Mhz 32-Bit STM32F427 Cortex M4, 256KB RAM, 2MB Flash, 14 PWM / servo outputs as well as connectivity options for additional peripherals (UART, I2C, CAN) and redundant power supply inputs as well as an automatic failover. Regarding peripheral sensors we are currently using only GPS, Airspeed sensor, Sonar, LiDar and Optical Flow, but the Pixhawk is not restricted to these and additional sensors can be added. The Pixhawk is licensed under the Creative Commons License (Open-Source HW).

Regarding the setup of system: the control unit as well as the visualization tool ((1) and (4), respectively, in Fig. 1) are realized in a control station (a PC or a laptop), which communicates through a wireless network with the members of the swarm (cf. Fig. 3, next page).

The following software was used:

- **NEC MSP Control Module**: programmed in C++. The UAV sends basic instructions to autopilot through ROS.
- **Flight Module**: using APM Flight Stack (GPLv3 License) which supports planes, copters and rovers. It connects to the navigation sensors (e.g. GPS) and controls basic flight/navigation dynamics.
- **MAVROS**: communicates the autopilot's / SITL's mavlink data to the network and the GCS (Ground Control Software) and relays the UAVs Command Module's instructions to the autopilot.
- **Ardupilot SITL (SW in the loop)**: this instance of the autopilot software creates simulated platforms that act as real platforms. Ardupilot is licensed under the GPLv3 License.

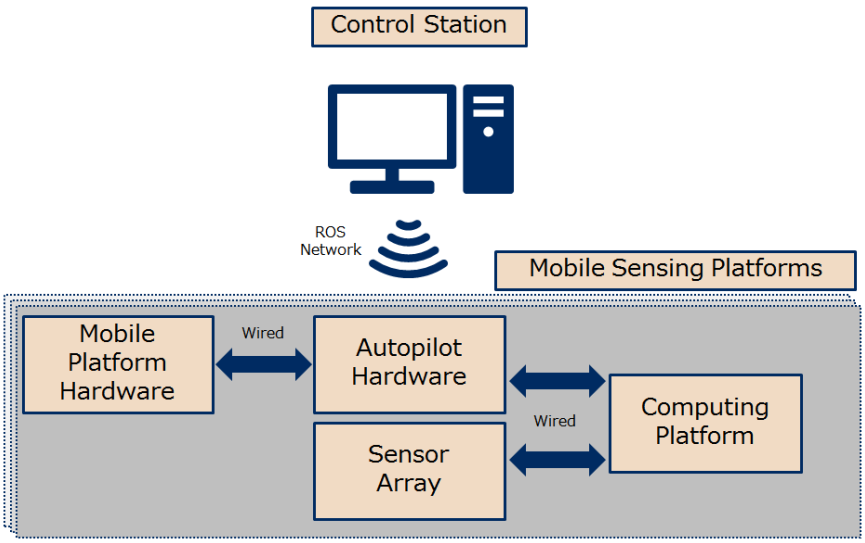

Fig. 3. A conceptual overview of the hardware components.

3 Architecture

We distinguish a number of components and modules (cf. Fig. 4):

- the control station houses the *system control* (SC), a *dispatch module* (D), an *environment module* (E) as well as the default visualization module (i.e. a screen where the swarm is displayed).
- the system control (SC) is the core and heart of the platform. This component initiates and starts demonstrations and all other components refer back to it, directly or through other components.

- the dispatch module (D) is the interface through which the devices communicate with the operator in a simulation. Through D the swarm can be fed new data and existing data can be amended.
- the environment module (E) simulates the interface through which updates about the physical environment are communicated to the swarm (traffic and weather conditions, flight corridors, etc).
- the Mobile Sensing Platform consist of up to three physical components: the mobile platform (e.g. the UAV), the sensor platform and the computing platform (e.g. a Raspberry Pi).
- the computing platform runs up to three separate software components: the NEC proprietary control module (CM) and, optionally, the simulated mobile platform and the simulated sensor platform.
- the control module (CM) is where the implemented swarm algorithms are executed.

Fig. 4 (on the next page) gives us a closer look at the architecture, detailing the different hardware and software components and visualizing the setup of the Mobile Sensing Platforms (which is a conceptual unit).

The hardware components of a UAV are physically connected by wires and we treat an UAV as a self-contained device. Regarding the communication between the individual components we distinguish two wireless connection types: (a) the system level wireless communication that allows the components to connect with the system control (SC); and (b), the simulated communication channel. The former is used to initialize all software components, to add units to the simulation and to gather the data for the visualization component of the simulation. The latter is simulating the communications of the swarm with dispatch (D) and environment (E).

The demonstration platform uses the ROS network as communication framework as it provides all functionalities required.

Within each Mobile Sensing Platform we separate the following hardware components (a) the Computing Platform (CP, in our case a Raspberry Pi 2) where the *NEC control module* (CM) is implemented. The CM is where both the simulated sensing platform, as well as the simulated mobile platform (Ardupilot SITL) are located and where the control / swarm algorithms are executed. Furthermore, we have (b) a Sensor Platform (SP, i.e. some onboard sensor array) and (c) the mobile hardware platform (MP), which in our case is the UAV shown in Fig. 2).

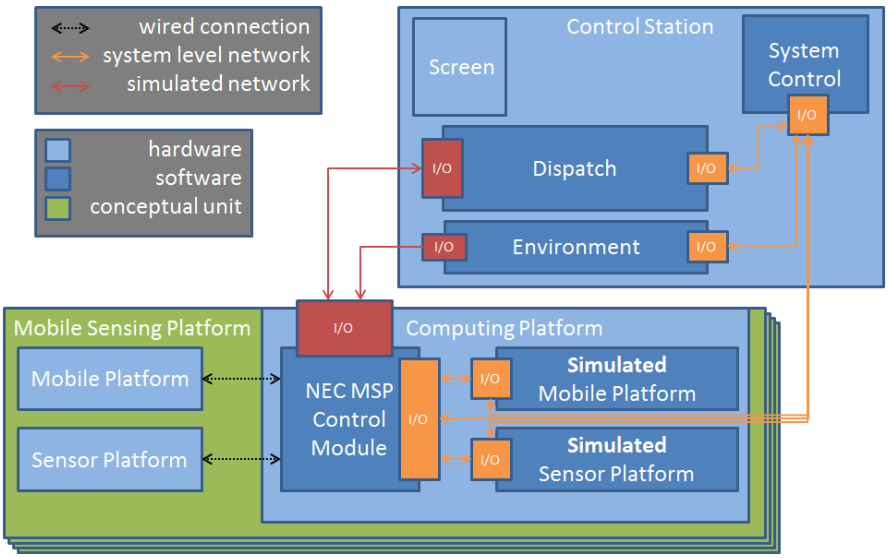

Fig. 4. The components and communication links of the development platform: we distinguish between the wireless system communication, the simulated wireless communication between the simulated / real devices and the dispatch / environment module and the wired connection between the hardware components.

4 Conclusion, Intended Usage & Future Work

The development platform is part of an NEC internal research project on swarms of mobile sensors (i.e. swarms of UAVs equipped with sensor arrays used as mobile wireless sensor networks) for public safety applications such as environmental monitoring and disaster response. Currently, only quadcopters are used, but (as stated above), a variety of devices is considered and functionality for including rovers or fixed wing drones is available. This sets the stage for future projects and the collaboration with other research groups focusing on inter-swarm collaboration.

The current use of the platform includes the development and the evaluation of algorithms such as the ones reported in (Hildmann, 2014), (Hildmann, 2015), (Hildmann, 2016) and the approaches subject to the following patent applications (1) US 14/250,470, (2) PCT/EP 2015/067850, (3) PCT/EP 2015/061180, (4) PCT/EP 2015/062810 (all pending)). Future work on applying the above / implementing these approaches for other device types as well as swarms consisting of devices of multiple types is considered, project approval pending.

Acknowledgements

The presented work was undertaken at NEC Research Labs Europe in the context of the *Mobile Sensing Platforms for Public Safety* Project, funded by the Global Safety Division of NEC.

References

Coopmans, C. 2014. Architecture requirements for Ethical, accurate, and resilient Unmanned Aerial Personal Remote Sensing. Int. Conf. on Unmanned Aircraft Systems (ICUAS). Orlando, USA, pp. 1−8.

Hildmann H and Nicolas S. and Martin M. (inventors), **PCT/EP 2015/061180** (pending). Method for providing location for performing tasks of moving objects.

Hildmann H. and Martin M. (inventors), **US 14/250,470** (pending). Distributed task scheduling using multiple agent paradigms.

Hildmann H. and Nicolas S. and Martin M. (inventors), **PCT/EP 2015/062810** (pending). Method and system for providing data from a plurality of sensing devices.

Hildmann, H. and Kovacs, E. 2016. "Should I stay or should I go?" – Enabling autonomous mobile devices to optimize data collection performance. In Proc. RoboCity16– Future Trends in Robotics, Ch. XXXI, pp. 251-258.

Hildmann, H. and Martin, M. 2014. Adaptive scheduling in dynamic environments. 3rd Workshop on Information Technologies for Logistics (IT4L'14), Warsaw, Poland

Hildmann, H. and Martin, M. 2015. Resource allocation and scheduling based in emergent behaviors in multi-agent scenarios. 4th Int. Conf. on Operational Research in Enterprise Systems (ICORES), Lisbon, Portugal

Martin M. and Hildmann H. (inventors), **PCT/EP 2015/067850** (pending). Distributed scheduling under uncertainty for mobile multi-agent systems.

Ogan, R.T. 2014. Integration of manned and unmanned aircraft systems into U.S. airspace . IEEE SouthEastCon2014. Lexington, USA , pp. 1−4.

Schneider, D. 2014. Open season on drones? IEEE Spect. −51(1): 32-33

Wilson, R.L. 2014. Ethical issues with use of Drone aircraft. 2014 IEEE Int. Symp. on Ethics in Science, Tech. and Eng.. Chicago, USA, pp.1−4.

CHAPTER 34

DETECTING, LOCALIZING AND FOLLOWING DYNAMIC OBJECTS WITH A MINI-UAV

I. BAIRA, M. GARZON and A. BARRIENTOS

Centro de Automática y Robótica UPM-CSIC, Calle José Gutiérrez Abascal, 2. 28006 Madrid, Spain – ma.garzon@upm.

This paper presents an approach for the detection, localization and following of dynamic terrestrial objects using a mini-UAV. The development is intended to be used for surveillance of large infrastructures. The detection algorithm is based on finding several pre-defined characteristics of the target, such as color, shape and size. The process used to localize the target, once it is detected, is based on an inversion of the Pinhole camera model. The task of following the Summit XL was designed to keep the target inside the field of view of the camera, and it was implemented in the form of a PID controller. The system has been tested both in simulation and with real robots, showing promising results.

1 Introduction

Nowadays, the detection, localization and following of moving objects using Unmanned Aerial Vehicles (UAV) has grown up as an important task. This work is intended to be used for surveillance of large critical infrastructures, but its range of applications is very large.

The proposed system should be able to detect, localize and follow a moving target in a complex environment. This means that the system must be able to deal with unknown obstacles, as well as changes in the movement of the target.

Following moving objects might be seen as a trivial function for living beings. However, it is a complex task for autonomous robots, because it requires several sub-tasks, such as detection, differentiation from obstacles or other elements in the surroundings. It also requires to obtain the global

or relative position of the object and to define a strategy to be able to adapt to the target's movements.

In previous years, some developments have used the drone camera to detect terrestrial objects, but they did not autonomously follow it or localized it without an external reference (Garzón et al., 2013). Also, (Huang et al., 2010) proposed an approach based on frames differentiation, but it did not perform well enough when facing high frequency vibrations, which are very common when using mini-UAVs. Another development uses LIDAR sensors in order follow objects (Leslar et al., 2011). Yet another approach proved to be able to follow a 3D moving object and keep a distance with it, based on the visual information given by an adaptive tracking method based on the color information (Mondragon et al., 2011). The work presented here differs from previous works because it is able to perform all three sub-tasks in a fully integrated way, it only uses a camera and an ultrasound sensor to perform the following and it uses a GPS to localize the target in global coordinates.

2 Detection

The target detection strategy used in this work is based on comparing a set of characteristics from the objects present on the aerial image against those of the target, which are pre-defined or can be extracted from an initial image. The main characteristics used are color, shape and size.

The color is obtained in the HSV color space, to make the system robust against illumination changes. Once it is defined, a binarization method is applied to every pixel of the image. This is done by establishing a threshold in each one of the channels (Hue, saturation and value). The objective of this step is to create a binary image in which every pixel that has the same color as the target will stand out in white over a black background. As mentioned before, the color of the target can be pre-defined or selected in the calibration step.

After this, a post-processing step is applied to the binary image, which includes noise reduction filters, as well as dilation and erosion. The objective of this step is to obtain an image with clearly defined outlines. Moreover, this filtering process can be adapted or fine-tuned according to the scenario where the following will be performed.

After the image is filtered, the shape and size of the objects is analyzed, so as to select only those figures that match the size and form of the target. It is possible to define a correct size of the target in the image plane, because the height at which the UAV is flying is known, and this height pro-

vides a good approximation to the distance from the camera to the object. Also, it should be pointed out that other geometrical characteristics can be included at this point, in case similar objects are found in the surroundings.

Once the target is found in the image, its geometric center is calculated; it represents the position of the target in the image plane, and will be used for the localization process described in Section 3. The final step for the detection process is to highlight the outline of the object in the original image so as to show to the user what is being detected. The overall process is illustrated with Fig. 1.

(a) (b) (c)

Fig. 1. Steps for image treatment: (a) Binarized image, (b) Prepared image, (c) Target highlighted.

3 Localization

The process used to obtain the position of the target in a global coordinate system, is based on an inversion of the Pinhole camera model, which describes the mathematical relationship between the location of a point in the space $(X,Y,Z)^T$ and its projection onto the image plane $(u,v)^T$ of the camera.

The model is shown in Equation (1), where the transformation matrix includes characteristic parameters of the camera. An intrinsic calibration of the camera is needed in order to obtain the parameters of the transformation matrix.

$$\lambda\begin{pmatrix} u \\ v \\ 1 \end{pmatrix} = \begin{pmatrix} f & \tau & \sigma_x & 0 \\ 0 & \eta f & \sigma_y & 0 \\ 0 & 0 & 1 & 0 \end{pmatrix}\begin{pmatrix} X \\ Y \\ Z \\ 1 \end{pmatrix} \tag{1}$$

where λ is the scale factor, $(u,v)^T$ the projection of the point onto the image plane expressed in pixels, f the focal distance, τ is the skew parameter which indicated whether the pixels are skew or not, and it will be 0 in case

there is no skew, $(\sigma_x, \sigma_y)^T$ are the coordinates of the center of the image plane, $(X, Y, Z)^T$ are the coordinates of the target in relation to the camera, and η indicates the form of the pixel, if it is 1, then the pixel is a square. The coordinate Z is known because the drone has an ultrasound sensor pointing downwards. It should be as precise as possible to obtain a correct estimation of the position. Therefore, the flight conditions of the drone should be smooth and they should avoid pronounced inclinations, speeds or angular accelerations.

Since the UAV will fly at a height of 8 meters or more, it is possible to assume that the target is flat and ignore its height to the ground. Having this assumption, the matrix model of Equation (1) can be inverted. Moreover, if $(u, v)^T$ is substituted by the coordinates of the centroid of the detected target, it is possible to obtain its position in a reference frame located on the camera optical frame.

The final step of the localization process is to transform this position, from the camera's optical frame to an external, fixed reference frame. This is done by applying a coordinate's transformation to the position of the target. The values of this transformation will be extracted from the localization system of the UAV itself. Moreover, if a GPS is mounted on-board, the position of the target will also be given in global reference frame. Otherwise it will be given in the UAV's odometry frame. Regardless of which external frame is used, the UAV will be able to perform the following step, because this step is based on relative changes of the position of the target.

4 Following algorithm

The objective of this algorithm is to keep the target inside the field of view of the camera, and therefore to extend the tracking as long as possible. A PID controller was selected as the solution for this due to its flexibility, robustness and popularity among industrial environments. And it proved to be capable of controlling the drone effectively.

The position error is defined as the distance in meters between the center of the camera image and the target position, according to the $(x, y)^T$ axis of the coordinate system of the drone.

The regulation actions consist in linear speed commands in each axis. Since the UAV's response for each axis are assumed to be decoupled, two different PID controllers were designed, for x and y axes respectively. Both, the simulated system and the real system were controlled using this method.

In order to adjust the PID controller, the Ziegler-Nichols' closed loop method was used (Quevedo et al., 2000). This selection was made because it is flexible and easy to adjust, and mainly because it does not require a system identification step. This is especially useful if different UAVs are to be used, as is this case.

However, after implementing those PIDs, the result was a slow response of the UAV, and it was not able to perform its task correctly. This behavior is foreseeable since Ziegler-Nichols' methods were designed for industrial plants which have slow dynamics (in contrast to our system, where fast reactions are essential). As a result, these estimations were used as a starting point for the following heuristic adjustment. Moreover, a different adjustment was necessary also for the real drone, and in this case the integral value was minimized because the error in steady state is not a priority, whereas a fast reaction is crucial. The results of the heuristic adjustment are presented in Table 1.

Table 1. Results for PID controller adjustment.

	Ziegler-Nichols'		Simulations		Real world	
	x axis	y axis	x axis	y axis	x axis	y axis
K_p	0.342	0.336	0.35	0.35	0.04	0.04
K_d	0.342	0.388	0.003	0.003	0	0
K_i	0.0427	0.0726	0.025	0.025	0.01	0.01

This PID demonstrated that it could respond to extreme situations such as sudden changes of direction or maximum speed of the Summit XL, keeping the target in every moment inside the framework of action of the ventral camera.

5 Software Architecture

The entire software is supported by the software framework ROS (Robot Operating System). A diagram of the simplified proposed software platform is found in Fig. 2, where the main components are marked by double lines. An external controller was created so as to be able to take off and position the drone at the desired altitude, and takeover control if necessary. Another component is the detection-localization where all the image processing occurs and the last one is the following where the PID controller is implemented.

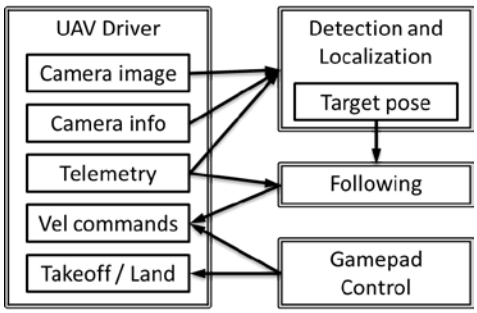

Fig. 2. Simplified nodes and topics of the system.

6 Experiments and results

The experiments are divided in two, simulations and real world tests. For both type of tests, the UGV was tele-operated along the scenario and the UAV perform the autonomous detection, localization and following.

6.1 Simulations

The simulations were done using the Gazebo 3D simulator, using models for the UAV and the UGV. Also, a virtual scenario similar to a critical infrastructure was created for the tests (See Fig. 3).

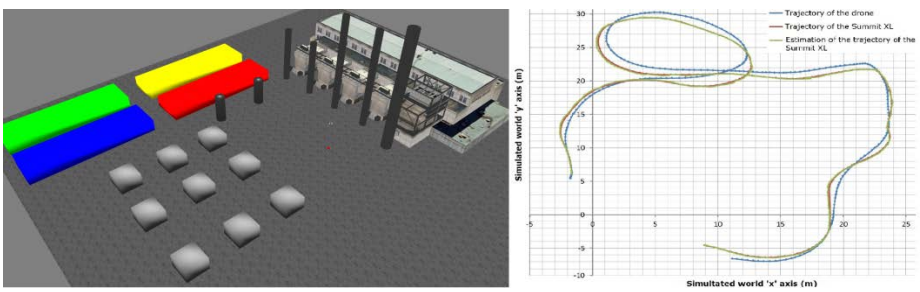

Fig. 3. Simulated world (Left). Example of routes of UGV and UAV (Right).

Several variables were observed along 10 different routes. These routes included big obstacles, red objects (same color as the target), changes of the target's speed (0-3m/s), etc.

6.2 Real world experiments and results

Since the localization of the real UAV is not reliable, the real world tests were done only for the detection and following capabilities. The tests were carried out indoors, with the UAV flying at a height of 6 meters, which can be a handicap because a higher altitude would improve the results by covering a bigger area with the ventral camera. However, the system proved its detection and following capabilities as shown in Fig. 4.

A summary of the results of both simulations and real world experiments is presented in Table 2. It can be seen that a correct detection was achieved in 98.47% of the cases for the simulation and 93.35% for the real world tests. The following task has also a good performance, as shown by the very small mean error obtained (0.18m). It should be pointed out that, in order to avoid errors on the localization, some images are rejected according to the aforementioned flying restrictions, and the reason is that high inclinations of the drone may trigger a bad localization of the target. Those rejections however do not affect the following task.

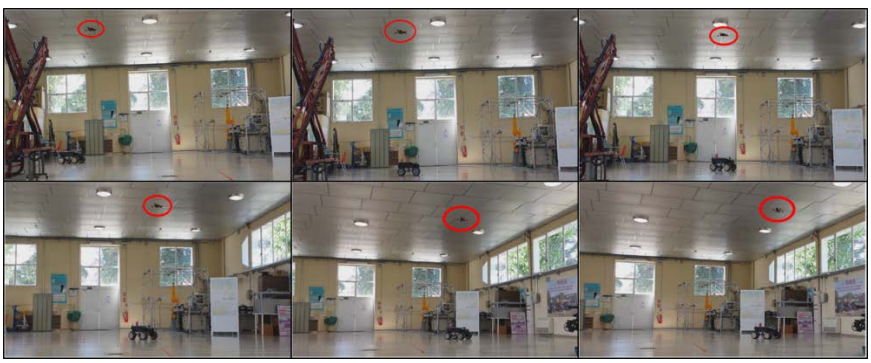

Fig. 4. Image sequence for real world tests.

Table 2. Results summary.

	Total Images	False negatives	False positives	UGV path length	Mean error
Simulations	10519	1.53%	0%	800m	0.18m
Real world	18.705	6.65%	0.54%	n/a	n/a

7 Conclusions

A system that detects, localizes and follows a mobile ground robot using a mini-UAV is presented. The proposed detection algorithm is simple

enough to be executed on real time and provides a very good detection ratio. The following technique is also robust, and allows following the UGV in long routes always keeping it in the camera's field of view.
The localization of the UGV in a global reference frame was possible only on simulations because of the lack of a good localization with the real robot, however it have proved to be a promising technique for obstacle or mobile objects localization in complex scenarios. The results, both in simulations and with real robots show that the proposed technique can successfully perform its tasks in realistic scenarios and work in real time.

Acknowledgements

This work has received founding by PRIC (Protección Robotizada de Infraestructuras Críticas; DPI2014-56985-R) and RoboCity2030-III-CM project (Robótica aplicada a la mejora de la calidad de vida de los ciudadanos. Fase III; S2013/MIT-2748), funded by Programas de Actividades I+D en la Comunidad de Madrid and cofunded by Structural Funds of the EU.

References

Garzón, M., Valente, J., Zapata, D., Barrientos, A. 2013. An Aerial-Ground Robotic System for Navigation and Obstacle Mapping in Large Outdoor Areas. Sensors, 13(1), 1247-1267.

Huang, C.-H., Wu, Y.-T., Kao, J.-H., Shih, M.-Y., Chou, C.-C. (2010). A Hybrid Moving Object Detection Method for Aerial Images. In Advances in Multimedia Information Processing - PCM 2010, 6297, pp. 357-368.

Leslar, M., Wang, J.-g., & Hu, B. (2011). Comprehensive Utilization of Temporal and Spatial Domain Outlier Detection Methods for Mobile Terrestrial LiDAR Data. Remote Sensing, 3(8), 1724--1742.

Mondragon, I., Campoy, P., Olivares-Mendez, M., & Martinez, C. (2011). 3D object following based on visual information for Unmanned Aerial Vehicles. Robotics Symposium, 2011 IEEE IX Latin American and IEEE Colombian Conference on Automatic Control and Industry Applications (LARC), (pp. 1-7).

Quevedo, J., & Escobet, T. (2000). Digital Control: Past, Present and Future of PID Control. Elsevier Science Inc.

CHAPTER 35

EXPERIMENTAL EVALUATION OF THE LOCOMOTION OF A HEXAPOD ROBOT

L. MENA[1], H. MONTES[1, 2], R. FERNÁNDEZ[1], J. SARRIA[1], and M. ARMADA[1]

[1]Centre for Automation and Robotics – CSIC-UPM; [2]Universidad Tecnológica de Panamá, hector.montes@csic.es

This work presents some experimental results of the locomotion in discontinuous and continuous gait of a hexapod robot of medium size. However, first is presented a brief summary of the configuration of the hexapod robot and its direct and inverse kinematics. Besides, the hardware architecture of the robot is also described. The gaits experimented on the robot use the alternating tripod mode in both cases, continuous and discontinuous gait.

1 Introduction

Autonomous legged locomotion has been of great interest for several researchers of robotics for many years, with the aim of replicating the movements of the animals when they are moving (Bekey, 2005). There have been important contributions to the advancement of walking robots

Important contributions to the advancement of walking robots have been carried out during more than 30 years, among them can be highlighted the hexapod robot ASV (Adaptive Suspension Vehicle) (Waldron and McGhee, 1986), which demonstrated the feasibility of using legs for transportation in rough terrain conditions; the Quadruped used to explore running on its legs (Raibert, 1986); the Dante (Bares & Whittaker, 1993), which combined legged and rappelling mobility system for remote exploration.

Development of new technologies has allowed the design and implementation of several prototypes of legged robots in the last decade. For ex-

ample, Boston Dynamics has developed several walking robots, as LittleDog, a quadruped robot used for research on learning locomotion (Kolter & Ng, 2011); BigDog, a rough-terrain robot that walks, runs, climbs and carries heavy loads (Raibert et al., 2008); LS3, a rough-terrain robot designed to go anywhere Marines and Soldiers go on foot, helping carry their load (Boston Dynamics, 2010). Additionally, there are other important legged robots that have contributed to the advancement of this technology, such as the Tri-ATHLETE, that is a vehicle is with wheel-on-limb developed to support the return of humans to the lunar surface (Heverly et al, 2010); the StartlETH, a quadruped robot with the ability to run and climb over rough grounds (Hutter et al., 2012).

On the other hand, the Field & Service Robotics Group of the Centre for Automation and Robotics (CAR) CSIC-UPM, since the early nineties, has designed and implemented several legged robots for various applications. Some of them are the ROWER, quadruped robot with a special gripper system in its legs used for welding tasks in processes of shipbuilding (Gonzalez de Santos et al., 2000); REST, a climbing hexapod robot intended for welding tasks in ferromagnetic walls (Grieco, 1997); SILO4, a quadruped robot used as a testbed for research topics on locomotion strategies (Gonzalez de Santos et al., 2006); ROBOCLIMBER, a teleoperated climbing and walking robot designed to carry out consolidation tasks on mountainsides to avoid the rock fall (Montes et al., 2004; Montes, 2005; Montes & Armada, 2016).

In this chapter some experimental evaluations of the locomotion of a hexapod walking robot are presented, which has been designed and manufactured by CAR CSIC-UPM. The main objective of this hexapod walking robot is carry out tasks for localisation of antipersonnel mines, taking on board a manipulator arm with a metal detector installed on it. However, this hexapod robot is able to carry out other applications.

This chapter is organized as follows: the configuration of the hexapod robot and its direct and inverse kinematics models are presented in Section 2. In Section 3 some experimental results of the hexapod robot locomotion are described. Finally, in Section 4 are presented some conclusions about this work.

2 Hexapod robot configuration

The hexapod robot presented in this work consists of a rectangular body and six equally spaced legs from each other in both sides. Its body not only serves as a support platform for the legs, but also as a support for subsys-

tems that allow controls of the robot and, besides, to support other systems in order to carry out other applications, e.g., humanitarian demining tasks (Montes et al., 2015a; Montes et al, 2015b; Mena et al, 2015). In Fig. 1 the general configuration of the robot is presented.

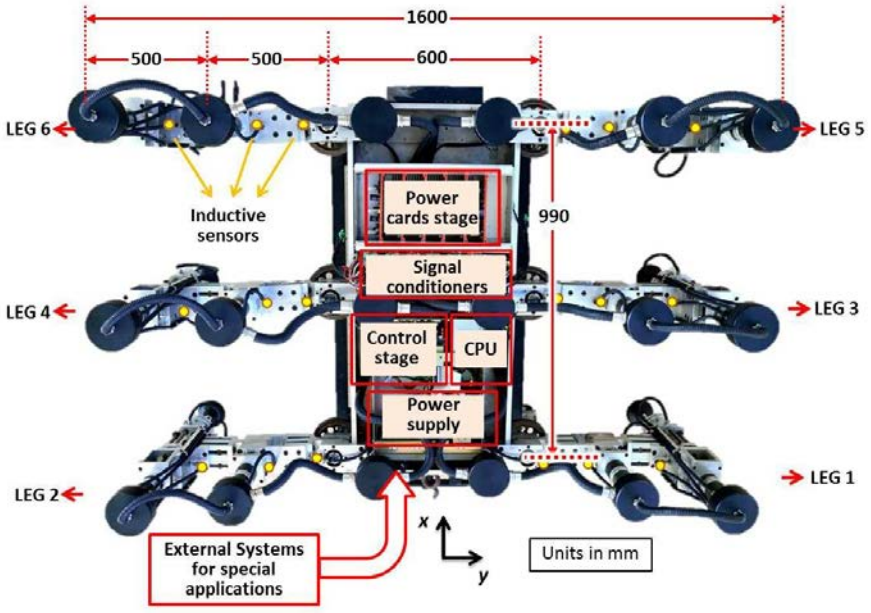

Fig. 1. General configuration of the hexapod robot.

The robot hardware consists of an on-board computer, control electronic cards, power cards, data acquisition boards, signal conditioner cards, several types of sensors, DC motors, Wi-Fi communication system, DGPS, batteries, and other devices and accessories. Each leg is controlled by means of a control electronic card, which drives three power cards, one by DC motor. Additionally, the system has a HMI in order to send to the hexapod robot the control commands to generate different locomotion patterns. These command controls can be sent by means of Ethernet connection or Wi-Fi (Mena et al., 2015). In Fig. 2 the hardware architecture of the hexapod robot is presented.

On the robot is possible to add a secondary on-board computer and other devices o mechanisms, which it would be responsible for executing specific tasks necessary for certain types of application. For example, a scanning manipulator to carry out searching tasks of antipersonnel landmines for

humanitarian demining applications (Montes et al., 2015a; Montes et al, 2015b).

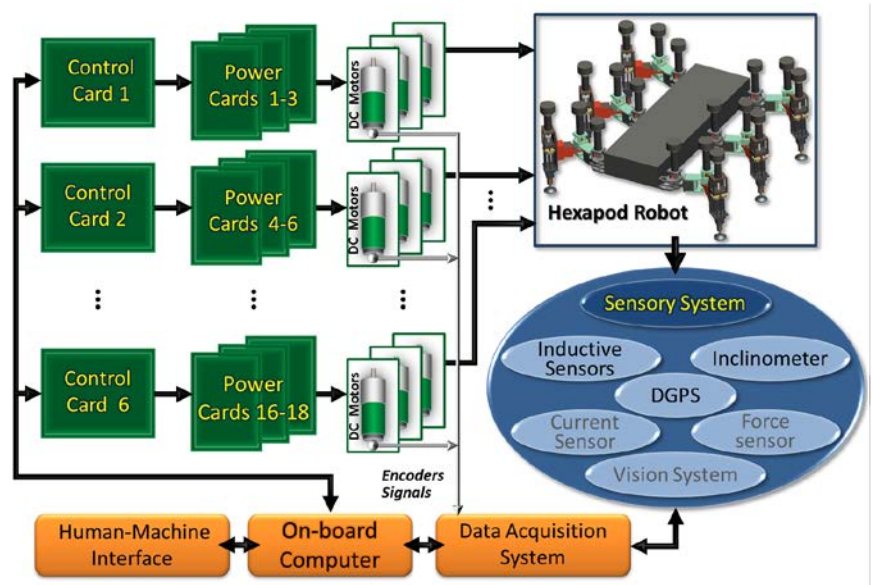

Fig. 2. Hardware architecture of the hexapod robot.

The robot legs have a SCARA configuration with three degree of freedom. Therefore, the formulation of the direct and inverse kinematics is relatively easy to obtain. Besides, this kind of legs configuration allows low energy consumption when the robot performs trajectories on a quasi-flat terrain. The Fig. 3 shows the configuration of one leg of the robot and the parameters used to obtain the direct and inverse kinematics.

The homogeneous transformation matrix of the hexapod robot leg and the Cartesian position of the foot centre is Equation (1).

$$T = \begin{bmatrix} C_{12} & -S_{12} & 0 & L_1C_1 + L_2C_{12} \\ S_{12} & C_{12} & 0 & L_1S_1 + L_2S_{12} \\ 0 & 0 & -1 & -d_3 \\ 0 & 0 & 0 & 1 \end{bmatrix} \tag{1}$$

$$x = L_1C_1 + L_2C_{12};\quad y = L_1S_1 + L_2S_{12};\quad z = -d_3$$

where, $C_1 = \cos(q_1);\ C_{12} = \cos(q_1 + q_2);\ S_1 = \sin(q_1);\ S_{12} = \sin(q_1 + q_2);$

The inverse kinematics of the robot legs has two types of responses depending on elbow joint position, i.e., with elbow-up and elbow-down configurations, which it is well known in the literature. From Equations (2) and (3), the inverse kinematics formulation with the configuration above mentioned are presented, respectively.

$$q_2 = \operatorname{atan}\frac{\sqrt{1-\cos^2\theta}}{-\cos\theta};\quad q_1 = \operatorname{atan}\frac{y}{x} - \operatorname{atan}\frac{L_2\sin(q_2)}{L_1 + L_2\cos(q_2)} \tag{2}$$

$$q_2 = \operatorname{atan}\frac{-\sqrt{1-\cos^2\theta}}{-\cos\theta};\quad q_1 = \operatorname{atan}\frac{y}{x} + \operatorname{atan}\frac{L_2\sin(q_2)}{L_1 + L_2\cos(q_2)} \tag{3}$$

where, $\theta = \pi - |q_2|$

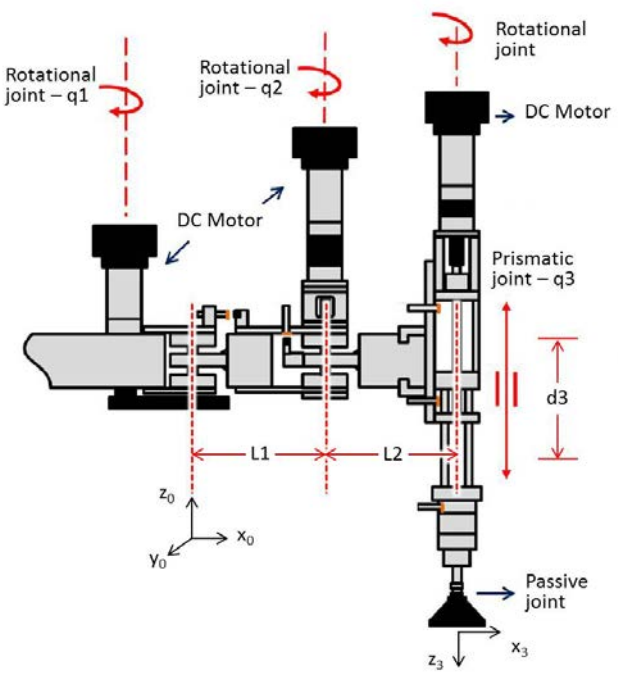

Fig. 3. Configuration of the robot leg and the parameters of its kinematics.

3 Experimental results

Several experimental tests have been carried out with different gaits, using the hexapod robot presented in this work. One of the gaits implemented in the hexapod robot has been the alternating tripod discontinuous gait, carried out periodically and with coordinated motions. Fig. 4 shows an experimental result during the execution of a discontinuous gait using the alternating tripod mode. In this case only the joint positions of the Leg1 and Leg2 are shown, because each leg belong to a different tripod. It is possible to see, in Fig. 4, the coordination between both tripods.

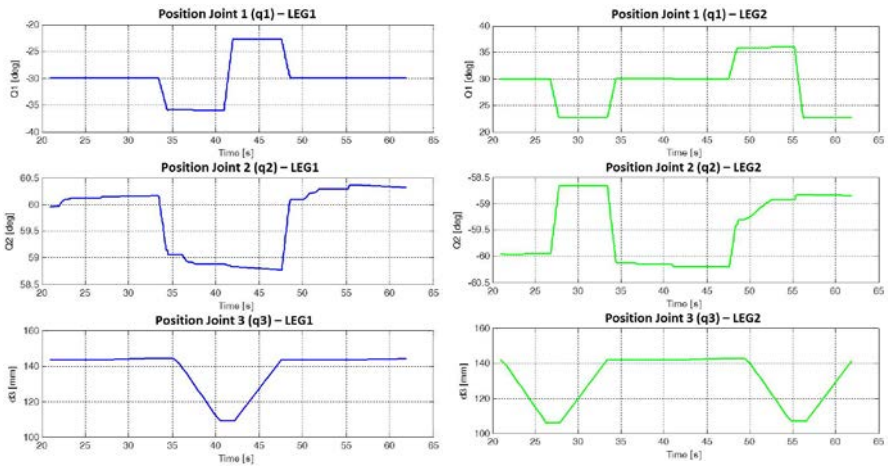

(a) (b)

Fig. 4. The alternating tripod mode in a discontinuous gait of the hexapod robot. (a) Joint positions of the Leg1, (b) joint positions of the Leg2.

Fig. 5 shows an experimental result during the execution of a continuous gait using the alternating tripod mode. In similar way, only the joint positions of the Leg1 and Leg2 are shown, because each leg belong to a different tripod. It is possible to see on the graphics of the joint 3 of both legs a delay in the execution of step. This is to avoid the frictions of the robot leg with the soil.

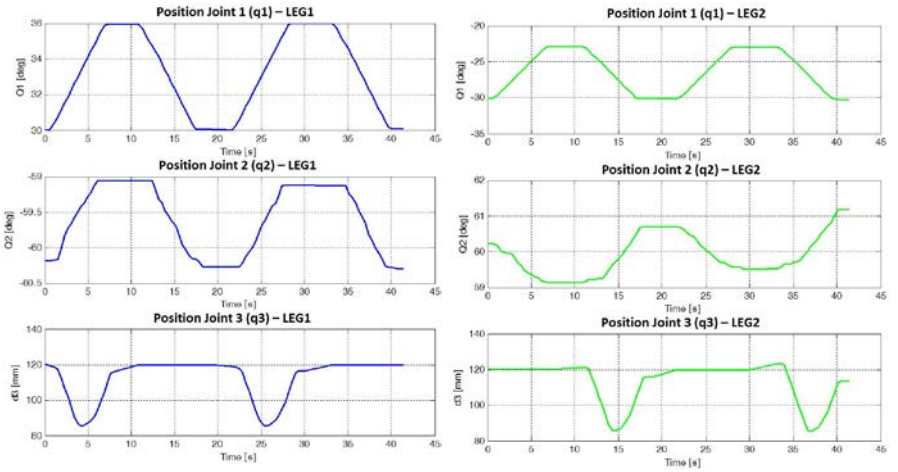

(a) (b)

Fig. 5. The alternating tripod mode in a continuous gait of the hexapod robot. (a) Joint positions of the Leg1, (b) joint positions of the Leg2.

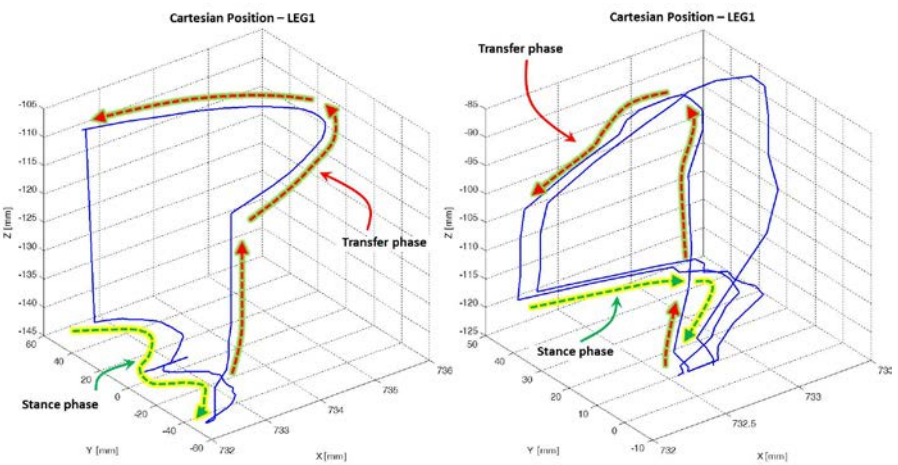

(a) (b)

Fig. 6. Transfer and stance phases of Leg1. (a) Using a discontinuous gait, (b) using a continuous gait.

The transfer and stance phases of the Leg1 during one step in discontinuous gate and two steps in continuous gait are shown in Fig. 6. Fig. 6(a) shows a small error in the trajectory of the foot of the Leg1 during the stance phase, but 1 mm, approximately, is negligible for the size of the ro-

bot. Fig. 6(b) shows a small error along 'x' axis, besides of the small error between each step. However, this error is negligible, too.

4 Conclusions

In this chapter some experimental results have been presented about the evaluation of the locomotion of a hexapod walking robot developed by the CAR CSIC-UPM.

Discontinuous and continuous gaits using alternating tripod mode have been presented, with one or two steps, in order to see the details of the steps. It is possible to compare the evolution of the joint positions of each robot tripod by referencing the Leg 1 and Leg 2. Besides, it is possible to see the transfer and stance phases of one of the leg of the robot in both modes, discontinuous and continuous gait.

This hexapod robot can be used for several applications on several kinds of terrains with velocities relatively low. However, this legged machine can bear loads relatively high, up to 300 kg.

Acknowledgements

The authors acknowledge funding of this work under TIRAMISU Project - Grant Agreement Nº 284747 of the 7FP, and partial funding from the RoboCity2030-III-CM project (Robótica aplicada a la mejora de la calidad de vida de los ciudadanos. Fase III; S2013/MIT-2748), funded by Programas de Actividades I+D en la Comunidad de Madrid and cofunded by Structural Funds of the EU. Dr. Héctor Montes also acknowledges support from Universidad Tecnológica de Panamá.

References

Bares, J.E. & Whittaker, D. S. 1993. Configuration of autonomous walkers for extreme terrain. The International Journal of Robotics Research,12(6), pp. 535-559.

Bekey, G. 2005. Autonomous Robots: From Biological Inspiration to Implementation and Control. MIT Press, Cambridge, Massachusetts.

Boston Dynamics. 2010. Boston Dynamics Wins DARPA Contract to Develop Legged Squad Support System (LS3). Report. Retrieved from http://www.cs.cmu.edu/~cga/humanoids-ugrad-10/bdi.pdf

Gonzalez de Santos, P., Armada, M.A., Jimenez, M.A. 2000. Ship building with ROWER, IEEE Robotics and Automation Magazine, 7(4), pp. 35-43.

Gonzalez de Santos, P., García, E. and Estremera, J. 2006. Quadrupedal Locomotion, An Introduction to the Control of Four -legged Robots, Springer, London.

Grieco, J.C. 1997. Robots Escaladores. Condiciones de Diseño, estabilidad y Estrategias de Control. Tesis doctoral, Universidad de Valladolid.

Heverly, M., Matthews, J., Frost, M., Quin, C. 2010. Development of the Tri-ATHLETE Lunar Vehicle Prototype. In Proc. 40th Aerospace Mechanisms Symposium, NASA Kennedy Space Center, pp. 1-10.

Hutter, M., Gehring, C., Bloesch, M., Hoepflinger, M., Remy, C. D., and Siegwart, R. 2012. StarlETH: A compliant quadrupedal robot for fast, efficient, and versatile locomotion. Adaptive Mobile Robotics: pp. 483-490.

Kolter, J.Z. & Ng, A.Y. 2011. The Stanford LittleDog: A learning and rapid replanning approach to quadruped locomotion. The International Journal of Robotics Research, 30(2), pp. 150-174.

Mena, L., Montes, H., Fernandez, R., Sarria, J., and Armada, M. 2015. Reconfiguration of a climbing robot in an all-terrain hexapod robot. ROBOT2015: Second Iberian Robotics Conference. Advances in Intelligent Systems and Computing Series, Vol. 418, pp. 197-208.

Montes, H., Nabulsi, S., Armada, M., and Sanchez, V. 2004. Design and Raibert, M. 1986. Legged robots that balance. The MIT Press, Cambridge, Massachusetts.

Montes, H. 2005. Análisis, diseño y evaluación de estrategias de control de fuerza en robots caminantes, Tesis doctoral, Universidad Complutense de Madrid.

Montes, H., Mena, L., Fernández, R., Sarria, J., González de Santos, P., Armada, M. 2015a. Hexapod Robot for Humanitarian Demining. In: Proc. RISE 2015, 8th IARP Workshop on Robotics for Risky Environments.

Montes, H., Mena, L., Fernandez, R., Sarria, J., and Armada, M. 2015b. Inspection platform for applications in humanitarian demining. CLAWAR 2015, Assistive Robotics, pp. 446-453.

Montes, H., and Armada, M. 2016. Force Control Strategies in Hydraulically Actuated Legged Robots. Intl J. Advanced Robotic System, 13(50). Retrieved from: http://www.intechopen.com/download/pdf/50046

Raibert, M., Blankespoor, K., Nelson, G., Playter, R., and BigDog Team. 2008. BigDog, the Rough-Terrain Quaduped Robot. Proc. 17th World Congress The Int. Federation of Automatic Control, Seul, Korea, pp. 10822-10825.

Waldron, K. J. and McGhee, R. B. 1986. The adaptive suspension vehicle. IEEE Control Systems Magazine, pp. 7-12.

CHAPTER 36

A TOPOLOGICAL NAVIGATION SYSTEM BASED ON MULTIPLE EVENTS FOR USUAL HUMAN ENVIRONMENTS

C. GOMEZ[1], A. C. HERNANDEZ[2], J. CRESPO[3] and R. BARBER[4]

RoboticsLab, Universidad Carlos III de Madrid, [1]claragobla@gmail.com, [2]alejandracarolina.hernandez@alumnos.uc3m.es, [3]jocrespo@ing.uc3m.es, [4]rbarber@ing.uc3m.es

This work aim is to develop a navigation system that allows a mobile robot to move autonomously in an environment using perceptions of multiple events. The topological navigation system is based on events that imitate humans' sensorial navigation, guiding the robot to its goal. Its design enhances the addition of new elements due to its modularity and decoupling. The innovation of this work resides in the use of an interface to integrate multiple events, leading to a more advanced navigation system. Finally, experiments have been carried out in mobile robots, their results show the feasibility and the practical validation of the navigation system proposed.

1 Introduction

Navigation has been a main field of study in mobile robotics since its beginning. In case of humans, navigation is determined by physiological needs and several abstraction levels (Gonzalez, 2008). This work is focus on providing a robot with navigation capabilities similar to humans' ones.

In this work, navigation is studied from the topological viewpoint (Thrun, 1998), based on reference elements and translations amidst them. The topological approach can be based on natural landmarks (Madhavan, 2004), detecting objects of an environment; or artificial landmarks (Jang, 2005), adding modifications to the environment. It can be classified also regarding its representation, whether it is based on geometric representations (Konolige, 2011) or on movements (Marinakis, 2010).

The main objective of this work is to develop the capabilities required in order to navigate autonomously through an indoor environment using mainly topological representations combining natural and artificial landmarks. This work is focused on topological navigation but it settles a first step towards semantic, topological and geometrical navigation integration.

2 Topological navigation model

This model is categorized as a topological representation based on movements. Nodes are associated with elements of the environment and arches with translations between them.

The system is formed by different modules: a perception interface, an event manager, a planner and a navigator. As shown in the distribution of the modules, Fig. 1, the perception interface is decoupled It receives different perceptions, but its output is generic in order to enhance the robustness and versatility of the system.

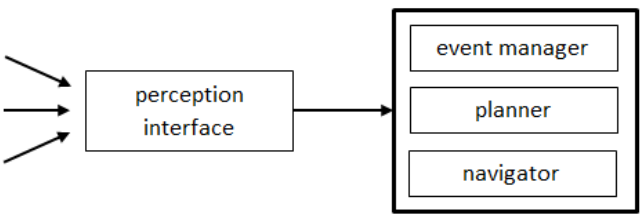

Fig. 1. Topological system model.

The perception interface is in charge of receiving the sensorial data from extereoceptive events and translating it into a general structure. The planner determines the path to get to the target using a topological map built at the beginning of each planning stage. The navigator performs the required behavior for each arc until the target is reached. This navigator is complemented with an obstacle avoidance algorithm to guarantee safe navigation.

2.1 Topological software scheme

The topological diagram, shown in Fig. 2, includes the topological navigation modules, the sensorial event modules (as *ARToolKit*) and the basic motor and camera configuration modules.

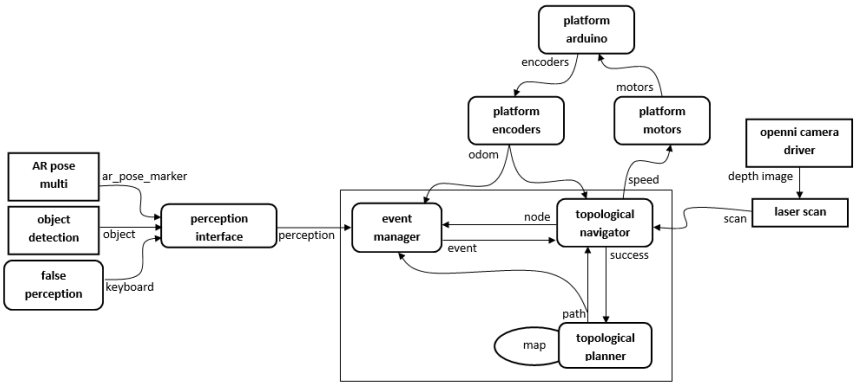

Fig. 2. Topological modules diagram.

2.2 Topological planner

As topological representations are based on graphs, a graph path-planning algorithm has to be used: a Dijkstra algorithm (Skiena, 1990) is chosen. Dijkstra algorithm is designed to obtain the shortest path between nodes in a graph. Given an initial node it evaluates adjacent nodes, prioritizing the ones with shorter distance, and iterates until the goal node is reached or every connection between nodes has been explored. The path-planning algorithm implemented is a modified Dijkstra, in which the cost of a translation can be varied, using it as feedback of previous executions or as a personality factor (Egido, 2004). The path obtained is a succession of nodes that is sent to the navigator, which will execute the trajectory.

The topological graph is given to the planner as an a priori text file, shown in Fig. 3. The graph representation used is oriented, meaning that the path is unidirectional: to go from A to B is different than going from B to A. In the topological map, nodes are associated to their event type (i.e. odometry) and arches are associated to their ability (i.e. GP, go to point).

```
0{0 1}GP|odometry<0 1>
1{1 2}R|marker 0<3.14>
2{2 3}R|marker 1<1.57>
3{1 4}R|marker 2<1.57>
4{3 4}R|marker 2<2.36>
5{4 0}GP|odometry<0 0>
```

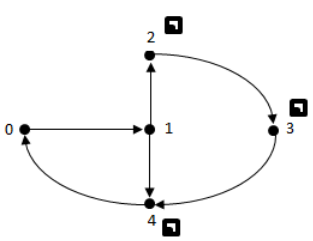

Fig. 3. Map structure and graphic representation.

2.3 Topological navigator

The navigation system is in charge of performing the path and reaching the goal analyzing events and abilities. Abilities are orders the robot has to execute to reach coming nodes, it is intrinsically related to motor control. Events are signs indicating the robot has reached a node, through sensorial perception. This system is formed by several abilities and events. The abilities implemented are Go to point, Turn, Contour follow and Go to object.

Once the navigator receives the path, it gets the ability of the first transition and executes it until the event corresponding to the second node is received. It iterates this functionality until the event corresponding to the last node of the path is received. Navigation is assisted by an obstacle avoidance module in order to guarantee safe navigation.

2.4 Perception interface

Extereoceptive events are managed through the Perception Interface. It is decoupled from the system and it manages events and translates them into a predefined structure. The extereoceptive modules integrated are:

- Perception of artificial landmarks, sourced by *ArToolKit*. Artificial landmark vision is related to markers added to the environment in order to enhance navigation.
- Object detection module, in charge of natural landmarks perception. Natural vision is related to the detection of objects and elements that are naturally in a room. This module uses computer vision techniques in order to classify several objects commonly found in a room.
- Simulated perception, a module design to generate external perceptions allowing the user to interact with the robot.

2.5 Event manager

The Event Manager module centralizes every process involving event communication between modules. This module receives information from the perception received by the Perception Interface, odometry coming from the encoders, the path to follow and the next node to reach, with this information it manages the concurrent communication and execution of the whole system. The module publishes the required information about the events received and determines when an event has been reached. Desired for the event, the robot will move towards it.

3 Experimental results

These experiments present the topological navigation and planning results in several indoor environments. The experiments were developed using two robots: a developed robotic platform (Gomez, 2015) and Turtlebot 2 platform.

3.1 Topological planification results

Regarding planning results, the planner used is a modified and self-designed Dijkstra whose aim, as in every Dijkstra algorithm, is to find the shortest path from the initial to the goal node, introduced by the user. The map representation used in this experiment is shown in Fig. 4.

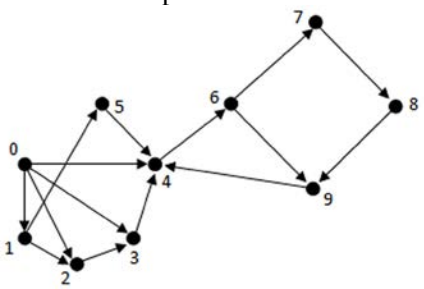

Fig. 4. Topological map used in planification experiments.

Several experiments have been developed related to planification according to the different possible situations: a simple path, a simple path with modified cost, an unsuccessful path and a replanified path. Their results are shown in Fig. 5.

Start: 0 Goal: 9 Sol: 0 4 6 9	Start: 0 Goal: 9 Sol: 0 3 4 6 9	Start: 5 Goal: 3 No solution	Start: 0 Goal: 4 Sol: 0 4 Replanification Sol: 0 3 4
(1)	(2)	(3)	(4)

Fig. 5. Results for different planification situations.

In Fig. 5 (1), the robot is asked to plan a trajectory from Node 0 to Node 9, as observable in the topological map the shortest path is 0-4-6-9. In Fig.

5 (2), the robot is asked to plan the same trajectory but the translation cost from Node 0 to Node 4 is incremented, it could be justified by any difficulty to reach the node. As a result, the planner avoids that translation changing the solution to 0-3-4-6-9. In Fig. 5 (3), the system is commanded to perform a translation that is not defined in the map, so no solution is found. Finally, in Fig. 5 (4), the robot is asked to plan the path to move from Node 0 to Node 4. Originally, this path is 0-4 but during the execution a problem occurred and replanification was needed, obtaining the solution 0-3-4.

Based on the results obtained it is possible to conclude that the system is able to plan and replan trajectories successfully in different situations.

3.2 Topological navigation experiment with object detection

This experiment involves the real-time functioning of the object detection module allowing the recognition of common objects. The navigation system receives the data of the detected object, if this information corresponds to the desired for the event, the robot will move towards it.

The robot performs the path shown in Fig. 6. In this case, the robot is asked to move using the ability Turn. The first event to reach is a Chair, whenever the robot detects the Chair it will move towards it using the ability Go to object. The second (and last) event to reach is a Closet, the same process will take place and when reached the robot will stop.

Fig. 6. Scenario and path for object detection experiment.

The result for this experiment is shown in Fig. 7 as a succession of the positions of the robot performing the path and the recognition of objects. Based on the proposed path, the observation of the images obtained during the execution and the captures obtained from the robot vision when the objects were detected, it is possible to conclude that the experiment was developed successfully.

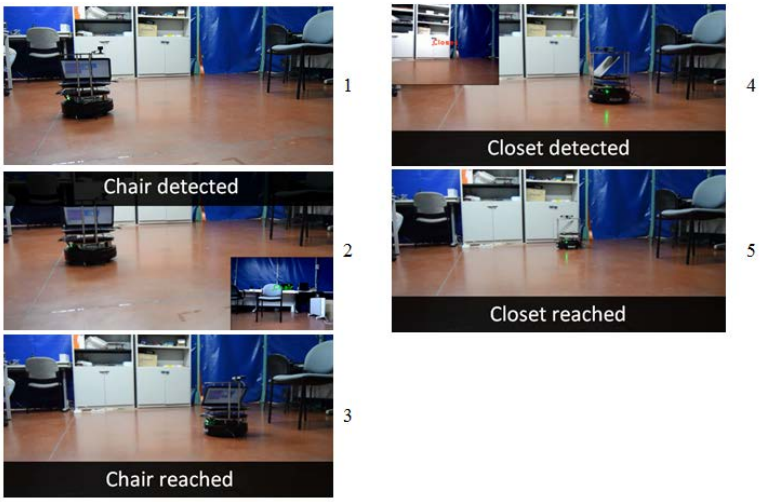

Fig. 7. Result for navigation with object detection experiment.

4 Conclusions and future works

The main objective of this work was to develop a mobile robot and to provide it with the capabilities required in order to navigate autonomously using mainly topological representations and developing behaviors similar to the ones of humans. Based on the results, it is successfully achieved:

- The developed topological software is able to plan successful trajectories over a given map and navigate through the environment following the path planned and reaching the proposed goal.
- It is able to avoid obstacles and plan a new path in case of failure.
- The system is multidisciplinary regarding the inputs admitted and the outputs offered: it is able to work with different types of perception and it performs different behaviors to reach the goal.
- The modular and detached design of the system enhances its versatility and facilitates the implementation of new functionalities.

Although the main objectives were achieved satisfactorily, there are still improvements to be done in the system. The future works are improving the motor skills of the robot enabling more natural movements; widening its perception capabilities by implementing more input methods; and including a topological explorer. The purpose of this work was to set the first steps towards robot navigation integration between the main three levels so the future lines are going to pursue the development of new navigation strategies that involve topological and semantic navigation levels.

Acknowledgements

The research leading to these results has received funding from the RoboCity2030-III-CM project (Robótica aplicada a la mejora de la calidad de vida de los ciudadanos. fase III; S2013/MIT-2748), funded by Programas de Actividades I+D en la Comunidad de Madrid and cofunded by Structural Funds of the EU.

References

Gonzalez, M. C., Hidalgo, C. A., and Barabasi, A. L. 2008. Understanding individual human mobility patterns. Nature, 453(7196), 779-782.

Thrun, S. 1998. Learning metric-topological maps for indoor mobile robot navigation. Vol. 99, p. 21-71. Elsevier, Netherlands.

Madhavan, R. and Durrant-Whyte H. F. 2004. Natural landmark-based autonomous vehicle navigation. Robotics and Autonomous Systems, 46(2), 79-95.

Jang, G., Kim, S., Kim, J. and Kweon, I. 2005. Metric localization using a single artificial landmark for indoor mobile robots. IROS, (pp. 2857-2862).

Konolige, K., Marder-Eppstein, E., and Marthi, B. 2011. Navigation of Hybrid Metric-Topological Maps. ICRA.

Marinakis, D. and Dudek, G. 2010. Pure topological mapping in mobile robotics. IEEE Trans. Robot., vol. 26 , no. 6 , pp.1051 -1064.

Skiena, S. 1990. Dijkstra's Algorithm. Implementing Discrete Mathematics. Addison-Wesley, 225-227.

Egido, V., Barber, R., Boada, M. J. L. and Salichs, M. A. 2004. A planner for topological navigation based on previous experiences. Parameters, 2, 3.

Gomez, C., Hernandez, A.C., Crespo, J. and Barber, R. 2015. A Ros-based middle-cost robotic platform with high-performance. Int. Conf. of Education, Research and Innovation (ICERI).

CHAPTER 37

UGV NAVIGATION IN ROS USING LIDAR 3D

A. LÁZARO[1], R. BAREA[2], L.M. BERGASA[3] and E. LOPEZ[4]

[1]Robesafe group, Universidad de Alcalá, [2]Robesafe group, Universidad de Alcalá, [3]Robesafe group, Universidad de Alcalá, [4]Robesafe group, Universidad de Alcalá, alberto2991lazaro@gmail.com.

This paper addresses to give a step more forward the achievement of robust Unmanned Ground Vehicles (UGVs), which can drive in urban environments. More specifically, it focuses in the management of a four wheeled vehicle in ROS using mainly the inputs provided by a LIDAR 3D. Simulations are carried out in ad-hoc scenarios designed and run using GAZEBO. The vehicle and the LIDAR sensor physical models have been added to the simulation environment in order to get a higher degree of reality. Navigation tests will be provided in the final version.

1 Introduction

Unmanned Ground Vehicles (UGVs) are becoming more and more used every single day. They can carry out lots of different tasks with no human supervision, achieving lower costs or working in areas where it would be dangerous for humans to work in. Those are the reasons why they are commonly used in industrial environments.

Industrial applications have a particularity, which makes easier the management of these vehicles, the environment is controlled. According to the guided systems the unmanned vehicles use, they can be classified as shown in Fig. 1.

In other applications where the environment is uncontrolled the sensors and manage systems should be more complex to ensure success in the vehicle autonomous management. This is our approach, because our goal is the UGV navigation in urban scenarios.

In this work, an UGV is managed through ROS using a LIDAR 3D sensor. This management is carried out in GAZEBO, a simulator where the needed models have been built.

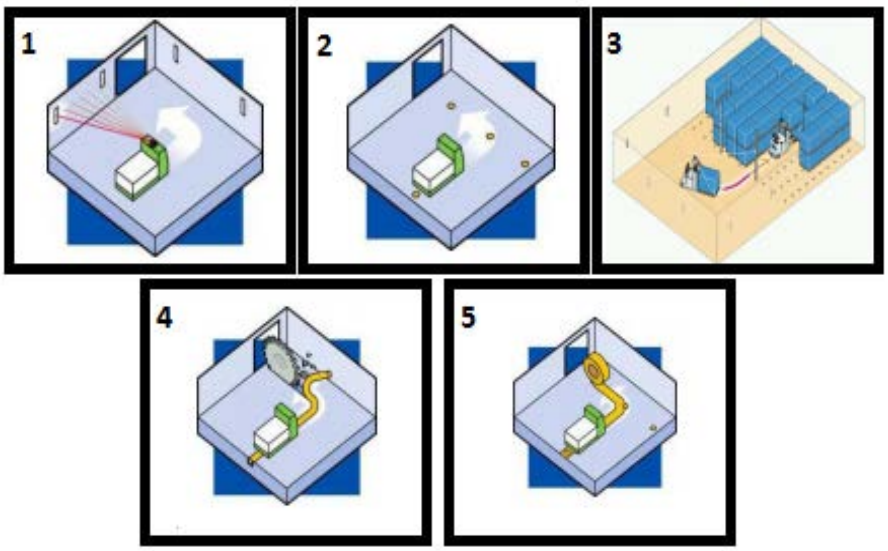

Fig. 1: (1) Laser UGV (2) Magnetic UGV (3) Dual UGV (4) Rail guided UGV (5) Optical band UGV.

The reason why GAZEBO world has been build is to create a virtual reconstruction of real scenarios, where testing the perception and vehicle management systems. Virtual simulations are usually used in the first implementation steps of autonomous vehicles. It allows us to test the developed systems as many times as needed in a safety way with reduced costs.

The sensor used to be mounted in the vehicle is the VLP-16 (Velodyne Lidar Puck). It creates a 360º 3D images using 16 laser/detector pairs mounted in a compact housing. The housing rapidly spins to scan the surrounding environment. The lasers fire thousands of times per second, providing a rich, 3D point cloud in real time.

VLP-16 includes the following characteristics:

- Horizontal Field of View (FOV) of 360°
- Rotational speed of 5-20 rotations per second (adjustable)
- Vertical Field of View (FOV) of 30°
- Returns of up to 100 meters (useful range depends on application)

2 State of the art

Nowadays, an interesting research line is the development of unmanned robotic systems. This target has multiple different purposes such as goods transportation, people transportation, etc.

These robots can be classified in 3 different categories: UGVs (Unmanned Ground Vehicles) (Lane, 1991), UAVs (Unmanned Aerial Vehicles) (Faessler, 2015) and UUVs (Unmanned Underwater Vehicles) (Eren, 2016).

Perception systems make possible unmanned vehicles. They let the vehicle know how the environment around it is and if there is any object around them. These perception systems can consist on several sensors such as cameras (Ahmed, 2007) or laser (Liu, 2015).

There are different types of 2D and 3D laser sensors. Comparison shows the advantages that 3D laser sensors provide (Nieuwenhuisen, 2015).

Navigation systems are also necessary to complete the intelligence of Unmanned Vehicles. Their target is to plan trajectories avoiding obstacles or hurdles found in the vehicle´s way (Aeschimann, 2105) (Quigley, 2009).

In this work several platforms has been used to develop the system which manages the autonomous vehicle such as ROS (Quigley, 2009 and GAZEBO (Roberts, 2003).

Different works can be found where these platforms have been used for similar purposes such as (Gupta, 2015) but there is no work that joins the power or both platforms with LIDAR 3D sensors, GPS, cameras and IMUs.

3 Work description

The steps which have been tackled to get the final goal are the following ones:

- Build a proper GAZEBO world to run the simulations.
- Build the UGV model with the sensor attached to it to make them move in solidarity.
- Prepare a ROS node which depicts the information obtained through RVIZ.
- Develop a management system which drives the car using the available information.

A general scheme of our system architecture is shown in Fig. 2.

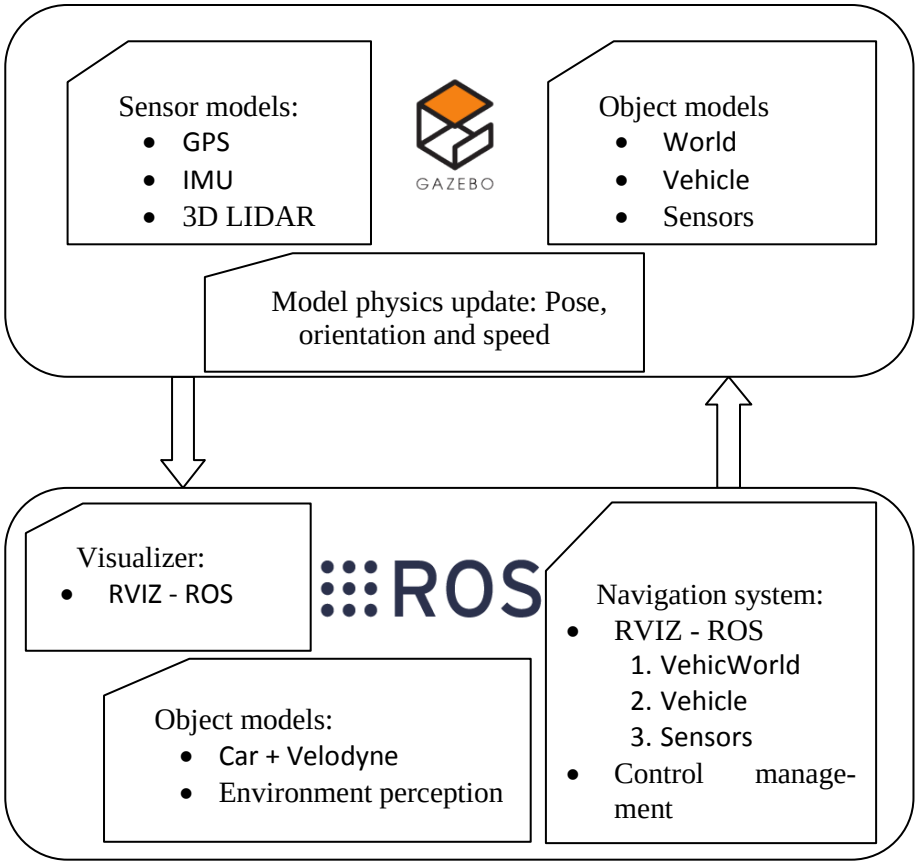

Fig. 2: Proposed system architecture.

3.1 Simulation world

The world is the environment where the UGV will be managed. To build it a grass plane has been used as base of the world. Different models from the DRCSim GAZEBO version have been added to the base. The models used are the ones which are shown hereafter:

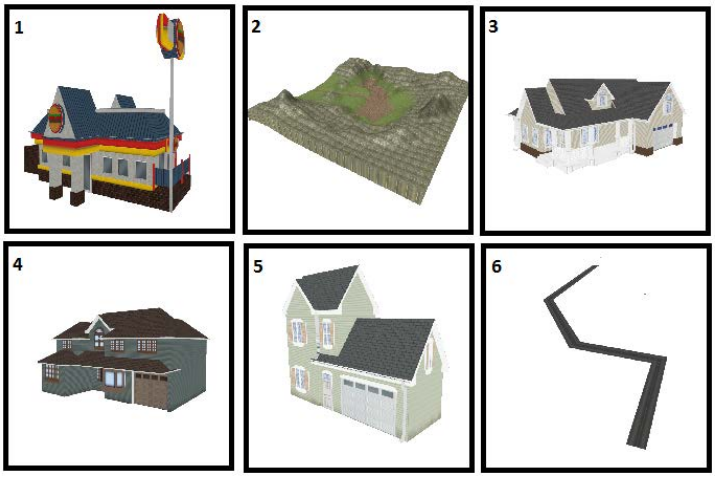

Fig. 3: (1) Fast food restaurant (2) Mountains landscape (3) House 1 (4) House 2 (5) House 3 (6) Road.

Furthermore, curbs have been added along both sides of the road. These curbs have been added in ten sections, one on the right, another one on the left of each section and two more at the start and at the end. The length of these curbs depends on the length of each section. Fig. 4 shows a picture of our simulation world.

Fig. 4: Simulation world.

3.2 UGV model

The Vehicle used is the DRC Vehicle, which can be found in the DRCSim GAZEBO version. Its model has been modified to add to it the VLP-16 (Velodyne Lidar Puck). After adding the model different constraints have been defined to make the VLP-16 move in solidarity with the Vehicle.

Fig. 5. (1) DRC Vehicle. (2) DRC Vehicle + VLP-16.

3.3 RVIZ sensors representation.

In Fig. 6 the real world simulation and the VLP-16 are depicted. Here it can be seen that the useful range is quite big while obtaining high precision.

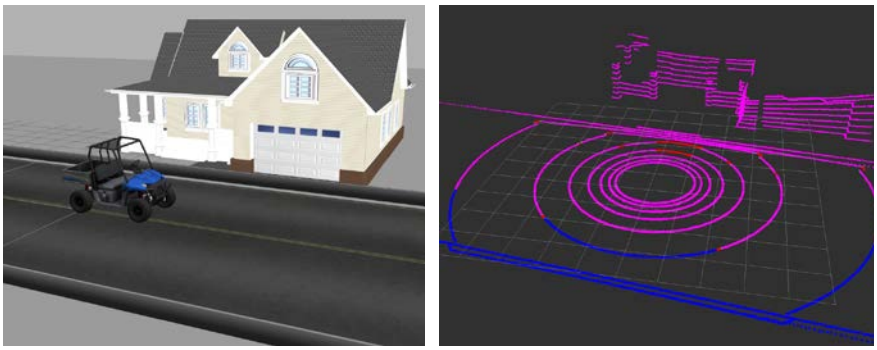

Fig. 6. (1) Real world simulation. (2) VLP-16 detection depicted RVIZ.

3.4 Navigation system.

A ROS node has been implemented to manage the UGV. It receives information of the environment provided by the sensors and information that shows the state of the DRC Vehicle such as position and speed.

All this information is processed and used to act in the control systems of the UGV managing the hand wheel, the gas pedal, the brake pedal, etc. Control architecture will be included in the trial version of the paper.

4 Experimental results

Experimental results consist on navigation text on the designed world in an autonomous way avoiding static and moving obstacles. We are working on it and they will be included in the final version.

5 Conclusions

The work presented in this paper addresses to achieve the management of an UGV in an urban scenes using ROS. It provides as novelty the jointly use of ROS, GAZEBO and a Velodyne sensor. Currently we are working in the control system, which is the reason why control architecture, experimental results and conclusions will be completed in the final version of the paper.

Acknowledgements

This work was supported in part by the MINECO SmartElderlyCar (TRA2015-70501-C2-1-R) project and by the RoboCity2030 III-CM project (S2013/MIT-2748) funded by Programas de I+D en la Comunidad de Madrid and cofunded by Structured Funds of the UE.

References

Gupta, N. Vijay R. Korupolu P.V.N. Bansal J. and Kapuria A. (2015). Architecture of autonomous vehicle simulation and control framework.. AIR.

Lane G. R. Lescoe P. Cooper S. 1991. Unmanned Ground Vehicle control technology. Telesystems Conference, 1991. Proceedings. Vol.1., NTC '91., National.

Aeschimann R. and Borges P. V. K. 2015. Ground or obstacles? Detecting clear paths in vehicle navigation. 2015 IEEE International Conference on Robotics and Automation (ICRA).

Ahmed J. Shah M. Miller A. Harper D. and Jafri M.N. 2007. A Vision-Based System for a UGV to Handle a Road Intersection", AAAI Twenty-Second Conference on Artificial Intelligence.

Nieuwenhuisen M. Droeschel D. Beul M. and Behnke S. 2014. Obstacle detection and navigation planning for autonomous micro aerial vehicles. Unmanned Aircraft Systems (ICUAS), 2014 International Conference on.

Quigley, M. Conley, K. Gerkey B.P. Faust J. Foote T. Leibs J. Wheeler R. and Ng A.Y. 2009. ROS: an open-source Robot Operating System. In ICRA Workshop on Open Source Software .

Eren F. Pe'eri S. Rzhanov Y. Thein W. M. and Celeikkol B. 2016. Optical Detector Array Design for Navigational Feedback Between Unmanned Underwater Vehicles (UUVs). IEEE Journal of Oceanic Engineering.

Faessler, M., Fontana, F., Forster, C., Mueggler, E., Pizzoli, M. and Scaramuzza, D. 2015, Autonomous, Vision-based Flight and Live Dense 3D Mapping with a Quadrotor Micro Aerial Vehicle. J. Field Robotics. doi: 10.1002/rob.21581

Liu S. Atia M.M. Karamat T.B. and Noureldin A. 2015. A LiDAR-Aided Indoor Navigation System for UGVs. Journal of Navigation.

Roberts D. Wolff R. Otto O. and Steed A. 2003. Constructing a Gazebo: Supporting Teamwork in a Tightly Coupled, Distributed Task in Virtual Reality. Presence.

CHAPTER 38

PEDESTRIAN MOTION PREDICTION: A GRAPH BASED APPROACH

D. GARZÓN-RAMOS, M. GARZON and A. BARRIENTOS

Centro de Automática y Robótica UPM-CSIC, Calle José Gutiérrez Abascal, 2. 28006 Madrid, Spain, dgarzon@etsii.upm.es

A novel pedestrian motion prediction technique is presented in this paper. Its main achievement regards to none previous observation, any knowledge of pedestrian trajectories nor the existence of possible destinations is required; hence making it useful for autonomous surveillance applications. Prediction only requires initial position of the pedestrian and a 2D representation of the scenario as occupancy grid. First, it uses the Fast Marching Method (FMM) to calculate the pedestrian arrival time for each position in the map and then, the likelihood that the pedestrian reaches those positions is estimated. The technique has been tested with synthetic and real scenarios. In all cases, accurate probability maps as well as their representative graphs were obtained with low computational cost.

1 Introduction

Nowadays, the need of improving the surveillance and security systems in critical infrastructures has led to develop novel strategies that minimize security weaknesses and provide solutions for responding efficiently and on-time to potential threats. In this sense, human motion prediction arises as a powerful tool to enhance the detection capabilities and reaction in possible presence or approximation of intruders to restricted or vulnerable locations. For these reasons, in this paper a novel approach for pedestrian motion prediction that can be used in any given scenario with the minimum requirements of situational information is presented.

Most of previous work on pedestrian motion prediction has been focused on identifying motion patterns from previous observations, and then,

those patterns are used to predict future trajectories or goals (Kitani et al., 2012). Nevertheless, that is not an option in security applications where it is needed to model behaviors that differ from the common situations. Other approach employs the sub-goal concept to model and predict the pedestrian behavior (Ikeda et al., 2013). In this case, the scenario is discretized in a set of sub-goals that can be reached by the pedestrian. Unfortunately, the sub-goals are also obtained from the analysis of large set of pedestrian trajectories. Regarding to the sub-goal approach, previous work was developed in order to obtain a topological representation of an unknown environment (Ramaithitima et al., 2016). Although, it is not necessary the previous knowledge to build the map, it discards a lot of information due to its reduced representation of the scenario as a single path. In this sense, the construction of a topological map could be employed to define the sub-goals and subsequently these sub-goals might be used to calculate a probability distribution and to predict the displacement of the pedestrian in the scenario.

The main novelty of this work is that it does not require any previous observation of pedestrian trajectories nor possible goals to estimate the likelihood that the pedestrian reaches any location in the map, including in long-term predictions. Also, due to the technique only needs the map of the scenario and the pedestrian position as inputs, it can be easily implemented in large infrastructures with different kind of security resources.

The rest of the paper is organized as follows: the methodology overview and the main process involved in the technique are presented in Section 2. The experiments and results of the methodology implementation are discussed in Section 3. Then, the conclusions of the work are provided in Section 4.

2 Methodology

The process starts when a new 2D representation of the scenario is received, the input for the algorithm can be defined as two-dimensional occupancy grid pictures as well as maps designed or acquired in the standard ROS (Robot Operating System) format. Then, the map is transformed into a representative cost-map that allows improving the efficiency of the other algorithms at the same time that it includes information about predefined behaviors of the pedestrians. The next step is performed by the Fast Marching Method and it includes the cost-map and the pedestrian position in order to obtain the arrival time of the pedestrian at each point in the map.

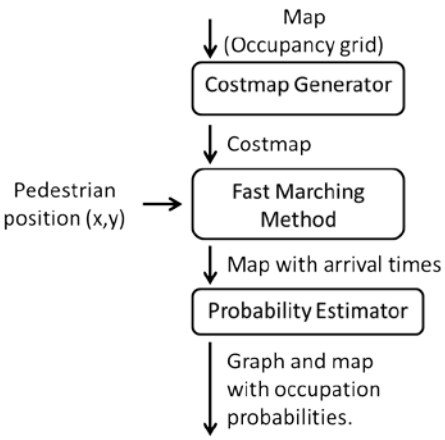

Fig. 1. Methodology overview.

Later, the map with the arrival times is used to generate an arrival time graph that corresponds to possible trajectories that can be followed by the pedestrian when he stands in the initial position. Finally, the graph is employed to calculate the probability distribution for the nodes and that distribution is translated into a new probability map. The methodology overview is shown in Fig. 1.

2.1 Cost-map generation

The cost-map is a modified representation of the original map that includes two main changes: scaling and distance transformation. The scale change refers to the increasing or decreasing the map resolution. In the proposed technique is desirable to reduce the number of pixels because the FMM and the probability estimator acts over the whole map and high resolutions could lead to a slow response in the algorithms. The scaling process is done by using a bilinear interpolation technique that ensures that the position in the resulting map have a correct translation to the original one.

From there, an increasing cost variation is added around the obstacles. This distance transformation allows modeling the behavior of pedestrians that move avoiding obstacles at the same time that stay away from the walls. In Fig. 2 is shown the cost-map representation of a hallway. In this case the original map was scaled from *0.05* to *0.35 m per pixel* and the distance transformation can be observed as a gray scale gradient near the walls.

2.2 Fast Marching Method

The required input for the FMM is a velocity map, so the cost-map obtained previously is transformed in a velocity map where the velocity achieved by the pedestrian at each position is directly proportional to the cost value in the same place. In order to simplify the case of study, it is assumed that the pedestrian will move continuously with a constant velocity over the unobstructed areas and he only will decrease the velocity when is close to the walls or obstacles.

Afterwards, the FMM (Sethian, 1999) is used to compute the amount of time that the pedestrian needs to reach each position in the map, and then, that information is employed to generate a new map that includes the arrival times. In Fig. 2 is shown the arrival time map obtained with the FMM when a pedestrian is located in the center of the hallway. In the image, blue pixels indicate near positions, red pixels refer to far places and yellow pixels are unreachable locations.

2.3 Probability estimation

The probability estimation algorithm is developed in two main steps: arrival time graph generation and probability distribution estimator. First, the values in the arrival time map are discretized. The set of discrete time values $T = \{t_1, t_2, t_3, \ldots, t_n\}$ is obtained by defining a constant time step from the pedestrian position to the farthest place in the map. So, the arrival time map is modified again by rounding its values to the larger nearest discrete value. This transformation allows clustering time connected positions; where the size of the cluster is directly proportional to the time step.

Next, a connected component labeling is performed in order to define a space-time differenced set of areas $A = \{a_1, a_2, a_3, \ldots, a_m\}$. This segmentation is realized with the aim of getting into the time clusters and dividing areas that can be reached in the same time (t_n) but they are not spatially connected (e.g. In a hallway, two opposite exits (a_1,a_2) could be reached in the same time (t_n), but they are not directly connected in the map) . After that, the arrival time graph is generated using the elements of A as nodes and the spatial connections between them as edges.

The discretized arrival time map and the corresponding arrival time graph are shown in Fig. 2. In this case, it was used a set of discrete time values composed by 10 elements: $T = \{t_1, t_2, t_3, \ldots, t_{10}\}$ that can be observed as opening circles that start in the pedestrian position (t_1) and end in the farthest points . Nevertheless, it was obtained a set of areas with 18 elements: $A = \{a_1, a_2, a_3, \ldots, a_{18}\}$, which means that some elements in A be-

long to the same cluster in T (e.g. The elements (a_6,a_8) belongs to the same cluster (t_5)).

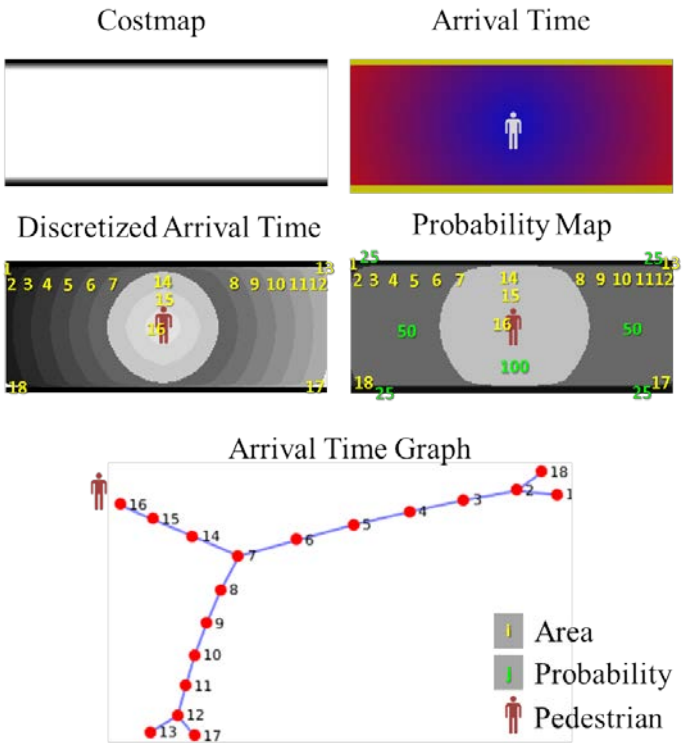

Fig. 2. Pedestrian motion prediction technique.

Table 1. Data from **Probability Map** and **Arrival Time Graph** in Fig. 2 .

Area	1	2	3	4	5	6	7	8	9
Prob. [%]	25	50	50	50	50	50	100	50	50

Area	10	11	12	13	14	15	16	17	18
Prob. [%]	50	50	50	25	100	100	100	25	25

Thereby, the probability estimation is easily achieved regarding the graph obtained above. The area that encloses the pedestrian position has *100%* of probability of being reached by the pedestrian. It is a normal assumption due to the closeness of the pedestrian to the positions included in this area. After that, if the parent node has only one child the probability is entirely passed to the next node, on the other hand, if the parent node has more than one child the probability is split and it is passed in equal parts to each child. In this point, a filtering process is performed in order to avoid

the probability assignment for small areas. If the area (a_n) does not have the number of pixels over an arbitrary threshold, the area receives the same probability as its parent and it is not taken into account as a child for probability division. This distribution is iteratively done until all nodes in the graph are filled. The final probability assigned to each node is the sum of the probability given by its parents. (i. e. A node can have more than one parent). Finally, a new probability map is built using the information obtained in the last step. This map represents the likelihood that the pedestrian reaches any position in the scenario.

In Fig. 2 is shown the probability map. The probability values for each area are shown in the Table 1. In the picture, the pedestrian is located in the area (a_{16}), so this area has the *100%* of probability. Then, the areas (a_{15}, a_{14}, a_7) do not have siblings, so they receive the entire probability from their parents. The area (a_7) has two children (a_8, a_6), and the probability is split in equal parts and each of them receives the *50%*. Same situation can be observed in the areas (a_2, a_{12}).

3 Experiments and Results

The Simulated Map 1 is a room with a small free space in the middle, but with none entrance to go inside. From the start point, the pedestrian can achieve the other side of the room by two different trajectories, which means dividing the probability in two separate paths with *50%* each. Nevertheless, when the trajectories are joined in the other side, the probability fuses again and that area gets *100%*. In addition, it can be observed that the unconnected room in the middle is not taken into account in the prediction; due it cannot be reached by the pedestrian.

The Simulated Map 2 has the same scenario, but in this case the small space has two different entrances that can be reached by the pedestrian at different times. Thus, the new connections generated by the room entrances can be observed in the graph. First, the probability is completely passed from the area surrounding the pedestrian to its child. Then, there are three possible paths: up, center and down, so the probability is divided by three and each child receives a *33.3%*. Then, the center and down path are joined in the middle room, and the probability reaches the *66.6%*. Like in the previous experiment, the area in the other side of the room gets the *100%* as the sum of *33.3%* and *66.6%* provided by its parents.

The last experiment is the prediction technique applied in a real scenario. The map was built with a LIDAR sensor mounted over an Unnamed Ground Vehicle (UGV) and it is a 2D reconstruction of a street intersec-

tion. The graph and the probability map shows how the proposed technique can operate in non-trivial scenarios and it can make long-term predictions. The experiments and resulting maps and graphs can be observed in Fig. 3.

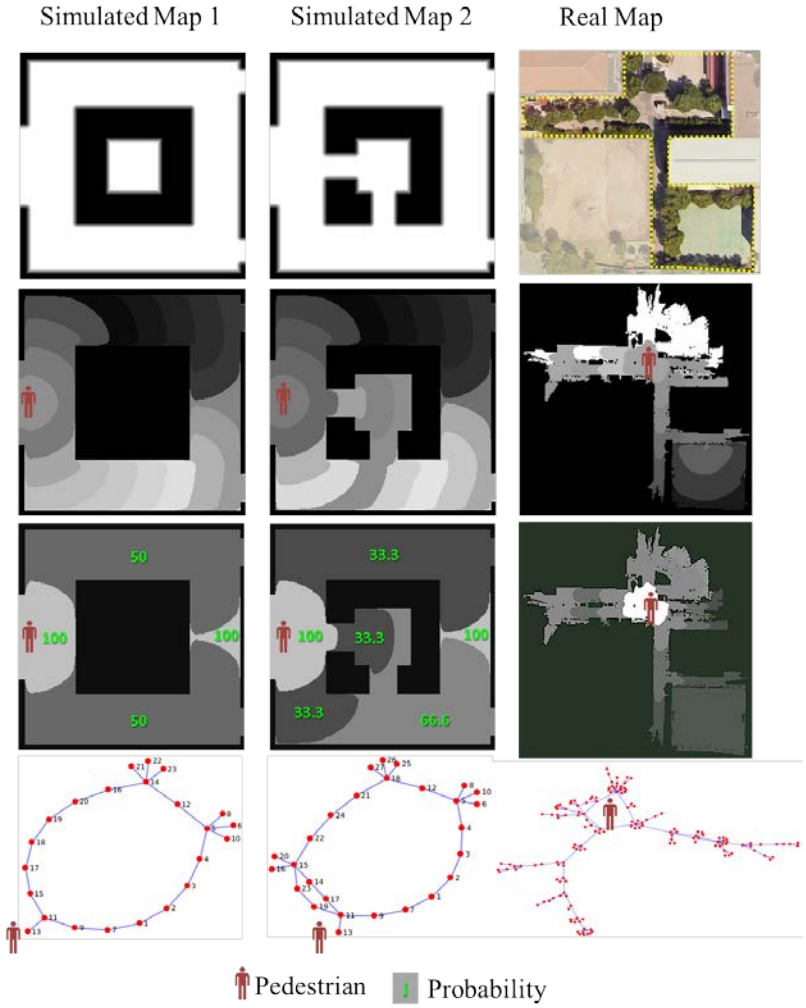

Fig. 3. Pedestrian motion prediction in simulated and real Scenarios.

4 Conclusions

An approach for pedestrian motion prediction was presented. The experiments and results show that it is possible getting probability estimations

about the likelihood that the pedestrian reaches any position in the scenario, only using the pedestrian position and the map as inputs.

The proposed technique do not uses specific paths or possible destinations, so the calculations are made for the whole map. In this sense, an adequate cost-map generation is necessary in order to improve the performance of the FMM algorithm and the probability estimation.

A long-term prediction was acquired for large scenarios. Future works will be aimed to do an on-line implementation of the technique with a pedestrian in continuous motion as well as the integration of new information sources in order to get a better prediction in dynamic environments.

Acknowledgements

This work was supported by the Robotics and Cybernetics Group at Universidad Politécnica de Madrid (Spain), and funded under the projects: PRIC (Protección Robotizada de Infraestructuras Críticas; DPI2014-56985-R), sponsored by Spanish Ministry of Economy and Competitiveness and RoboCity2030-III-CM project (Robótica aplicada a la mejora de la calidad de vida de los ciudadanos. fase III; S2013/MIT-2748), funded by Programas de Actividades I+D en la Comunidad de Madrid and cofunded by Structural Funds of the EU.

References

K. M. Kitani, B. D. Ziebart, J. A. Bagnell and M. Hebert. 2012. Activity Forecasting. In Computer Vision – ECCV 2012, edited by A. Fitzgibbon, Berlin, pp. 201−214.

Ikeda, T. Chigodo, Y. Rea, D. Zanlungo, F. Shiomi, M. and Kanda, T. 2013. Modeling and prediction of pedestrian behavior based on the subgoal concept. Robotics, p. 137.

Ramaithitima, R. Whitzer, M. Bhattacharya, S. and Kumar, V. 2016. Automated Creation of Topological Maps in Unknown Environments Using a Swarm of Resource-Constrained Robots. IEEE Robotics and Automation Letters, vol. 1, no. 2, pp. 746-753.

Sethian, J. A. 1999. Fast marching methods. SIAM Review, 41(2). pp. 199–235.

CHAPTER 39

PATH PLANNING ON MARS USING VFM

S. GARRIDO, L. MORENO and D. ALVAREZ

RoboticsLab, Universidad Carlos III de Madrid, sgarrido@ing.uc3m.es

This paper presents the application of the Fast Marching Method, with or without an external vectorial field, to the path planning problem or robots moving in spatial environments. The resulting trajectory has to take into account the obstacles, the slope of the terrain (gradient of the height), the roughness (spherical variance) and the type of terrain (presence of sand) that can lead to slidings. When the robot is in sandy terrain with a certain slope, there is a landslide (usually small) that can be modelled as a lateral current or vectorial field in the direction of the negative gradient.

1 Introduction

Planetary exploration with robots has increased in the last decades. Different robots, such as the Mars Exploration Rovers (MER) (Volpe, 2000) Spirit or Opportunity, have been placed in planets, like Mars, or asteroids, like Ceres or Vesta, in order to obtain valuable samples for the scientific community and enlarge our knowledge of the universe. These activities require safe and accurate movements to be executed combined with onboard decision making, especially due to the long time the information needed to travel. These robots are equipped with different kind of sensors to evaluate their environment. Stereo-vision systems are commonly used, although other type of sensors such as active vision LIDAR systems or six-axis Inertial Measurement Units are also being tested (Ishigami, 2007).

Once the environment is recognised, path planning is essential either for exploration or for reaching interesting goals. The objective of a path planner for a mobile robot operating in environments with obstacles is to calculate collision-free trajectories with the best possible characteristics. General desired path characteristics are safety (in terms of obstacle avoidance) and or shortness (for energy optimization). Besides, in the case of plane-

tary exploration, it is common to take into account the height or roughness (unevenness) (Garrido, 2008) of the terrain, and the possible sliding of the robot due to, i.e. sandy slopes (height gradient). This paper presents a methodology to: 1) build a cost function taking into account the nature of the terrain and 2) plan paths with desirable characteristics. Obviously, it assumes the knowledge, with a degree of uncertainty, of the main attributes of the environment in which the robot has to move.

The path planer presented is based on the Fast Marching Method (FMM), which essentially computes the time of arrival of a wave to the different points in the environment. Then, the gradient descent algorithm is used for path ex- traction. The intrinsic nature of FMM and a proper definition of the velocities at which the wave (robot) can move, makes the computed path to assure safety, and shortness (Garrido, 2008; Valero, 2013). In order to define the robot speed over the environment, the method uses the height information and evaluates the roughness of a surface based on its spherical variance. It also takes into account both the absolute value of the height and its gradient, and the distance to obstacles. Then, it combines these data with the robot movement limitations to generate a weighted matrix. This matrix can be seen as a cost function and defines the different velocities at each point of the map.

Finally, robots not always can avoid difficult terrains. This may lead to small slidings while moving. An approach for considering these slippings is presented. These undesired movements are modelled as a vectorial field, which depends on the terrain and the height gradient of the surface, and its effect is considered using the Fast Marching Method subjected to a vectorial field (FMVF).

2 The Eikonal Equation and the Fast Marching Planning Method

In robotics, the path planner of the mobile robot must drive it in a smooth, safe and fast way to the goal point. In nature, there are phenomena that work in the same way, such as electromagnetic waves. If at the goal point there is an antenna that emits an electromagnetic wave, then the robot could drive himself to the destination following the waves to the source. The idea of the electromagnetic wave is especially interesting because the potential magnetic field has all the good properties desired for the trajectory, such as smoothness (that is, C^{∞}) and the absence of local minima. In a similar manner, Fermat's principle in optics says that the path of a beam of monochromatic light follows the path of least time. When the refractive index is constant, the wave fronts are circles, which represent

different arrival times, and the paths are straight lines. In the case of two media with different indices of refraction, rays are bent as shown in the left side Fig. 1, resulting in the refraction of the path, known as Snell's law effect. In the case that the refractive index varies continuously, the light beam is also continuously bent, as shown in in the right side Fig. 1 (Sethian, 1996; Gomez, 2015).

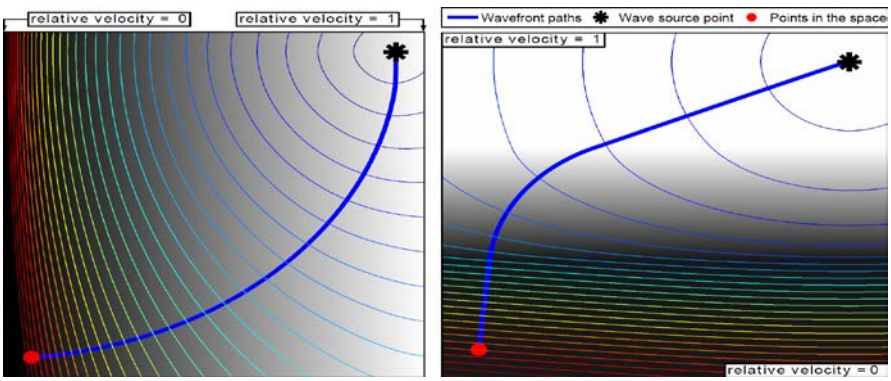

Fig. 1. Paths (or light rays) obtained with the Fast Marching Method when there are two media of different refractive indexes (air and water, for example) and when the refractive index changes continuously from 0 to 1.

3 Fast Marching Method subjected to a Vectorial Field (VFM)

From a physical point of view, the velocity of propagation over any medium belongs to [0, c], where c is the light speed, but it can be normalised to the interval [0, V], where V represents the maximum velocity of propagation of our vehicle. Besides, the refractive index n = c/F belongs to the interval [0, 1], with 1 representing the maximum possible speed of the wave propagation (or robot velocity). Therefore, the cost function f = 1 − n belongs to the interval [0, 1], being f = 0 the minimum cost and f = 1 is the maximum cost of the function. Thus, the optimal route minimizes the time between the starting point xs and end point xg:

$$T = V \cdot \min_{C(s) \subset D} \int_{x_s}^{x_g} f(C(s))\,ds \tag{1}$$

where C(s) represents any path in the domain D.

In the vectorial case, it is necessary to normalise the total cost function:

$$\tilde{f} = f_{dif} + f_{vect} \tag{2}$$

where fdif is the cost function due to the difficulty of the terrain and the obstacles, and it is computed as fdif = 1 − W , being W a cost matrix that will be explained in section 4. The second part corresponds to the external vectorial field.

This way, the influence of the vectorial field over the velocity of the vehicle depends on the magnitude of the two of them and on the angle between them, i.e., it depends on scalar product, and therefore the fvect can be defined as:

$$\text{fvect}(i, j) = 1 - (\vec{V}_{i,j} \cdot \vec{F}_{i,j}) \qquad (3)$$

Physically, this is equivalent to say that a force favours the vehicle when both external vectorial field and vehicle are pointing to the same direction.

It is very important to highlight that the new cost function defined in equation 3 must to be always positive, because in the Fast Marching methods the wave front cannot move backwards. More details on the algorithm can be consulted in (Petres, 2007).

In Fig. 3 is shown the expansion or a wave (FMM) with a rectangular obstacle in the middle a). And the expansion of a wave subjected to a unitary vectorial field, to the right in the upper part, zero in the middle and a unitary vectorial field to the left in the lower part (VFM) b).

Furthermore, in this paper, we have applied the VFM method on a matrix of difficulty for trajectories that optimise a cost function while they are subject to a vectorial field, which in the case of paths for a Rover on Mars can be caused by the sideslip due to the sand.

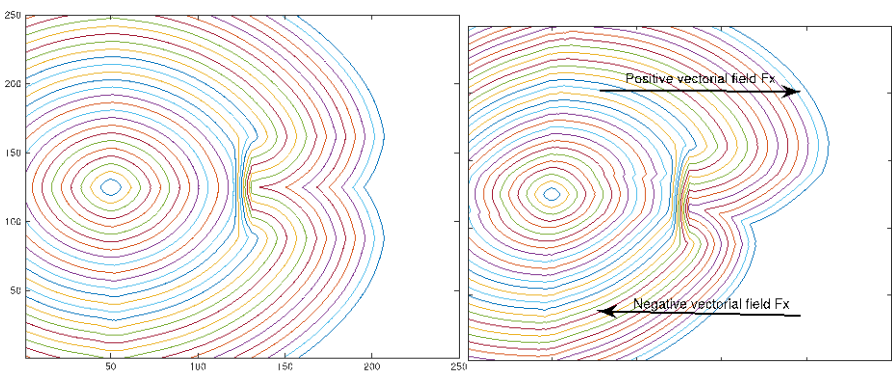

Fig. 3. Fast marching expansion wave with an rectangular obstacle in the middle a) and Fast Marching subjected to a vectorial field (VFM) wave expansion and b) subjected to a unitary vectorial field to the right in the upper part, zero in the middle and a unitary vectorial field to the left in the lower part.

4 Matrix W: Difficulty Map or Cost Function

As expressed in section 1, the proposed technique is based on the FMM. This algorithm uses a velocity (refraction) index of the wave front to compute the time-of-arrival in the map. If we build this map based on the 3D characteristics of the environment and the robot limitations, desirable path attributes are obtained. The trajectory is not going to be the simple geodesic (computed when we have constant velocity of the wave), but it is going to be modified according to the robot and task needs. The proposed method creates a weight matrix W, which is built based on: the spherical variance, the saturated gradient of height, and the height.

In (Castejon, 2000) a method to calculate the roughness degree is presented. The spherical variance finds the roughness of a surface to determine the level of difficulty for the robot to move through it. The spherical variance is obtained from the orientation variation of the normal vector at each point. In a uniform terrain (low roughness), the normal vectors will be approximately parallel and, for this reason, they will present a low dispersion. On the other hand, in an uneven terrain (high roughness) the normal vectors will present great dispersion due to changes in their orientation.

The saturated gradient of the height magnitude consists of giving a limit value to the gradient of each point over the surface. The gradient limit depends on the robot capabilities; the maximum inclination that the robot is able to cross will be the limit value for the saturated gradient.

As previously explained, with this matrix the algorithm can modify the path that the robot is going to follow across the 3D surface by having a proper velocity value for each point on the surface. We can add as many characteristics as we need to get different paths including several attributes of the terrain.

In our case, the saturated gradient, the spherical variance, and the height are three matrices G, Sv, and H with the same size as the environment map. To build matrix W, we give a weight factor to each surface characteristic and we can determine which one is the more important depending on the task requirements. The values of the three matrices are normalized, and therefore they vary from 0 to 1. The components of matrix W with a value of 0 will be points in the environment with maximum speed. Hence, these are points which the robot can cross without any problem and at its maximum speed. The components of W with a value of 1 will be points in the vertex with a minimum speed. This means that the robot will not be able to pass across them.

$$W = a1 \cdot G + a2 \cdot Sv + a3 \cdot H \tag{4}$$

where a1, a2 and a3 are weighting factors with sum equal to 1.

After matrix W is generated, the FMM is run over the modified map to calculate the best trajectory. With the FMM we can assure that the path found will be the one of less time in the W metrics.

5 Numerical Simulations

Several tests on different environments have been carried out in order to test the usability of the algorithm and the influence of the weighted matrix and the external vectorial field on the planned paths.

Then, experiments are done using a height map of the area around the Gale crater in Mars, which can be seen in Fig. 4. In this case, possible slidings while moving inside the crater are modelled applying a vectorial filed proportional to the gradient of the terrain surface. The different resultant paths can be seen in Fig. 4 a) and b).

Finally, both the roughness and the changes of height are considered together in the construction of the difficulty map, which can be seen in Fig. 5 c). Different values a_i in the weighting factor when computing the map W lead to different paths. In Fig. 5 a), the changes in height along the path are more penalised than in Fig. 5 b), in which the roughness of the terrain is more penalised.

6 Conclusions

The algorithm we have presented is a novel methodology for considering the most important aspects of path planning for exploration of planets or asteroids. The main characteristics considered as: height, roughness, magnitude of slope, path length and clearness among obstacles.

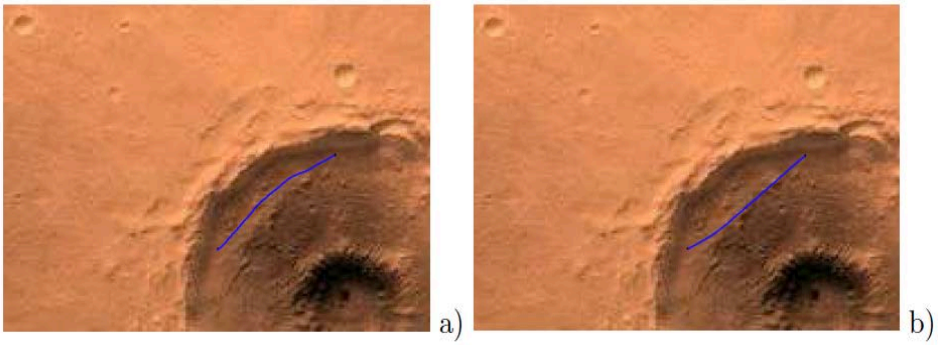

Fig. 4. Two different paths in the Mars Gale crater taking into account the lateral sand landslide proportional to the gradient. a) without landslide, b) with landslide.

They are used to build a velocities map that is later used by the Fast Marching Method for computing the time of arrival of a wave expansion. Then, the path is extracted using gradient descent. Also, possible slidings due to slopes or terrain conditions are modelled as an external Vectorial Field, and taken into account using Fast Marching Method subjected to a Vectorial Field. Numerical simulations show promising results on the application of this methodology. Different results show the influence of the combination of several characteristics of the environment in the resulting path. In all cases, obstacles and difficult terrain are avoided. Besides, possible sliding problems are taken into account in the path-planning phase.

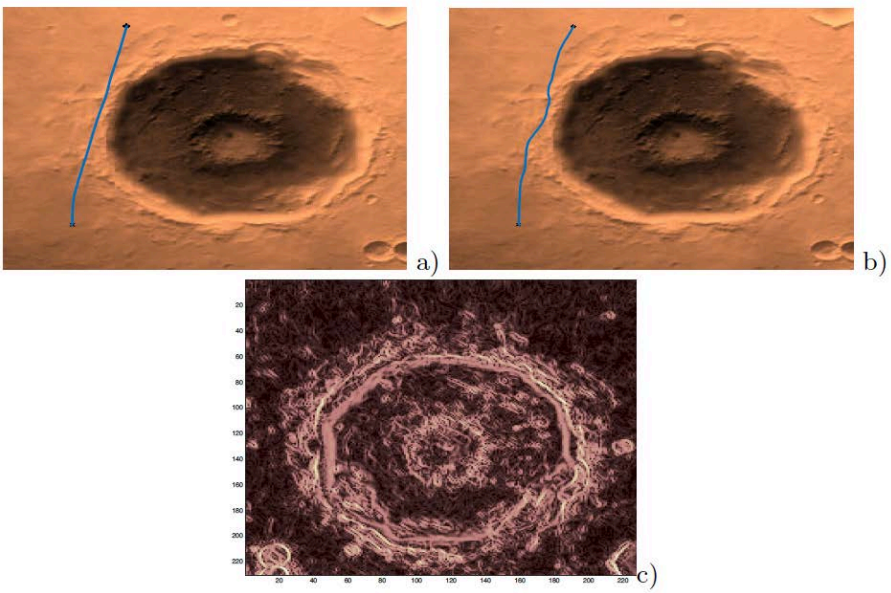

Fig. 5. Path calculated using mountains map penalising the change in height, when there is an external field a) downside, b) upside and c) original map.

References

Castejon, C., Boada, B., Blanco, D., Moreno, L. 2000. Traversable region modeling for outdoor navigation. J. Intelligent and Robotic Systems, vol. 43, pp. 175-216.

Garrido, S., Moreno, L., Blanco, D. 2008. Exploration of a cluttered environment using voronoi transform and fast marching method. In: Robotics and Autonomous Systems, vol. 56, pp. 1069-1081.

Gomez, J.V., Alvarez, D., Garrido, S., Moreno, L. 2015. Fast methods for eikonal equations: an experimental survey. ArXiV abs/1506.03771.

Ishigami, G., Nagatani, K., Yoshida, K. 2007. Path Planning for Planetary Exploration. Rovers and Its Evaluation based on Wheel Slip Dynamics of the terrain. In: IEEE Int. Conference on Robotics and Automation, pp. 2361-2366.

Petres, C., Pailhas, Y., Patron, P., Petillot, Y., Evans, J., Lane, D. 2007. Path Planning for Autonomous Underwater Vehicles. In: IEEE Transactions on Robotics, vol. 23(2), pp. 331-341.

Sethian, J.A. 1996. Theory, algorithms and applications of level set methods for propagating interfaces. Acta numerica, Cambridge University Press, pp. 309-395.

Sethian. J. A. 1996. Level set methods, Cambridge University Press.

Valero-Gomez, A., Gomez, J.V., Garrido, S., Moreno, L. 2013. The Path to Efficiency: Fast Marching Method for Safer, More Efficient Mobile Robot Trajectories. In: IEEE Robotics and Automation Magazine, vol. 20(4), pp.111-120.

Volpe, R., Estlin, T., Laubach, S., Olson, C. 2000. Enhanced Mars Rover Navigation Techniques. In: IEEE International Conference on Robotics and Automation, vol. 1, pp. 926-931.

CHAPTER 40

A CROPS INSPECTION VEHICLE BASED ON A BATTERY-POWERED ELECTRIC CAR

J.M. BENGOCHEA-GUEVARA, D. ANDÚJAR, J.CONESA-MUÑOZ and A. RIBEIRO

Centre for Automation and Robotics (CSIC-UPM), jose.bengochea@csic.es, dionisioandujar@hotmail.com, jesus.conesa@csic.es, angela.ribeiro@csic.es

The concept of Integrated Pest Management (IPM) has emerged in recent years to achieve sustainable use of pesticides by reducing their risk and impact on human health and the environment. A key element is the monitoring or continuous inspection of crops to ensure early detection thereof. This article presents the development of a mobile robotic platform able to inspect two types of scenarios: annual crops (maize, cereal, etc.) and multiannual crops (orchards, vineyards, etc.).

1 Introduction

Agricultural use is the main use of land in the European Union (EU) with 40% of the total land area covered (Eurostat, 2016). In 2012, more than 60% of this agricultural land was devoted to annual crops (cereal, maize…) while 6% was dedicated to multiannual crops (olive trees, vineyards, fruit trees…). But not all of this agricultural land is productive, factors such as pests (pathogens of plants, invertebrates and weeds) can significantly reduce agricultural production, reaching in some cases up to 40% overall reduction in crop yield (Oerke et al., 1994) by disease transmission, competition with the crop plants (weeds) or feeding on crops. To get an idea, it is estimated that the amount of crops eaten by insects would be enough to feed more than one billion people (Birch et al., 2011). This scenario may worsen with the establishment of exotic pests favored by climate change. Thus, the increasingly warm and humid climate of north-

ern Europe will favor the development of diseases, while drier and warmer conditions in southern will originate insect pests. In fact, literature indicates that every 10 months a new agricultural pest enters in southern Europe moving north as conditions change (Reddy, 2015). Today most farmers and producers in the EU depend on broad spectrum chemical pesticides, although the negative effects lead to difficult problems as the emergence of secondary pests and resistance, which has led the EU to pass a legislation banning an important number of synthetic chemical pesticides (Regulation (EC) No 1107/2009 and Directive 2009/128/EC of the European Parliament and of the Council). This new scenario drives actions to achieve sustainable use of pesticides by reducing their risk and impact on human health and the environment, promoting the concept of Integrated Pest Management (IPM) in which a key element is the monitoring or continuous inspection of crops to ensure early detection thereof. While operators can scout small fields, it is unmanageable in large areas where only sampling observations currently are taken.

In this context, the Ministerio de Economía y Competitividad (MINECO) funded, within its Programa Estatal, the research project titled: *Integration of multisensory information and machine learning for detection, characterization and accurate recognition of natural structures in fields* (*3DWeed*). The main goal of this project is to provide technological tools required in the development of Integrated Weed Management Systems (IWMS). The project is structured around two scenarios: the dry-land cereal production systems prevailing in Central Spain and the vineyard systems more widely used in these same areas, based on the use of deficit irrigation. In both scenarios we are currently developing crops inspection systems composed by a ground autonomous platform that integrates a multisensory system. The information provided by on-board sensory system is currently being used for characterization and recognition of crop plants (cereal and vine) and weeds (B. diandrus, P. rhoeas, C. dactylon and C. arvensis). Thus, the heterogeneous acquired information is integrated in both 2D and 3D crops maps with the aim of performing preventive and predictive inspection of plants, which is vital to optimize operations performed continuously on the crop. In few words, the project purpose is to generate the basic technology from which to build a system of early detection (i.e., days before human detection) of symptoms in plants caused by pests and diseases. This early detection is an essential step in the Integrated Pest Management which results in making more effective treatments saving in the amount of pesticide used.

At present we are working on a ground platform to integrate a remote control navigation. Indeed, two types of navigation will be integrated in the vehicle in order to it can autonomously inspect a crop field with full coverage. The platform will be able to navigate: 1) guided by information provided by the GPS receiver with RTK correction; an appropriate navigation for narrow row crops, such as cereal crops or woody crops, and 2) guided by real-time detection of some element of interest, such as the crop row; an appropriate navigation for wide row crops, such as maize crops, where the vehicle must not tread on the crop. To achieve the goal of an autonomous navigation, our group has the experience of having previously developed a prototype, a small autonomous vehicle for inspection (Bengochea-Guevara et al., 2016).

2 Equipment

The mobile base platform is a Renault Twizy Urban 80 model (Fig. 1a). It is a compact electric vehicle, with zero-emissions in use. It has a length of 2.32 metres, a width of 1.19 metres and a height of 1.46 metres. Twizy Urban 80 model can drive up to 80 km/h. It is powered by a 13 kW electric motor, with a smooth one-speed automatic transmission and a light and compact lithium-ion battery pack. Thanks to its electric motor, the vehicle has no vibrations, which is a great advantage for information capture with sensors. Furthermore Twizy can travel at the required speeds for the sampling in the field, about 3 Km/h. It can move around 80 km after a 3.5 hours charge from a standard household electrical supply. Furthermore, the mobile platform integrates the two cameras described below for the crop inspection purpose.

One of the two on-board cameras, is a Kinect; a RGB-D sensor developed by Microsoft. Its second generation, Kinect v2 (Fig. 1b), acquires a 512×424 pixels depth map and a 1920×1080 pixels RGB image with a frame rate up to 30 Hz. The Kinect v2 depth sensor is based on the ToF (time-of-flight) technology, which allows it to work outdoors, unlike Kinect v1 very sensitive to the sunlight due to the use of a structured light pattern to obtain the depth information.

Kinect v2 is connected to an on-board computer with an Intel Core i7-4771@3.5GHz processor, 16GB of RAM, and a single NVIDIA GeForce GTX 660 graphic card.

In addition to Kinect v2, the platform is equipped with a second camera: a digital single-lens reflex camera, Canon EOS 7D. The camera is connected to an on-board laptop (a Panasonic Toughbook CF-19, equipped

with an Intel Core i5-2520@2.5GHz processor and 2 GB of RAM) via a USB connector, providing in real time around five frames, of 1056×704 pixels resolution, per second. The vehicle equipment is complemented with a Hemisphere R220 GPS receiver with RTK correction for geo-referencing the gathered data. The RTK-GPS receiver provides 10 locations per second with a great accuracy (an error below 2 cm).

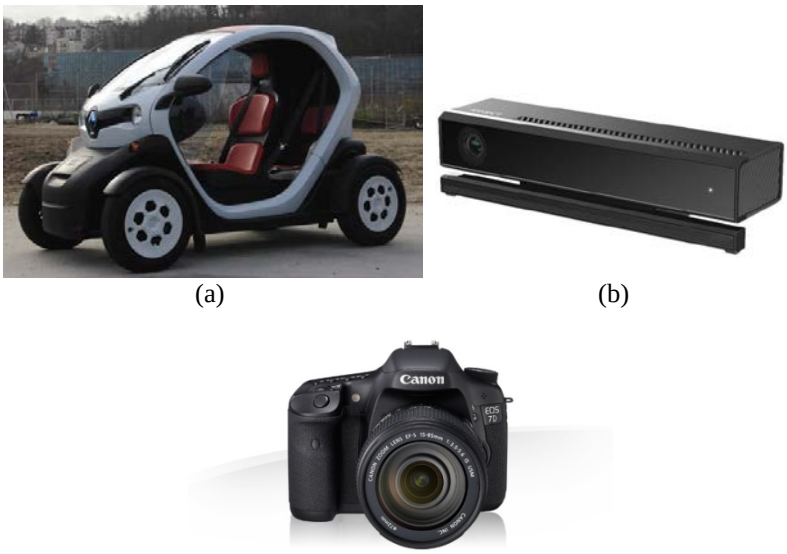

(a) (b) (c)

Fig. 1. (a) Renault Twizy (b) Kinect v2 (c) Canon EOS 7D.

3 First samplings

Once the initial version of the prototype was integrated, the first sampling was made in late February 2016. They all were performed in Lleida (Spain) in the vineyards of the Raimat winery, owned by Codorniu S.A, and in the cereal field of Muller. Fig. 2 shows the mobile platform during the sampling.

In vineyard parcels, the Kinect v2 sensor was focused to the vineyards in order to capture the vineyard structure so that it could be characterized by their 3D reconstruction. Furthermore, 3D maps can be built thanks to the data provided by the RTK-GPS receiver. On the other hand, the Canon

camera was focused to the street to capture information of the vegetation cover for weed detection purposes.

Fig. 2. The inspection platform during the sampling.

Fig. 3 shows an example of information provided by Kinect v2 sensor.

(a) (b)

Fig. 3. (a) Color image taken by Kinect v2 sensor (b) Depth image taken by Kinect v2 sensor.

The image on the left of the figure (Fig. 3a) illustrates the RGB information, which is a faithful color image of the real scene, whereas the image on the right (Fig. 3b) shows a color representation of the depth information (distance of objects in the scene) provided by the sensor; in

particular near objects appear red, distant ones are blue and objects in-between show up in various shades of orange, yellow, and green.

Some examples of the images acquired by the Canon camera can be seen in Fig. 4, where it can be distinguished different states of vegetation cover and different types of weeds. Fig 4a, 4b, 4c were taken in Raimat vineyards with different lighting conditions, whereas Fig. 4d shows a shot of the cereal at the Muller field.

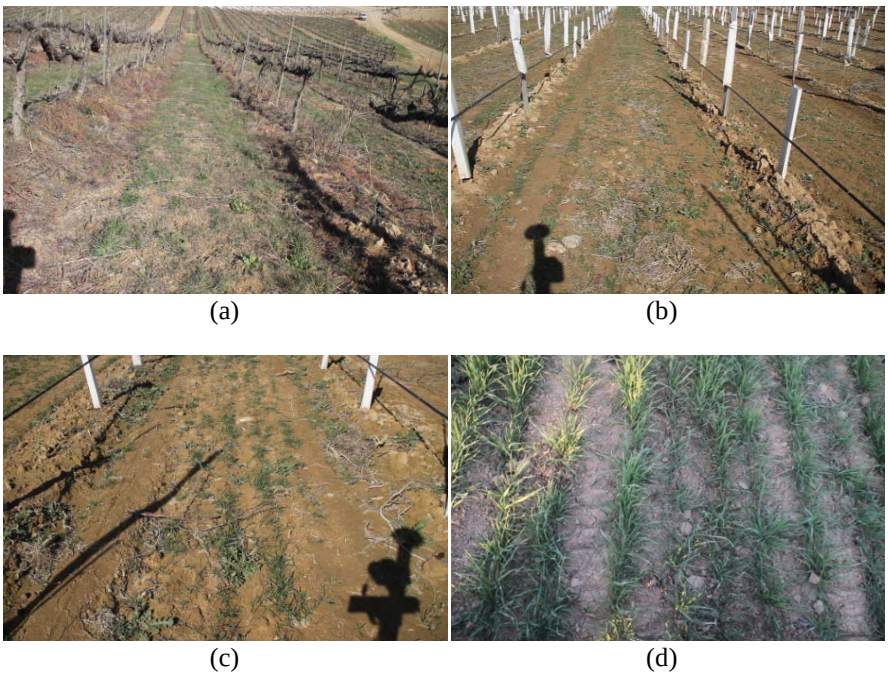

(a) (b)

(c) (d)

Fig. 4. Images from (a) to (d) show different examples of images acquired by Canon camera.

4 Conclusions and future work

The concept of Integrated Pest Management has emerged in recent years to achieve sustainable use of pesticides by reducing their risk and impact on human health and the environment. In this paper, some very early results of research accomplished in the project *3DWeed* have been presented. The project objective is to provide the technological tools required in the development of Integrated Weed Management Systems.

After an initial integration of different sensors in a battery-powered electric car, a mobile inspection platform has been built able to perform scouting on two types of scenarios: annual crops (corn, cereal, etc) and multiannual crops (orchards, vineyards, etc). Proper operation of the vehicle in the first sampling in actual fields has been shown.

With the acquired information, our group are working on the detection, characterization and recognition of crop plants (cereal, vine) and weeds (B. diandrus, P. rhoeas, C. dactylon, C. arvensis), and in the generation of crop maps (2D and 3D). Furthermore, our group is working in the navigation control of the platform with the aim that it can autonomously inspect fields with full coverage. Two types of navigation will be integrated in the next months: 1) guided by information provided by the RTK-GPS receiver, appropriate for navigation in narrow row crops, such as cereal crops, vineyards, etc., and 2) guided by detecting some interest elements such as crop rows.

Acknowledgements

The Spanish Government has provided full and continuing support for this research work through project AGL2014-52465-C4-3-R (3DWeed). The authors wish to thank Jordi Recasens and his team (Weed Science and Plant Ecology Research Group of the UdL) for their invaluable help in the field trials. The authors wish to acknowledge the invaluable technical support of Damian Rodriguez.

References

Bengochea-Guevara, J. M., Conesa-Muñoz, J., Andújar, D., & Ribeiro, A. 2016. Merge Fuzzy Visual Servoing and GPS-Based Planning to Obtain a Proper Navigation Behavior for a Small Crop-Inspection Robot. Sensors, 16(3), 276.

Birch, A.N.E., Begg, G.S. & Squire G.R. 2011. How agro-ecological research helps to address food security issues under new IPM and pesticide reduction policies for global crop production systems. Journal of Experimental Botany 62: 3251-3261.

Eurostat. 2016. http://ec.europa.eu/eurostat/web/agri-environmental-indicators/overview.

Oerke, E.C., Dehne, H.W., Schnbeck, F. & Weber, A. 1994. Crop production and crop protection: estimated losses in major food and cash crops. Elsevier, Amsterdam, Netherlands.

Reddy, P. P. 2015. Climate Resilient Agriculture for Ensuring Food Security. Springer, India.

CHAPTER 41

FUTURE TRENDS IN PERCEPTION AND MANIPULATION FOR UNFOLDING AND FOLDING GARMENTS

D. ESTEVEZ, J. G. VICTORES and C. BALAGUER

RoboticsLab, Universidad Carlos III de Madrid, destevez@ing.uc3m.es

This paper presents current approaches for robotic garment folding-oriented 3D deformable object perception and manipulation. A major portion of these approaches are based on 3D perception algorithms that match garments to a model, and are thus model-based. They require a full view of an extended garment, in order to then apply a preprogrammed folding sequence. Other approaches are based on 3D manipulation algorithms that are focused on modifying the pose of the garment, also oriented at matching it with a model. We present our own garment-agnostic algorithm, which requires no model to unfold clothes, and works using a single view from an RGB-D sensor. The unfolding algorithm also has been validated through experiments using a garment dataset of RGB-D sensor data, and additional validation with a humanoid robot platform. Finally, conclusions regarding the current state of the art and on the future trends of these research lines are discussed.

1 Introduction

Every day, humans encounter garment manipulation tasks in both domestic (e.g. laundry) and industrial (e.g. garment manufacturing) environments. A growing need exists for automated solutions to help us to perform these tasks, as they are tedious and repetitive. Additionally, another critical factor involved in this increase in demand is the increasing aging of the world population. This is because of the decrease in mobility associated with elder age. Currently, the only existing automated solutions are bulky and ex-

pensive, as can be seen in Fig. 1 (right). They are intended to be used in an industrial environment, so they are not suitable for domestic use.

Fig. 1. Current clothes folding solutions available for garment folding. On the left, human workers folding clothes in a textile factory. On the right, an automated solution available in the market, manufactured by Texgraff©.

Robots, more specifically, humanoid robots, arise as a sensible choice. Humanoid robots are designed to work in human environments and to have human-like locomotion and manipulation capabilities. However, working with garments involves deformable 3D objects. This is not a trivial task for robots. Modeling is especially complex due to the almost infinite number of poses into which a textile article can be brought. The situation becomes even more complex in the presence of several garments, as they can easily be entangled, increasing the amount of occlusions and complicating the recognition of each individual garment using 2D or 3D computer vision techniques. Bringing garments to a desired configuration from an arbitrary initial pose is a very challenging issue.

The way humans perform laundry has inspired most of the works that can be found throughout robotic literature. The human pipeline usually begins with the extraction of a garment from a washing or drying machine. Garments are placed on a pile, from where deformable 3D object perception allows them to be picked up one at a time, initiating an iterative sequence. Deformable 3D object manipulation is used to extend and flatten the garment, either in the air, or with the help of a flat surface such as a table. The extended garment is then classified and fit into a garment model according to its category. Finally, the garment model is used to execute a preprogrammed folding sequence on the garment. Once a garment is folded, the next garment is picked up from the pile.

This paper focuses on past and current approaches in robotic garment perception and manipulation, and on exploring the robotic trends of the future.

2 State of the art

One of the main contributors within the existing model-based work has been the computer graphics community (Chen, Yin, & Su, 2009). Model-based approaches focus on classifying garments in categories according to a model when the garments are grasped or extended on a flat surface.

Kita et al. use deformable models to estimate the state of hanging clothes based on 3D observed data (Y. Kita, Saito, & Kita, 2004)(Yasuyo Kita, Ueshiba, Neo, & Kita, 2009). Several candidate shapes are generated through physical simulations of hanging clothes. They are later compared to the observed garment data. Further deformation of these candidate shapes is allowed to make the model fit the data more accurately. The shape which is more consistent with the data is finally selected.

Miller et al. present a method for modeling garments once they are extended on a flat surface in (Miller, Fritz, Darrell, & Abbeel, 2011). Parameterized shapes are used as model, where some parameters are fit from garment data and other parameters are computed using the fit parameters. Each garment category requires a different model, and parameters allow each model to adapt to the garment shape within each category.

A method for classifying and estimating the poses of deformable objects is presented in (Li et al., 2015). It consists in creating a training set of deformable objects by off-line simulation of different garments, extracting depth images from different points of view. A codebook is built for a set of different poses of each deformable object. With this codebook, classifying deformable objects on different categories and estimating their current pose is possible, for later regrasping or folding the garment.

Clothing article manipulation is the other main approach to garment folding. Osawa et al. propose in (Osawa, Seki, & Kamiya, 2006) a method to unfold garments in order to classify them. It consists in alternatively regrasping clothing from the lowest point and attempting to expand them using a two-arm manipulator.

The method introduced by Cusumano-Towner et al. in (Cusumano-Towner, Singh, Miller, O'Brien, & Abbeel, 2011) allows a bi-manipulator robot to identify a clothing article, estimate its current state and achieve a desired configuration, generalizing to previously unseen garments. For that purpose, the robot uses a Hidden Markov Model (HMM) throughout a sequence of manipulations and observations, in conjunction with a relaxation of a strain-limiting finite element model for cloth simulation that can be solved via convex optimization.

In (Li et al., 2015) Li presents a method for unfolding deformable objects with a bi-manipulator robot. With this method, the robot is capable of

taking a clothing article from an unknown state to a known state by iterative regrasping, detecting the most suitable grasping points in each state to achieve its goal. For locating the most suitable grasping points, the 3D point cloud obtained by the robot is matched to the mesh model that incorporates the information about the best regions to grasp in order to unfold the garment.

In (Willimon, Birchfield, & Walker, 2011) Willimon et al. use several features obtained from a depth image, such as peak regions and corners location, to determine the location and orientation of points where the robot later interacts with the garment.

CloPeMa[1] is a recent EU-FP7 research project (2012-2015) whose objective is to advance the state of the art in perception and manipulation of fabric, textiles and garments. As part of the CloPeMa project, a method to detect single folds has been presented by Mariolis et al. in (Mariolis & Malassiotis, 2013)(Mariolis & Malassiotis, 2015). In order to detect such folds, first, a dataset of unfolded clothes templates is built. These templates are later used to perform a shape matching between the folded garment shape, obtained by the camera, and the unfolded garment model. This process is iterative, and the initial results are served as feedback to adapt the model for a better fit. Stria et al. propose in (Stria, Pruša, Hlaváč, Wagner, & Petrik, 2014)(Stria, Pruša, & Hlaváč, 2014) a polygon-based model for clothes configuration recognition using the estimated position of the most important landmarks in the clothing article. Once identified, these landmarks can be used for automated folding using a robotic manipulator. The clothes contour is extracted from an RGB image and processed using a modified grab-cut algorithm, and dynamic programming methods are used to fit it to the polygonal model. Doumanoglou et al. follow in (Doumanoglou, Kargakos, Kim, & Malassiotis, 2014) an approach based on Active Random Forests in order to recognize clothing articles from depth images. The classifier allows the robot to perform actions to collect extra information in order to disambiguate the current hypotheses, such as changing the viewpoint.

3 A Garment-Agnostic approach to unfolding

Existing work found in the literature has focused in garment recognition and modeling once the garment is extended, as well as in developing folding algorithms using those models. For this reason, our work has focused

[1] http://www.clopema.eu/

on the step previous to having an unfolded garment, which is how to unfold a clothing article that has been picked up from a pile of clothes and is placed on a flat surface. The original algorithm has been recently published in (Estevez, Victores, Morante, & Balaguer, 2016). Fig. 2 depicts the outline of the algorithm, which uses a single RGB-D sensor view for rapid processing of the deformable 3D object perception algorithm.

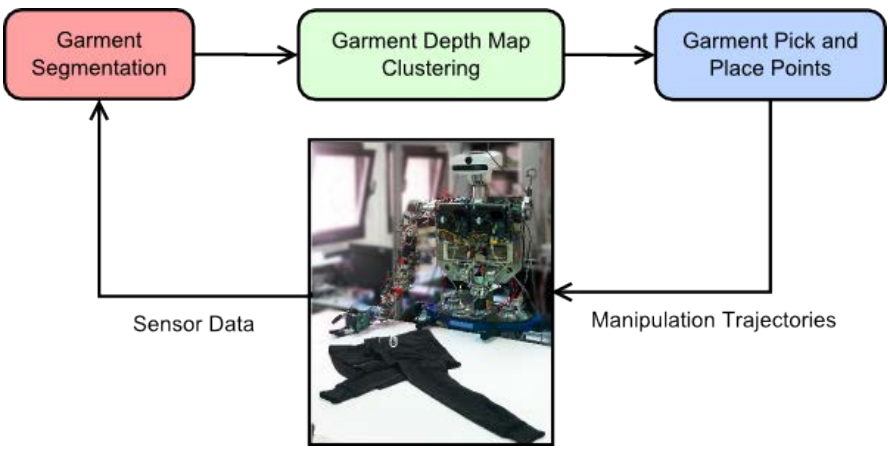

Fig. 2. Pipeline of the Garment-Agnostic Approach to Unfolding algorithm.

The depth information provided by the RGB-D sensor is converted into a grayscale image. Garment Segmentation is performed in the HSV space, and then Garment Depth Map Clustering is performed using a watershed algorithm. This algorithm provides us with labeled regions, each having a different height. In this labeled image, we assume that the highest height region belongs to the fold. Starting on this region, and ending in the garment border, tentative paths are created by the Garment Pick and Place Points stage, in several directions to analyze the height profile. For each profile, a *bumpiness* value B is computed as in Equation (1).

$$B = \sum_{i=1}^{n} \left| path(i) - path(i-1) \right| \qquad (1)$$

The lowest one is selected as the unfolding direction. A final extension on this line is performed to create a pick point on the fold border, and a place point outside the garment. Experiments for evaluation of the algorithm were performed over a dataset of RGB-D sensor data, and additional validation with a humanoid robot platform as seen in Fig. 3.

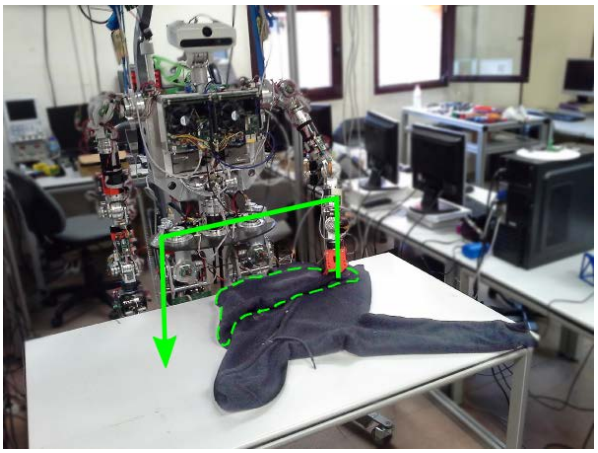

Fig. 3. Humanoid robotics clothes folding scenario. The clothes are placed on a flat white table, while a RGB-D sensor is positioned on the top.

4 Conclusions and future work

In this paper we have reviewed several model-based approaches, and also garment manipulation-based approaches for garments, in the context of deformable 3D object perception and manipulation. Finally, a model-free garment-agnostic algorithm to unfold clothes was presented. Results show that our approach to garment-agnostic unfolding is promising to be included in a complete pipeline of clothes folding. The main contribution of our work is its analysis of the garment not dependent of a prior model. Using only depth information for detecting overlapped regions (except for Garment Segmentation, where other algorithms could be used), as opposed to using RGB images, makes our algorithm independent of the colors and patterns present in the garments.

Our future lines of research include implementing a pre-processing stage in which a perspective transformation is performed (to perceive the garment as if a bird's eye point of view were used), using multiple views of the deformable 3D object (e.g. KinFu with GPU acceleration), and performing large-scale experiments in perception and manipulation with large datasets and prolonged physical trials (e.g. with industrial manipulators).

In a broader sense, we expect the robotics community to aim its efforts towards perceiving and manipulating deformable 3D objects. They represent a grand portion of our everyday life whether in domestic, office, or outdoor environments. While our first approaches have been aimed at this tedious household and industrial chore, the long term goal of this work is

to allow robots to perform any kind task that requires addressing the difficulties of perceiving and manipulating these objects.

Acknowledgements

The research leading to these results has received funding from the RoboCity2030-III-CM project (Robótica aplicada a la mejora de la calidad de vida de los ciudadanos. Fase III; S2013/MIT-2748), funded by Programas de Actividades I+D en la Comunidad de Madrid and cofunded by Structural Funds of the EU.

References

Chen, Q., Yin, Y., & Su, A. F. (2009). Review of Cloth Modeling. 2008 International Workshop on Education Technology and Training and on Geoscience and Remote Sensing, ETT and GRS 2008, 1, 238–241.

Cusumano-Towner, M., Singh, A., Miller, S., O'Brien, J. F., & Abbeel, P. (2011). Bringing clothing into desired configurations with limited perception. Proceedings - IEEE International Conference on Robotics and Automation, 3893–3900.

Doumanoglou, A., Kargakos, A., Kim, T.-K., & Malassiotis, S. (2014). Autonomous Active Recognition and Unfolding of Clothes Using Random Decision Forests and Probabilistic Planning. Proc. IEEE International Conference on Robotics and Automation (ICRA14), 987–993.

Estevez, D., Victores, J. G., Morante, S., & Balaguer, C. (2016). Towards Robotic Garment Folding: A Vision Approach for Fold Detection. In IEEE International Conference on Autonomous Robot Systems and Competitions (ICARSC).

Kita, Y., Saito, F., & Kita, N. (2004). A deformable model driven visual method for handling clothes. IEEE International Conference on Robotics and Automation, 2004. Proceedings. ICRA '04. 2004, 4, 0–4.

Kita, Y., Ueshiba, T., Neo, E. S., & Kita, N. (2009). Clothes state recognition using 3d observed data. Proceedings - IEEE International Conference on Robotics and Automation, 1220–1225.

Li, Y., Xu, D., Yue, Y., Wang, Y., Chang, S., Grinspun, E., & Allen, P. K. (2015). Regrasping and Unfolding of Garments Using Predictive Thin Shell Modeling. In ICRA.

Mariolis, I., & Malassiotis, S. (2013). Matching folded garments to unfolded templates using robust shape analysis techniques. Lecture Notes in Computer Science (Including Subseries Lecture Notes in Artificial Intelligence and Lecture Notes in Bioinformatics), 8048 LNCS (PART 2), 193–200.

Mariolis, I., & Malassiotis, S. (2015). Modelling folded garments by fitting foldable templates. Machine Vision and Applications, 26(4), 549–560.

Miller, S., Fritz, M., Darrell, T., & Abbeel, P. (2011). Parametrized shape models for clothing. Proceedings - IEEE International Conference on Robotics and Automation, 4861–4868.

Osawa, F., Seki, H., & Kamiya, Y. (2006). Unfolding of Massive Laundry and Classification Types. Journal of Advanced Computational Intelligence and Intelligent Informatics, 457–463.

Stria, J., Pruša, D., & Hlaváč, V. (2014). Polygonal Models for Clothing.

Stria, J., Pruša, D., Hlaváč, V., Wagner, L., & Petrik, V. (2014). Garment Perception and its Folding using a Dual-arm Robot, (Iros).

Willimon, B., Birchfield, S., & Walker, I. (2011). Model for unfolding laundry using interactive perception. IEEE International Conference on Intelligent Robots and Systems, 4871–4876.

CHAPTER 42

HYBRID CONNECTOR DESIGN FOR MODULAR ROBOTS TITLE

S. SEGOVIA, A. BRUNETE and E. GAMBAO

Centro de Automática y Robótica- UPM-CSIC,
sergio.segovia.gonzalez@alumnos.upm.es

Docking systems are very important in modular robots because they serve not only as a connection element, but also as a communication line and power-transmission amongst the modules. It is especially important in self-reconfigurable modular robots, because they are the only mean to attach to other modules. The different characteristics that must be present in a docking system of a self-reconfigurable modular robot are described in this paper, leading to the proposal of a new design which combines the advantages of different types of mechanisms (electromagnetic and mechanical) in order to achieve the objective of building a robust, strong and automatic system for carrying out the processes of connection and disconnection between modules.

1 Introduction

Modular robots are robotic systems which are composed of independent modules, which are not capable of performing a particular task by themselves, but joined together in a certain position and orientation are able to perform specific tasks.

Therefore, one of the most important elements in this type of robot is the coupling element, which must be present in each of the modules to achieve the connection between them. To adapt to different environments, the coupling must be robust and able to transmit power and communications between the modules. The connection and disconnection process must be fast, precise and consume almost no energy.

In this article, we present a first version of a docking element to unify into a single mechanism, several essential features that must be present on a self-reconfigurable modular robot docking system.

First, a brief description of the main features of an ideal docking system is performed. Then, we review the different types of mechanisms used in the development of the docking elements for the connection between modules within the world of modular robotics. Finally, we will present the mechanical design of our docking element, as well as a brief description of each of its most important elements, to finish with an explanation of its basic operation in the connection and disconnection process.

2 State of the art

The robot coupling mechanisms can be classified from the point of view of the main elements used to carry out the connection and disconnection between the modules. The different types of existing connectors are described in the following sections.

2.1 Magnetic Connectors

Magnetic connectors were firstly used in Modular Transformer (M-TRAN) (Murata, 2002). In this case, magnets and Shape Memory Alloy (SMA) are mainly used for the construction of the type of docking shown in Fig. 1.

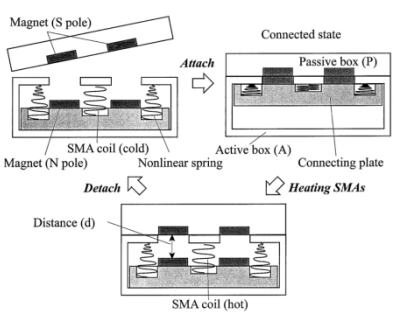

Fig. 1. M_TRAN Magnetic Docking Connection.

2.2 Electromechanical connector

In this type of connectors, there are various types of elements used for the connection and disconnection among modules.

- *Pins and holes*: in this case there are usually two types of modules, active and passive. Normally the active module has holes (where pins penetrate) and shape memory alloys (SMA) allow to disconnect. The passive element has pins that penetrate into the holes of the active element. This type of connector is use in PolyBot G2 (Yim, 2002) and CONRO (Castano, 2002).
- *The hooks:* because SMAs are slow and consume high power, some modular robots used hooks to make connection and disconnection between modules. It is the case of the M-TRAN III (Murata, 2002) or Roombot (Sproewitz, 2009).
- *Geared worm actuated locking wheel:* this type of connector is called Cone Bolt Locking Device (CoBoLD) (Liedke, 2011) and can be seen in Symbrion and Replicator (Kernbach, 2008). It uses a motor, which moves a worm that is geared with a locking wheel, in such a way that when one pin or hook goes into the hole, this is locked by the wheel. For the disconnection process, springs are used.
- *Motorize Jaws,* in this case, the connector uses motorized jaws, so that, when it squeezes together, they establish the connection and when they do not, the modules are disengaged. These elements for mechanical connector can be seen in SuperBot (Kovac, 2009).

2.3 Mechanical magnetic connector

SMORES (Dvey, 2012) modules employ four magnets (two north-pole and two south-pole) arranged alternatingly around the docking face, at 90º from each other. Each SMORES module has three active connectors and one passive connector.

Fable II modular robot (Pacheco, 2013) presents a genderless docking system, which is 90º symmetric. Two different (small and medium) size connectors, which are cross-compatible, are used in this system. The connector uses a pair of (north and south pole) magnets, a flange and a groove per 90º segment of the circular connector. Only manual disconnection between modules is possible in this system.

M^3Express (Wolfe, 2013) features a hybrid docking system that carries a pair of permanent magnets and a pair of steal screws for magnetic connection, in addition to four spring loaded tapered pins and four holes, arranged in pairs at 90º from each other, for mechanical connection.

3 Main features of a modular robot docking system

A docking system should have the following main characteristics (Neubert, 2014).

- *Size:* its size will have a great influence on the overall size of the module. Due to this, the docking must be as small and thin as possible.
- *Mechanical Strength:* the mechanism used is essentially intended to make the connection between two different modules, implying that the joint should be as strong as possible.
- *Ability to transmit information:* the docking system should allow the transmission of information between modules.
- *Ability to transmit power:* one or more modules may not have elements of energy storage, so it is necessary that the modules having these elements transmit power to all other modules.
- *Repeatability***:** the modules must be able to make the connection and disconnection, and they must be able to make this several times during the performance of the task.
- *Speed of Connection and Disconnection*: the modules are constantly being connected and disconnected, and therefore, the docking element must handle these processes as fast as possible.
- *Accuracy*: the process of connection between two modules is the precision with which this is done. Therefore, the connection system must help with the alignment among modules.
- *Power consumption*: it is necessary that in the process of connection and disconnection, the power consumption is minimal or null.
- *Gender and orientation*: the docking should allow the connection, regardless of the position in which the modules are at any time. The docking should not restrict the orientation of the modules to perform the connection process.

4 Mechanical designs

In this section, the mechanical design of the connector that we propose is described. The prototype shown here is designed to satisfy the ideal characteristics that a coupling for modular robotic systems must have. The goal is to achieve an automatic docking element that does not have the need of a manual intervention in the process of connecting or disconnecting with another module.

For this reason, it has been decided to choose the mechanical magnetic connector explained in section three. This type of connector unifies the features of the magnetic and mechanical connectors, in order to overcome their disadvantages and acquire their advantages.

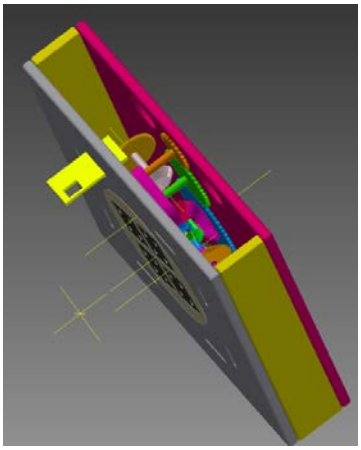

Fig. 2. Docking Connector.

4.1 Magnetic Part

This part consists of a rotating system that contains four neodymium magnets, which are disc magnets polarized in an axial way. The magnets are positioned in four holes equidistantly distributed from each other (Fig. 3).

As already mentioned, the magnets are strategically placed so that contiguous magnets have different polarity. Starting with the top left corner, the magnet has north polarity, the top right corner has south polarity, the bottom right corner has north polarity, and finally, at the bottom left corner, the magnet has south polarity.

In this way, in the connection process, when a module is faced with another identical system, the magnets are matched up, north-south, thus contributing, on one hand to better alignment and on the other hand to a better connection between the modules, adding strength for assemble.

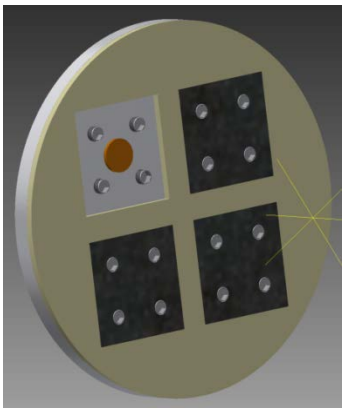

Fig. 3 Magnetic Part.

In the disconnection process, the rotation system begins turning the magnets so that each of them faces another magnet of different polarity. The magnets of a module (rotating) and the magnets of the other module (still), suffer a repulsive force that separates the modules.

4.2 Mechanical Part

The mechanical part (Fig. 4) has as main objective to strengthen the connection between modules connected together, because there may be situations in which the attractive force between the magnets is not enough. Therefore, this part has hooks and holes, one on each side of a rectangular piece that encloses the coupling element.

The operation of this coupling part is as follows: as the gear system rotates, the element with the hole (module 1) goes inside the other module (module 2), while, at the same time, the hook of module 2 advances until it meets the hole of the element of module 1, forming a fix connection system between the two modules.

The rotation of the gear system produces not only the movement of the mechanical part described above, but also the rotation of the circular system where the magnets are. This implies that we must use one system that allows carrying out two independent movements with only one motor.

The system used for this purpose is a differential gear, which allows the simultaneous movement of both parts and also allows the individual movement of each part if the other has reached the desired position, so only one motor is needed.

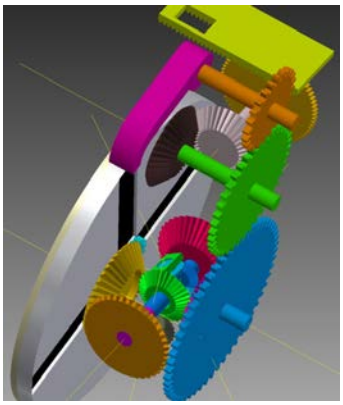

Fig. 4 Mechanical Part.

5. Conclusions and Future Works

The most known modular robot connections systems have been presented. After a thorough study of the necessary features of the docking systems, a new proposal of mechanical design has been introduced. This docking system design takes advantage of both, magnetic and mechanical connection principles, trying to unify the best features to achieve the ideal specifications of a coupling system.

The first version of the design has been described showing the most important working principles. The main elements of the docking system have been also introduced, and the complete system has been mechanically simulated to assess the performance.

In the following steps the design will be refined from the kinematic and dynamic analysis of the system. This work will allow manufacturing a real prototype that could be tested in real working conditions.

References

Castano, A., Behar A., and Will, P. “The Conro modules for reconfigurable robots,” IEEE/ASME Trans. Mechatronics, vol. 7, no. 4, pp. 403–409, Dec. 2002.

Davey, J., Kwok, N., & Yim, M. (2012, October). Emulating self-reconfigurable robots-design of the SMORES system. In Intelligent Robots and Systems (IROS), 2012 IEEE/RSJ International Conference on (pp. 4464-4469). IEEE.

Kernbach, S., Thenius, R., Corradi, P., Ricotti, L., Meister, E., Schlachter, F., Jebens, K., Szymanski, M., Liedke, J., Laneri, D., Winkler, L. and Schmickl, T. "Symbiotic robot organisms: REPLICATOR and SYMBRION projects," in Proceedings of the 8th Workshop on Performance Metrics for Intelligent Systems - PerMIS '08, 2008, p. 62.

Kovac R. and Rubenstein, M. "SINGO: A single-end-operative and genderless connector for self-reconfiguration, self-assembly and self-healing," in 2009 IEEE International Conference on Robotics and Automation, 2009, pp. 4253–4258.

Liedke, J., and Worn, H. "CoBoLD — A bonding mechanism for modular self-reconfigurable mobile robots," in 2011 IEEE International Conference on Robotics and Biomimetics, 2011, no. section III, pp. 2025–2030.

Murata, S., Yoshida, E., Kamimura, A., Kurokawa, H., Tomita, K. and Kokaji, S., "M-TRAN: self-reconfigurable modular robotic system," IEEE/ASME Trans. Mechatronics, vol. 7, no. 4, pp. 431–441, Dec. 2002.

Neubert, J., Rost, A., & Lipson, H. (2014). Self-soldering connectors for modular robots. Robotics, IEEE Transactions on, 30(6), 1344-1357.

Pacheco, M., Moghadam, M., Magnússon, A., Silverman, B., Lund, H. H., & Christensen, D. J. (2013, May). Fable: Design of a modular robotic playware platform. In Robotics and Automation (ICRA), 2013 IEEE International Conference on (pp. 544-550). IEEE.

Sproewitz, A., Billard, A., Dillenbourg, P. and Ijspeert, A. J. "Roombots-mechanical design of self-reconfiguring modular robots for adaptive furniture," in 2009 IEEE International Conference on Robotics and Automation, 2009, no. c, pp. 4259–4264.

Wolfe, K. C., Moses, M. S., Kutzer, M. D., & Chirikjian, G. S. (2012, May). M 3 Express: A low-cost independently-mobile reconfigurable modular robot. InRobotics and Automation (ICRA), 2012 IEEE International Conference on (pp. 2704-2710). IEEE.

Yim, M. and Duff, D. "Modular robots," IEEE Spectr., vol. 39, no. 2, pp. 30–34, 2002.

CHAPTER 43

CASCADE CONTROL OF THE PUMA 560 MOTORS USING SIMULINK AND ARDUINO

D. BLANCO, S. ALONSO and M. DOMÍNGUEZ

SUPPRESS Research Group, Escuela de Ingenierías Industrial e Informática. Universidad de León. Campus de Vegazana SN, 24071 León, Spain
E-mail:*{dblanm00.estudiantes, saloc, manuel.dominguez }@unileon.es*

In this paper, a low-cost rapid prototyping approach to control the PUMA 560 robot arm is presented. This approach is proposed as an educational tool in robotics and control field by presenting a torque, velocity and position cascade control architecture. Arduino was used as a Data Acquisition Server, reading the PUMA sensors and sending the signals to the motor drivers. Simulink was responsible for the main control system, computing all the data and communicating with Arduino for the proper robot control. The motor driver is in charge of delivering the corresponding current to the motors. In this paper, the control architecture is set up and tested for one motor, but it can be easily extended to the remaining motors of the robot.

1 Introduction

Education in engineering sciences deals with many difficult concepts in electronics, robotics and control, to name a few. The understanding of these fields can become straightforward when instructors use practical examples to demonstrate what it is being explained. In particular, control engineers have to deal with real-world systems, which involve imperfect models and perturbations. Education using real-world systems gives students a chance to learn how to design control systems for real plants such as robotic arms, resulting from applied approximations (Dormido et. al., 2008).

Quite frequently, outdated and simple robots are used by the institutions to widen the experiments in their courses, due to the high-price of new sys-

tems. These systems are usually obsolete, making hardware replacement difficult to find. Furthermore, IT technologies involve new requirements for these systems, which cannot usually be used as educational tools in remote laboratories, such as LRA-ULE (Candelas Herías et al., 2004; Prada et al., 2015). Because of this fact, the hardware and software need to be updated, being rapid prototyping and low-cost hardware a great option (Reguera et al., 2015).

PUMA 560 robot arm is a good example of obsolete equipment. It is commonly used in many universities for learning robotics and control. However, for that, it requires replacing its old controller and adapting the whole system (Wyeth et al., 2000). In this paper, a new control architecture for Puma 560 based on Simulink and Arduino is proposed. These technologies have been chosen because of its extensive use and accessibility in educational institutions and rapid prototyping. The aim of this work is to update the original control system of the PUMA 560 (Moreira et al., 1996). As an example, the application of this new control architecture to one of the six joints of the robot is presented here.

The rest of the paper is organized as follows: Section 2 presents the state of the art of Puma 560. In Section 3, the signal acquisition and motor driver as well as the three control loops are described. Some experimental results are presented in Section 4. Finally, the paper gives a conclusion in Section 5.

2 Puma 560 robot arm

PUMA 560 robot arm is well known in industry, teaching and research areas, which makes it suitable for educational purposes. Puma 560 has six joints, i.e. motors, 3 located in the body and 3 in the wrist. Each joint is driven by a 40V brushed DC motor. The motors in the wrist are rated at around 80W and the ones in the body are rated at around 160W. Body joints incorporate a 24V electromagnetic brake which must be released before operating these joints. All the joints are provided with sine-cosine encoders and potentiometers for giving position and velocity feedback to the controller (Wyeth et al., 2000). Furthermore, encoder 30mV quadrature signals must be processed and adapted. one of the six joints of the robot is presented here.

All motor signals (motors, encoders, potentiometers, etc.) use specific colored wires (Potgieter et al., 2005), facilitating the connection and adaptation.

3 Proposed Control Architecture

3.1 Data Acquisition

In this section, we present the signal acquisition and conditioning from/to the PUMA sensors and motors. Also, we explain the option used to communicate Simulink and Arduino. Motor driver features and the control loops implemented in Simulink are described here.

3.1.1 Signal filtering and conditioning

Potentiometer signal includes noise and so, it needs to be filtered via a low-pass filter. The cutoff frequency was determined using a Fourier transform. The signals from the encoders are sine-cosine waves in a range of 30mV. These high frequency signals cannot be read correctly by the Arduino board, so a conditioning electronic circuit is required to convert the 30 mV sine-cosine waves into a 0-5V TTL signals. First, the signals are amplified using an LM741 and then, they are compared with a threshold to obtain 0-5V TTL signals.

3.1.2 Arduino Mega 2560

An Arduino Mega 2560 board is used to acquire signals from potentiometers, encoders and to send data to motor driver.

One Analog Input (AI) is used for acquire the filtered signal from the potentiometers. Encoders signal are high frequency signals, therefore, they are obtained using the external interrupts mapped to digital input pins.

There are three outputs towards the motor driver, two Digital Outputs are used to point out the direction of the joint; and one digital PWM to indicate the velocity of the motor. In addition, one AI is used to receive the motor current from the motor driver (see Table 1.).

Table 1. Pinout of Arduino Meg 2560 board signals.

Signal	Signal From/To	Arduino Pin
Potentiometer	From PUMA 560	Analog Pin 0
Motor Current	From Motor Driver	Analog Pin 1
Encoder	From PUMA 560	Digital Pin 2
Motor CW/CCW	To Motor Driver	Digital Pin 4 & 5
PWM	To Motor Driver	Digital Pin 9

3.1.3 ArduinoIO

Among all existing techniques to communicate Arduino boards with Matlab, we chose ArduinoIO package (Campa, 2016) and modified it, extending the package functionalities.

ArduinoIO package implements the algorithms for the usage of the Arduino board as a Data Acquisition Server (DAS). The Arduino board will act as a listener awaiting strings from Simulink to configure each I/O pin function. The output values will return to Simulink as a string using the same format.

ArduinoIO package has been modified, including encoder pulse counter functionality using the external interrupts of the Arduino board. Matlab's algorithm has also been changed to include the communication with Arduino's pulse counter function. Moreover, a Simulink Pulse Counter block has been developed in order to achieve the velocity control loop.

3.2 Motor Driver

As a motor driver, the ESCON Module 50/5 DC by Maxon Motor has been chosen, replacing the old and incompatible driver target. The operating voltage and current (50V; 5A), the type of inputs and outputs and the operating modes are some of the reasons because it has been selected. It should be emphasized that the PWM range of the motor driver is limited to values between 10-90%. The current range is limited to protect the motors.

On the other hand, the selected driver measures the current of the motors and provides it in order to be used in torque control loop. This signal is delivered to the Arduino board and is scaled according to the input pin range.

3.3 Control Algorithms

The control architecture adopted is defined by the Arduino Mega 2560, working as a DAS; the cascade control loop developed in Simulink; the motor driver; and the sensor signal conditioning (see Fig. 1).

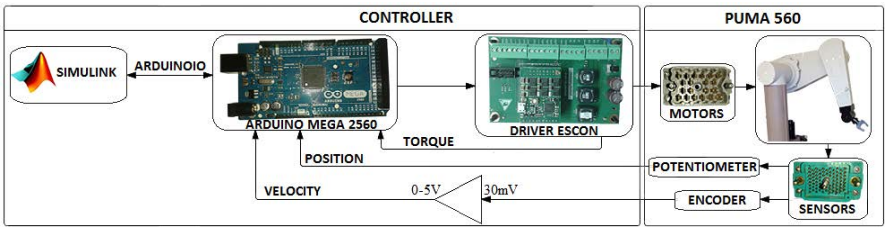

Fig. 1. Control architecture proposed.

To develop a proper cascade control the following steps have been followed: potentiometer scaling; motor position control; encoder signal scaling; velocity and position cascade control; current signal scaling; and final nested control structure.

3.3.1 Position Control Loop

This control is based on the error computation between the position set-point, given in degrees; and the filtered signal acquired from the potentiometer.

Once the error is computed, a comparison block defines the direction of the motor as clockwise (CW) or counter-clockwise (CCW). Then, a PI controller is applied and the output signal is scaled and saturated according to the PWM motor driver limits.

3.3.2 Position and Velocity Control Loop

First of all, the ratio between the encoder pulses per revolution (PPR) and the voltage supplied to the joint was found. Next, PPR is compared with the position error to define when the velocity loop needs to take action. The output of this comparison is multiplied by a constant, so that, when the position error is maximum, the velocity will be higher, and as the motor approaches to the desired position, the velocity will slow down.

Position loop needs to be scaled into the maximum voltage supplied by the motor driver, so the velocity and position loop are in the same range. Next, the velocity loop applies a PI controller, followed by a gain to convert the voltage units into the Arduino's PWM range.

3.3.3 Position, Velocity and Torque Control Loop

As well known, the torque generated by a DC motor is proportional to its current. The proposed torque loop will use the ratio between the input

voltage and the motor current. This loop determines the error between the read current and the estimated current. In case that the current read is greater than the estimated, the power supplied will be higher to compensate the motor's load if necessary. The estimated current corresponds to the PWM sent to the driver motor. Read and estimated current need to have the same range to be compared, so both are converted to the motor driver limits. As in the velocity loop, if the position error is high, the torque loop will have higher influence. After the estimated and read current comparison, a PI controller is applied, followed by the signal saturation. The final nested control architecture implements the previously loops commented (see Fig 2.).

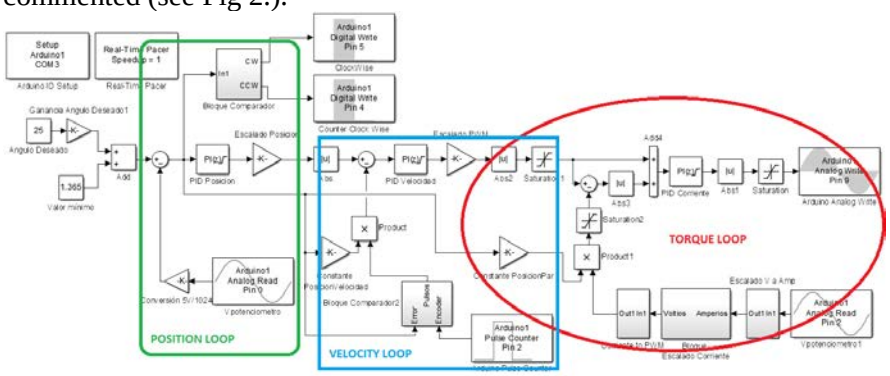

Fig. 2. Position, velocity and torque cascade control loop.

4. Experimental Results

In order to find the different ratios and parameters that would affect the cascade control loop, the following experiments were carried out using one of the motors in the wrist. First, we determined signal ranges (potentiometer and encoder) and ratios (input voltage - encoder's pulses per revolution, motor current) in order to adjust the control parameters of a wrist motor.

Position control was tested using different PI controller parameters and it can be pointed out that the control works reaching the position setpoint correctly but slower as expected. Afterwards, the position and velocity control was tested with a PI controller, tuned empirically using Ziegler-Nichols rules. Finally, position, velocity and torque cascade control with PI controllers were tuned empirically as mentioned above (see Fig.3. and Fig.4.). The results obtained using last cascade control showed how a growth in the motor current was correctly compensated, so that the position setpoint was reached with certain accuracy (a bit slower), likewise no load was presented. Thus the control worked as expected.

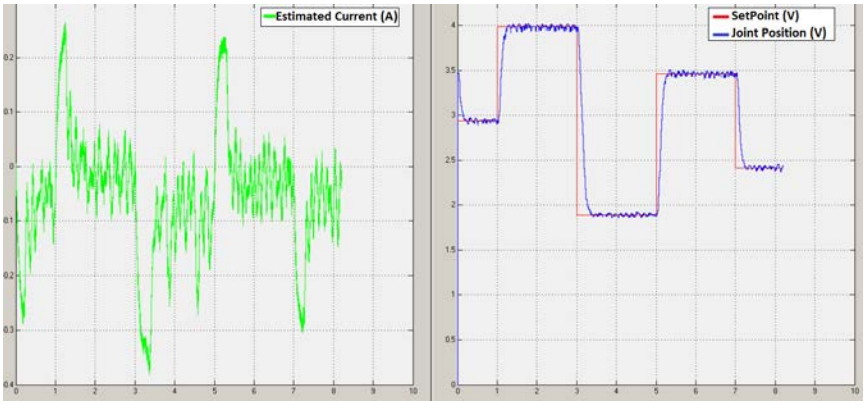

Fig. 3. Motor cascade control without load.

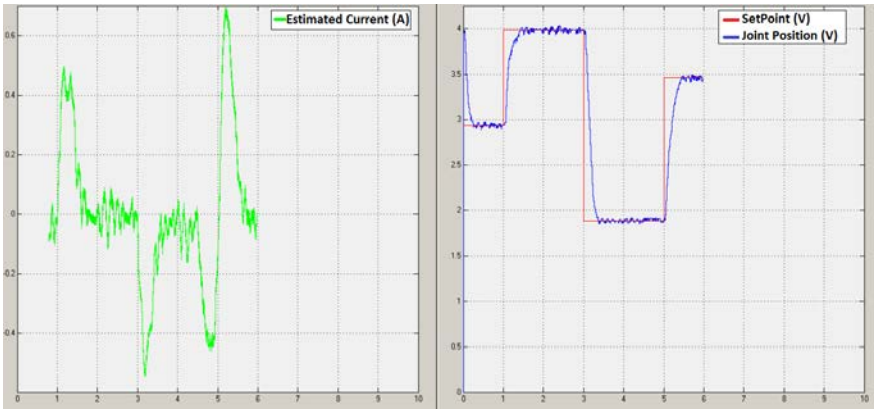

Fig. 4. Motor cascade control with load.

5 Conclusions and Future Work

In this paper, a cascade control architecture has been presented. It was implemented and tested using a joint of the PUMA 560, confirming that Arduino and Simulink can be used for the purpose. The proposed architecture is a low-cost updating of the previous architecture, adapting the PUMA 560 to new IT requirements and putting this robot closer to its incorporation into the LRA-ULE, as educational tool.

Future works could be led to implement in LRA-ULE in order to students can modify different parameters and Simulink blocks and to analyze the results driven by this changes. Moreover, the cascade control could be replicated for the six joints of the robot. Also, the kinematic model of Puma 560 could be considered in the control architecture.

References

Campa, G. (2016). Legacy MATLAB and Simulink Support for Arduino - File Exchange - MATLAB Central. [online] Mathworks.com. Available at: http://www.mathworks.com/matlabcentral/fileexchange/32374-legacy-matlab-and-simulink-support-for-arduino [Accessed 20 Apr. 2016].

Candelas Herías, F. A., Torres Medina, F., Gil Vázquez, P., Ortiz Zamora, F. G., Puente Méndez, S. T., & Pomares Baeza, J. (2004). Laboratorio virtual remoto para robótica y evaluación de su impacto en la docencia.

Dormido, R., Vargas, H., Duro, N., Sanchez, J., Dormido-Canto, S., Farias, G., Esquembre, F., & Dormido, S. (2008). Development of a web-based control laboratory for automation technicians: The three-tank system. Education, IEEE Transactions on, 51(1), 35-44.

Moreira, N., Alvito, P., & Lima, P. (1996, September). First steps towards an open control architecture for a PUMA 560. In Proc. 2nd Portuguese Conf. On Automatic Control. Porto (Portugal).

Potgieter, J., Zyzalo, J., & Diegel, O. (2005). Reconfigurable Mechatronic Robotic Plug-and-Play Controller. INTECH Open Access Publisher.

Prada, M. A., Fuertes, J. J., Alonso, S., García, S., & Domínguez, M. (2015). Challenges and solutions in remote laboratories. Application to a remote laboratory of an electro-pneumatic classification cell. Computers & Education, 85, 180-190.

Reguera, P., García, D., Domínguez, M., Prada, M. A., & Alonso, S. (2015). A LOW-COST OPEN SOURCE HARDWARE IN CONTROL EDUCATION. CASE STUDY: ARDUINO-FEEDBACK MS-150. IFAC-PapersOnLine, 48(29), 117-122.

Studenny, J., Belanger, P., & Daneshmend, L. K. (1991, December). A digital implementation of the acceleration feedback control law on a PUMA 560 manipulator. In Decision and Control, 1991., Proceedings of the 30th IEEE Conference on (pp. 2639-2648). IEEE.

Wyeth, G. F., Kennedy, J., & Lillywhite, J. (2000). Distributed digital control of a robot arm. In Proceedings of the Australian Conference on Robotics and Automation (ACRA 2000), August.

CHAPTER 44

GRABBING OBJECTS THROUGH A ROBOTIC ARM AND HAND IN A SAFETY WAY

A. LÁZARO, J. MORIANO, L.M. BERGASA, R. BAREA and E. LOPEZ

Robesafe group, Universidad de Alcalá, alberto2991lazaro@gmail.com.

This paper presents a system for grabbing objects in an industrial environment through a robotic arm and a hand grip in a safety way including three dimensional obstacle avoidance. The environment information is provided by a vision system, based on a RGBD camera, through the Robotic Operating System (ROS) (Quigley, 2009). A comparison between the different solvers is also carried out for a typical industrial scenario and experimental results with an IRB120 robotic arm are also shown.

1 Introduction

Industrial robotics systems tend to autonomously be able to complete more complex tasks with the minimal human intervention. In last years, taking advantage of the newest object recognition techniques in computer vision, it is possible to automatically classify the detected objects in different groups.

In a working space with several different objects, once the vision system has classified every object in the group it belongs, it is possible to physically classify and grab all of them by means of a robotic arm and a robotic hand. In the proposed work, the trajectory calculation for grabbing and placing the target object, comparing different solvers, is faced. These trajectories are calculated avoiding collisions with the rest of detected objects in a three-dimensional way.

The employed vision system using a RGBD camera is explained in (Lázaro, 2016) and it includes object classification, pose and dimension estimation. The communication between the vision and robotic modules has been implemented taking advantage of ROS communication facilities.

The main goal of this paper is, by reconstructing a scene with the provided information, in which the objects, the robot arm and its environment are included, be able to interact with the different objects placed in the working scene in a safety way, avoiding damages in the robot and in the manipulated objects. Different planner strategies have been analyzed and compared to select the one that better fits with the required needs.

2 State of the art

Regarding to the topic of automatic objects classification employing robotic arm, several projects have been carried out. Hereafter we show some of the most important.

In (Szabo, 2012), (Bdiwi, 2012) and (Li, 2014) object classification and sorting is faced depending on the object color or shape. They also employ industrial robots for grabbing the different objects and placing them. These works are mainly focus in computer vision algorithm for detection and classification of the different objects.

Our proposal, as difference with the above works, employs different techniques for robotic arm planning and they are compared to choose the one that best fits our requirements. The selected planning techniques in ROS are employed to develop the robot manage system and to carried out comparison results between the different OMPL (Open Motion Planning Library).

Furthermore, the trajectories are calculated at the computer employing a robotic CAD model. This way the system is easily portable for a different robotic arm. Using OMPL planners and incorporating the detected objects to the scene, the path is calculated as a non-collision path.

3 Set up and robot Control

All the communication processes have been implemented by means of ROS, employing different nodes and topics. The vision system is set up as a unique ROS node while the robotic system is separated in several ROS nodes. The communication is established through a common topic where the vision system is publishing continuously.

To carry out the trajectories planning, an URDF model which includes the IRB 120 robotic arm shape and its configuration parameters, was developed using the robot CAD models as it is depicted in Fig. 1. The robot

parameters, that are set up in the URDF file, define the axes and the joints movement limits.

Once the model is completed it is introduced into the "MoveIt!" software, where the robot environment is added with the provided information (object class, position, orientation and dimensions), so trajectories plan can be faced.

Due to several objects can be touched by the robot when some of them is grabbed, in the grabbing maneuvers the rest of the objects will be defined as "collision objects", which cannot collide with any part of the robot. A safety area is added around the collision object in order to increase the security of the maneuver.

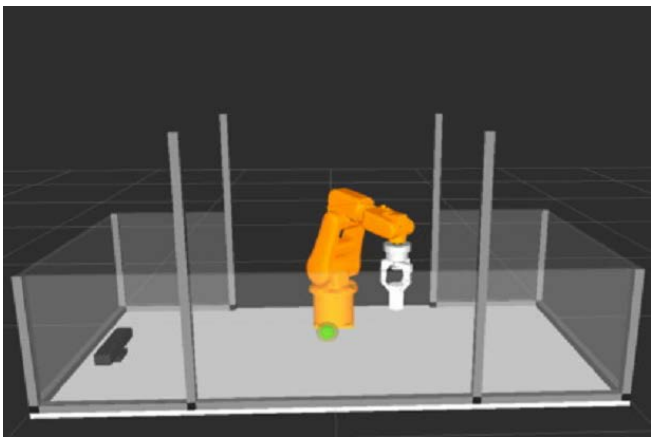

Fig. 1. Robot Model: the robot model and its working environment are shown. There are two different objects placed in the working scene: a can (cylinder) and a ball (sphere), which is depicted with a safety area around it

4 Robot Control

Once all the objects placed in the working scene are detected and the virtual environment is created, the robot recognizes the different objects according to the explained methods. The robot classifies the objects from the biggest to the smallest. Different grab processes have been developed to optimize the hand-grip taking into account the shape the objects have.
The robot uses the information of the vision system to estimate the height where the robotic hand should close.

After grabbing an object, it is placed in the assigned position according to the class it belongs as it can be seen in Fig. 2. The locations where the

objects are deposited are filtered by the system, so once they are placed they disappear in the computer reconstruction.

Fig. 2. Object sorting: Different objects are shown once the robot has sorted them

4.1 Collision avoidance

Due to the fact that the number of objects placed in the working scene is usually bigger than one, a planner which is able to find free-collision-paths is required. Different motion based planners (PRM planners and Tree based planners) (Hsu, 1999), (Sanchez, 2003), (Suçan, 2009) and (Muja, 2009), which are available in OMPL are compared in our scenario.

The maximum distance among nodes is the most important parameter. The dimensions of the objects and the whole distance trajectory should be taken into account to choose it properly. This distance should reach a compromise between processing time and safety. After several tests, the maximum distance that returns better results in terms of performance is 5 cm, which is the reason why this distance is the one that has been established to estimate the trajectories.

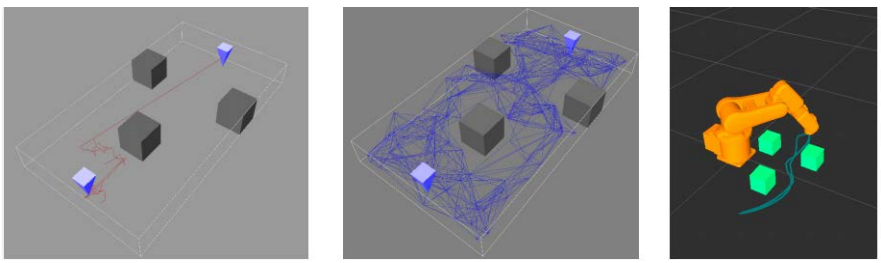

Fig. 3. In this figure the differences between probabilistic road-map and tree-based planning strategies are shown using KPIECE (left image) and PRM planner (center image). They are employed on an environment close to the real cases they will be faced. These

Simulations have been carried out thanks to OMPL application. In the right image the KPIECE planner is tested in the simulated environment and different paths were planned meeting the constraints and avoiding the three collision objects.

All the planners were tested solving the same case several times in which the robot needs to avoid three box obstacles (10x10x10 cm). The robot is forced to find a free three dimensional collision trajectory with a constrain of 10 cm in height. Average values of the obtained results are shown in Table 1 to choose the planner that has more interesting features. This analysis reveals that KPIECE and BKPIECE planners are the ones that stay closer to the desired requirements. Time costs are shown for the different tested planners in the next table:

Table 1. Planners times with 3 obstacles.

Planner	Average time (s)
BKPIECE	22.5
KPIECE	25.71
LBKPIECE	90
EST	90
PRM	45
PRM Star	180
RRT	60
RRT Connect	90
RRT Star	-
TRRT	-
SBL	36

In 3D environments, tree-based planners are really interesting because they can find a path without collisions in a small time, reducing the calculations. In the Fig. 3, the two planner categories (three-based and probabilistic) are compared applying them to the same problem.

KPIECE tree-based planner was selected as the better option because it is one of the fastest planners for our scenario and the paths are smooth enough to get our goals. Due to this planner carries out a discretization, it takes longer, compared with random ones, to define the better path.

4.2 Application Test

To test our whole application different objects such as balls, cans and boxes are used. The objects are detected by the vision system which provides to the robot the position where all of them are located so it can reach their position. According to the objects class they are grabbed and deposited by

the robot in different places. The robotic system receives the path through an ROS–ABB socket.

Firstly, the robot moves to the initial position, which is high enough to allow the vision system captures properly the working scene. Afterwards the working scene simulation is updated according to the information it receives.

The robot goes to the location of the biggest object in the scene and grabs it setting the finger angles to the established position, then robot deposits the grabbed object in a predefined location according to the class it belongs. Finally, the robot goes back to the initial position out of the Kinect vision field and the process starts again in the same way. The working scene stops updating while the robot is in the Kinect vision field.

It should be delighted that through the feedback of robotic hand and arm states it is possible to get in real time a simulated view of the whole process thanks to RViz.

In Fig. 4 an example of the application is shown in simulation and with the real arm (IRB120 of ABB) and hand (BH8-262 of BarrettHand). In this figure it can be seen how the box is not included in the simulated scene due to the fact that it has been previously placed by the robot in its proper location employing a position filter the box is no longer included in the scene. Therefore, there are just two objects in the working scene: a can and a ball. The can is the target object for the robot in the shown case because it is the biggest one. Therefore, the ball is considered as collision object.

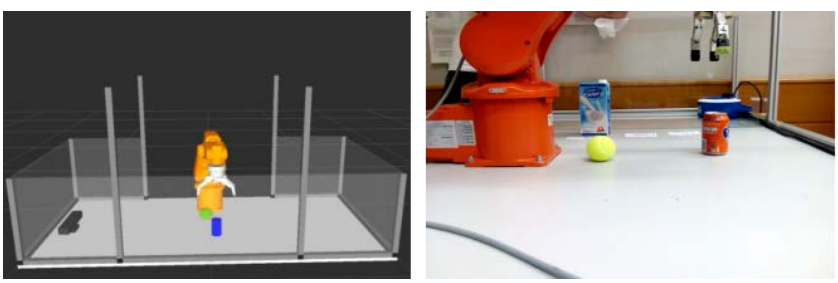

Fig. 4. Application example: The left figure shows the simulated working scene while the right one depicts the real working scene from the Kinect's point of view. Both images were taken at the same time.

5 Conclusions and future work

This paper has addressed the trajectory planning for object grabbing in a 3D free collision way, both in simulation and in a real industrial environ-

ment. To achieve the robot movement ensuring there is no collision an optimum movement planner, which is able to avoid hurdles, is used. Although it has been presented a real time solution for the addressed problem an enhancement will be done on working on reducing the processing time in order to make our system able to recognize and move objects faster than a human.

Acknowledgements

This work was supported in part by the MINECO SmartElderlyCar (TRA2015-70501-C2-1-R) project and by the RoboCity2030 III-CM project (S2013/MIT-2748) funded by Programas de I+D en la Comunidad de Madrid and cofunded by Structured Funds of the UE.

References

Bdiwi, M. 2012. Robot Control System with Integrated Vision / Force Feedback for Automated Sorting System. , pp.31–36.

Cruz, L. 2012. Kinect and RGBD images: Challenges and applications. Proceedings: 25th SIBGRAPI - Conference on Graphics, Patterns and Images Tutorials, SIBGRAPI-T 2012, pp.36–49.

Hsu, D. 1999. Path Planning in Expansive Configuration Spaces. International Journal of Computational Geometry & Applications, 09(04n05), pp.495–512.

Lázaro, A. 2016. 3D Object recognition and pose estimation using VFH descriptors. Open Conf. on Future Trends in Robotics (Robocity,'16').

Li, K. 2014. Robotic object manipulation with multilevel part-based model in RGB-D data. Proceedings - IEEE International Conference on Robotics and Automation, pp.3151–3156.

Muja, M. 2009. Fast Approximate Nearest Neighbors with Automatic Algorithm Configuration. International Conference on Computer Vision Theory and Applications (VISAPP '09), pp.1–10.

Quigley, M. 2009. ROS: an open-source Robot Operating System. In ICRA workshop on open source software (Vol. 3, No. 3.2, p. 5).

Rusu, R.B. 2011. 3D is here: point cloud library. IEEE International Conference on Robotics and Automation, pp.1 – 4.

Sanchez. 2003. A single-query bi-directional probabilistic roadmap planner with lazy collision checking. Robotics Research, pp.403–417.

Şucan, I. A. 2009. Kinodynamic motion planning by interior-exterior cell exploration. In Algorithmic Foundation of Robotics VIII (pp. 449-464). Springer Berlin Heidelberg.

Szabo, R. 2012. Automated colored object sorting application for robotic arms. 2012 10th International Symposium on Electronics and Telecommunications, ISETC 2012 - Conference Proceedings, pp.95–98.

CHAPTER 45

ELECTROMECHANICAL DESIGN OF A HUMANOID ROBOTIC HAND

C. MORILLO, M. HERNANDO and A. BRUNETE

Centro de Automática y Robótica, Universidad Politécnica de Madrid, Madrid, Spain.

Contributions in the field of humanoids robots have been focused on developing one of the most defining features of human: bipedism. But it is important not to forget another characteristic feature of our race derived from the previous, hand morphology. The evolution has made the hand a versatile and complex tool capable of doing a wide range of tasks such as grasping or communicating. To be able to adapt itself to the different situations a perfect cooperation among muscles, electrosignals and skin receptors is required. In terms of robotics, this means a lot of degrees of freedom in a confined space. A new design of a humanoid robotic hand is presented in this paper, proposing an electromechanical layout in order to preserve the freedom within the hand space and without using forearm's.

1 Introduction

In the last decade, many robotic hands have been developed in order to satisfy two main requirements: prosthetic hands and robotic hands. Even though those purposes seem to achieve practically the same objective, a mechanical design electronically controlled, the requirements on each case are significantly different. Prostheses tend to be simpler due to the fact that they need to be controlled by human interactions as muscle contractions or nerve signals. For this reason the quantity of degrees of freedom is much lower than in computationally controlled hands, which can simulate the whole movements of his real counterpart.

In spite of replicating the totality of the DoF, the hand can be approximated to a simpler model that allows doing the basic movements and

grasps that human usually done. For each DoF it is necessary an actuator that makes the function of the muscle. There are different options in this area, electric motors, SMA (Shape Memory Alloy) (Lagoudas, 2008), SMP (Shape Memory Polymer) (Behl et al., 2007), air compress actuators... It is also important the way the movements are transmitted to his correct articulation, being possible keep the actuators far from the related mechanism and stored in a specific place where space is not such a problem. This is a common use on robotic hands as Shadow Hand (Armando de la Rosa et al., 2012), where actuators are placed in the forearm. For the developed robotic hand treated in this paper, actuators will not dispose of any part beyond the wrist.

Thanks to the 3D printing techniques it is possible to design a prototype able to adapt itself to the hand requirements and to keep all the electronic and mechanical elements on the inside. Many hands have been developed using this technology, for example the project InMoov (Langevin G., 2014) has designed a fully 3D printed hand which is actuated by wires contraction; or Talon Hand, that uses a mechanism activated by the wrist to close the fingers.

In order to suit small spaces where the hand components should be placed, for the hand proposed in this paper it has been elaborated mechanisms adapted to the articulations and a global electromechanical design which consist on the utilization of the electronic components as an important part of the hand structure.

2 Design requirements

The main objective is the creation of a robotic gestural hand that provides the most natural sensations in its movements. Because of this, the robot will not need to support external charges and non rigid materials could be used.

2.1 3D Printing

Humanoid robots need to be light to be carried easily in order to keep the stability. For that reason 3D printed plastic pieces have been chosen as main structural components. There are different options in this way: PLA, ABS, plastic mixed with other materials, elastic plastic… For this project PLA has been chosen instead of ABS due to its thermal response that makes it easy to work with (Casavola et al., 2015). In addition, the stress

supported by PLA is much higher than ABS's, which provides resistance and extra protection to the hand.

2.2 Hand Grasps

Human hand anatomy should to be known to be able to make a good design of a robotic hand which seeks to imitate its behavior (Drake et al., 2014). Hand consists of 27 bones and 34 muscles which, in addition to forearm muscles provides the hand 20 degrees of freedom.

It is a difficult task to replicate each muscle with an actuator, so a simplification is done in order to get a commitment between simplicity and functionality. To quantify that dependency there are some tests as *Cutkosky Grasp test* that check sixteen different positions on the hand. Robonaut 2 hand from NASA completes fifteen of these tests with 14 DoF in total (Bridgwater et al., 2012).

For the robotic hand approached it has been proposed a total of 17 DoF to resemble a real hand: 3 for each finger, 4 for the thumb and 1 for the opposing hand palm capacity. To give a natural position on idle state, each finger has a different angle.

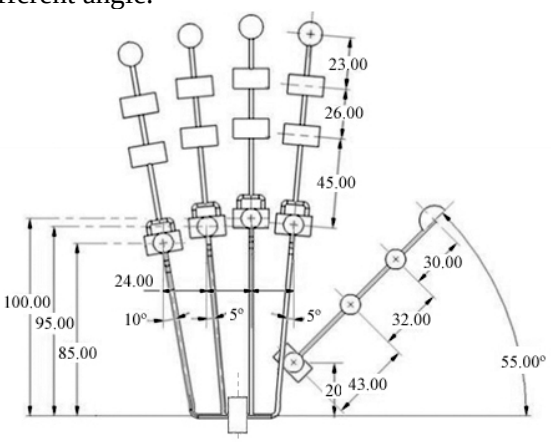

Fig. 1. Schematic design of the proposed hand.

2.3 Actuators

After some tests with servomotors, SMA or SMP, DC motors with gearbox have been chosen as the actuator due to its small size, good movement features, rapid response and relative easy control. It will be necessary one motor per degree of freedom.

DC motors. This kind of actuators appears in many applications. It can be found in a wide range of sizes, even miniaturized, that gives the possibility of including a lot of them in a confined space. However, there is an important drawback; high rotation velocity should be transformed in order to increase the torque. Some motors include an optimized gearbox that allows the reduction only taken a small space.

2.4 Sensors

A good control requires some feedback information such as actuators position, velocity or force. Hand includes infrared distance sensors to measure motor movement and as a result, provide the information about finger position. For each motor there will be one sensor, thus the hand should keep 17 sensors in total.

Due to this project try to save as money as possible to get a low cost design, IR sensors have been proposed from the beginning. In addition, this kind of sensors avoids mechanical friction and produces less noise than other such as variable resistors.

3 Electro-mechanic design

Once that robotic hand basic structure and components have been selected, it is necessary to distribute all inside the hand volume. As it has been said before, space limitations are the most difficult issue to deal with.

3.1 Interphalangeal joints

This joint is constituted by two different articulations, distal interphalangeal joint and proximal interphalangeal joint. Both of them constitute the two final finger articulations.

According to grasping tests, human natural grasps do not use those joints independently each other, so robotic model uses only one motor to actuate both at once. To get this it has been designed a four-bar linkage as shown in Fig. 2; it transmits the movement from proximal joint to distal as in Robonaut 2 hand (Bridgwater et al., 2012).

Movement is generated by an actuator located in the proximal phalange. To transmit the movement from the motor to the proximal interphalangeal joint, represented by number ‘1’ in Fig. 2, it is necessary to change the axis of rotation 90 degrees. Instead of using conical gears difficult to adapt within that little space, a new idea has been proposed, use a spring as

transmitter. The spring is bended 90 degrees connecting the motor axis with the proximal phalange axis. In case of external impacts given to the finger, the spring will absorb the forces avoiding cracks on the internal structure. The IR sensor could be found within the distal phalange taking measure of the variable distance to a plastic piece in order to map it to a finger rotation.

Fig. 2. Four-bar linkage in the interphalangeal joints.

3.2 Metacarpophalangeal joints

In the finger base is situated the metacarpophalangeal joint, which has two DoF due to this is a universal joint. In this case, it is used parallel robotics that use the combination of two motors located in the hand palm to get that 2 DoF of the knuckle. A rod-crank as shown in Fig. 3 mechanism has been developed to transmit the actuators movement. DC motor actuate directly on the rod, characterized for its linear movement, so a screw has been used to convert the rotation into a travel. If screw metric is low, so the lead distance is, thus instead of a screw, a hard compression spring has been used. This spring will not compress due to its hardness and lead is larger so the linear movement will be faster. Moreover, in case of impact, in case of impact, the spring absorbs the shock avoiding damage to the structure. In Fig. 3 only one mechanism is shown, however in the other side of the knuckle there is another one to get the parallel actuation.

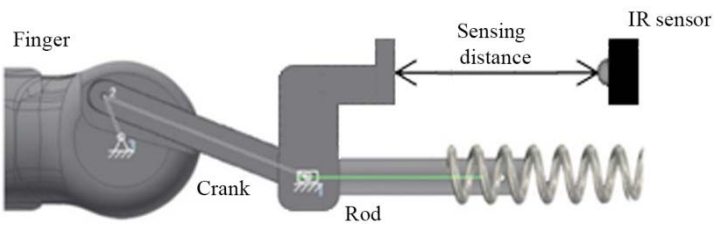

Fig 3. Lateral view of the knuckle rod-crank mechanism.

The convertion from rotation to linear movement allows an easier way to place IR sensors. Sensors are welded on te controller board and face a

smooth plastic piece which moves attached to the rod. Moreover, as will be seen later, these sensors are fully integrated on the controller board that contains all the aditional electronics to simplify hand control.

Mechatronical controller design. In order to control all the electronic components such as DC motors or IR sensors, it has been designed a controller board that contains everything needed to be controlled except the microcontroller. Instead of finding a position inside the hand to place it, the board will be an essential structural component, composing the enclosure of the hand palm. In that way, thanks to the fully mechatronic driver desing, not only it is possible space saving, even confers the hand extra robustness due to all IR sensors of the actuators placed in the palm are welded on the board, positioning them facing the rod that the optical sensor should meassure as in Fig. 3. This avoids mounting errors that could affect directly on the measurement quality.

The electronic circuit is separated in two sections: sensors control and actuator control. Sensing part requieres a lot of analog inputs so with the demultiplexer which the board includes they are reduced to one. Controlling DC motors is simplified due to H-bridges and as in sensig part, actuation requires a lot of digital outputs, so three shift registers decrease that number to three.

Fig. 4 shows the designed circuit in two layers for two fingers: index and middle. Its particular form allows the board to adapt to the hand and avoid collisions when finger moves. The white rectangles on the first circuit show where the IR sensors are placed, using one pair to each finger.

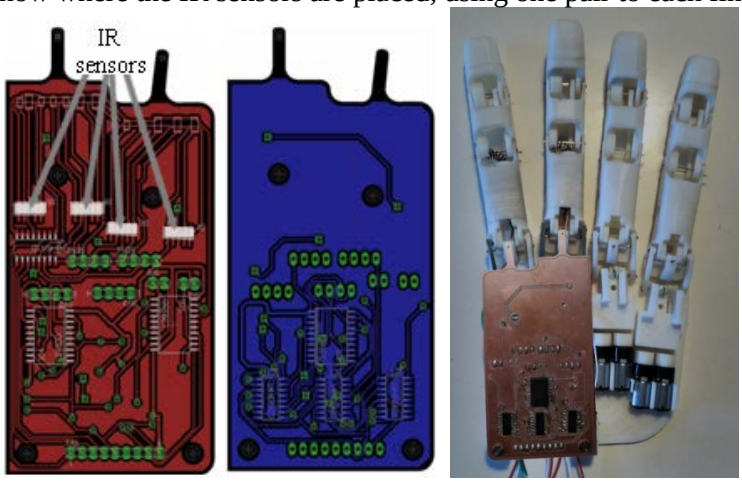

Fig 4. Controller board A) Bottom. B) Top. C) Controller board on hand structure.

Schematics. For the ring and little finger, the schematic circuit is exactly the same, only the form changes in order to enclosure the part of the hand palm that belongs to these fingers. The reason for separate both circuits is that there is an extra articulation between them, which allows hand opposing movements.

On Fig. 4c it could be seen the different spaces dedicated to each pair of fingers (index-middle and ring-little) and how the axis of rotation of the fingers fit on the electromecanical enclosure.

3.3 Thumb design

The main characteristic in human hands is the opposed finger, the thumb. It has been developed an initial design in order to distribute the finger degrees of freedom. The carpometacarpal joint has 2 DoF, however is not spherical but a saddle joint. To get this articulation effect, that allows the opposition, abduction and all characteristic movements of the thumb, it has been disposed two cylindrical joints but with a certain discrepancy so the axis of rotation do not intersect. Thumb, unlike the other fingers has an independent actuation in all articulations due to it is the most important point to get a realistic human hand. Thumb is in process of development.

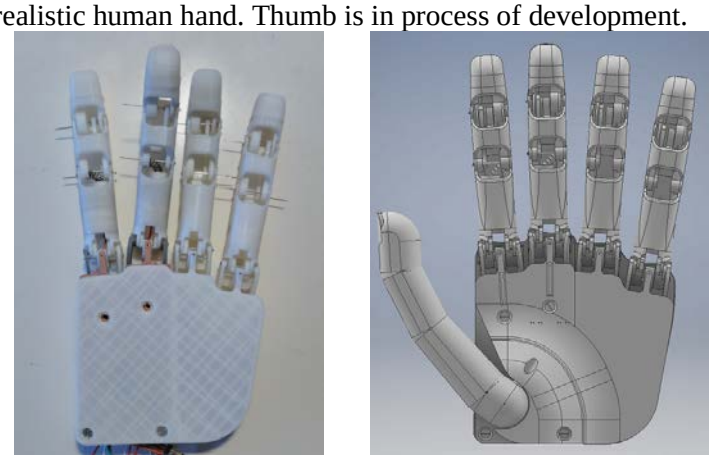

Fig 5. A) Final hand appearance. B) Complete hand with thumb

4 Conclusions and future work

The creation of the robotic hand with electromechanical techniques has developed new designing concepts based on the combined design between

mechanical structures and electronic devices. That electromechanical approach has been crucial to get the design of a hand with 17 degrees of freedom and all elements included within the hand volume. Movements are realistic thanks to the parallel robotics, which are specifically designed to allow the movements within the logical ranges. Springs gives flexibility to the hand without losing movement capacity, being able to resist external forces absorbing its effects and avoiding cracks. Thanks to the controller board, the hand can be controlled easily by a microcontroller such as Arduino. Hand costs are very low, total hand estimated costs are 150€ for a hand with 17 DoF. That means that for each DoF the costs are less than 9€.

The future work consist on develop a robust control of the whole hand, being able to perform different postures and grasps in order to add the hand to a humanoid robot capable of interact with the environment.

References

Armando de la Rosa T., Gavin Cassidy & Hugo Elias 2012, 21 December 2012-last update, Shadow dexterous hand technical specification. [2008, 1 June 2008].

Behl, M. & Lendlein, A. 2007, "Shape-memory polymers", Materials today, vol.10, no. 4, pp. 20-28.

Bridgwater, L.B., Ihrke, C., Diftler, M.A., Abdallah, M.E., Radford, N.A., Rogers,J., Yayathi, S., Askew, R.S. & Linn, D.M. 2012, "The robonaut 2 hand-designed to do work with tools", Robotics and Automation (ICRA), 2012IEEE International Conference onIEEE, , pp. 3425.

Casavola C., Cazzato A., Moramarco V., Pappalettere C. 2015. “Orthotropic mechanical properties of fused deposition modelling parts described by classical laminate theory”.

Drake, R., Vogl, A.W. & Mitchell, A.W. 2014, Gray's anatomy for students,Elsevier Health Sciences.

Lagoudas, D.C. 2008, "Shape memory alloys", Science and Business Media,LLC.

Langevin, G., 2014. InMoov-Open Source 3D printed life-size robot. pp. URL: http://inmoov. fr, License: http://creativecommons. org/licenses/by–nc/3.0/legalcode.

AUTHOR INDEX

GOBIERNO DE ESPANA
MINISTERIO DE ECONOMIA Y COMPETITIVIDAD

CSIC
CONSEJO SUPERIOR DE INVESTIGACIONES CIENTÍFICAS

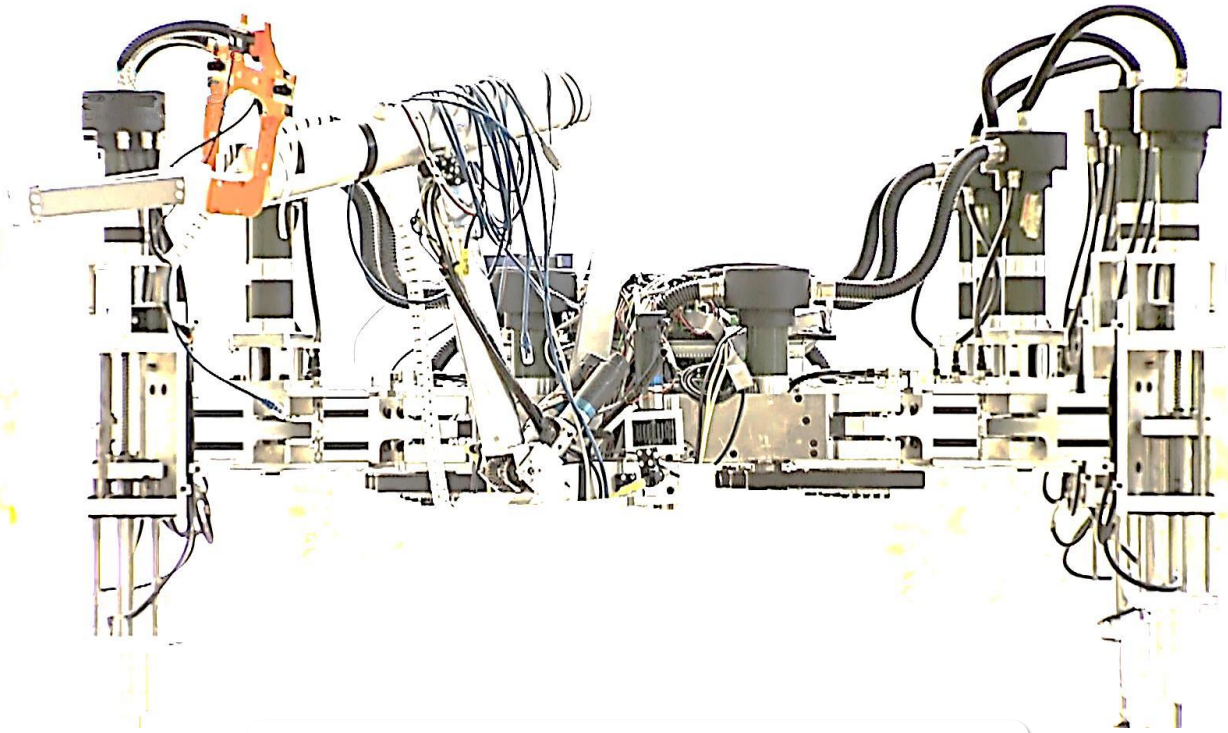

RoboCity2030.org

Comunidad de Madrid

UNIÓN EUROPEA
Fondos Estructurales
Invertimos en su futuro

Universidad Carlos III de Madrid

CSIC
CONSEJO SUPERIOR DE INVESTIGACIONES CIENTÍFICAS

POLITÉCNICA

Universidad de Alcalá

Universidad Rey Juan Carlos

UNED

ISBN: 978-84-608-8452-1

9 788460 884521

The research leading to these results has received funding from the RoboCity2030-III-CM project (*Robótica aplicada a la mejora de la calidad de vida de los ciudadanos*. *fase III; S2013/MIT-2748*), funded by *Programas de Actividades I+D en la Comunidad de Madrid* and cofunded by Structural Funds of the EU.